

DEVELOPMENT OF ELECTROCHEMICAL STEPS FOR GLUCOSE ELECTROOXIDATION TO VALUE-ADDED PRODUCTS

Giulia Moggia

Thesis submitted in the fulfilment of the requirements for the degree of
Doctor in Applied Engineering
(doctor in de toegepaste ingenieurswetenschappen)

Promotor:

Prof. Dr. Ing. Tom Breugelmans

Co-Promotor:

Dr. Joost Helsen

Printed by:

©2024 Giulia Moggia

All rights reserved. No parts of this book may be reproduced or transmitted in any form or by any means, electronic, mechanical, photocopying, recording or otherwise without the prior written permission of the author.

Development of electrochemical steps for glucose electrooxidation to value-added products

Giulia Moggia

Members of the jury:

Prof. Dr. Vera Meynen

President of the jury
University of Antwerp
Faculty of Science
Laboratory of adsorption and catalysis (LADCA)

Prof. Dr. Ir. Sammy Verbruggen

Member of the jury
University of Antwerp
Faculty of Science
Sustainable Energy, Air and Water technology
(DuEL)

Prof. Dr. Ing. Tom Breugelmans

Promoter
University of Antwerp
Faculty of Applied Engineering
Research group Applied Electrochemistry &
Catalysis (ELCAT)

Dr. Joost Helsen

Co-Promoter
Vlaamse Instelling voor Technologisch Onderzoek
(VITO)

Dr. Sander Neukermans

Secretary
University of Antwerp
Faculty of Applied Engineering
Research group Applied Electrochemistry &
Catalysis (ELCAT)

Prof. Dr. Patricia Benito Martin

External Member of the jury
University of Bologna
Faculty of Science

Prof. Dr. Amanda Garcia

External Member of the jury
University of Amsterdam
Faculty of Science

Declaration

I, Giulia Moggia, confirm that the work described in this thesis is my own and has not been supported by the Climate, Infrastructure and Environment Executive Agency of the European Commission. The views expressed in this thesis have not been adopted or in any way approved by the European Commission and do not constitute a statement of the European Commission's views.

Giulia Moggia

Ringraziamenti

Dedico questo studio e questi anni di lavoro alle mie due nipotine, con la promessa di continuare a fare del mio meglio per lasciare a loro un mondo in cui possano godersi questa unica vita, tanto quanto hanno potuto le generazioni prima di me, e tanto più di me.

Ringrazio chi é con me sempre, e mi ha spinto a non mollare, reggendomi forte: João, mamma e papà, Silvia, Antonello, Conc, Chris e Marianne, e tutti i miei amici.

Riconosco il supporto professionale di Dr. Nick Daems, il supporto tecnico di Thomas Kenis e di tutti i colleghi di ELCAT che hanno collaborato al lavoro condotto per questa Tesi. Riconosco il gentile supporto amministrativo ed organizzativo di Sofie Delanoye ed An Bellens. Ringrazio Prof. Tom Breugelmans per avermi dato questa opportunità, e la giuria tutta per il tempo dedicato a migliorare la mia Tesi e per la grande disponibilità per aver partecipato alla mia discussione privata e pubblica.

“Volli, volli, e fortissimamente volli”, citazione di mia nonna, Caterina Augusto, in un suo libero adattamento di Vittorio Alfieri.

Acknowledgments

I dedicate this study and these years of work to my two nieces, to whom I promise to continue doing my best to leave them a world in which they can enjoy this unique life, as much as the generations before me could, and even more so as me.

I thank those who are always with me, and who pushed me to never give up, holding me strong: João, mum and dad, Silvia, Antonello, Conc, Chris and Marianne, and all my friends.

I acknowledge the professional support of Dr. Nick Daems, the technical support of Thomas Kenis and of all ELCAT colleagues who collaborated to this work. I also acknowledge the kind, administrative and organizational, support of Sofie Delanoye and An Bellens. I thank Prof. Tom Breugelmans for giving me this opportunity, and this jury all for the time spent improving my thesis and for participating in my private and public discussions.

“I willed, and always willed, and strongly willed”, quoting my grandmother, Caterina Augusto, in her free adaptation of Vittorio Alfieri.

Summary

Carbohydrates are renewable, inexpensive and available organic raw materials. Only 3–5% of carbohydrates have industrial use, the rest decays and recycles along natural pathways. One interesting finding in this field has been the recognition that aldonic and aldaric acids, sugar acids, have potential uses in fine chemistry. The carboxylic group is, in fact, able to react selectively with different amines, alcohols and vinyl derivatives forming products with new application profiles like aldonolactones, which are used in the preparation of N-alkyl aldonamide surfactants. However, the reasons for the limited use of carbohydrates as raw materials in fine chemistry are related to their over functionalization and also their poor solubility in most of the commonly used organic solvents. The challenge is to achieve a direct and region-selective oxidation of saccharides in aqueous media, which is difficult by classical chemical methods without a preliminary protection strategy. Electroorganic approaches have currently fascinated academicians and industrial researchers because of their high potential prospects for industrial ventures. Electrocatalytic organic synthesis provides a powerful tool to control the reaction rate and selectivity through electrode potential and current. Furthermore, electrosynthesis is naturally suited to obey the principles of Green Chemistry, owing to several environmentally favorable features: i.e., reduced energy consumption, use of renewable raw materials, decreased emission of pollutants or toxic raw materials. For this reason, the use of electrochemical organic synthesis represents a promising alternative to the traditional industrial methods.

Despite its sustainable nature and its potential to electrify the industry, as such replacing traditional, non-sustainable production processes of a broad range of fine chemicals, electrochemical synthesis methods are still very underdeveloped as compared to their traditional alternatives. More research is needed to better understand electrochemical processes and address the main challenges that prevent their application at industrial scale: i.e., the still unsatisfactory selectivity and/or productivity, the electrodes' limited lifetime and the insufficient know-how on up-scaling towards industrial scale.

This PhD thesis is specifically dedicated to the study of electrocatalytic routes for the selective oxidation of glucose to gluconic and glucaric acid (both of which are commercially relevant carbohydrates). To achieve this, it is of crucial importance that the exact reaction mechanism is understood. The aim here is thus to investigate the factors that determine the selectivity of the reaction towards the two products of interest, including the choice of the catalyst and the reaction conditions, and, as such, unravel the reaction mechanism beyond it. To this end, a combination of electrochemical and analytical techniques is used where microscopical surface analysis, used for the morphological characterization, is linked to its electrocatalytic performance.

This research starts with the investigation of the electrocatalytic activity of MnO₂-based catalysts towards glucose oxidation, to understand the underlying mechanism and its potential application for the production of gluconic and glucaric acid. MnO₂ films are first synthesized by electrodeposition and chemical impregnation methods on various supports and then tested in a batch cell for glucose electrooxidation at various reaction conditions. Electrochemical evaluation reveals that the catalyst with the smallest porosity (average pore size 45 nm), also results in the highest electrocatalytic activity in presence of glucose (~10.5 mA cm⁻²), but it does not yield the desired products in significant quantities, as shown by chromatographic analysis, and is therefore discarded for further studies. Next, the mechanism of three noble metals (Cu, Pt and Au) towards glucose electrooxidation is investigated using rotating disk electrodes in a batch cell. For all three,

a strong relationship is found between potential and reactivity of the functional groups in the glucose molecule. The Au electrode shows the highest activity (2 to 4 mA cm⁻²) and selectivity to gluconic (86.6 %) and glucaric acid (13.5 %), owing to two distinct oxidation peaks, one, at low potential (0.55 V_{RHE}), for the oxidation of the aldehyde group on C1, the other, at higher potential (1.34 V_{RHE}), for the oxidation of the hydroxymethyl group on C6. These experiments thus suggest that the reaction takes place in two separate steps: first, the oxidation of glucose to gluconic acid and, then, the further oxidation to glucaric acid. Given its promising electrochemical performance, Au is selected for further studies.

In the second part of this work, to help unravel the glucose electrooxidation mechanism on Au, we systematically investigate the influence of different operational parameters, i.e., pH, initial substrate concentration, applied potential, reaction temperature and time, for both oxidation steps. To this purpose long-term electrolysis experiments are conducted in a batch cell at different reaction conditions after which the products are analyzed by liquid chromatography. Results show that, in the first oxidation step, glucose to gluconic acid, the maximum selectivity (97.6 %) is achieved at moderately high pH, low temperature and low initial concentration of glucose, and is mainly limited due to the presence of competitive, base-catalyzed, chemical reactions. In the second electrooxidation, gluconic to glucaric acid, these parameters do not have a significant impact on the selectivity, that reaches a maximum of 89.5 % at 1.1 V_{RHE}, but only limited concentrations of glucaric acid are obtained due to early deactivation of the Au electrode possibly caused by fouling by glucaric acid itself. This is established as the most likely cause for deactivation after discarding all potential other options including e.g., Au leaching, which is investigated by analyzing the reaction solution after operation.

In the final section of this work, a novel electrocatalyst is developed with a higher electroactive surface area, 39.5 cm² compared to the 0.702 cm² of the bulk electrode, and a gold loading of 9.3 %, to be feasible for larger scale applications. To this aim, an Au-based catalyst consisting of Au nanoparticles deposited over a porous activated carbon is synthesized using a straightforward chemical impregnation method. The final material is characterized electrochemically and analyzed by various physical characterization techniques. Its electrocatalytic activity is determined by the EASA and tested for gluconic acid oxidation by electrolysis in batch and flow cell. While further optimization of the catalyst is needed for its effective application for glucose and gluconic acid electrooxidation, results suggest that this catalyst could have a potential use for a broad range of applications, including reactions of small gas molecules such as O₂, CO₂, CH₄ and N₂.

In conclusion, in this work, a promising electrocatalytic route for the selective oxidation of glucose to glucaric acid is developed and the electrochemical process explained. Much research is still needed to make this process possible at a large scale.

Overzicht

Koolhydraten zijn goedkope, hernieuwbare en beschikbare organische ruwe materialen. Slechts 3-5% van de koolhydraten worden industrieel gebruikt de rest verdwijnt en recycleert op natuurlijke wijze. Een van de belangrijkste, recente bevindingen in dit domein is de vaststelling dat aldonische en aldarische zuren en suikerzuren mogelijke toepassingen hebben in de fijnchemie. De groep van de carboxylicen is namelijk in staat om selectief te reageren met verschillende amines, alcohols en vinyl derivaten, om producten te vormen met nieuwe toepassingen zoals aldonolactonen die gebruikt worden in de bereiding van N-alkyl aldonamide oppervlakreactieve stoffen. De redenen voor het beperkt gebruik van koolhydraten als ruwe materialen in de fijnchemie zijn echter de overfunctionalizatie en ook hun slechte oplosbaarheid in de meest gangbare organische solventen. De uitdaging is om een directe en zone-selectieve oxidatie van saccharides? in een waterig milieu te bekomen. Dit is moeilijk met de klassieke chemische methodes zonder een preliminaire beschermingsstrategie. Electro-organische benaderingen fascineren momenteel academici en industriële onderzoekers wegens hun hoog potentieel voor industriële toepassingen. Electrocatalytische organische synthese is een krachtig instrument om de reactiesnelheid en selectiviteit te controleren door de elektrode potentiaal en de stroomsterkte. Verder voldoet electrosynthese op natuurlijke wijze aan de principes van Groene Chemie en dit ten gevolge van verschillende omgevingsvriendelijke kenmerken: verminderd energie verbruik, gebruik van hernieuwbare ruwe materialen, verminderde emissie van pollutanten en toxische ruwe materialen. Om deze reden is het gebruik van electrochemische organische synthese een veelbelovend alternatief voor de traditionele industriële methodes. Ondanks hun hernieuwbare karakter en hun potentieel om de industrie te elektrifiëren en zo de traditionele, niet-hernieuwbare productie processen van een breed gamma van basischemicaliën te vervangen, zijn electrochemische synthese methodes nog steeds sterk onderontwikkeld in vergelijking met de traditionele alternatieven. Er is bijkomend onderzoek nodig om de electrochemische processen beter te begrijpen en de belangrijkste uitdagingen aan te pakken die hun toepassing op industriële schaal in de weg staan, zoals de nog steeds onvoldoende selectiviteit en/of productiviteit, de beperkte levensduur van de elektroden en de onvoldoende know-how om op te schalen naar een industriële niveau.

Deze doctoraatsthesis is specifiek gericht naar de studie van electrocatalytische manieren voor de selectieve oxidatie van glucose naar gluconzuur en glucarinezuur (die beide commercieel relevante koolhydraten zijn). Om dit te bereiken is het essentieel dat men het exacte reactiemechanisme begrijpt. Het doel hier is dus om de factoren te onderzoeken die de selectiviteit bepalen van de reactie naar de twee producten van belang met inbegrip van de keuze van de katalysator en de reactie condities, en, alzo, het achterliggende reactie mechanisme te onthullen. Om dit te bereiken wordt een combinatie van electrochemische en analytische technieken gebruikt, waarbij microscopische oppervlakte analyse, gebruikt voor de morfologische karakterisatie, gekoppeld wordt aan haar electrocatalytische performantie. Dit werk start met het onderzoek naar de electrocatalytische activiteit van MnO_2 -gebaseerde katalysatoren voor glucose oxidatie, om het onderliggend mechanisme te begrijpen en de mogelijke toepassing voor de productie van gluconzuur en glucarinezuur. MnO_2 -films worden eerst gesynthetiseerd door elektrodepositie en chemische impregniatiemethoden op verschillende dragers en vervolgens getest in een batchcel op glucose-elektro-oxidatie bij verschillende reactieomstandigheden. MnO_2 -films worden eerst gesynthetiseerd door elektrodepositie en chemische impregniatiemethoden op verschillende dragers en vervolgens getest in een batchcel op glucose-elektro-oxidatie bij verschillende

reactieomstandigheden Elektrochemische evaluatie toont dat de katalysator met de grootste specifieke oppervlakte en de kleinste porositeit (gemiddelde poriegrootte 45 nm), de meeste electrocatalytische activiteit vertoont in de aanwezigheid van glucose ($\sim 10.5 \text{ mA cm}^{-2}$). Het levert echter niet de gewenste producten in significante hoeveelheden, zoals blijkt uit chromatografische analyse, en wordt daarom niet verder onderzocht. Vervolgens, wordt het mechanisme van drie edele metalen (Cu, Pt en Au) onderzocht voor glucose elektro-oxidatie onderzocht gebruikmakend van een roterende schijf-elektrode in een batchcel. Voor alle drie is er een sterk verband tussen de spanning en de reactiviteit van de functionele groepen in de glucose molecule. De Au elektrode vertoont de hoogste activiteit (2 tot 4 mA cm^{-2}) en selectiviteit voor glucon- (86,6 %) en glucarinezuur (13.5 %) bezit twee verschillende oxidatiepieken, één met een laag potentiaal ($0.55 V_{\text{RHE}}$) voor de oxidatie van de aldehydegroep op C1, de andere met een hoger potentiaal ($1.34 V_{\text{RHE}}$) voor de oxidatie van de hydroxymethylgroep op C6. Deze experimenten laten dus zien dat de reactie plaatsvindt in twee afzonderlijke stappen: eerst de oxidatie van glucose tot gluconzuur en daarna de verdere oxidatie tot glucarinezuur. Gezien zijn veelbelovende elektrochemische prestaties, wordt Au geselecteerd voor verdere studies.

In het tweede deel van dit werk, om het glucose-elektro-oxidatiemechanisme op Au te helpen ontrafelen, onderzoeken we systematisch de invloed van verschillende operationele parameters, d.w.z. pH, initiële substraatconcentratie, toegepast potentieel, reactietemperatuur en tijd, voor beide oxidatiestappen. Hiertoe worden langdurige elektrolyse-experimenten uitgevoerd in een batchcel onder verschillende reactiecondities, waarna de producten worden geanalyseerd met vloeistofchromatografie. De resultaten tonen aan dat in de eerste oxidatiestap (glucose naar gluconzuur) de maximale selectiviteit (97.6 %) wordt bereikt bij een matig hoge pH, lage temperatuur en lage initiële glucoseconcentratie, en voornamelijk beperkt is door de aanwezigheid van competitieve, base-gekatalyseerde, chemische reacties. Bij de tweede elektro-oxidatie (gluconzuur naar glucarinezuur) hebben deze parameters geen significante invloed op de selectiviteit, die een maximum van 89.5 % bereikt bij $1.1 V_{\text{RHE}}$, maar er worden slechts beperkte concentraties glucarinezuur verkregen vanwege de vroege deactivering van de Au-elektrode veroorzaakt door de blokkering van de actieve sites door onomkeerbare adsorptie van glucarinezuur zelf. Dit is vastgesteld als de meest waarschijnlijke oorzaak voor deactivering na het negeren van alle mogelijke andere opties, waaronder bijvoorbeeld Au-uitloging, wat wordt onderzocht door de reactieoplossing na gebruik te analyseren. In het laatste deel van dit werk wordt een nieuwe elektrokatalysator ontwikkeld met een veel hoger elektroactief oppervlak 39.5 cm^2 vergeleken met de 0.702 cm^2 van de bulkelektrode, en een goudlading van 9.3 %, om haalbaar te zijn voor toepassingen op grotere schaal. Voor dit doel wordt een op Au gebaseerde katalysator bestaande uit Au-nanodeeltjes afgezet op een poreuze actieve kool gesynthetiseerd met behulp van een eenvoudige chemische impregniatiemethode. Het uiteindelijke materiaal wordt elektrochemisch gekarakteriseerd en geanalyseerd met verschillende fysische karakteriseringstechnieken. De elektrokatalytische activiteit wordt bepaald door het EASA en getest op gluconzuuroxidatie door elektrolyse in batch- en flowcellen. Hoewel verdere optimalisatie van de katalysator nodig is voor een effectieve toepassing ervan voor elektro-oxidatie van glucose en gluconzuur, suggereren de resultaten dat deze katalysator potentieel kan worden gebruikt voor een breed scala aan toepassingen, waaronder reacties van kleine gasmoleculen zoals O_2 , CO_2 , CH_4 en N_2 . Concluderend wordt in dit werk een veelbelovende elektrokatalytische route voor de selectieve oxidatie van glucose tot glucarinezuur ontwikkeld en wordt het elektrochemische proces uitgelegd. Er is nog veel onderzoek nodig om dit proces op grote schaal mogelijk te maken.

List of abbreviations and symbols

AC	Activated Carbon
Ag/AgCl	Silver-silver chloride (reference electrode)
BET	Brunauer–Emmett–Teller
CV	Cyclic Voltammetry
EASA	Electrochemically Active Surface Area
EC	Electrochemical and Catalytic (mechanism)
ECE	Electrochemical Catalytic Electrochemical (mechanism)
EDL	Electrode double layer (capacitance)
EDX	Energy-Dispersive X-ray
FTIR	Fourier-transform infrared spectroscopy
GC	Gas Chromatography
GC	Glassy Carbon
GHG	Greenhouse Gas
HAADF-STEM	High-angle annular dark-field scanning transmission electron microscopy
HPLC	High Performance Liquid Chromatography
ICP-MS	Inductively Coupled Plasma-Mass Spectrometry
LC	Liquid Chromatography
M	Molar
nm	Nanometer
NP	Nanoparticle
ORR	Oxygen Reduction Reaction
PDA	Photo diode array (detector/spectrum)
PhD	Doctor of Philosophy
PZC	Point of zero charge
RDE	Rotating Disk Electrode
RHE	Reversible Hydrogen Electrode
SEM	Scanning Electron Microscopy
SI	Supporting Information
TEMPO	2,2,6,6-tetramethyl-1-piperidiny1 free radical
XRD	X-ray Diffraction
3D	Three dimensional
μm	Micrometer

List of Publications and Conference Presentations

Publications

G. Moggia, T. Kenis, N. Daems, T. Breugelmans, Electrochemical Oxidation of D-Glucose in Alkaline Medium: Impact of Oxidation Potential and Chemical Side Reactions on the Selectivity to D-Gluconic and D-Glucaric Acid. **ChemElectroChem**, vol. 7 (2020) issue 1, pages 86-95. Impact Factor: 4.782, citations: 50. <https://doi.org/10.1002/celec.201901592>

G. Moggia, T. Kenis, N. Daems, T. Breugelmans, Electrochemical Oxidation of D-Glucose in Alkaline Medium: Impact of Oxidation Potential and Chemical Side Reactions on the Selectivity to D-Gluconic and D-Glucaric Acid. **ChemElectroChem**, vol. 7 (2020) issue 1, pages 2-2, Cover Feature. Impact Factor: 4.782, citations: 1. <https://doi.org/10.1002/celec.201901960>

G. Moggia, J. Schalck, N. Daems, T. Breugelmans, Two-steps synthesis of D-glucaric acid via D-gluconic acid by electrocatalytic oxidation of D-glucose on gold electrode: Influence of operational parameters. **Electrochimica Acta**, vol. 374 (2021) special issue: "Electrochemistry towards Excellence (ISE 2020)", article number: 137852. Impact Factor: 7.336, citations: 23. <https://doi.org/10.1016/j.electacta.2021.137852>

G. Moggia, S. Hoekx, N. Daems, S. Bals, T. Breugelmans, Synthesis and Characterization of a Highly Electroactive Composite based on Au Nanoparticles Supported on Nanoporous Activated Carbon for Electrocatalysis. **ChemElectroChem** vol. 10 (2023) issue 21, pages n/a. Impact Factor: 4.782, citations: 1. <https://doi.org/10.1002/celec.202300293>

International Conference Presentations

G. Moggia, T. Kenis, N. Daems, T. Breugelmans, "On the impact of the oxidation potential on the conversion of D-glucose to D-glucaric acid in alkaline medium", International Society of Electrochemistry (ISE) Conference GEI 2019 Giornate dell'elettrochimica italiana, Padua, Italy, 8-12 September 2019, (*oral*).

G. Moggia, J. Schalck, N. Daems, T. Breugelmans, "Two steps synthesis of D-glucaric acid by electrocatalytic oxidation of D-glucose on a gold electrode: influence of operational parameters", 71st Annual ISE Meeting 2020 - Belgrade Online, 31 August-4 September 2020, (*oral*).

Table of Contents

Declaration.....	i
Ringraziamenti.....	ii
Acknowledgments.....	iii
Summary.....	iv
Overzicht.....	vi
List of abbreviations and symbols.....	viii
List of Publications and Conference Presentations.....	ix
Table of Contents.....	x
Chapter 1.....	1
Introduction and scope of the thesis.....	1
1.1 Climate change.....	2
1.2 Electrochemistry as green alternative to traditional processes.....	3
1.3 Biomass as feedstock for production of value-added products.....	5
1.4 Glucaric acid: a glucose derivative.....	6
1.4.1 Applications.....	6
1.4.2 Current synthesis methods.....	8
1.4.2.1 Nitric acid oxidation.....	8
1.4.2.2 Catalytic oxidation.....	8
1.4.3 Electrochemical methods.....	12
Homogeneous electrocatalysis.....	12
Heterogeneous electrocatalysis.....	13
1.5 Scope and strategy.....	14
1.6 Thesis outline.....	16
Chapter 2.....	17
MnO ₂ electrocatalysts for glucose electrooxidation.....	17
2.1 Introduction.....	18
2.2 Experimental.....	18
2.2.1 Chemicals and reagents.....	18
2.2.2 Preparation and physical characterization of MnO ₂ catalysts.....	19
2.2.3 Electrochemical characterization of the catalysts.....	19
2.2.4 Long-term electrolysis.....	20

2.3	Results and discussion	20
2.3.1	MnO ₂ layer deposition and impact of morphology on the electrode surface area	20
2.3.1.1	Anodic deposition of MnO ₂ over Pt, Au and GC electrodes	22
2.3.1.2	Cathodic deposition of MnO ₂ over a Pt electrode	24
2.3.1.3	Chemical deposition of MnO ₂ over a Ti electrode	26
2.3.2	Electrochemical characterization in a batch cell.....	27
2.3.3	Long-term electrolysis	29
2.4	Conclusions.....	31
2.5	Supporting information.....	32
Chapter 3		37
Role of oxidation potential and chemical side-reactions on the selectivity to D-gluconic and D-glucaric acid.....		37
3.1	Introduction.....	38
3.2	Experimental	38
3.2.1	Chemicals and reagents.....	38
3.2.2	Electrochemical setup	38
3.2.3	Product Analysis	39
3.3	Results and discussion	40
3.3.1	Oxidation of D-glucose at copper, platinum and gold electrodes	40
3.3.2	Voltammetry study on glucose derivatives	43
3.3.3	Long-term electrolysis	47
3.4	Conclusions.....	50
3.5	Supporting information.....	51
Chapter 4		53
Two-steps synthesis of D-glucaric acid via D-gluconic acid on gold electrode: influence of operational parameters		53
4.1	Introduction.....	54
4.2	Experimental	54
4.2.1	Chemicals and reagents.....	54
4.2.2	Electrochemical setup	54
4.2.3	Reaction procedure	55
4.2.4	Catalyst stability.....	57
4.3	Results and discussion	57
4.3.1	The oxidation of glucose to gluconic acid: impact of the operational parameters	58

pH	58
D-glucose initial concentration	60
Reaction temperature	62
Oxidation potential and reaction time	64
4.3.2 The oxidation of gluconic acid to glucaric acid: impact of the operational parameters	66
4.3.3 The two steps in cascade	68
4.3.4 Catalyst stability	69
4.4 Conclusions	71
4.5 Supporting information	72
Chapter 5	81
Synthesis, Characterization of a Highly Electroactive Composite based on Au Nanoparticles Supported on Nanoporous Activated Carbon for Electrocatalysis	81
5.1 Introduction	82
5.2 Experimental	82
5.2.1 Chemicals and reagents	82
5.2.2 Preparation of AuNPs supported on activated carbon	82
5.2.3 Physical characterization of the Au/AC catalyst	83
5.2.4 Electrochemical setups	84
5.2.5 Electroactive surface area measurement	86
5.3 Results and discussion	86
5.3.1 Physical characterization of the catalyst	87
5.3.2 Catalytic activity testing	91
5.4 Conclusions	95
5.5 Supporting information	96
Chapter 6	101
Conclusions and future perspectives	101
6.1 Conclusion	102
6.1.1 Electrocatalysts for glucose oxidation to gluconic and glucaric acid	102
6.1.2 Investigation of the influence of the reaction parameters	103
6.1.3 Synthesis of gold nanoparticles	104
6.2 Future perspectives	104
6.2.1 Mesoporous carbon supports and gold direct deposition	104
6.2.2 Bi-metallic catalysts and promoters	105

6.2.3 Optimization of the AuNP@AC catalyst and application for NRR	105
List of Figures.....	107
List of Tables	111
Bibliography	112

Chapter 1

Introduction and scope of the thesis

1.1 Climate change

Research on future scenarios predict climate change will have a dramatic effect on natural environments, plants and animals, leading to acceleration in biodiversity loss in some areas. The impacts will have knock-on effects for many communities and sectors that depend on natural resources, including agriculture, fisheries, energy, tourism and water [1]. Nowadays the main environmental challenges include: the problem of disposal of the ever-growing amount of wastes produced by human activity (e.g. industrial, civil, agricultural), the emission of CO₂ which accumulates into the atmosphere causing Global warming and the depletion of natural resources (water depletion, deforestation, mining for fossil fuels, soil erosion, etc...) [2]. To overcome these challenges, the European Union has set targets with the ambition to achieve: net zero emissions of greenhouse gases by 2050, economic growth decoupled from resource use, reducing inequalities (European Green Deal) [3]. This set of proposals aim to make the EU's climate, energy, transport and taxation policies fit for reducing net greenhouse gas emissions by at least 55% by 2030, compared to 1990 levels.

The main strategy that has been identified to overcome this challenge is the **electrification of the economy and the better and larger exploitation of renewable energy**, which is expected to lead to a third industrial revolution [4]. Specifically, the energy sector is expected to rely 40% more on renewable energy by 2030.

Electrification means switching away from fossil fuels towards the use of clean and renewable electricity as the main source of energy for all our applications in society (Fig. 1.1): for transport, heating and cooling of buildings, but also in Industry. First and foremost, transport, which has to be made more sustainable, with a **drastic reduction of the CO₂ emissions of vehicles**: 55% reduction of emissions from cars by 2030, 0% emissions from new cars by 2035 (with electric vehicles). Also, the use of renewable energy in heating and cooling in the buildings, expected to achieve +1.1 % each year, until 2030.

In this context, industry (especially the chemical branch) is one of the most difficult sectors to decarbonize through electrification [5] because it involves huge capital investments and know-how to switch from combustion-based technologies to electricity. Nevertheless, economically competitive electrified industrial processes coupled with zero-carbon electricity sources can sharply reduce greenhouse gas emissions (GHG) compared to manufacturing processes that rely on fossil fuels as they are sustainable and environmentally benign in nature.

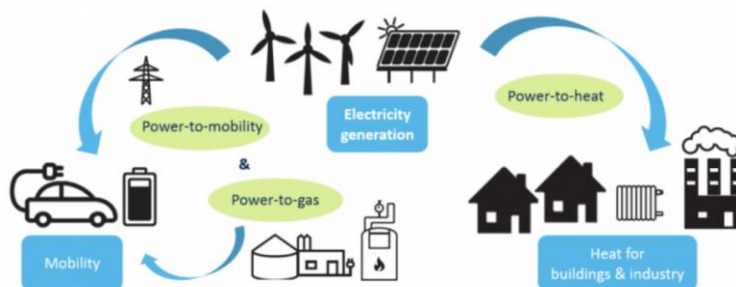


Figure 1.1. Electricity as the main source of energy for all our applications in society [6, 7].

On top of this, another objective of the European Green deal is, to restore Europe's forests, soils, wetlands and peatlands, as such increasing absorption of CO₂ and make the environment more resilient to climate change (natural carbon removal: -268 Mt current vs. -310 Mt future). This also includes reducing the consumption of natural supplies by finding alternative sources like waste materials and biomass, fitting in the concept of a circular economy (Fig 1.2).

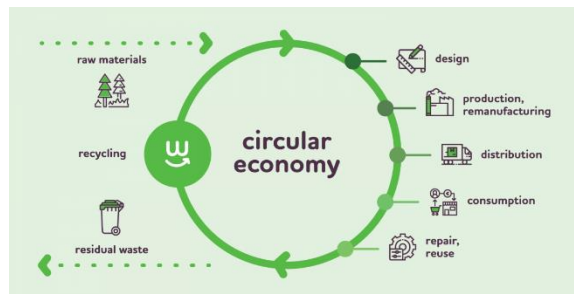


Figure 1.2. Schematic representation of a circular economy [8].

1.2 Electrochemistry as green alternative to traditional processes

Green chemistry has been defined as the utilization of a series of principles that reduce or eliminate the use or generation of dangerous substances during the design, fabrication, or application of chemical products [9, 10]. The Green chemistry's 12 principles are [11]:

1. Prevent waste: Design chemical syntheses to prevent waste. Leave no waste to treat or clean up.
2. Maximize atom economy: Design syntheses so that the final product contains the maximum proportion of the starting materials. Waste few or no atoms.
3. Design less hazardous chemical syntheses: Design syntheses to use and generate substances with little or no toxicity to either humans or the environment.
4. Design safer chemicals and products: Design chemical products that are fully effective yet have little or no toxicity.
5. Use safer solvents and reaction conditions: Avoid using solvents, separation agents, or other auxiliary chemicals. If you must use these chemicals, use safer ones.
6. Increase energy efficiency: Run chemical reactions at room temperature and pressure whenever possible.
7. Use renewable feedstocks: Use starting materials (also known as feedstocks) that are renewable rather than depletable. The source of renewable feedstocks is often agricultural products or the wastes of other processes; the source of depletable feedstocks is often fossil fuels (petroleum, natural gas, or coal) or mining operations.
8. Avoid chemical derivatives: Avoid using blocking or protecting groups or any temporary modifications if possible. Derivatives use additional reagents and generate waste.
9. Use catalysts, not stoichiometric reagents: Minimize waste by using catalytic reactions. Catalysts are effective in small amounts and can carry out a single reaction many times. They are preferable to stoichiometric reagents, which are used in excess and carry out a reaction only once.
10. Design chemicals and products to degrade after use: Design chemical products to break down to innocuous substances after use so that they do not accumulate in the environment.
11. Analyze in real time to prevent pollution: Include in-process, real-time monitoring and control during syntheses to minimize or eliminate the formation of byproducts.

12. Minimize the potential for accidents: Design chemicals and their physical forms (solid, liquid, or gas) to minimize the potential for chemical accidents including explosions, fires, and releases to the environment.

Electrochemistry is naturally suited to obey to most of these principles. There are several environmentally favorable features of electrochemical transformations including [12–14] (a) electrons are intrinsically clean reagents; (b) most of the reactions may take place in mild conditions, which reduces energy consumption, the risk of corrosion, material failure, and the cost associated to temperature controls; (c) reactions may occur in low or null volatility solvents, and this reduces accidental solvent releases to the atmosphere; (d) electrodes are used as heterogeneous catalysts, which are easy to separate from the products; (e) controllability: the selectivity can be controlled by adjusting the operating voltage or current density; (f) when the heterogeneous electron-transfer is naturally slow, electrochemically active mediator species may help and later be electrochemically recovered; (g) flexibility: it can be used to treat neutral, positive, or negatively charged species and induce the production of precipitates or gaseous species by pH changes or charge neutralization; it can deal with solids, liquids or gases and with inorganic, organic or biochemical substances; (h) cost-effectiveness, since the required equipment and operations are normally simple and, if properly designed, they can also be made less expensive than other techniques.

For all these reasons, the use of electrochemical organic synthesis represents a promising alternative to the traditional industrial methods (e.g., heterogeneous and homogeneous catalysis), as well as with emerging methods (e.g., enzymatic catalysis, photocatalysis) [12]. While all these synthesis methods require application of energy to accomplish the transformation of raw materials, the electrochemical synthesis specifically involves application of a potential, in the presence of active electrode surfaces, and the resulting flow of current drives the oxidation or reduction and subsequent recombination of reactants. Some examples of electroorganic syntheses that use renewable raw materials, improve atom efficiency, use less toxic raw materials, or decrease emissions compared to their conventional alternatives are: electrochemical reduction of CO₂ to methanol, synthesis of organic carbamates via O₂⁻ and CO₂, electrochemical activation to replace chlorine. These processes are still in development, as further research is needed to enable replacement of current ones.

While some industrial firms such as BASF are well known for commercial utilization of electrochemical synthesis, it is not widely practiced in industry [12]. The potential for green synthesis is real, but there are still several remaining hurdles to overcome. Electrochemical processes do not scale up in the same manner as traditional petrochemical processes, primarily because of the mass transfer limitations associated with bulk electrodes, making this a big challenge for future research. Coating, corrosion, and deactivation of electrodes are other frequent problems, limiting the lifetime of typical electrolyzers and thus their economic potential. Additionally, selectivity and productivity of said processes still need to be further improved before they can compete with traditional processes. Nevertheless, given its sustainable nature and promising advances in the recent past, they still have great potential to electrify the industry of fine chemicals in the future. However, at the moment, it is not possible to justify replacement of existing processes (i.e. Fisher-Tropsch) based on marginal or uncertain improvements in new technology [12]. For these and other reasons, electrochemistry is currently only being adopted for

small-scale syntheses of pharmaceuticals and other high-value, low-volume specialty products [12, 15].

1.3 Biomass as feedstock for production of value-added products

Green chemistry [16] encompasses utilization of renewable feedstocks. The production of chemicals has to reduce its dependence on petroleum-based feedstocks, and encourage, instead, the use of waste biomass (estimated at up to 138 million tons per year in the European Union alone [17]), fitting with the concept of circular economy. The production of value added chemicals from biomass represents a key opportunity for the chemical industry [18].

Biomass is renewable organic material that comes from plants and animals. Biomass sources include [6]: wood and wood processing wastes, black liquor from pulp and paper mills; agricultural crops and waste materials (i.e. corn, soybeans, algae, food processing residues); biogenic materials in municipal solid waste (i.e. paper, cotton, wool and food wastes); animal manure and human sewage (Fig. 1.3).

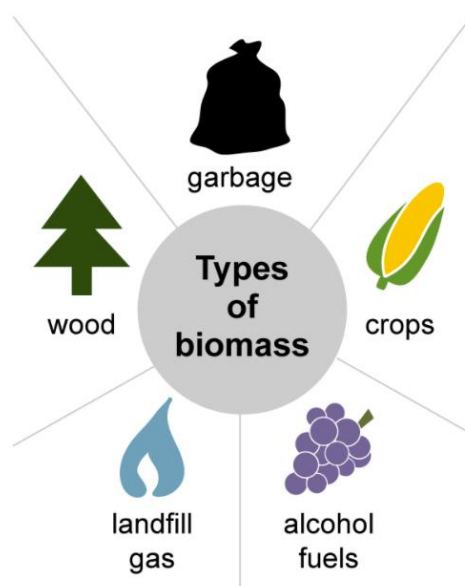


Figure 1.3. Types of Biomass (adapted from [6])

In addition to generating electricity and fuels, biomass can be used to create valuable chemicals and materials, known as “bioproducts” [19]. Bio-based chemicals and materials can serve as renewable alternatives to many of the products derived from petroleum or natural gas, such as plastics, fertilizers, lubricants, and industrial chemicals. Manufacturing bioproducts from biomass involves a variety of industrial techniques where biomass is first broken down into relatively stable chemical building blocks, which are then converted into a wide range of marketable products using a combination of biological, thermal, and chemical processes [19]. A key component in developing a diverse, robust, and resilient bioeconomy is the establishment of integrated biorefineries, where biomass is converted into chemicals alongside biofuels and power. As refineries, biorefineries can provide multiple chemicals by fractionating the initial raw material, biomass, into multiple intermediates (carbohydrates, proteins, triglycerides) that can be further converted into value-added products [20].

Carbohydrates constitute the major part of the total biomass, e.g. 75% of the dry weight of herbaceous and woody biomass are carbohydrates [21]. However, despite the low costs and easy access, only 3-5% of carbohydrates have industrial use, with the great majority remaining unused [22]. This has consequently led to an increase of the research efforts focused on harvesting the potential use of carbohydrates derived from lignocellulosic biomass residues resulting from the forestry and agricultural activities [22, 23]. Among various carbohydrates, cellulose and glucose are of particular interest in green chemistry since they can be used to generate a wide range of valuable compounds. Cellulose is a polysaccharide consisting of a linear chain of D-glucose units and constitutes 45% of the total annual production of biomass [23]; glucose is the monosaccharide obtained by depolymerization of said cellulose.

1.4 Glucaric acid: a glucose derivative

Glucaric acid (Fig. 1.4), molecular formula $C_6H_{10}O_8$, also known as glucarate or D-saccharic acid, is an acid derivative of glucose belonging to the aldaric acid family, i.e., both the aldehyde group in C1 and the hydroxymethyl group in C6 are fully oxidized to carboxylic groups. Glucaric acid exists in all living organisms [24].

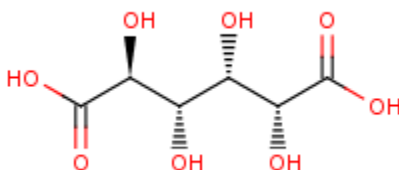


Figure 1.4. Chemical structure depiction of D-glucaric acid, the D-enantiomer of glucaric acid (adapted from [25]).

1.4.1 Applications

In 2004, the US Department of Energy has classified glucaric acid as one of the 12 “Top Value Added Chemical from Biomass” [26] because of its extensive commercial potential. According to a market report by Grand View Research, Inc. its global market size was estimated at USD 550.4 million in 2016 and is expected to reach USD 1.3 billion by 2025 [27]. In fact, thanks to its high functionalization, glucaric acid, and its derivatives (Fig. 1.5), constitute building blocks for the production of a variety of commodity products (Fig. 1.6) i.e. detergents [28], polymers [29–32], including methacrylates [30], hydroxylated nylons [31] and other ester/amide polymers [32]. It is also used as food additive, due to its health benefits as a dietary supplement claimed to help maintain healthy cholesterol levels [33] and prevent cancer [34–36], in construction as cement and concrete additives [37], thanks to its corrosion inhibition properties [38, 39], and as retarding agent for metallic mordants in the dyeing of textiles [40]. Of particular interest is the use of glucaric acid in the manufacture of detergents. In fact, recent disincentive policies have been adopted in the EU and US to ban the use of phosphates in detergents, as they are responsible for a decrease in water quality [41–44]. Glucaric acid represents the ideal candidate to replace phosphates due to its chelating properties in sequestering cations [45–47].

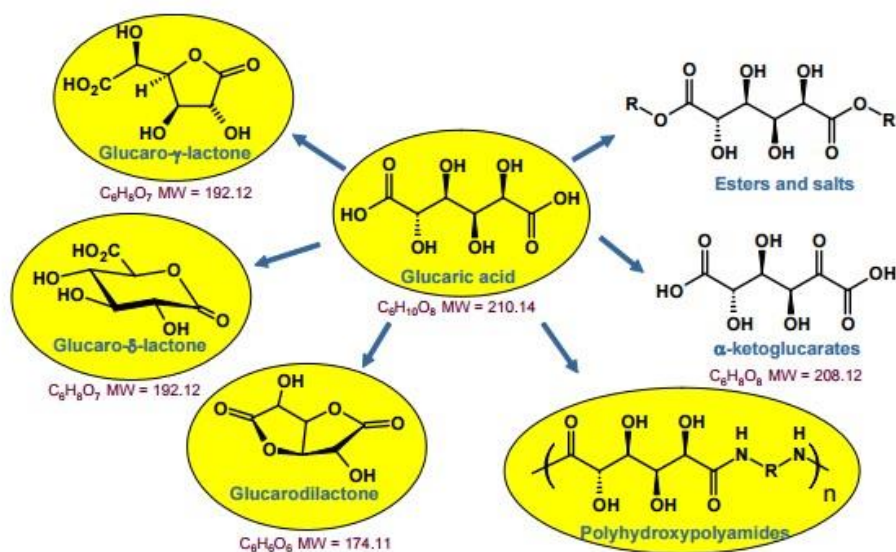


Figure 1.5. Derivatives of Glucaric acid (adapted from [26]).

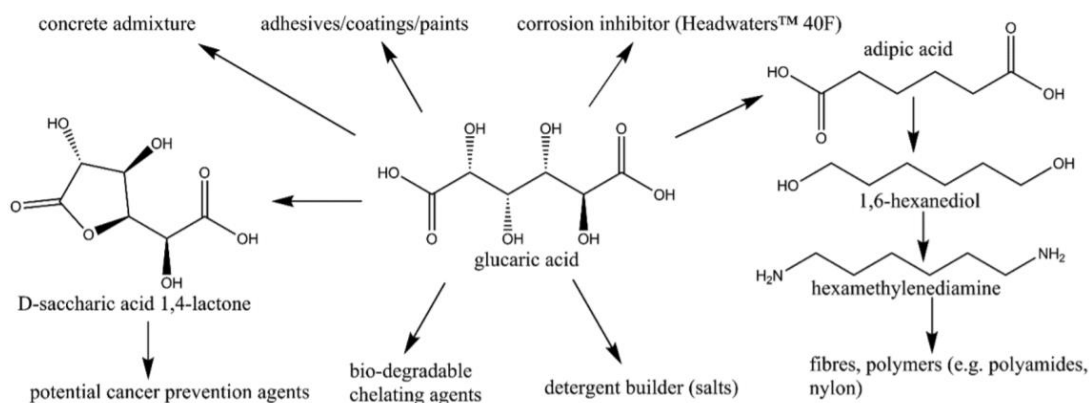


Figure 1.6. Scheme of the variety of applications of glucaric acid in different sectors (adapted from [18]).

Probably the most relevant application of glucaric acid is its use as precursor for the production of bio-derived adipic acid [48, 49], which represents a more sustainable alternative to fossil-fuel derived adipic acid. Most of the adipic acid produced is employed in the nylon industry, a lower amount in the production of plasticizers and polyurethanes, but it is also used in other areas, including the food and pharmaceutical industries [50]. The total amount of adipic acid produced worldwide per year is nearly 3 million tons, with a market value of almost USD 6 billion, growing at a compound annual growth rate of 3–5% [50].

To conclude, the production of bio-based glucaric acid represents a multi-billion dollar market, but the current supply of glucaric acid is very limited and not sufficient for such a large market [18]. In addition, current technologies are either highly inefficient or highly polluting. For instance, the industrial route of choice utilizes nitric acid as an oxidant causing the release of harmful N_2O gases. Thus, in order to further exploit the use of glucaric acid a new, environmentally friendly production technology is currently being sought after [26].

1.4.2 Current synthesis methods

1.4.2.1 Nitric acid oxidation

The preparation of D-glucaric acid from glucose has been first reported by the authors Sohst and Tollens in 1888 [51], who isolated it as monopotassium D-glucarate using nitric acid as oxidant [52]. In what followed, a method was developed [40, 53] and carried out on a larger scale (a pilot plant) in 1954, with the production of 43% yield of 98 to 99% pure potassium acid saccharate [54], but it was never commercialized [52]. Despite it being poorly selective, due to the competing side-reactions, and despite its unsustainable nature (it leads to the formation of 85 kg of waste nitric acid (toxic) per 100 kg of glucaric acid produced [18]), the oxidation of glucose with nitric acid (Fig. 1.7) still remains an attractive method for commercialization because of its simplicity since HNO_3 serves as both the solvent and the oxidizing agent [55].

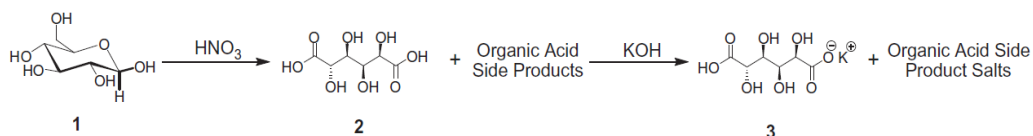


Figure 1.7. Nitric acid oxidation of D-glucose (1) to D-glucaric acid (2) isolated as monopotassium D-glucarate (3) (adapted from [52]).

In an attempt to lower the consumption of nitric acid, this technology has been modified in 2010 by conducting the reaction under an atmosphere of oxygen in a closed reaction flask in order to effect a catalytic oxidation process using oxygen as the terminal oxidant, fostering regeneration of spent nitric acid and lowering the required amount [52]. Despite the better control over the highly exothermic reaction, allowing the oxidation to occur at relatively low temperatures (25–30 °C), the modification did not increase the selectivity of the process, which remained very low, leading to modest yields of glucaric acid (ca. 40–45 %). Besides, expensive separation units were required for the removal of nitric acid from the product solution, including nanofiltration and diffusion dialysis [52]. Despite these limitations, Rivertop Renewables, a Montana-based specialty chemicals company, in collaboration with DTI, a custom manufacturer of fine and specialty chemical products based in Danville, Virginia, started a first commercial plant using the recycling technology claiming to be able to produce 10 million dry pounds of sodium glucarate product per year [56]. Nevertheless, the scarce selectivity and limited yield, together with the high risks and cost, make this technology extremely unsustainable, thus, for the last fifty years, there has been an intensive research effort to find alternative production methods that avoid the release of N_2O , associated with nitric acid oxidation [18]. This resulted in the study of several other greener and more sustainable oxidation methods including catalytic, electrocatalytic and microbiological routes. These technologies will be highlighted in the following sections.

1.4.2.2 Catalytic oxidation

Given the disadvantages of the direct oxidation of glucose (*vide supra*) and in order to develop a Green Chemistry process, first, the use of such toxic and dangerous substances must be abolished [57] and second, methods for regioselective, controlled oxidation of glucose are required. The use of a catalyst represents a potential solution to this problem [58], which is the reason of the extensive

research, over the last decade, on catalyst-controlled methods for the regioselective oxidation of glucose. The catalytic oxidation is carried out using a non-toxic oxidizing agent, a catalyst (homogeneous or heterogeneous) and, sometimes, a co-catalyst.

Homogeneous catalysis

A water soluble oxidation catalyst, 2,2,6,6-tetramethyl-1-piperidinyloxy free radical (TEMPO), was first applied by the authors Thaburet et al. for the oxidation of various maltodextrines and glucose [59]. The reactive intermediate in the oxidation with TEMPO is the oxoammonium salt which is generated in situ under phase-transfer conditions employing an appropriate co-oxidant (or terminal oxidant), generally sodium hypochlorite (NaOCl, bleach) in aqueous phase [60]. Thaburet et al. employed the system NaOCl-NaBr-2,2,6,6-tetramethylpiperidine-1-oxyl (TEMPO) under strongly basic conditions ($\text{pH} > 11.5$) and at 5°C , to avoid the rapid increase of temperature due to the exothermicity of the reaction, and obtained D-glucaric acid in a yield of 90% (isolated as sodium glucarate) [59]. In this study the authors evidence that the oxidation of glucose with the TEMPO-NaOCl-NaBr system is selective only at high pH (11.5-12), while at lower pH the oxidation mainly leads to degradation products like sodium tartrate, oxalate and carbonate, formed by oxidative diol cleavage [59, 61]. In a following study, the authors perform the oxidation of glucose using 4-acetamido-TEMPO, the acetamido derivative of TEMPO, which is more stable and less volatile than TEMPO and is also commercially available [62]. This time the catalyst is used in combination with two different oxidants, sodium hypochlorite (bleach) and potassium hypochlorite, and sodium or potassium bromide as co-catalysts. The catalytic cycles are shown in Fig. 1.8.

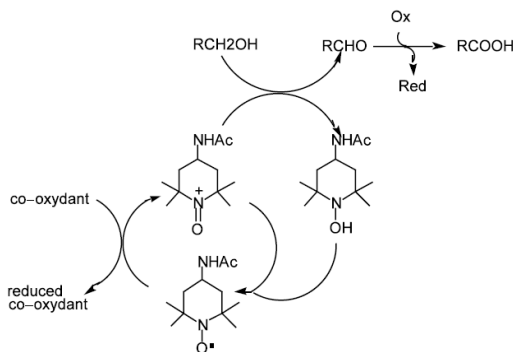


Figure 1.8. Redox system for TEMPO-like nitroxide mediated oxidations [62].

It was found that the use of 4-acetamido-TEMPO instead of TEMPO as catalyst allows more freedom for the reaction conditions because of its greater stability and much lower volatility and reduces the price [62]. More than 85% yield of glucaric acid, isolated as the monopotassium salt, was obtained at pH values between 11.4 and 11.6 and at temperatures between 0 and 5°C .

Hypohalites, like sodium hypochlorite (NaOCl), appeared to be essential as they act as terminal oxidants in the oxidation of glucose to glucaric acid with 4-acetyl-amino-2,2,6,6-tetramethyl-1-piperidinyloxy (4-AcNH-TEMPO). Halogens dissolved in aqueous solutions at high pH disproportionate to generate hypohalites and halogenides [63, 64]. In order to gain mechanistic insights of the overall reaction, Merbouh et al. investigated the use of elemental chlorine or bromine or chlorine gas as the terminal oxidant in the oxidation of D-glucose catalyzed by a

nitroxide/bromide catalysts/co-catalyst system at high pH [64]. They report a 70% yield of monopotassium gluconate obtained with the bromine oxidation method [64], which was found to be best suited for the synthesis at lab scale. On the other hand, the chlorine oxidation method is reported to be more suitable for commercial development, because of the use of an economical oxidant in aqueous solution and a readily available catalysts/co-catalysts system, [64]. In this case, a yield of disodium gluconate of 85% for a conversion of glucose > 97% was obtained when using Cl₂ gas bubbled into the reaction solution as terminal oxidant [64].

In all cases, the resulting product was separated from the reaction solution by precipitating the corresponding salt after addition of concentrated aqueous HCl, to reach a final pH of ~8 [64].

Using GC and NMR, the authors Ibert et al. developed a fast method for the determination of the short-chain carboxylic acids produced by the nitroxide-mediated oxidation of glucose to gluconic acid using bleach as terminal oxidant and proposed a reaction pathway [61]. They discovered that, while the oxidation of glucose to gluconic acid is fast and leads to the formation of few side products [64], the N-oxide oxidation of the primary alcohol of the gluconate to carboxylate is much slower and accompanied by extensive over-oxidation [61]. In fact, it was found that the oxoammonium salt, as well as the terminal oxidant, are capable of over-oxidizing gluconic acid, which is the reason why low concentrations of oxidants led to higher selectivities [61]. Fig. 1.9 shows the degradation products generated when gluconic acid is exposed to the oxidation conditions, rationalized by the following steps: C3-C4 cleavage forms tartronic acid, C2-C3 cleavage produces meso-tartaric acid and C4-C5 produces L-tartaric acid. The low selectivity to gluconic acid obtained with this process is due to an uncontrolled reaction leading to over-oxidation, which, of course, makes it economically unfeasible.

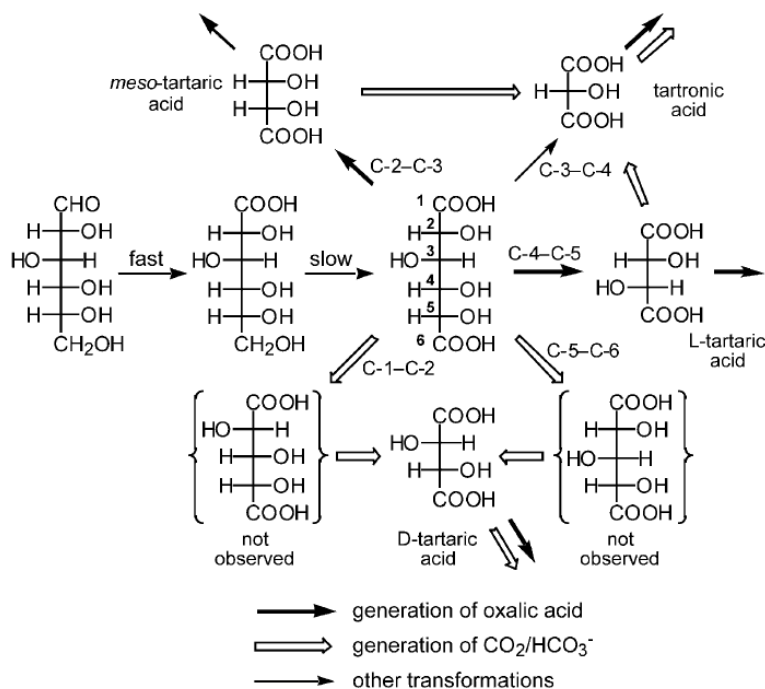


Figure 1.9. Proposed genealogy of the degradation products observed in the nitroxide-mediated oxidation of D-glucose to D-gluconic acid [61].

The remaining concerns of this oxidation method regard mainly the separation and recovery of TEMPO, which is a homogeneous catalyst and, as such, it remains dissolved into the reaction mixture. To address this problem, the authors Merbouh et al. mention, in their work, the possibility of using solid phase-bound nitroxide catalysts, that can be separated by simple filtration [64]. Although, to date, no study has been ever reported on the use of such immobilized TEMPO systems, for glucose oxidation to glucaric acid. Moreover, the use of toxic and polluting oxidizing agents as chlorine and bleach, make this method unsustainable from a safety and environmental point of view.

Heterogeneous catalysis

In the last decades, there has been a growing interest in finding an efficient catalytic system for glucose oxidation that responded better to the sustainability requirements: 1) the catalyst being in a solid phase (heterogeneous catalyst), to allow an easy separation and recovery after reaction; 2) the use of non-toxic and highly abundant oxidants. Motivated by these reasons, catalytic aerobic oxidation using noble metals as catalysts and O₂ from air as oxidant has been studied for many years, and has reached already promising results, so that it is currently considered, besides electrochemical oxidation, one of the best candidates to replace the unsustainable nitric acid oxidation.

The first mention of glucaric acid synthesis by means of heterogeneous catalysis has been reported by the authors Alexander and Mehlretter in a patent in 1949 [18, 65]. They employed a 10% Pt/C catalyst to oxidize dextrose with oxygen from air bubbled at atmospheric pressure inside a continuously stirred solution containing potassium bicarbonate, to keep the pH alkaline. They obtained 54% yield of potassium D-glucosaccharate in 12h at 50°C [65].

Afterwards, in 1971, Acres and Budd patented another heterogeneous catalytic process to produce both gluconic and glucaric acid using 1% Pd/ α -Al₂O₃ for gluconic and 3% Pt/C for glucaric acid [66]. The process was conducted in a continuous system, under basic conditions, using 1 M sodium bicarbonate for the first oxidation and 0.5 M sodium carbonate for the second [66]. They obtained 100 and 84.6% conversion of the substrate after, respectively, 6.25 and 3 h, at 50°C and 1500 mL/h oxygen [66].

In the next years, various catalysts based on transition metals on different supports have been developed for base-free aerobic oxidation of glucose to glucaric acid in water by Rennovia Inc., a specialty chemicals company based in Santa Clara (CA), focused on novel processes for the production of chemicals from renewable feedstocks [18, 67, 68]. In their first patent, from 2010, they used a commercial 1.5% Au/TiO₂ catalyst promoted by 1.5% Pt and obtained 55% yield of glucaric acid after 5 h at 100°C. Even before the patent's release, the high activity of noble metals like Au and Pt in the selective oxidation of glucose was well known in literature [69]. Indeed, to date, they are the most effective catalytic systems for this reaction and remain the most studied ones [70, 71]. In a second patent, the authors Murphy et al. obtained a yield of glucaric acid up to 71% at 100% conversion after 3 h reaction at 119°C using pressurized oxygen as oxidant [68]. This time they used an optimized catalyst made of AuPt nanoparticles between 8-12 nm deposited on TiO₂, with a composition 1:1 of Au and Pt and a loading of 4 wt. % of each metal [68]. In 2015, Rennovia started, in partnership with Johnson Matthey, a pilot plant for the conversion of glucose to glucaric acid using this technology. In this facility, the glucaric acid produced undergoes a second catalytic step that transforms it into adipic acid. Nowadays, the technology has been

licensed to a third company, Archer Daniels Midland Company, with the intent of commercialization.

Recently, Lee et al. reported 74% selectivity to glucaric acid at >99% glucose conversion obtained over a commercial Pt/C catalyst under base-free conditions, at 80°C and 13.8 bar oxygen pressure, over 10 h [72].

Since the best results that can be obtained with mono-metallic systems are not yet satisfactory, researchers moved their attention to bimetallic systems, as they typically result in improved performance in terms of activity and selectivity and improved stability (low metal leaching) [73, 74]. However, to date, this has not yet been achieved for the glucose oxidation (best selectivity obtained was 44% using PtPd on TiO₂ at 100% conversion after 72 h) [73]) leaving the process performance still unsatisfactory for commercialization.

In conclusion, catalytic oxidation, despite exceeding nitric acid oxidation, still relies on traditional driving forces: on heat, to reach the desired temperatures for the reactions (typically above 80°C) and high partial pressure of the oxidant, O₂. Moreover, it remains still difficult to control the reactions, thus leading to unsatisfactory selectivity.

1.4.3 Electrochemical methods

Electrochemical synthesis possesses have major benefits compared to traditional chemical synthesis [75]: 1) the driving force is electricity, which can be produced by renewable sources; 2) electrons are clean reagents as they do not generate any waste; 3) since reactions occur by a direct electron transfer at the electrode, the systems usually do not require any other activation, thus the conditions are mild resulting in high selectivities; 4) the atom economy is high compared with processes that use moderate- to high-molecular-weight reagents; 5) although the electrochemical cells are not simple, due to the extensive history of reactor design in this field, they are surprisingly inexpensive. One potential drawback of electrochemical synthesis is that, if the redox potential of the substrate is close to that of the solvent, then the process will waste significant amount of energy and will partially transform the solvent, which may generate waste.

Homogeneous electrocatalysis

Because of their great reactivity in mild conditions, 2,2,6,6-tetramethyl-1-piperidinyl free radical (TEMPO) and its derivatives has been extensively used as homogeneous mediators in alcohols' oxidation and, as a consequence have also been applied in the chemical oxidation of glucose (Section 1.4.2.2). Following the success of the method, the authors Ibert et al. decided to employ TEMPO in the electrooxidation of glucose in alkaline media in an attempt to target glucaric acid as main product [76]. Glassy carbon was used as working electrode, with as main function the electrocatalytic regeneration of TEMPO, thus eliminating the need of co-oxidants, as it was the case in the simple catalytic process (*vide supra*). The authors analyzed the impact of various parameters as the catalyst amount, the temperature and the pH on the current density by cyclic voltammetry measurements and demonstrated the central role of the pH in such transformation. Once the optimal parameters (0.0005 mol TEMPO at a temperature of 5 °C, a pH of 12.2 and applied current of 600 mA with 74% Faraday efficiency) were selected, they applied them to conduct the oxidation starting from a solution containing 0.1 mol of sodium D-gluconate, the sodium salt of D-gluconic acid, instead of glucose, having the hemiacetal function already oxidized. In these conditions they obtained a yield of D-glucaric acid of ca 85% after 20 h. In a

following study, the authors attempted a TEMPO-mediated electrochemical oxidation of glucose targeting glucaric acid, first in an undivided cell, which was unsuccessful due to the lack of control over the reaction parameters, then in a jacketed reactor which allowed control over the pH and temperature of the mixture [77]. In these conditions, they achieved full conversion of glucose (with 80% Faraday efficiency) but obtained a poor yield of glucaric acid with the formation of a large number of by-products (i.e., oxalic, tartaric and malonic acid). One of these by-products was a tricarboxylic acid whose structure was identified for the first time by the authors using a combination of NMR and GC analysis and which was named “maribersonic acid” (Fig. 1.10).

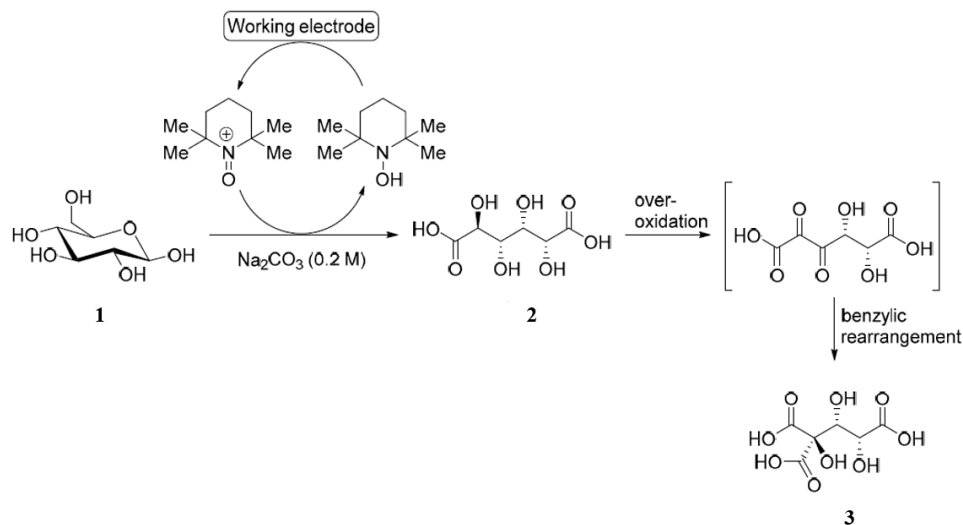


Figure 1.10. TEMPO-mediated electro-oxidation of D-glucose (1) to D-glucaric acid (2) and the tricarboxylic acid (3) (adapted from [78]).

Although the electrochemical regeneration of TEMPO eliminates the need of dangerous co-oxidants as chlorine and bleach, the separation and recovery of TEMPO, which is a homogeneous catalyst dissolved into the reaction mixture, remains an unsolved problem that translates into exceedingly high costs and difficulty of the downstream processing for industrial applications. Moreover, as for the oxidation of glucose to glucaric acid, the poor yield of glucaric acid and the low selectivity of the reaction make this technology still not sustainable for larger scale applications.

Heterogeneous electrocatalysis

The first work addressing the heterogeneous electrooxidation of glucose for the production of both, gluconic and glucaric acid, is that of Bin et al., who employed MnO₂ deposited on a tubular porous Ti support [79]. The authors adopted a reactor configuration that allowed them control over the flow rate during the electrolysis to avoid over-oxidation of the products. In contrast with literature, they did not note a strong dependence of glucose conversion on the pH: their conversion was always >90%, irrespective of the pH (from pH 2 to pH 10) [79] and the selectivity was at a maximum at neutral pH. Under the optimized conditions, they obtained a conversion of glucose of 93% after 19 min reaction time, with 42% yield of gluconic acid and 44% of glucaric acid, with a current density of 4 mA cm⁻² starting from an aqueous glucose solution of 50.5 mmol L⁻¹ [79]. To date, only two studies have reported relevant values of glucaric acid yield/selectivity at more industrially relevant current densities (i.e. 100 mA cm⁻² and above) by making use of more

complex catalytic systems [80, 81]. The first study, by Liu et al., reports a glucaric acid yield of 83% after 2 h obtained from glucose electrolysis on NiFeO_x and NiFeN_x catalytic systems [81]. The second, by Zhao et al., reports a glucaric acid selectivity of 97.9 % obtained by electrooxidation of sodium gluconate (the sodium salt of gluconic acid) over a Ni₃(BTC)₂/NiF bifunctional catalyst, at 100 % conversion of the substrate after 20 h [80]. In both cases, highly concentrated solutions of NaOH have been used as electrolyte, respectively, 1 [81] and 8 [80] M. Indeed, a major downside of these methods is the use of such large amounts of hydroxide salt (370 tons per 1000 tons of glucaric acid produced [57]) that requires specialized equipment for corrosion resistance. A summary of the most relevant literature studies on electrocatalytic production of glucaric acid and the resulting performances is reported in Table 1.1. From these studies it is clear that the electrochemical oxidation of glucose for the production of glucaric acid using heterogeneous catalysts, without addition of any mediator or oxidative agent, is not only possible but can be economically advantageous [81]. What is also clear is the major role of the catalytic system used in determining the overall process performance in terms of selectivity and yield, which still needs improvement.

Despite the growing interest shown recently, the production of glucaric acid by electrocatalytic oxidation of glucose still remains an undeveloped research topic, especially when compared to other electrocatalytic processes (i.e., CO₂ reduction and oxygen reduction reaction, ORR). Indeed, further efforts are required to develop new catalytic systems (or improving the old ones) which are efficient, long lasting and stable and whose fabrication requires simple materials and synthesis methods and are easily up-scalable. Most importantly, the process must operate in sustainable working conditions, producing the least amount of waste and avoiding expensive and energy-consuming downstream processing.

Table 1.1. Summary of the most relevant electrocatalytic systems investigated so far for glucaric acid production and resulting performance, reported as selectivity or yield (%).

Electrocatalyst	Reference	Substrate	Selectivity (%)	Yield (%)	Time
<i>TEMPO</i> (mediator)	Ibert et al. (2010) [76]	sodium D-gluconate	/	85	20 h
<i>MnO₂/Ti</i>	Bin et al. (2014) [79]	D-glucose	/	44	19 min
<i>NiFeO_x, NiFeN_x</i>	Liu et al. (2020) [81]	D-glucose	/	83	2 h
<i>Ni₃(BTC)₂/NiF</i>	Zhao et al. (2019) [80]	sodium gluconate	97.9	/	20 h

1.5 Scope and strategy

The ultimate scope of this PhD is to unravel new environmentally-friendly routes for the selective transformation of biomass-derived glucose into one of its most valuable derivatives, glucaric acid, which is a very high demand critical raw material used as starting substance in a variety of industrial processes.

The main goals are:

- (1) contributing to the decarbonization of the chemical industry effectively reducing its environmental footprint and GHG emissions by leveraging the exploitation of electricity from renewable sources to enable economically competitive electrified chemical processes,

thus contributing to the electrification and future competitiveness of the industry in accordance with the latest European policy directives;

(2) replacing traditional synthesis methods with electrochemical reactions which follow the principles of Green Chemistry, with a special attention to: waste reduction, by focusing on high selectivity; safer chemical processes based on water as a solvent; real-time monitoring and control of the reaction to minimize waste generation;

(3) enabling circular economy best practices by using second-life biomass-derived glucose instead of fossil fuels derivatives as feedstock;

(4) reducing the overall energy requirements, as the reaction requires mild conditions, and the electrodes used are heterogeneous catalysts, which are easy to separate from the products;

(5) contributing to the sustainable increase of the production capacity (within Europe) of a critical raw material, that plays a central role as a precursor in a variety of applications across a wide range of strategic industries, such as the production of nylon, plasticizers, polyurethanes, and pharmaceutical products, and its role as a food preservative.

While extensive research has been devoted to investigating different metal and metal oxide electrodes for their activity towards glucose electrooxidation, mainly for applications such as glucose sensors and fuel cells, only a few recent studies are dedicated to the analysis and optimization of the reaction products, with an emphasis on the electrosynthesis of gluconic and glucaric acid. This space is still very unexplored and much research effort is still needed to unravel the potential of an electro organic route to produce glucaric acid from glucose. In fact, to prove feasibility of such process for large-scale application, a very high selectivity, an optimal usage of the reagent, and low side-products formation must be achieved to avoid energy-demanding and expensive downstream separation processes. To this end, the selection and optimization of the electrocatalytic system and reaction conditions is critical and it will be the main goal of this Ph.D. thesis.

As a first step in this research, a suitable electrocatalyst has to be found for the electrochemical oxidation of glucose to the targeted product. Different types of electrocatalysts are investigated (1) manganese dioxide and (2) noble metals. Flat electrodes are tested for their electrocatalytic performance using a three-electrode electrochemical setup. The most suitable electrocatalyst is determined by the following set of electrochemical parameters: (1) electro-activity and (2) selectivity towards the target product. The physicochemical characterization is used to link the composition and structure of the electrocatalysts to their electrochemical performance with the aim to better understand their behavior and possibly further optimize them. Liquid chromatography techniques are used for the identification and quantification of the reaction products, to demonstrate the link between electrochemical parameters (i.e. applied potential and current), and the selectivity of the studied reaction.

In the second part, the optimal operational conditions need to be examined to maximize the selectivity towards the product of interest and minimize the occurrence of undesired side-reactions. The influence of reaction parameters such as pH, initial substrate concentration, reaction temperature and time, is investigated on the conversion and selectivity of the reaction using a combination of electrochemical and chromatography techniques.

The last part of this research work focuses on the optimization of the electrocatalyst morphology and EASA to improve its electrocatalytic activity while keeping limited usage of the expensive active phase. To this end, a catalyst made of nanoparticles deposited over a high specific surface carbon matrix is developed using a chemical synthesis method.

1.6 Thesis outline

This thesis describes the development of an electrosynthesis process for the conversion of glucose into valuable chemicals. The most suitable electrocatalyst material is identified and its morphology and performance optimised; the reaction parameters are analysed and optimised to maximise the selectivity.

In **Chapter 2 and 3**, the electrocatalytic activity of various catalysts for glucose electrooxidation and their selectivity towards the production of gluconic and glucaric acid is investigated. While in Chapter 2 the focus is on MnO₂-based catalysts, in Chapter 3 we studied the reactivity of three noble metals, copper, platinum and gold, as they all had shown electrocatalytic activity in presence of glucose. Amongst these, gold shows the best activity and selectivity to gluconic and glucaric acid. These first positive results motivated us to continue the investigations focusing on gold, with the intent to optimize selectivity and productivity of glucaric acid.

Chapter 4 builds on the results obtained on Chapter 3. In this chapter, we investigate the influence of and optimize different operational parameters, i.e., pH, initial substrate concentration, applied potential, reaction temperature and reaction time, for the efficient oxidation of glucose to gluconic acid and for the further oxidation of gluconic acid to glucaric acid.

In **Chapter 5**, a method to synthesize a Au-based catalyst with very high electroactive surface area and at the same time, low Au loading is developed and the resulting material is tested for gluconic acid electrooxidation. After describing the synthesis method, the AuNP/C composite is physically characterized and its electrocatalytic activity determined by calculation of the EASA. Finally, the as-developed system is tested for the desired reaction in batch and flow-reactors, to also see the impact of the flow conditions on the electroreactivity of the AuNP/C catalyst towards this reaction.

Conclusions and future developments are discussed in **Chapter 6**.

Chapter 2

MnO₂ electrocatalysts for glucose electrooxidation

2.1 Introduction

Gluconic acid and glucaric acid are two high value-added chemicals obtained from the oxidation of glucose [31, 82–85]. Currently, the main production method is still nitric acid oxidation, despite it being poorly selective and unsustainable [57]. Many other approaches have been investigated, including fermentation and catalytic oxidation [26, 58]. Recently, much attention has been paid to electrocatalytic methods because they allow a high degree of controllability over the reaction process, which results in selective reactions and fast kinetics [75]. In electrochemistry, an important role is played by the electrocatalyst as it has a big impact on the overall performance. For the glucose electrooxidation, the most studied catalytic systems are noble metals, since they showed high selectivity and good kinetics [86–91]. Nevertheless, their high-cost pushes scientists to find alternative, cheaper options, more suitable for industrial applications. In this respect, metal oxide electrodes are likely to be suitable for carbohydrate oxidation as they potentially speed up the carbohydrate adsorption through formation of hydrogen bonds with the oxide layer via their OH groups, as such facilitating the electron transfer [79, 81]. Amongst all metal oxides, MnO₂ is expected to be a promising electrocatalyst owing to the fact that it possesses a number of higher valent oxo-manganese species such as Mn(IV) and Mn(V), which are generally strong chemical oxidants [92–97]. This catalyst has attracted considerable attention due to its high energy density, low cost, natural abundance and environmentally friendly nature. Moreover, Bin *et al.* obtained a glucaric acid yield of 44% over MnO₂/Ti catalysts in a tubular flow reactor, which is of particular interest to us as this was the first study to specifically target glucaric acid as a glucose electrooxidation product [79]. Indeed, many previous works had investigated different metal and metal oxide electrodes for glucose electrooxidation, but without specific focus on the reaction products [98–102]. In their study, Bin *et al.* [79] not only analyze the reaction products, but they also propose a reactor configuration that, according to their findings, leads to the highest productivity of the two main products: gluconic and glucaric acid, albeit without unraveling the reaction mechanism. Our main purpose here was thus to understand the underlying mechanism and understand the potential application of MnO₂ for the production of glucaric acid. To this end, we synthesized MnO₂ catalysts by electrodeposition and chemical deposition methods on various supports and tested them in a batch cell for glucose electrooxidation at various reaction conditions. In order to identify and quantify the reaction products, we developed an analytical method using high performance liquid chromatography (HPLC) specifically tailored to complex mixtures of sugars and sugar-derivatives.

2.2 Experimental

2.2.1 Chemicals and reagents

The synthesis baths for the anodic deposition were prepared using Manganese (II) sulfate hydrate, MnSO₄ · xH₂O (Sigma-Aldrich, ≥ 99.99%), Sodium sulfate anhydrous, Na₂SO₄ (Sigma-Aldrich, Merck) and ultrapure water (Synergy UV system). The solutions for the cathodic deposition were prepared using Manganese (II) chloride, MnCl₂ (Sigma Aldrich, ≥ 99.99%) and NaCl (≥99.0% ACS, VWR Chemicals BDH®). The supporting electrolytes for the electrochemical tests in batch were prepared with ultrapure water (Synergy UV system), sodium carbonate (Sigma-Aldrich, 98%) and sodium hydroxide (Sigma-Aldrich, 98%). For the sol-gel chemical deposition, the following chemicals were used: oxalic acid anhydrous for synthesis (Sigma-Aldrich) and Manganese (II) nitrate tetrahydrate, Mn(NO₃)₂ · 4H₂O (Sigma-Aldrich). Anhydrous D-glucose

(VWR, 99.5%) and Sodium sulfate anhydrous, Na₂SO₄ (Sigma-Aldrich) were used for the electrochemical tests in batch. All chemicals were used without further modifications. Platinum (Pt), gold (Au), glassy carbon (GC), stainless steel (SS) RDE electrodes (AISI 304, Goodfellow) were used for the anodic and cathodic depositions. A 3D-printed Ti rod (2x2x0.5 cm) was used for the chemical deposition. A Pt plate (9x10x0.5 mm) where MnO₂ was anodically deposited was employed for the long-term electrolysis.

2.2.2 Preparation and physical characterization of MnO₂ catalysts

The catalysts were prepared using various deposition techniques (electrodeposition, anodic and cathodic, and chemical deposition) and employing different supporting materials (i.e., Pt, Au, GC, SS, Ti). For the anodic deposition, the bath consisted of a solution of 0.01 M MnSO₄ and 0.5 M Na₂SO₄. A layer of MnO₂ was deposited over Pt, Au, GC and SS RDEs by chronoamperometry, applying a constant voltage of 1.91 V_{RHE} for 20 min [103]. A cathodic electrodeposition method developed by Nguyen et al. [104] was also applied in order to induce homogeneously distributed macro-holes and crumpled nanosheets in the structure of the film to increase its surface area. This method consisted of 2-steps: in the first step, hydrogen bubbling was used as dynamic template for the catalyst deposition at a potential of -0.7 V_{RHE} for 10 min, in a solution with 0.1 M MnCl₂ and 0.1 M NaCl; in the second step, the films were stabilized by potential cycling in the range 0.6 -1.6 V_{RHE} in 0.1 M Na₂SO₄ for 10 cycles at 10 mV s⁻¹. For this method, SS and Pt RDEs were used as support electrodes. Finally, a sol-gel method was used for the chemical deposition of a MnO₂ thin film over the surface of a 3D-printed Ti rod, following the procedure exemplified by Bin et al. [79, 92, 105]. The sol-gel approach i.e. thermal decomposition of manganese (II) nitrate on the Ti electrode, is briefly described as follows [105]: the Ti electrode was first pretreated in 10 wt% boiled oxalic acid solution for 1 h, cleaned with large amounts of deionized water and dried at room temperature; then, for the deposition itself, the electrode was dipped for 30 min into 50 wt% Mn(NO₃)₂ solution, dried at room temperature, and then placed in a muffle furnace for calcination at 200-250 °C for 30 min. Finally, the electrode was cooled to room temperature naturally. This deposition could not be performed on the RDEs as it comprises thermal steps that would have damaged the resin of the electrode casing.

The morphology and pore structure of MnO₂ films was imaged by scanning electron microscopy (SEM). The chemical composition of the MnO₂ electrode was evaluated by energy dispersive spectrum (EDS) and X-ray diffraction (XRD). The microscope used was a Quanta 250 FEI operated at an acceleration voltage of 5kV and equipped with a Super-X EDX detector. XRD patterns were obtained using a Huber X-ray diffractometer equipped with a G670 Guinier camera (Huber GmbH&Co, Germany) using the Cu K α 1 radiation ($\lambda=1.5405981\text{\AA}$).

2.2.3 Electrochemical characterization of the catalysts

A thermostated three-electrode glass cell was used for both, the electrodeposition and the electrochemical characterization of the deposited catalysts. A silver-silver chloride electrode (Ag/AgCl) and a platinum wire were used as reference and counter electrodes, respectively. The working electrodes used in this study consisted of Pt, Au, GC and SS RDEs, and a Ti rod, where the MnO₂ film was deposited as described in 2.2. A two-compartment glass cell separated by a cation-exchange membrane (Nafion 117) was employed for the long-term electrolysis. The electrochemical instrumentation consisted of a Bio-Logic VSP-300 Potentiostat. All the electrode

activities are represented as current densities, utilizing the geometric area as active area and with respect to the reversible hydrogen electrode (V_{RHE}). The tested potential vs. Ag/AgCl was converted into potential vs. RHE using the Nernst equation (Eq. 1):

$$E_{RHE} = E_{Ag/AgCl} + \ln(10) \cdot \frac{RT}{F} \cdot pH + 0.197 \quad [1]$$

With R being the universal gas constant ($8.314472 \text{ J K}^{-1} \text{ mol}^{-1}$), F the Faraday constant ($96485.332 \text{ C mol}^{-1}$) and T the temperature.

Before every deposition, the working electrodes' surface was carefully polished with aluminum ($\Phi 1 \mu\text{m}$) slurry on a polishing cloth and then sonicated in MilliQ water for 5 min. Finally, the electrode was dried with high purity N_2 (99.999%). All the voltammograms shown correspond to the cycle once a stable state was reached.

2.2.4 Long-term electrolysis

To study the reaction products, long-term electrolysis experiments were performed on the $\text{MnO}_2@Pt$ electrode, obtained by anodic deposition. A two-compartment batch cell separated by a cation-exchange membrane (Nafion 117) was employed for the electrolysis. A silver-silver chloride electrode (Ag/AgCl) and a platinum rod were used as reference and counter electrodes, respectively. The electrochemical instrumentation consisted of a Bio-Logic VSP-300 Potentiostat. The long-term electrolysis experiments were performed in solutions containing 0.4 M of glucose and 0.5 M Na_2SO_4 , for neutral pH (7), and 0.4 M glucose and 0.1 M NaOH for alkaline pH (13). A CV was performed before each electrolysis to select the exact potential corresponding to the oxidation peak. The analysis of the reaction products was performed by high performance liquid chromatography (HPLC) using an ion-exclusion column (Shodex KC-811). A photodiode array (PDA) detector set to 210 nm was used to detect organic acids while a refractive index (RI) detector thermostated at 30°C was used to detect glucose. The aqueous solutions of HPLC references were prepared from standard products >99% of pure glucose, gluconic, glucaric, formic and oxalic acid.

2.3 Results and discussion

2.3.1 MnO_2 layer deposition and impact of morphology on the electrode surface area

It is believed that surface morphology, which depends on the preparation method and processing parameters, significantly affects the capacitive behavior of electrode materials. Therefore, the fabrication of materials with appropriate morphology has become an important strategy to enhance the electrochemical performance of electrode materials [97].

One-dimensional (1D) nanomaterials such as nanowires [106], nanorods [107], nanotubes [108] and two-dimensional (2D) nanosheets [109] are reported to exhibit outstanding charge storage properties, because they have large surface areas for charge storage and fast redox reactions. Manganese dioxide has attracted considerable attention due to its high energy density, low cost, natural abundance and environmentally friendly nature. There are many synthesis techniques for the fabrication of MnO_2 catalysts: wet chemical reaction [110], thermal decomposition [111], modified hydrothermal or water-bathing method [112, 113], sol-gel method [114] and redox

reaction with a strong reducing agent (i.e. $(\text{NH}_4)_2\text{C}_2\text{O}_4$) [115]. In recent years, electrodeposition techniques [116–122] have been increasingly explored to produce novel electroactive materials due to their relatively easy and accurate control of the surface microstructure of deposited films. Indeed, by changing deposition variables, such as the electrolyte, deposition potential and bath temperature the final structure can be precisely tuned [123, 124]. Many investigations have attributed the capacity of manganese dioxides to their structural, morphological and compositional characteristics [125, 126]. Generally, most important physicochemical properties of manganese dioxide deposits depend on electrokinetic phenomena during the synthesis process. [127–132].

Babakhani and Ivey studied the effects of the morphology and crystal structure of electrodeposited manganese oxide on its supercapacitive behavior [97]. The electrochemical analysis of manganese oxide electrodes revealed that oriented structures, such as manganese oxide rods and thin sheets, exhibited superior capacitive behavior relative to continuous coatings. An in-depth study of morphology-controlled growth of manganese oxide porous structures from acetate-containing aqueous solutions was conducted by varying the deposition parameters, including solution composition, pH value, deposition temperature and current density. As a result, a series of manganese oxide porous structures, including continuous coatings with equiaxed and fibrous features, petal- and flower-like morphologies, discrete oxide clusters, columnar structures and interconnected nanosheets, were anodically deposited on Au-coated glass [103]. The results showed that manganese oxide electrodes with oriented nanostructures, such as interconnected nanosheet architectures, exhibited superior performance (specific capacitance, rate capacity and electrochemical impedance response), when compared with electrodes with a continuous coating morphology (Fig. 2.1). In fact, porous electrode materials have become highly interesting for applications associated with energy conversion and storage due to their exceptional charge storage capacity. The latter property is measured by the capacitance of the electrode, which is believed to be mainly dependent on the nature of the material and on its geometry, primarily the specific surface area [133–135].

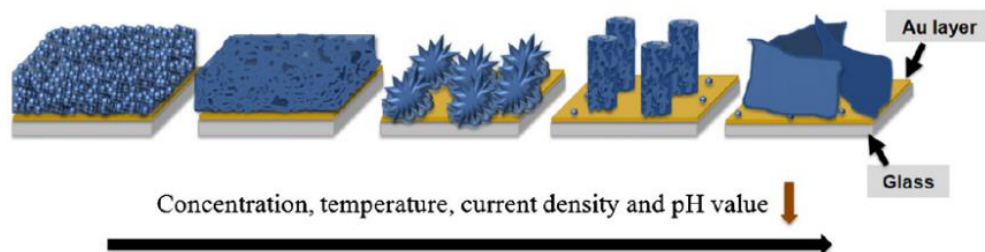


Figure 2.1. Schematic diagram to correlate deposition parameters change (decrease of Mn^{2+} concentration, temperature, current density and pH) with manganese oxide morphology, anodically deposited on Au-coated glass (adapted from [103])

Based on this, we chose to use synthesis methods that allowed the deposition of MnO_2 layers with interconnected nanosheet architectures in the attempt to optimize the electrochemical properties of the developed materials. The overall reaction in the electrochemical deposition of MnO_2 from an electrolyte containing Mn^{2+} ions is given by Eq. 2.



However, the reaction does not take place in a single step [132, 136–139], as will be shown in the next paragraphs.

2.3.1.1 Anodic deposition of MnO₂ over Pt, Au and GC electrodes

Das et al. have reported the use of MnO₂ prepared electrochemically by potentiostatic techniques and chemically from aqueous media as an anode catalyst for the oxidation of carbohydrates [93, 94, 96]. The authors studied the mechanism of potentiostatic (anodic) deposition of MnO₂ on Pt, the redox behavior of the resulting deposit and its electrocatalytic activity towards the oxidation of glucose and fructose, by using cyclic voltammetry, chronoamperometry, chrono-potentiometry and steady state polarization measurements. Fig. 2.2 shows the cyclic voltammetric response during the deposition of Mn²⁺ on a Pt working electrode from a solution, consisting of the precursor, i.e., 0.01 M MnSO₄, and the electrolyte, 0.5 M Na₂SO₄. In accordance with the observations of Das et al. [94], the anodic peak obtained at ca. 0.8 V_{RHE} is related to the oxidation of Mn²⁺ to a higher oxidation state, i.e. Mn³⁺, in a one-electron transfer process (Eq. 3). Mn³⁺ subsequently disproportionates to Mn²⁺ and Mn⁴⁺, at low acid concentration (Eq. 4) or hydrolyses to form an intermediate and insulating product, i.e., MnOOH, at high acid concentration (Eq. 5). Mn⁴⁺ can then hydrolyze to yield MnO₂, the final product, which forms a deposit on Pt (Eq. 6). Additionally, MnOOH will disproportionate to also produce MnO₂ deposits, while releasing a proton and an electron (oxidation step occurring at 1.60 V_{RHE}, Eq. 7). The cathodic peaks at 0.70 and 1.45 V_{RHE}, obtained during the reverse sweep and pointing to reverse process (reduction), are quite small. Additionally, upon increasing the Mn²⁺ concentration in the deposition solution, they do not increase while the corresponding anodic peaks do increase. Both observations suggest that the as-produced MnO₂ layer is rather stable [94].

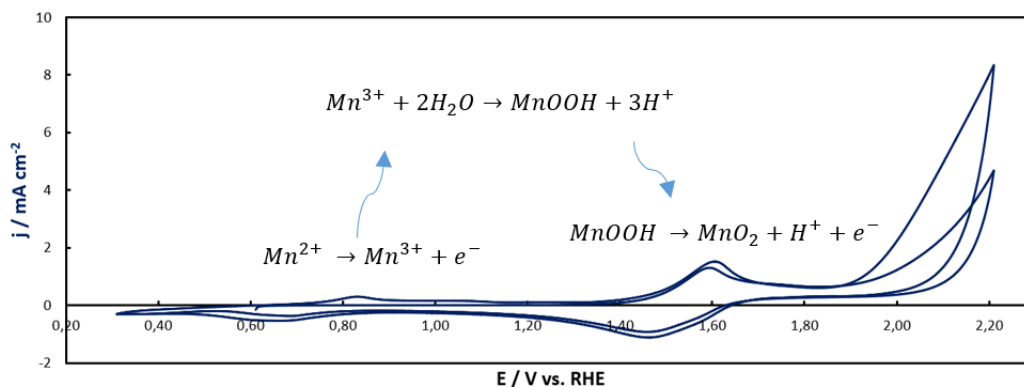


Figure 2.2. Cyclic voltammetric study of Pt in 0.01M MnSO₄ and 0.5M Na₂SO₄ solution recorded at a scan rate of 5 mV s⁻¹.

Next, we investigated the mechanism of the electrochemical deposition of MnO₂ over a glassy carbon electrode. Fig. 2.3 shows the cyclic voltammetry study of Mn²⁺ recorded in the deposition

solution consisting of the precursor, 0.01 M MnSO₄, and the electrolyte, 0.5 M Na₂SO₄. on a GC working electrode at 5 mV s⁻¹.

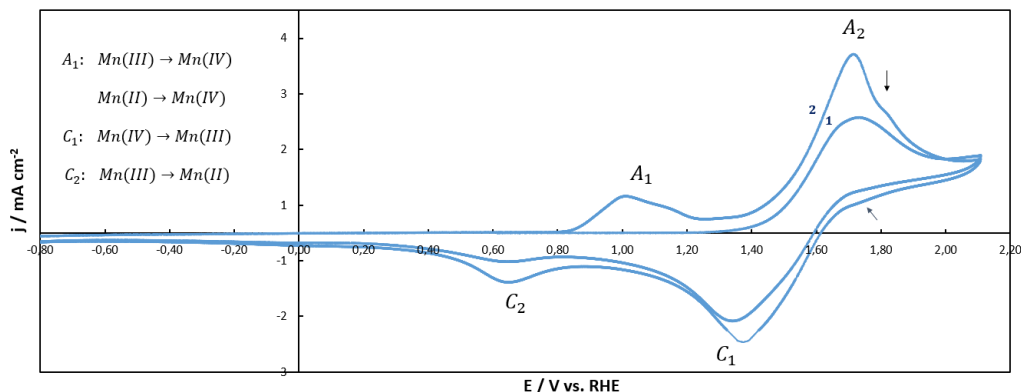


Figure 2.3. Cyclic voltammetric study of GC in 0.01 M MnSO₄ and 0.5 M Na₂SO₄ solution recorded at a scan rate of 5 mV s⁻¹.

In accordance with what was observed by the authors Wen-Zhi et al., there are two redox peaks, A_1 and A_2 in the cyclic voltammograms [140]. The anodic peak A_2 , which appears in the first cycle, is attributed to the two distinct oxidation mechanisms represented by Eqs. 3, 5, 7 (ECE mechanism) and Eqs. 3, 4, 6 (disproportionation mechanism) [141]. According to literature, the cathodic peak in the C_1 region may be due to the reduction of MnO₂ to MnOOH, which is further reduced to Mn (II) in C_2 [142]. In the second cyclic voltammogram, an additional anodic peak appears, namely A_1 , at around 1.0 V_{RHE}, with a broad right shoulder, which did not appear in the first cycle, indicating that its appearance resulted from the formation of MnO₂ at A_2 . A_1 is attributed to the oxidation reaction of Mn (III)/ Mn (IV) and Mn (II)/Mn (IV) species, respectively. Also, the other peaks (A_2 , C_1 , and C_2) all increased in the second cycle, indicating that the MnO₂ film can successfully and continuously grow on the GC surface by further potential scanning [143].

The morphology and nature of the MnO₂ deposit was studied after deposition at a constant potential of 1.91 V_{RHE} for 20 min from a solution of 0.01M Mn²⁺ in 0.5 M Na₂SO₄ and on different substrates including Pt, Au and GC. This potential was chosen on the basis of literature results, where it was found to result in the maximum deposition charge density (120 mC cm⁻²), smaller porosity of the deposit and higher specific surface [93, 94, 96]. The MnO₂@Pt electrode was characterized by SEM. Fig. 2.4 (a) and (b) show a deposit characterized by a petal-shaped, interconnected nanosheet structure, with pores with an average size of 300 nm. Fig. 2.4 (c) shows the energy dispersive X-ray (EDX) spectra of the synthesized MnO₂@Pt electrode, confirming the deposit is made up of Mn and O. Similar results were obtained for the system MnO₂@Au (Fig. 2.10 in SI) and MnO₂@GC (Fig. 2.11 in SI), showing that the anodic deposition of MnO₂ from Mn²⁺ solution is independent of the substrate.

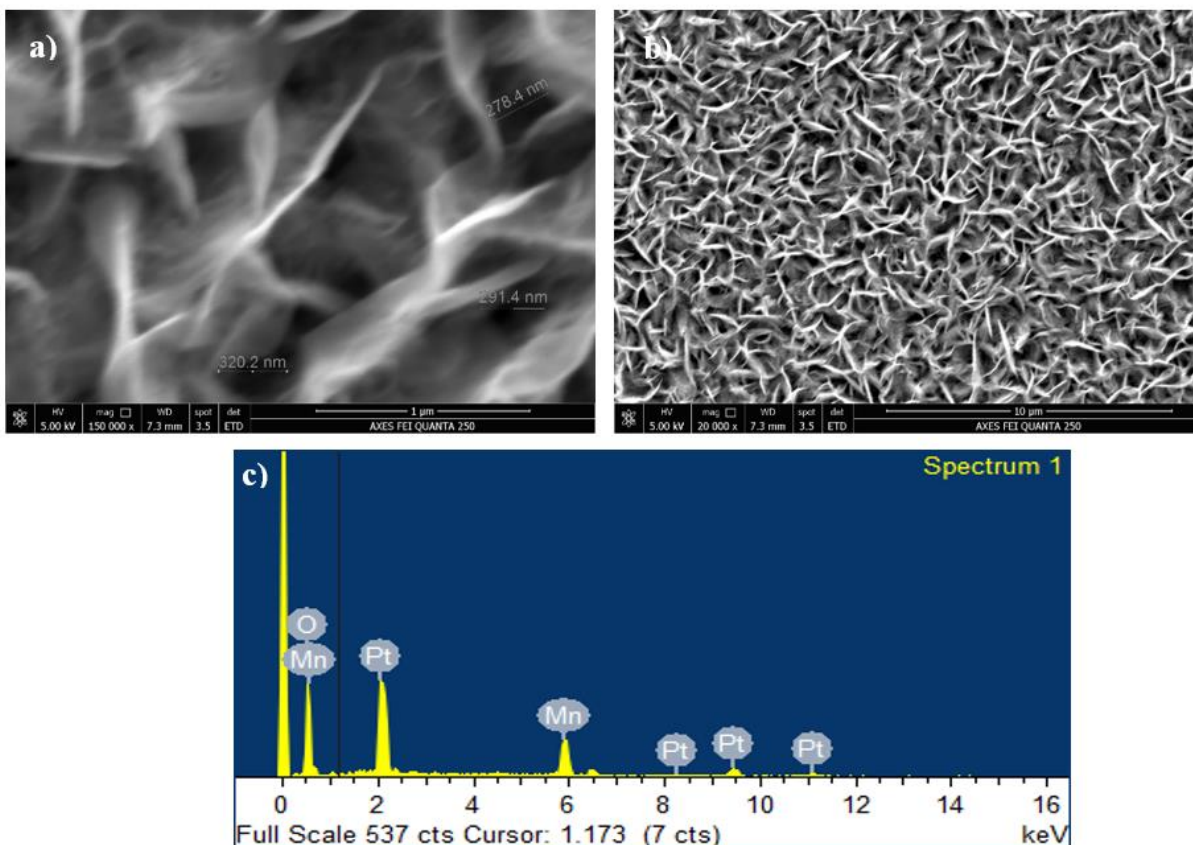


Figure 2.4. SEM images, (a) and (b), and c) EDX spectra of the MnO₂ inter-connected nanosheet layer deposited over the Pt electrode by anodic deposition at 1.91 V_{RHE} for 20 min from a 0.01M Mn²⁺ in 0.5M Na₂SO₄ solution.

2.3.1.2 Cathodic deposition of MnO₂ over a Pt electrode

Cathodic electrodeposition involving hydrogen evolution has been often used to create metallic foams of Ni, Cu, Pd, Ag, Pt, and Au [133, 144]. The hydrogen bubbles that continuously evolve from the substrate prevent the deposition of the metal on these sites, therefore, acting as a dynamic negative template that leads to the formation of porous metallic foams with controlled macro-pores [145]. It has been reported that the macro-pores created by hydrogen bubbling, together with other nanostructured features of oxide films formed by electrodeposition, can result in novel hierarchical electrodes and display improved capacitance linked to the surface-to-volume ratio [133–135]. For this reason, we followed a deposition procedure developed by Nguyen et al. [104], which consisted of using hydrogen bubbling as dynamic template to electrodeposit macroporous manganese oxide films onto Pt and SS RDEs, later to be applied for the electrochemical oxidation of glucose. The deposition was conducted in two steps: step 1 is the hydrogen bubbling, achieved in a solution containing 0.1M MnCl₂ and 0.1M NaCl for 10 min at constant potential of -0.7 V_{RHE}. During this step, hydroxyl ions (OH⁻) and hydrogen bubbles are generated via water electrolysis (Eq. 8) under a cathodic regime.



This is followed by the reaction of Mn²⁺ ions with generated OH⁻ to form Mn(OH)₂ deposited on the substrates, according to:



It must be noted that, by applying cathodic potentials, the undesired reduction reaction of Mn^{2+} to Mn can also take place:



However, the standard electrode potential (SEP) of water electrolysis is lower than that of Mn^{2+} reduction, thus thermodynamically more favorable resulting in only minor metallic Mn formation [104].

In step 2, the oxidation of the as-deposited $\text{Mn}(\text{OH})_2$ to form MnO_2 was performed by carrying out 10 voltammetry cycles in a 0.1 M Na_2SO_4 solution at 10 mV s^{-1} , in the potential range $E = \{0.6, 1.6\} \text{ V}_{\text{RHE}}$, allowing also the stabilization of the electrodeposited electrode [104].

The resulting $\text{MnO}_2@Pt$ electrode was characterized by SEM. Fig. 2.5 (a) and (b) show that, using hydrogen bubbling as dynamic template, it was possible to fabricate a multi-scale macro (hierarchical) porous manganese oxide film with pores of average size around 120 nm. Fig. 2.5 (c) shows the energy dispersive X-ray (EDX) spectra of the synthesized $\text{MnO}_2@Pt$ electrode, confirming the composition of the deposit. Similar results were obtained for the system $\text{MnO}_2@SS$ (Fig. 2.12 in SI), again showing that electrodeposition synthesis techniques do not undergo an influence of the substrate. It is thus clear that the hydrogen bubbling generates macroporous MnO_2 films characterized by well-distributed macro-pores with smaller size compared with those generated during anodic deposition, which possibly results in a higher surface-to-volume ratio. It is reported by the authors by Nguyen et al. that the macro-pores created by the hydrogen bubbling, together with other nanostructured features of oxide films formed by electrodeposition, result in highly hierarchical electrodes that display improved capacitance performance and surface area available for electrochemical reaction [104, 133, 146].

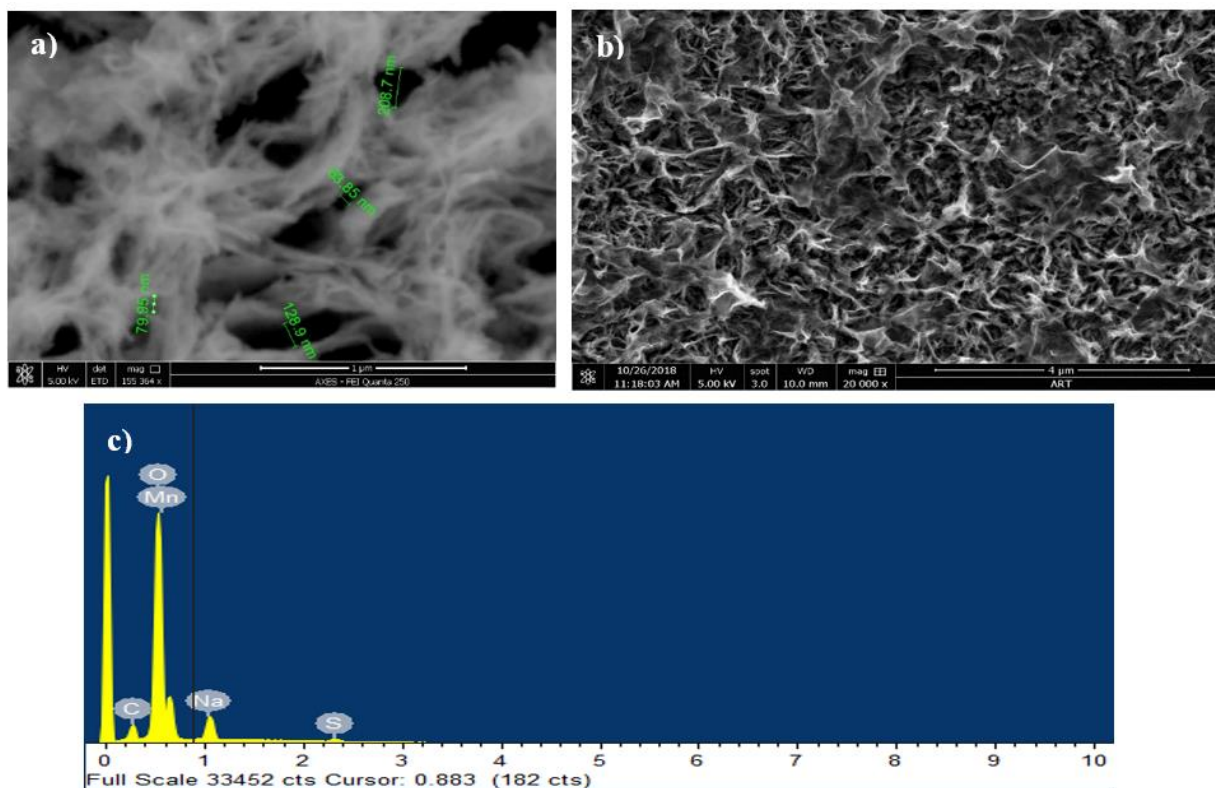


Figure 2.5. SEM images, (a) and (b), and c) EDX spectra of the multi-scale macroporous MnO₂ film fabricated by cathodic deposition using hydrogen bubbling as dynamic template over the Pt RDE.

2.3.1.3 Chemical deposition of MnO₂ over a Ti electrode

Finally, a chemical deposition method following the sol-gel approach developed by Mette et al. [147] was also applied for comparison. This method consists of the thermal decomposition of manganese (II) nitrate on the Ti electrode. This technique is well-established and typically results in loadings of only a few weight percent of the active component [147]. Such low loadings enable a high dispersion of the transition metal oxide and, thus, its efficient use thanks to a high surface-to-bulk ratio. Moreover, the increased presence of defects and strains leads to a further improvement of the intrinsic catalytic properties of electrodes, enhancing the electrode performance. SEM images indicated that the resulting porous MnO₂@Ti electrode consisted of a meso/macro-porous structure with average pores size of 45 nm, as shown in Fig. 2.6. The EDS result in Fig. 2.6 also clearly shows the presence of Mn, O, Ti and various other elements like Ca, Na, K derived from contamination during the synthesis.

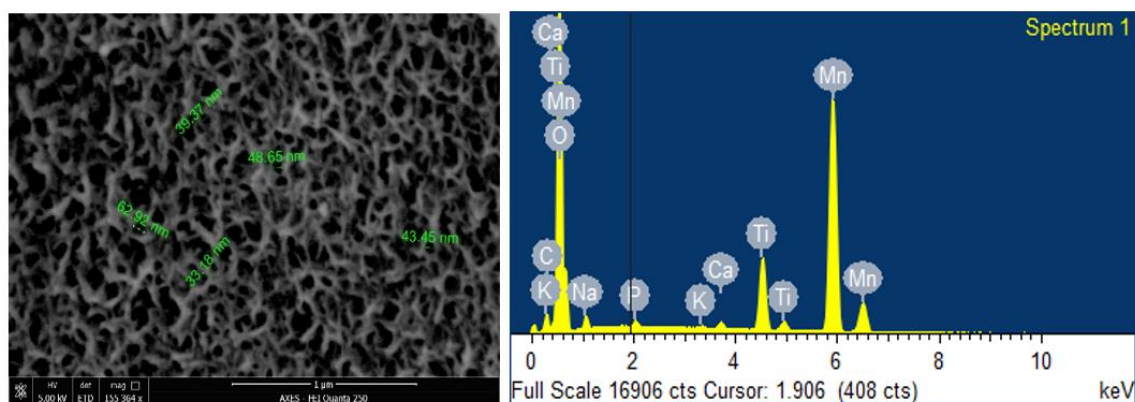


Figure 2.6. SEM image, left, and EDX spectra, right, of the meso/macro-porous MnO_2 film fabricated by sol-gel chemical deposition over a Ti rod electrode.

2.3.2 Electrochemical characterization in a batch cell

To understand the electrocatalytic activity of the as-synthesized $\text{MnO}_2@Pt$ electrode towards glucose oxidation, a cyclic voltammogram was recorded at ambient temperature, in 0.5M Na_2SO_4 solution (blank) with increasing amount of glucose (Fig. 2.7 (a)). The enhancement of the $\text{Mn(IV)} \rightarrow \text{Mn(V)}$ oxidation peak current at 1.8 V_{RHE} upon addition of glucose in the electrolyte indicates the reactivity of the electrode towards glucose oxidation.

As proof of concept, the same study was also conducted on the Pt electrode alone, which shows absence of oxidation peaks when glucose is added to the blank solution, confirming that MnO_2 is the active compound and not Pt (Fig. 2.7 (b)).

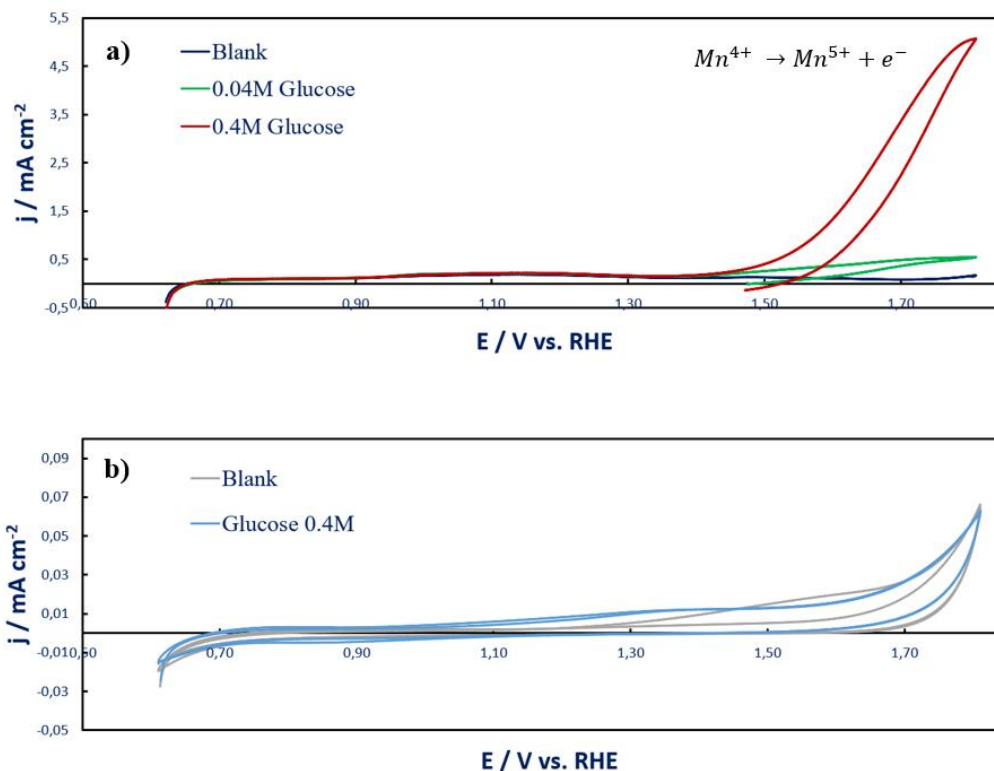
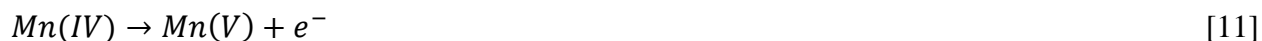


Figure 2.7. a) Cyclic voltammetric study of MnO₂@Pt in blank solution, 0.5 M Na₂SO₄, (blue line) and with increasing concentration of glucose (lines green, 0.04 M, and red, 0.4 M) recorded at 100 mV s⁻¹; b) cyclic voltammetry study of Pt in blank solution, 0.5 M Na₂SO₄, (grey line) and in a solution 0.4 M glucose (light blue line).

The electro-oxidation of glucose was found to proceed via an electrochemical and catalytic (EC) mechanism in which Mn(V) is generated electrochemically (Eq. 11) and consumed chemically in succession (Eq. 12), for both chemically and electrochemically prepared MnO₂@Pt electrodes [94–96, 148].



However, the mechanism behind the oxidation of the carbohydrate by Mn(V) species, Eq. 12, remains to be unraveled. It is postulated that Mn(V) is continuously generated electrochemically and consumed chemically and that gluconolactone is the product formed by the oxidation of glucose, but the latter has never been verified [94–96, 148].

Fig. 2.8 shows the difference in electrocatalytic activity between the MnO₂@Pt electrodes obtained by anodic deposition (20 min) and the cathodic deposition through hydrogen bubbling (10 min), and the MnO₂@Ti electrode obtained by chemical deposition (30 min).

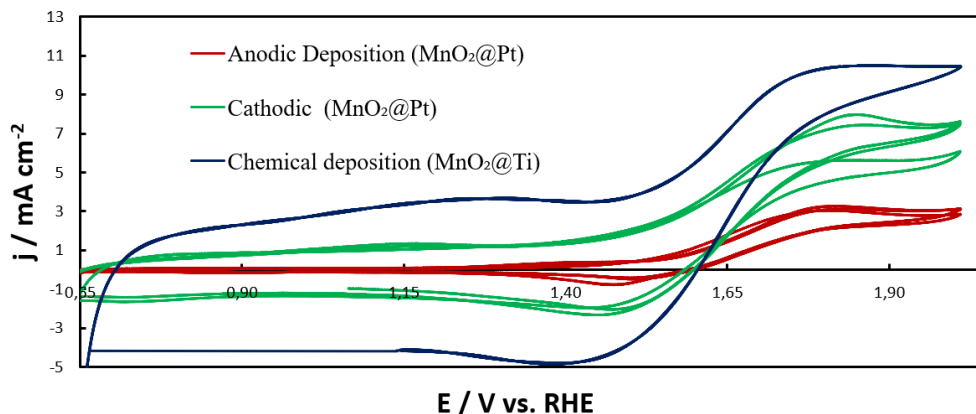


Figure 2.8. Cyclic voltammetric study in a solution 0.5 M Na₂SO₄ and 0.4 M glucose of MnO₂@ Pt obtained by anodic deposition (red line) and with cathodic deposition (green line), and MnO₂@ Ti obtained by chemical deposition (blue line), recorded at 100 mV s⁻¹.

It is evidenced that the chemically deposited MnO₂, characterized by an average pore size of 45 nm, shows the best electrocatalytic performance (~10.5 mA cm⁻²), followed by the cathodically deposited MnO₂, with an average pores size of 120 nm (~8.0 mA cm⁻²), and, finally, the anodically deposited one, with pores size of 300 nm (~3.0 mA cm⁻²). This suggests a possible correlation between porosity and reactivity of the catalyst.

2.3.3 Long-term electrolysis

In order to determine the electrooxidation products, long-term electrolysis experiments were conducted on MnO₂@Pt electrodes deposited with anodic and cathodic deposition methods and on the MnO₂@Ti electrode deposited by chemical deposition.

The long-term electrolysis of D-glucose (0.4 M) was carried out at room temperature (20 °C) first, in neutral medium, 0.5 M Na₂SO₄ (pH 7), and then in alkaline medium, 0.1 M NaOH (pH 13) (for comparison with the reference work [79]). After electrolysis, samples from the electrolyzed solutions were analyzed by HPLC. Despite the aging conditions of the applied HPLC column and the well-known difficulties encountered in the chromatographic analysis of sugar solutions [149–151], we were able to identify the chromatograms of standard solutions of the expected reaction products, gluconic and glucaric acid (Fig. 2.13 in SI). Surprisingly, even after 18 h of electrolysis, neither gluconic nor glucaric acid were detected under neutral conditions in the solutions resulting from the long-term electrolysis (Fig. 2.14 in SI). Only a very small peak appears at a retention time of 9.2 min, already after 1 h reaction time when conducting the electrolysis at 2.0 V_{RHE} and has been identified as formic acid (Fig. 2.15 in SI). This result is in contrast with what was found by the authors Bin et al., who report a total selectivity of 93% to gluconic and glucaric acid and a glucose conversion of 93% after 24 min reaction at a pH of 7, using a similar MnO₂ system. The authors have claimed that their exceptional results are a consequence of the flow reactor configuration used, since it ensures the systematic separation of the products from the reaction compartment into a permeate tank, thus avoiding over-oxidation. However, if oxidation of glucose to gluconic and glucaric occurred at the MnO₂ catalyst, we should be able to detect them at an early stage of the reaction, even when working in a batch system. In other words, if over-oxidation occurs in an un-controlled process as is for the batch system, we should, indeed, observe high levels of over-oxidation products (i.e., formic acid), but also, in part, the intermediates, gluconic

and glucaric acid. Similarly, if over-oxidation of gluconic and glucaric acid to formic acid and other, lower molecular mass, products does occur on MnO_2 catalysts, the authors should also detect, at least in part, these products, especially at the highest residence times. Unfortunately, we have thus far not found any explanation for the large difference in performance between our work and that performed by Bin *et al.*, other than the addition of flow, which we believe cannot be the sole explanation.

Different results were obtained when the reaction was conducted in alkaline medium. In fact, in the solutions resulting from the electrolysis of 0.4 M glucose in 0.1 M NaOH (pH 13) on the same, anodically deposited MnO_2 @Pt catalyst at 2 V_{RHE} , gluconic acid was detected (around 1000 ppm, which is still on the low side), as shown in the chromatogram in Fig. 2.16 in SI. A temperature of 5 °C was chosen in this case to inhibit chemical side-reactions that occur at ambient temperature and that are catalyzed by bases [152].

These observations seem to confirm the important role of the pH in the glucose oxidation reaction, as evident from literature [153–156]. Indeed, D-glucose exists in two anomeric forms, α and β -D-glucopyranose (Fig. 2.9), as well as, in minor part, in the free linear aldehyde form. Largeaud *et al.* investigated the stability of α - and β -D-glucose in acidic, neutral and basic media by using polarimetric measurements and their reactivity by cyclic voltammetry [157]. The authors attributed the enhanced performances of glucose oxidation in alkaline conditions to the shift of the equilibrium of D-glucopyranose to the β -anomeric form, which was found to be more reactive. In fact, the β -conformation allows a planar approach of the molecule to the surface of the catalyst, favoring a rapid interaction, explaining the improved performance shown here in alkaline medium for MnO_2 @Pt [157].

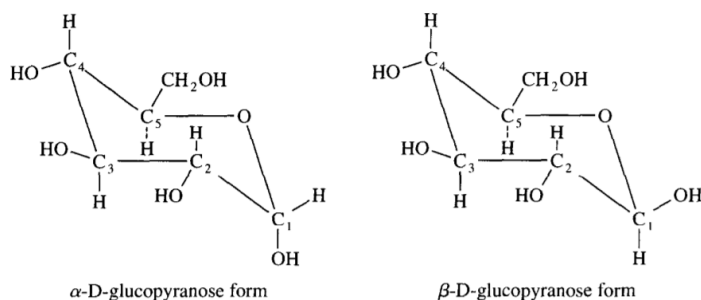


Figure 2.9. The two anomeric forms of D-glucopyranose: the difference between the two anomers lies on the position of the OH functional group on the anomeric carbon C1, axial in the α form and equatorial in the β form (adapted from [157]).

In conclusion, the mechanism of glucose electrooxidation on MnO_2 electrodes remains unclear even after our investigations. It has been postulated that the oxidation of Mn (IV) to Mn (V) (Eq. 11), corresponding to the oxidation peak appearing at 1.70-1.80 V_{RHE} in the voltammogram of MnO_2 in presence of glucose in neutral media (Fig. 2.8(a)), is followed by the chemical regeneration of Mn (IV) by a chemical reaction that converts glucose to gluconolactone (Eq. 12). However, the analysis of the solutions resulting from long-term electrolysis conducted in this work, does not reveal such species nor any other sugar derivative, in a relevant amount. In order to unravel the reaction mechanism, further studies are needed to identify the actual products formed during glucose electrooxidation on MnO_2 in neutral conditions, that seem to not be detected by HPLC. Given its very small concentration, even the gluconic acid detected after long-term electrolysis in alkaline media could be the result of the chemical, base-catalyzed degradation of

glucose rather than electrooxidation on MnO_2 [152]. Further investigations will be conducted to confirm this hypothesis. Given the evidences collected with this work and as the objective of this thesis was to find an electrocatalytic system for the selective oxidation of glucose to glucaric acid, we decided to not investigate MnO_2 systems further. On the contrary, we turned our attention to noble metal catalysts, that have been proven very promising for glucose oxidation and for which there is extensive literature on their reaction mechanism [86–91, 101, 157–164].

2.4 Conclusions

In this work we synthesized nanostructured MnO_2 porous films over various supports using anodic deposition (Pt, Au, GC), cathodic deposition (Pt, SS) and a chemical impregnation method (Ti). The morphology and elemental composition of the deposits was investigated by SEM and EDX. The analysis revealed, in all cases, a porous structure constituted of interconnected nanosheets. Different size of the pores was obtained with the different deposition methods, but independently of the nature of the support electrode. Pores with an average size of 300 nm were obtained when using anodic deposition, while an average pore size of 120 nm was obtained with cathodic deposition using hydrogen bubbling as dynamic template, and 45 nm was obtained with the chemical deposition (impregnation method). In this context, the best electrocatalytic system was obtained by chemical deposition (impregnation method), as it showed the highest electrocatalytic activity ($\sim 10.5 \text{ mA cm}^{-2}$). However, the anodic deposition method has the advantage of being simpler and faster to implement, as it involves only 1 step, requires ambient conditions and it does not make use of strong reagents. Long-term electrolysis performed in neutral media at the potential of 2 V_{RHE} , did not result in the formation of gluconic nor glucaric acid. The formation of gluconolactone in this potential range had been hypothesized in previous literature, but not proven. Apparently, some other oxidation product is being formed that cannot be detected by liquid chromatography. Gluconic acid appears, instead, in very small concentration, in the chromatogram of the solution resulting from long-term electrolysis in alkaline media. However, the latter could have also been generated by the base-catalyzed reactions that take place in alkaline media and involving sugars [152]. As the evidences collected with this work prove that MnO_2 is not an ideal catalyst for the selective oxidation of glucose to glucaric acid, we decided to move away from it and turn our attention to noble metal catalysts, that have been proven very promising for glucose oxidation.

2.5 Supporting information

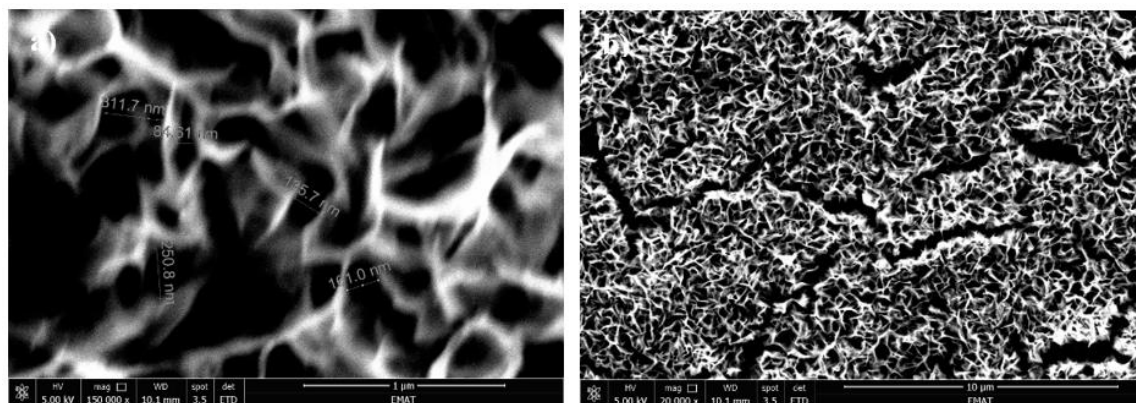


Figure 2.10. a) and b) show the SEM images of the MnO₂@Au electrode obtained by anodic deposition at a constant potential of 1.91 V_{RHE}, for 20 min at 50 mV s⁻¹ from a 0.01M Mn²⁺ in 0.5M Na₂SO₄ solution.

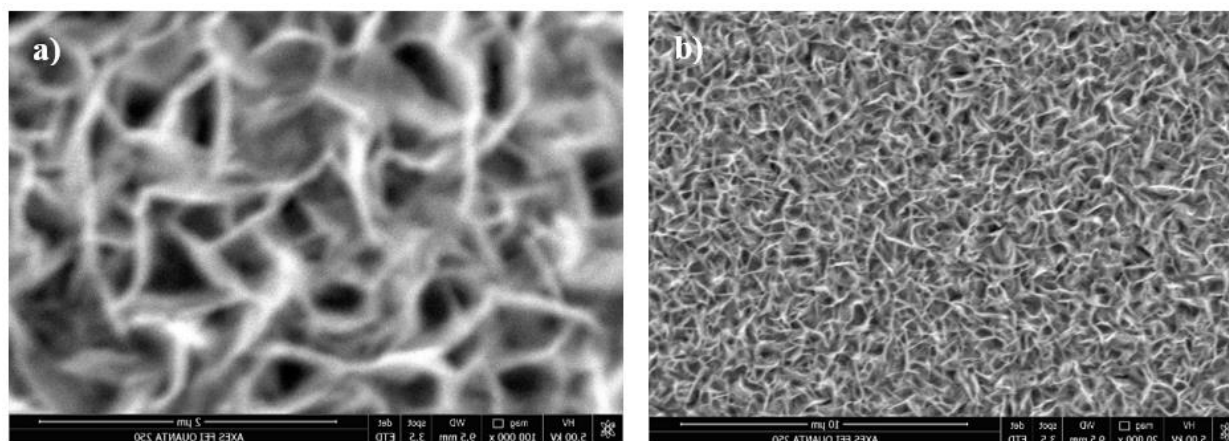


Figure 2.11. a) and b) show the SEM images of the MnO₂@GC electrode obtained by anodic deposition at a constant potential of 1.91 V_{RHE}, for 20 min at 50 mV s⁻¹ from a 0.01M Mn²⁺ in 0.5M Na₂SO₄ solution.

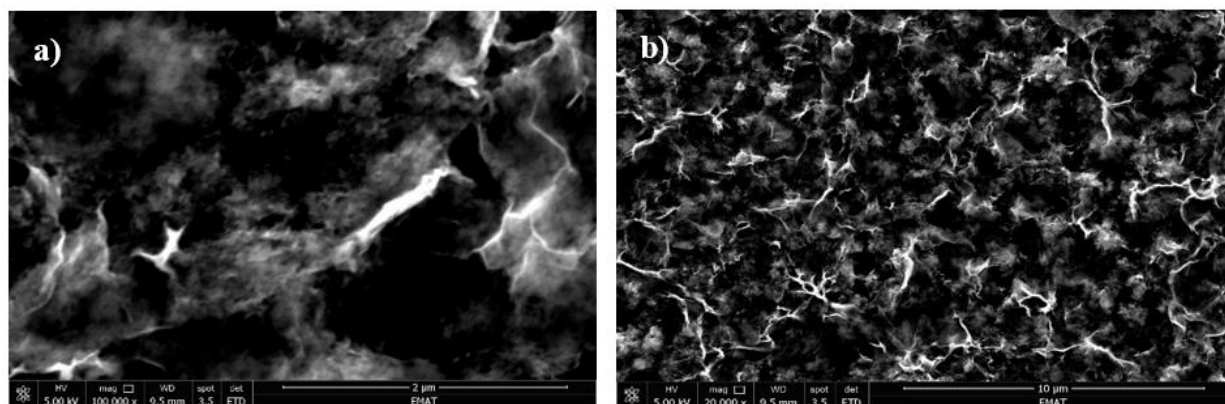
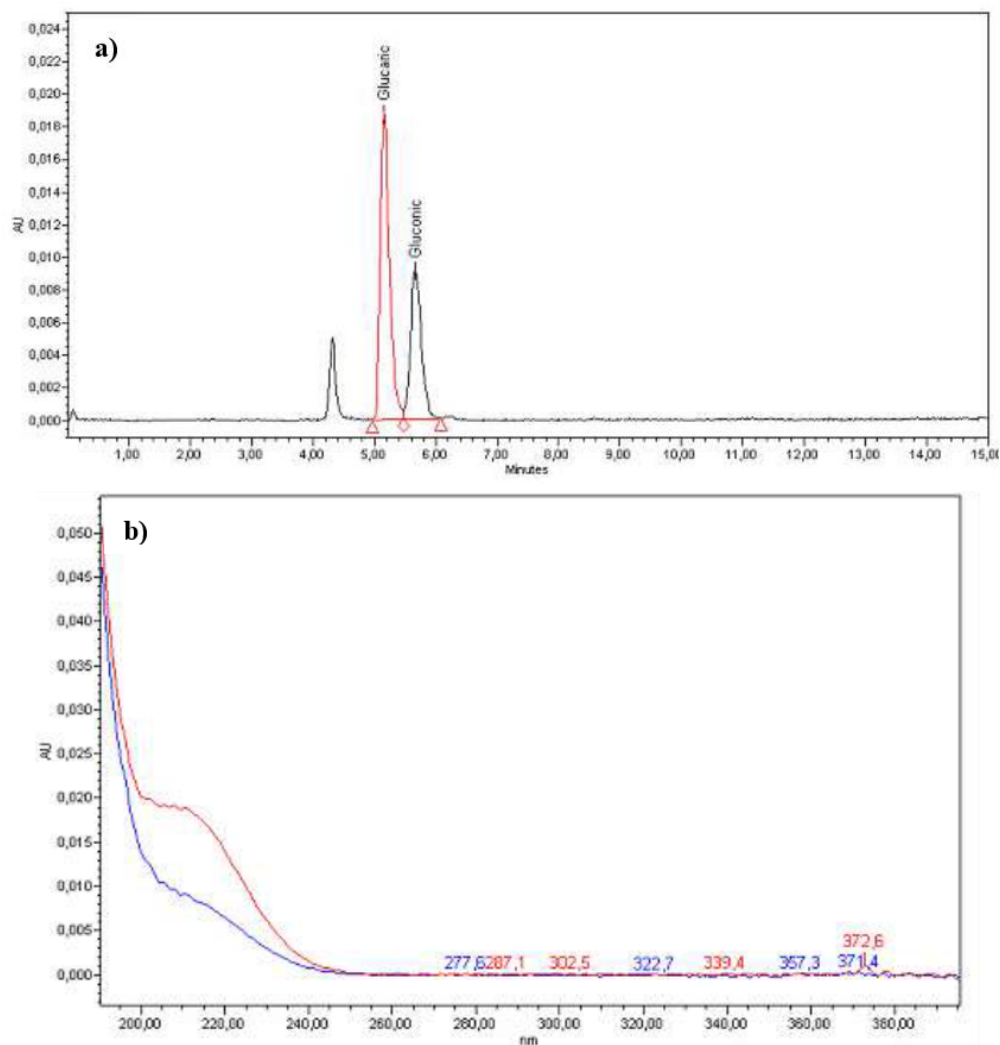


Figure 2.12. a) and b) show the SEM images of the MnO₂@SS electrode obtained by cathodic deposition: 10 min at -0.7 V_{RHE} and 10 mV s⁻¹ in 0.1M MnCl₂ and 0.1M NaCl (hydrogen bubbling, step 1); 10 cycles between 0.6 and 1.6 V_{RHE} in a solution: 0.1M Na₂SO₄ (electrooxidation, step 2).



Name	Retention Time (min)	Area (μV*sec)	Height (μV)	Width (sec)	Peak Lambda Max (nm)	N
Glucaric acid	5,156	195943	18909	31	190,4	5600
Gluconic acid	5,663	111532	9099	36	190,4	4828

Figure 2.13. Chromatogram (a) and corresponding PDA spectrum (b) of gluconic (black line in a) and blue line in b) and glucaric acid (red line).

Sample preparation: 1 mL of filtered sample (0.2 μm syringe filter) is added to 100 μL of 1.2 M HClO₄ solution in a sample vial and sonicated for at least 30 seconds until no bubbles are observed. Method parameters: eluent was for 80% a solution 0.1% HClO₄ in Milli-Q water and the remaining 20% ACN in Milli-Q water; 1 mL/min flow rate; column temperature 30°C; injection Volume 10 μL.

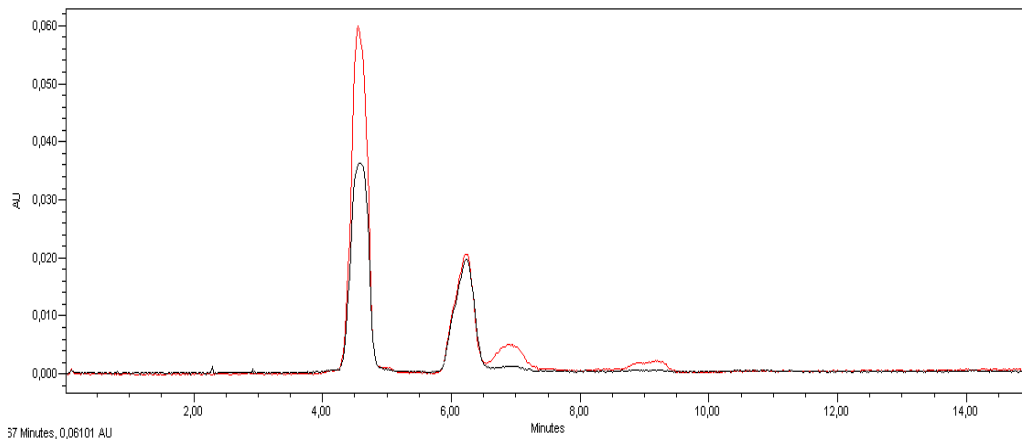


Figure 2.14. Chromatogram of the resulting solution of 18 h electrolysis of 0.4 M Glucose in 0.5M Na₂SO₄ at neutral pH on anodically deposited MnO₂@Pt at 20 °C and oxidation potential 1.61 V_{RHE} (black line) and 1.80 V_{RHE} (red line). All peaks visible in the chromatogram are smaller than the injection peak (at around 4.6 min), thus neglectable. None of them corresponds to gluconic (retention time 5.156 min) or glucaric acid (retention time 5.663).

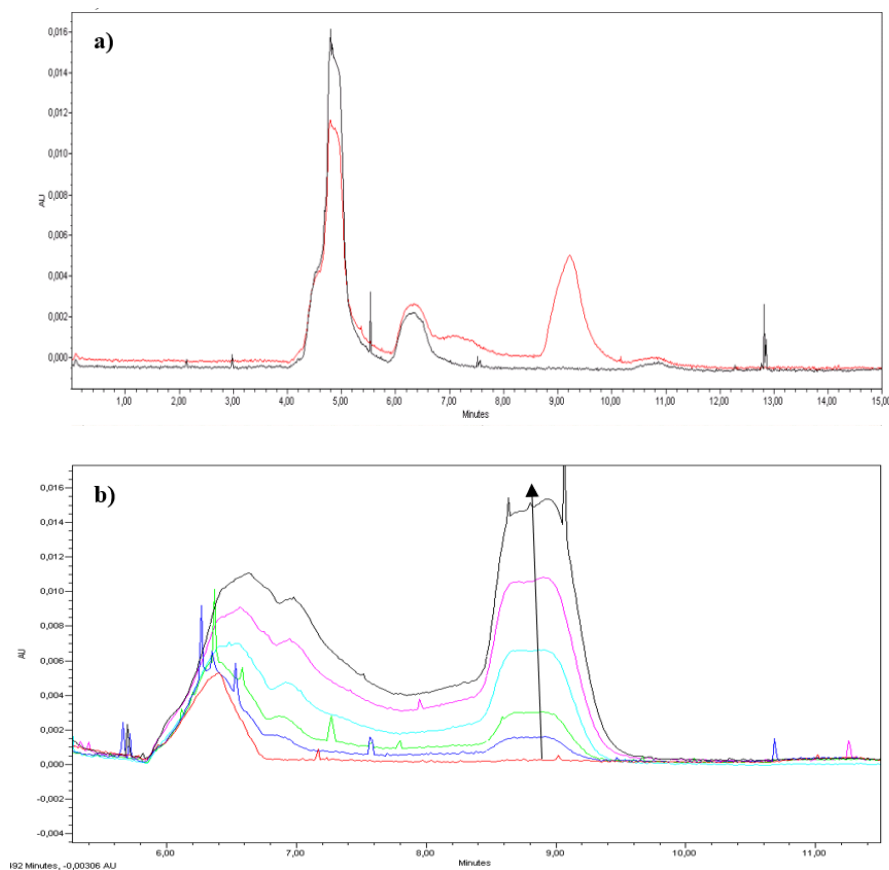


Figure 2.15. a) Chromatograms of the resulting solutions of the electrolysis of 0.4 M Glucose in 0.5M Na₂SO₄ at neutral pH on anodically deposited MnO₂@Pt at 20 °C and oxidation potential 2.0 V_{RHE}. a) is the chromatogram of the products after 1 h electrolysis (red line) compared with the chromatogram of the reaction solution before electrolysis (black line), obtained using an injection volume of 100 μL, in an attempt to better identify the products' peaks; b) is the chromatogram of the product solution at increasing electrolysis times, from 0 to 5 h, obtained using

an injection volume of 10 μL . All peaks visible in the chromatograms are smaller than the injection peak (4.6 min). None of them corresponds to gluconic (retention time 5.156 min) or glucaric acid (retention time 5.663).

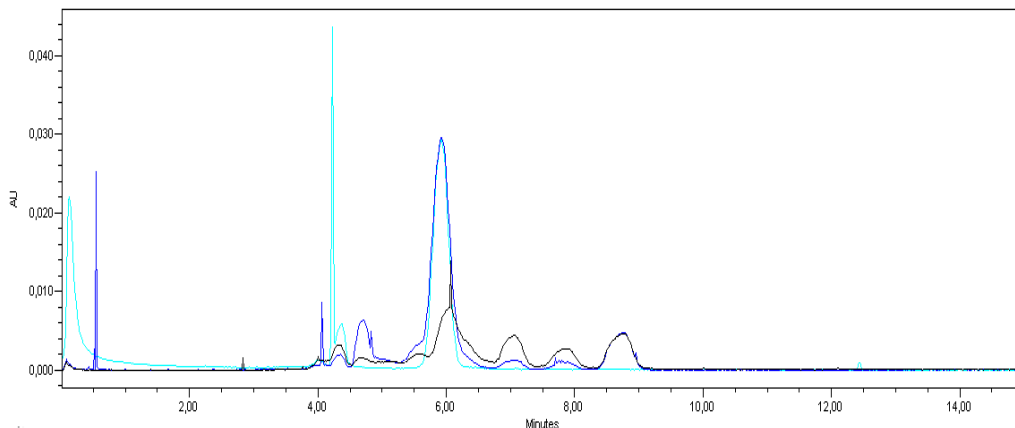


Figure 2.16. Chromatogram of the resulting solution of 65 h electrolysis of 0.4 M Glucose in 0.1M NaOH at pH 13 on anodically deposited $\text{MnO}_2@Pt$ at 5 $^\circ\text{C}$ and oxidation potential 2.0 V_{RHE} (blue line), compared to that of the starting solution (black line). One peak in the chromatogram is considered relevant as higher than the injection peak: the peak at ca. 5.8 min retention time, which corresponds to gluconic acid, as confirmed by overlapping the chromatogram with that of pure gluconic acid (light blue line). The other, smaller peaks remained unidentified but are sufficiently small to be neglectable.

Chapter 3

Role of oxidation potential and chemical side-reactions on the selectivity to D-gluconic and D-glucaric acid

This chapter has been published as a research paper: G. Moggia, T. Kenis, N. Daems, T. Breugelmans, “Electrochemical Oxidation of d -Glucose in Alkaline Medium : Impact of Oxidation Potential and Chemical Side Reactions on the Selectivity to D-Gluconic and D-Glucaric Acid”, ChemElectroChem, vol. 7 (2020) issue 1, pages 86-95.

3.1 Introduction

The first challenge encountered during the electrocatalytic oxidation of D-glucose in alkaline media is the low selectivity of the overall process which results in several reaction products including D-fructose and low molar mass carboxylic acids where the structure of the glucose molecule is disrupted [88, 159]. It has been reported in literature that, in alkaline conditions, D-glucose is consumed by two chemical reactions [152]: the isomerization of D-glucose to D-fructose and its thermal oxidative degradation. The former is a reaction controlled by a thermodynamic equilibrium and for which bases are common homogenous catalysts. The latter is a set of irreversible temperature-catalyzed reactions (aldolization/retroaldolization, β -elimination, and benzylic rearrangement) that take place simultaneously to isomerization and lead to several by-products (i.e. formic, oxalic, tartaric, glycolic acid) [152]. In this chapter, we preliminary investigate the stability of the reaction solution to find the operating conditions less favorable for these side-reactions in an attempt to limit their impact on the process (i. e. low temperature and concentration of the base). The oxidation of glucose to glucaric acid involves the oxidation of only the two terminal anomeric carbons in the glucose molecule, while keeping the six-atom structure unaltered. This overall process passes through the formation of an intermediate product, gluconic acid, by oxidation of the C1 group (aldehyde) to carboxylic group. For the further reaction to D-glucaric acid, also the C6 group (hydroxymethyl) needs to be fully oxidised to a carboxylic group. In an uncontrolled process, i. e., at high temperatures or in presence of high concentration of strongly reactive oxidants (radicals, ions), any carbon atom in the glucose backbone becomes a reactive site, leading to the cleavage of C-C bonds and formation of low molar mass carboxylic acids like formic and oxalic acid. Our objective is to develop an electrochemical method, using only heterogeneous catalysts, that allows a controlled oxidation with high selectivity towards the desired products (gluconic and glucaric acid) while at the same time preventing the formation of undesired side-products. Here, we want to demonstrate that, by adjusting an electrochemical parameter (applied potential), it is possible to achieve a region-selective oxidation of glucose to gluconic and glucaric acid. To this end, the electro-reactivity of the two terminal functional groups of D-glucose is investigated in this chapter by cyclic voltammetry in alkaline medium for three different metal electrodes (copper, platinum and gold), in order to find a relationship between potential and reactivity of the functional group. Once the optimal reaction conditions, maximally inhibiting undesired chemical side-reactions, are selected, this relationship is verified by analyzing the products of long-term electrolysis.

3.2 Experimental

3.2.1 Chemicals and reagents

The supporting electrolytes were prepared with ultrapure water (Synergy UV system) and sodium hydroxide (Sigma-Aldrich, 98%). Anhydrous d-glucose was purchased from VWR (99.5 %), gluconic acid potassium salt (98%) and D-saccharic acid potassium salt (98%) from Sigma Aldrich, and D-glucuronic acid sodium salt (99%) from Acros Organics. All chemicals were used without further modifications.

3.2.2 Electrochemical setup



Figure 3.1. Electrochemical set-up designed for the long-term electrolysis: (1) Pt counter electrode (CE), in the cathodic compartment; (2) Nafion membrane; (3) reference electrode (RE) and (4) working electrode (WE), both in the anodic compartment.

A thermostated three-electrode glass cell was used during the voltammetry study, while a two-compartment glass cell separated by a cation-exchange membrane (Nafion 117) was employed for the electrolysis (Fig. 3.1). A cation-exchange membrane was used to allow only protons to move between compartments. A silver-silver chloride electrode (Ag/AgCl) and a platinum rod were used as reference and counter electrodes, respectively. Copper (0.32 cm²), platinum (0.13 cm²) and gold (0.08 cm²) working electrodes used for the cyclic voltammetry experiments were purchased from AISI 304, Goodfellow. A copper rod (3.85 cm²), a platinum plate (2.91 cm²) and the gold (0.08 cm²) working electrode were used for the long-term electrolysis. The electrochemical instrumentation consisted of a Bio-Logic VSP-300 Potentiostat. All the electrode activities are represented as current densities, utilizing the geometric area as active area and with respect to the reversible hydrogen electrode (V_{RHE}). Before every electrochemical measurement, the working electrodes' surface was carefully polished with aluminum (Φ 1 μ m) slurry on a polishing cloth and then sonicated in MilliQ water for 5 min. Finally, the electrode was dried with high purity N₂ (99.999 %). The cyclic voltammetry studies were conducted between 0 and 2 V_{RHE} at 10 mV s⁻¹ at ambient temperature, while the long-term electrolysis experiments were performed for 65 hours at 5°C, in order to inhibit the thermal degradation of glucose in alkaline solution [152]. Solutions containing 0.04 M of glucose, gluconic acid, glucuronic acid and glucaric acid in 0.1 M aqueous NaOH were used for the cyclic voltammetry studies. All the voltammograms shown correspond to the cycle once a stable state was reached. An initial solution containing 0.04 M of glucose in 0.1 M NaOH (pH 13) was used for the electrolysis. A CV was performed before each electrolysis to select the exact potential corresponding to the oxidation peak.

3.2.3 Product Analysis

The identification of reaction products was carried out by gas chromatography coupled with mass spectrometry (GC-MS) using a RXI-1 ms (Restek) capillary (30 m, 0.32 mm i.d. and 0.25 μ m film thickness). The electrolytic solutions were treated before analysis according to the following procedure. The water was removed by lyophilization to leave dry samples of electrolyzed material. This material was trimethylsilylated using Supelco hexamethyldisilazane and

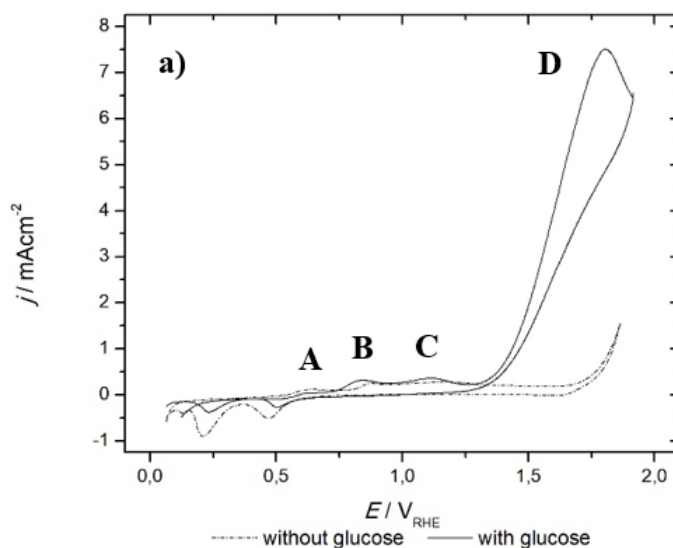
trimethylchlorosilane (HMDS+TMCS) + pyridine, 3:1:9 (Sylon HTP) Kit, as described in [165]. Authentic samples of the expected reaction products were also trimethylsilylated and their chromatographic data were used for the product identification. The quantitative analysis of the reaction products was performed by high performance liquid chromatography (HPLC) using an ionexclusion column (Shodex KC-811). A photodiode array (PDA) detector set to 210 nm was used to detect organic acids while a refractive index (RI) detector thermostated at 30°C was used to detect glucose and fructose. Gluconic acid and glucose peaks overlapped in the chromatograms obtained using the RI detector, however, it was possible to perform a quantitative analysis of glucose, by subtracting the gluconic acid concentration obtained with the PDA detector from the total gluconic acid and glucose concentrations obtained with the RI detector, as already done by Solmi et al. [50]. The aqueous solutions of HPLC references were prepared from standard products >99% of pure gluconic, glucaric, lactic, tartaric, formic and oxalic acid. The selectivity (mol%) was calculated as the number of moles of product formed per number of moles of glucose consumed taking into account the stoichiometry (Eq. 13):

$$\text{Selectivity [mol\%]} = 100 \cdot \frac{[\text{mol of product formed}] \cdot [\mu]}{[\text{mol of glucose consumed}] \cdot [v]} \quad [13]$$

For the results of the electrolysis, the selectivity refers only to the contributions of the electrochemical reaction. All the measurements were performed two times and the errors measured on the values of selectivity of the products were, in all cases, lower than 3%. The analysis of the gas phase was performed by Gas Chromatography (GC): no gaseous product was formed during the electrolysis.

3.3 Results and discussion

3.3.1 Oxidation of D-glucose at copper, platinum and gold electrodes



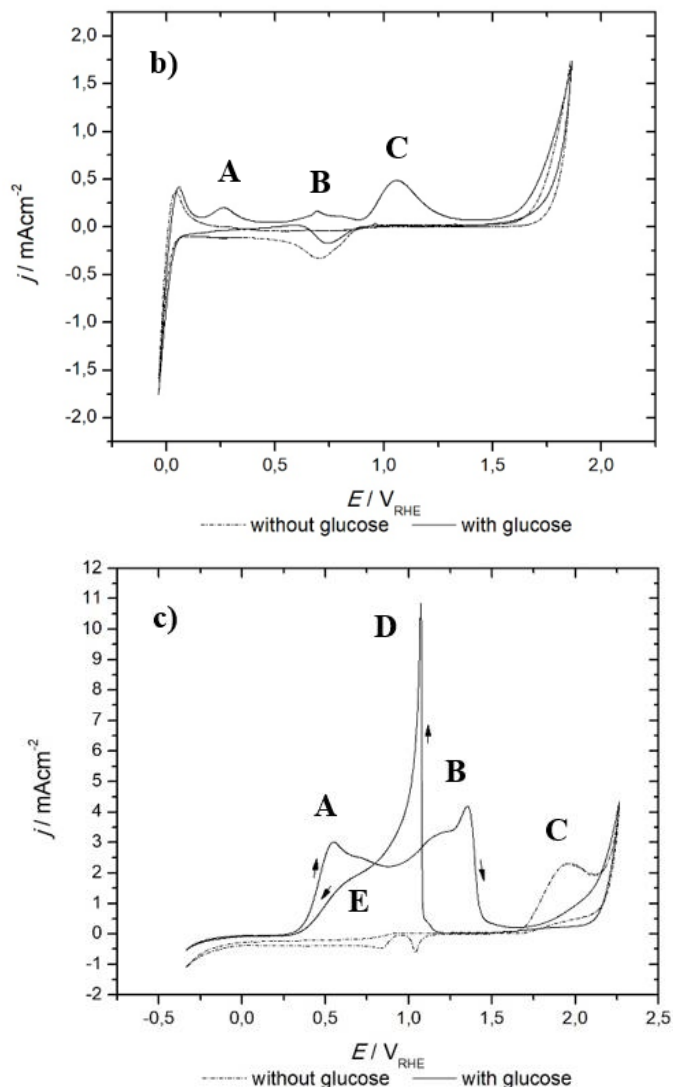


Figure 3.2. Voltammograms of a) copper, b) platinum and c) gold electrodes in alkaline medium (0.1 M NaOH) recorded at 10 mVs^{-1} , at $20 \text{ }^\circ\text{C}$ without (dashed lines) and with (solid lines) 0.04 M D-glucose.

The cyclic voltammograms of copper, platinum and gold recorded at ambient temperature in 0.1 M NaOH in the absence and presence of glucose (0.04 M) are given in Figure 3.2. For copper, four oxidation peaks can be observed during the positive potential sweep, at 0.61 (peak A), 0.84 (peak B), 1.11 (peak C) and 1.80 V_{RHE} (peak D) (Figure 3.2(a)). The oxidation at peak A has been reported by Kano et al. [166] to correspond to a one-electron transfer reaction between Cu and OH^- ions in solution with the formation of a Cu_2O monolayer as a result. Peak B has been mainly attributed to a two-electron transfer reaction directly from Cu, in combination with (to a smaller extent however) a one-electron transfer reaction from Cu_2O , resulting in the formation of CuO [166]. This species, in which copper has oxidation state +2, appears to be reactive towards glucose oxidation since the current density corresponding to its peak, in presence of glucose, is slightly higher than in the blank solution. Peak C has been found to increase with the solution alkalinity (up to 0.1 M NaOH) [166]; at higher NaOH concentrations it appears at less anodic potentials and eventually overlaps with B. Kano et al. did not attribute a specific reaction to this peak, but they

hypothesized the formation of a soluble product, either chemically or electrochemically, which diffuses away from the electrode surface and hence is not recovered in the cathodic sweep [166]. In our case, peak C is slightly more pronounced in presence of glucose and shows a reactivity similar to that of peak B, pointing us in direction of the formation of a soluble product from CuO. Finally, Peak D has been attributed to the formation of soluble reaction products, namely cuprite CuO_2^{2-} , from either Cu, through an (electro)chemical reaction from CuO, which diffuse away from the electrode surface, and hence are not recovered in the cathodic half-cycle [166]. We found that these species show the highest current density in presence of glucose and are thus the most interesting Cu species to perform the oxidation of glucose, which we believe results in the cleavage of the C-C bonds and formation of low molar mass carboxylic acids, i. e. formic acid, as was confirmed by HPLC analysis (*vide infra*). The two reduction peaks in the cathodic scan represent the reduction of, respectively, Cu(II) to Cu(I) and Cu(I) to Cu(0), which can be observed both in presence and in absence of glucose. Three oxidation peaks are visible on the platinum electrode during the positive potential sweep, at 0.26 (peak A), 0.70 (peak B) and 1.10 V_{RHE} (peak C) (Figure 3.2(b)) all in the presence of glucose. The presence of shoulders (which affect peak B especially) suggests that the peaks are complex and result from different contributions. Yei et al. [164] thoroughly studied the mechanism of glucose electrooxidation on platinum in alkaline medium. They concluded that: peak A corresponds to the oxidation of the adsorbed hydrogen produced by chemisorption of the glucose molecule, without poisoning of the surface and peak B corresponds to the direct oxidation of glucose from the bulk. Finally, for peak C it is more difficult to determine the involved reaction. This peak was hypothesized to correspond to the oxidation of the adsorbed species resulting from the chemisorption of glucose in the range of peak A [164]. The reduction peak in the cathodic half-cycle corresponds to the reduction of the oxidized Pt. Finally, the CV curve of the gold electrode in glucose alkaline solution shows three clear electrochemical processes during the anodic sweep and two during the cathodic return scan (Figure 3.2(c)). Pasta et al. [90] concluded that glucose electrooxidation on gold follows the same mechanism as on platinum. According to the authors: peak A (around 0.55 V_{RHE}) corresponds to the dehydrogenation of anomeric carbon under adsorption control; peak B at 1.34 V_{RHE} , with a large left shoulder has been attributed to several oxidative processes taking place in the potential range from 1 V_{RHE} to 1.34 V_{RHE} that lead to gluconate as oxidation product [90]; at 1.50 V_{RHE} (peak C) gold surface oxidation occurs, as demonstrated by Xiang et al. [167]. The oxidative peak around 1.00 V_{RHE} in the cathodic scan (peak D) is obtained as soon as the oxide layer is reduced to generate free O_2^- anions which react with glucose and then the Au surface undergoes re-oxidation by OH^- in solution [90]. Pasta et al. didn't give an explanation for the oxidation process taking place at E, 0.55 V_{RHE} , in the cathodic scan. It might be attributed, as further explained in the following paragraph, to the same oxidation process taking place at A. From these studies, it is clear that the electrocatalytic glucose oxidation is strongly influenced by the nature of the applied catalyst. For each examined metal, the different potential windows correspond with different oxidation processes. In some cases the metal is itself involved in the oxidation reaction (i. e. at peak B on Pt or at peak A and B on Au) in some other cases it is an oxide species of the metal that acts as catalytic mediator (i. e. the two oxides of Cu formed at peaks B and C or the platinum oxide at peak C) and, finally, soluble species can be generated at certain potentials that react with glucose in solution (namely the species cuprite CuO_2^{2-} at peak D on Cu or the free O_2^- anions generated by the reduction of the gold oxide layers at peak D).

3.3.2 Voltammetry study on glucose derivatives

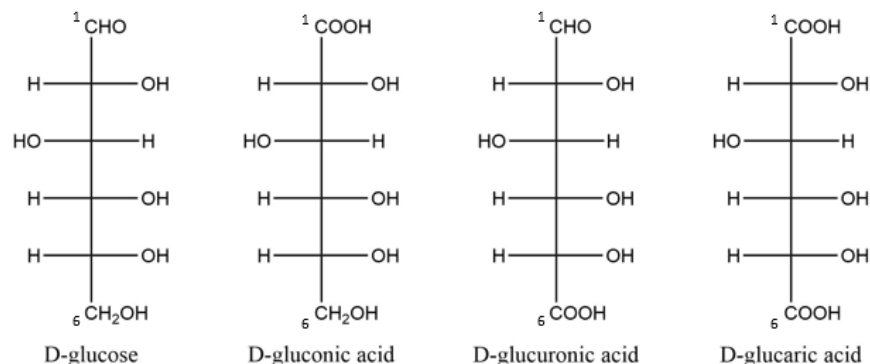
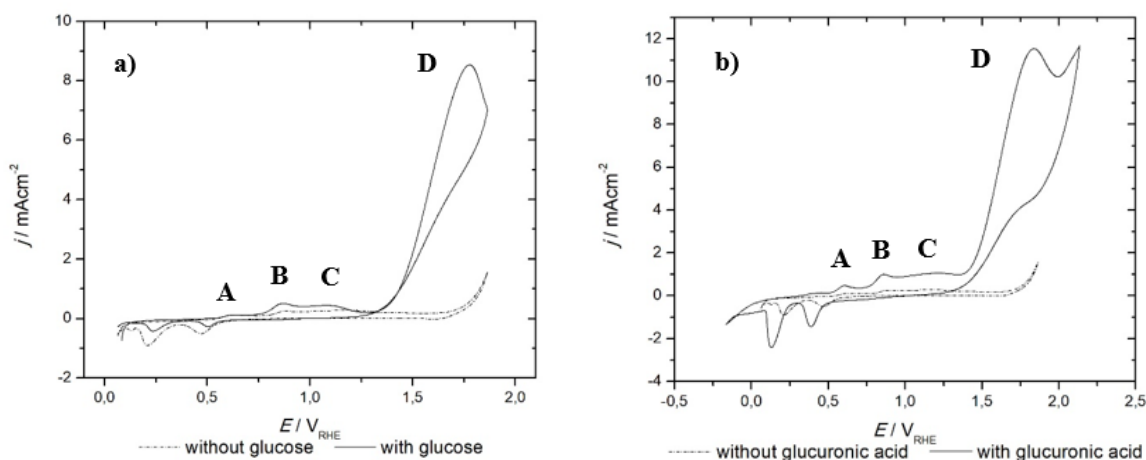


Figure 3.3. Structural formulas of D-glucose and its three derivatives.

The structural formulas of D-glucose (for simplicity we show the open-chain form) and its three derivatives, gluconic, glucuronic and glucaric acid, are shown in Figure 3.3. Gluconic acid is the glucose derivative resulting from the oxidation of the aldehyde group on C1, so it only has one remaining oxidizable functional group, on C6: the hydroxymethyl group; glucuronic acid is the glucose derivative that would result from the oxidation of the hydroxymethyl group on C6, so it also only has one remaining functional group, on C1: the aldehyde group; finally, glucaric acid is the derivative resulting from the complete oxidation of both groups, on C1 and C6, to carboxyl groups, leaving it without directly accessible and oxidizable sites. In the next paragraph, the reactivity of the glucose derivatives was examined by cyclic voltammetry on each of the three electrodes under investigation to understand the reactivity of the single functional groups of glucose in function of the oxidation potential.

Figure 3.4 shows the cyclic voltammograms of copper in the presence of glucose (Figure 3.4(a)), glucuronic acid (Figure 3.4(b)), gluconic acid (Figure 3.4(c)) and glucaric acid (Figure 3.4(d)).



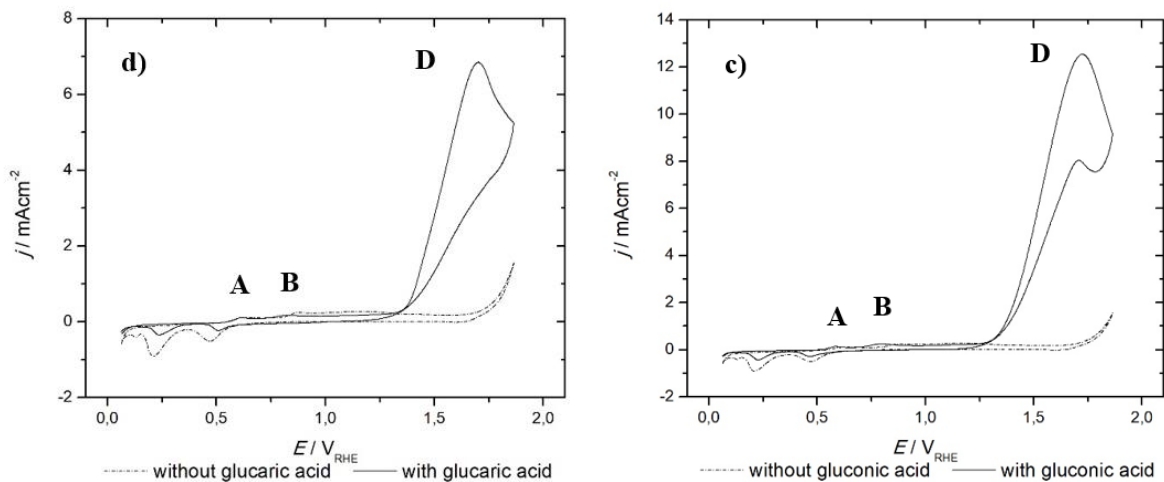


Figure 3.4. Voltammograms of copper electrode in 0.04 M a) glucose, b) glucuronic acid, c) gluconic acid and d) glucuronic acid (solid lines) in alkaline medium (0.1 M NaOH) recorded at 10 mVs^{-1} , at 20°C , compared with the blank solution (dashed lines).

Peaks A and B appear in all the voltammograms of the four solutions, as well as in the blank solution, and correspond to the oxidation of $\text{Cu}(0)$ to $\text{Cu}(\text{I})$ and $\text{Cu}(\text{II})$, respectively [166]. Peak B was already found to increase upon addition of glucose, and the same is true in presence of glucuronic acid. On the other hand, no increase is visible when gluconic and glucuronic acids are added to the solution. This could signify that $\text{Cu}(\text{II})$, which is formed at this oxidation potential, is able to predominantly oxidize the aldehyde group at C1, which is absent for gluconic and glucuronic acid. The same explanation can be given for Peak C that can only be observed in the voltammograms of glucose and glucuronic acid, and is thus expected to originate from the oxidation of the aldehyde group by a soluble species of copper similar to CuO . Based on these first observations, we believe that at peaks B and C, a reaction involving a two-electrons transfer takes place, leading to the oxidation of the C1 aldehyde group into a carboxyl group, generating gluconic acid. Finally, peak D, characterized by a much higher current density, is present in the voltammograms of all the four carbohydrates and thus clearly does not depend on the nature of the available functional groups present in the molecules. This can be explained by assigning this peak to the (undesired) cleavage of the C-C bond, which can possibly take place at this high overpotentials and is independent of the available functional groups. This ultimately leads to the formation of lower carboxylic acids, i. e. formic acid and is therefore undesirable. In conclusion, the oxidation of the hydroxymethyl group on C6 is not visible in the cyclic voltammogram, so we expect copper to selectively oxidize the C1 aldehyde group at low potentials ($0.8 - 1.2 \text{ V}_{\text{RHE}}$).

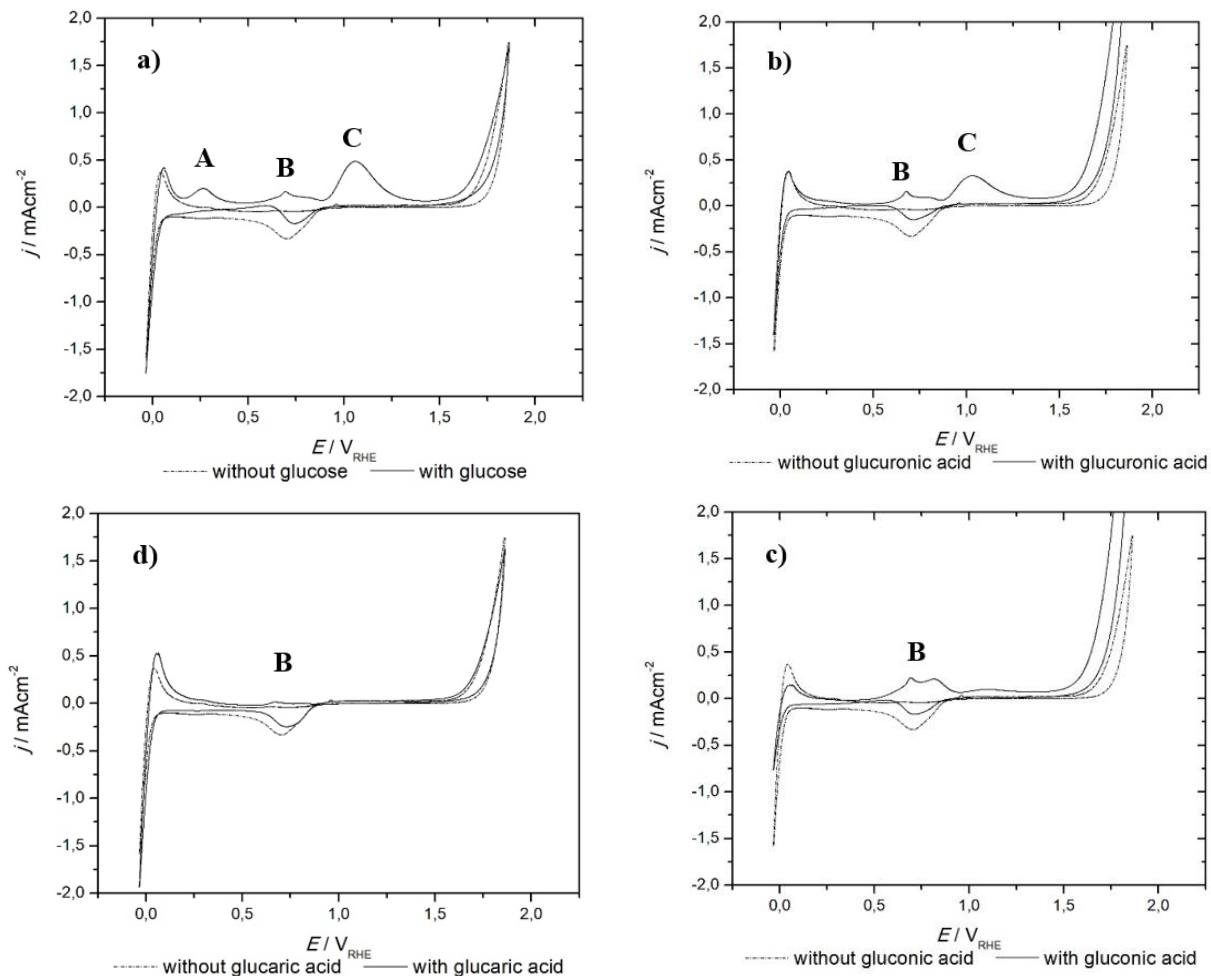


Figure 3.5. Voltammograms of platinum electrode in 0.04 M a) glucose, b) glucuronic acid, c) gluconic acid and d) glucaric acid (solid lines) in alkaline medium (0.1 M NaOH) recorded at 10 mVs^{-1} , at 20°C , compared with the blank solution (dashed lines).

The same study was then performed on platinum (Figure 3.5). None of the glucose oxidation peaks appear in the solution containing glucaric acid, meaning that neither oxidation processes nor cleavage of the C-C bond takes place on the Pt electrode. On the contrary, both peak B and C are present in the solution containing glucuronic acid and a more pronounced peak B appears in the solution containing gluconic acid. This might be explained by stating that peak C, that was assigned by Yei et al. [164] to the oxidation of adsorbed glucose on an already oxidized platinum surface, corresponds mainly to the oxidation of the aldehyde group, present in the glucuronic acid molecule but not in the gluconic one. Peak B, which is present in the voltammograms of both hydrocarbons, and that had been attributed by Yei et al. to the direct oxidation of glucose from the bulk, might be assigned to both oxidations, of the aldehyde and of the hydroxymethyl groups. In conclusion, both the oxidation of the hydroxymethyl group on C6 and of the aldehyde group on C1 are visible in the cyclic voltammogram of platinum that can therefore oxidize C6 at lower overpotentials and C1 at higher overpotentials.

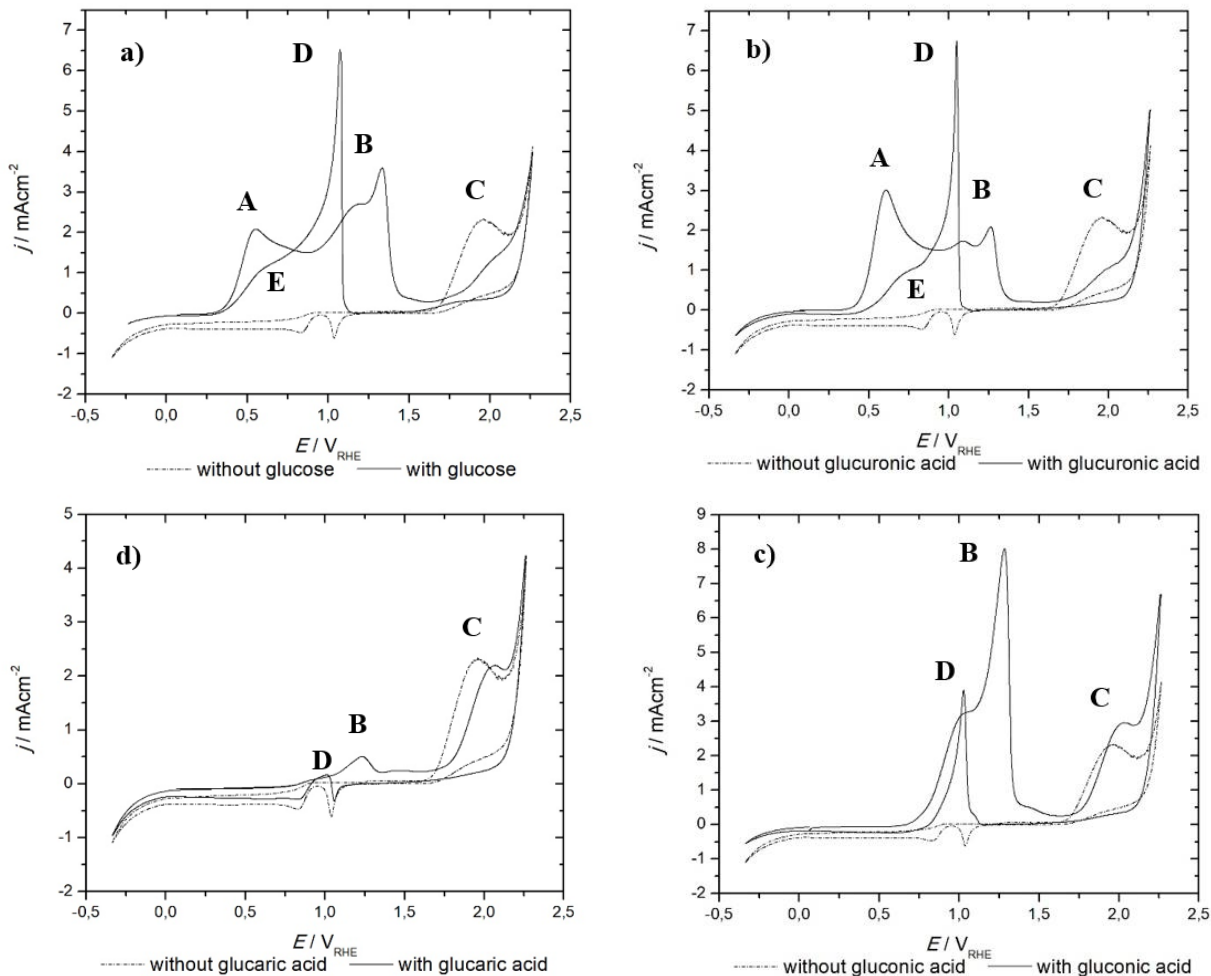


Figure 3.6. Voltammograms of gold electrode in 0.04 M a) glucose, b) glucuronic acid, c) gluconic acid and d) glucaric acid (solid lines) in alkaline medium (0.1 M NaOH) recorded at 10 mVs^{-1} , at 20°C , compared with the blank solution (dashed lines).

Finally, the electrocatalytic activity of gold was also studied in the solutions of the three glucose derivatives (Figure 3.6). Gold, in addition to exhibiting the highest electro-activity (excluding the undesired C-C cleavage at $1.8 \text{ V}_{\text{RHE}}$, which is more pronounced on copper), also shows distinct oxidation peaks for the aldehyde and for the hydroxymethyl groups. It is easy to see that the oxidation processes at $0.55 \text{ V}_{\text{RHE}}$, both in the anodic and in the cathodic scan (peaks A and E, respectively) only take place in the glucose and glucuronic acid solutions. For this reason we believe that they correspond exclusively to the oxidation of the aldehyde group. Peaks B and D, instead, are present in all the solutions. Nevertheless, peak B is significantly higher in the gluconic acid solution, and might thus be related to the oxidation of the hydroxymethyl group. Peak D, which was attributed to the reaction between free O_2^- anions and glucose from the bulk, is slightly less pronounced in the gluconic acid solution, so might be attributed predominantly to the oxidation of the aldehyde group, and in a lesser extent to the hydroxymethyl functional group. In conclusion, as for platinum, both the oxidation of the hydroxymethyl group on C6 and of the aldehyde group on C1 are visible in the cyclic voltammogram of gold that can therefore oxidize C1 at lower overpotentials and C6 at higher overpotentials.

3.3.3 Long-term electrolysis

In order to find the reaction conditions that inhibit the base-catalyzed isomerization of d-glucose to d-fructose and oxidative degradation to lower molar mass carboxylic acids, preliminary experiments were performed in absence of the catalysts at two different temperatures, 5 and 20°C. In absence of the base, glucose conversion did not occur, but in 0.1 M NaOH the sugar was quickly converted into a variety of products, mainly fructose but also gluconic acid, glycolic acid, tartaric acid, glucaric acid, oxalic acid and formic acid. Except for one minor product that remained unidentified, the carboxylic acids were analyzed by HPLC: the selectivity and the conversion of glucose after 65 h of reaction in absence of the catalyst are presented in Table 3.1. The products whose concentration were below 100 ppm are indicated as “traces”.

Table 3.1. Chromatographic analyses of the solutions of D-glucose after 65 h of reaction in absence of the catalyst at 5 and 20°C.

Product	Selectivity (%)	
	5°C	20°C
Glucaric acid	traces	traces
Gluconic acid	10.7	4.6
Formic acid	traces	traces
Oxalic acid	traces	traces
Tartaric acid	traces	2.6
Glycolic acid	traces	6.0
Fructose	79.8	84.5
Glucose conversion (%)	18.4	46.3

In the absence of the catalyst, the predominant product is D-fructose, as a consequence of the NaOH-catalyzed isomerization of d-glucose, and the conversion to this product increases with the reaction temperature. Besides, in accordance with previous studies [152], the aldose-ketose isomerization is accompanied by sugar degradation reactions, which lead to the production of low molar mass carboxylic acids (i. e. formic, oxalic, tartaric and glycolic acids) [152]. The authors [152] reported that the rate and extent of these side reactions are controlled mainly by the type of base cation, base concentration, and temperature. In particular, they indicate alkali and alkaline earth hydroxides as very active catalysts towards the isomerization reaction, but also unselective, promoting the oxidative degradations of glucose, especially when used at high concentration or for increased time and reaction temperature. In accordance with these previous studies, our experiments demonstrate that, at high concentration of the base and ambient temperature, the base-catalyzed isomerization reaction, together with the (thermal) oxidative degradation of glucose, dramatically affect the performance of the electrocatalytic process since they consume almost 50% of the glucose in the solution. Therefore, mild reaction conditions and a low alkali concentration are advisable to limit these undesired side-reactions, which is why all following experiments were performed at 5 °C. In order to determine the electrooxidation products, D-glucose (0.04 M) was oxidized at copper, platinum and gold electrodes in 0.1 M NaOH medium (pH 13) by means of longterm electrolysis (65 h) at a temperature of 5 °C. After electrolysis, samples from the

electrolyzed solutions were analyzed by HPLC (Fig. 3.7 in SI). In all the experiments, the identified products were the same as the ones obtained in absence of the catalyst. The long-term electrolysis of D-glucose on copper was carried out at 0.84, 1.11, and 1.80 V_{RHE} . The selectivity % of the products in the liquid phase after 65 h of reaction at 5°C is given in table 3.2. The products whose concentration is below 100 ppm are indicated as “traces”.

Table 3.2 Chromatographic analyses of the solutions of D-glucose after 65 h electrolysis on Cu at 0.84 V_{RHE} , 1.11 V_{RHE} and 1.80 V_{RHE} at 5°C.

Product	Selectivity (%)		
	$E_{ox}=0.84 V_{RHE}$	$E_{ox}=1.11 V_{RHE}$	$E_{ox}= 1.80 V_{RHE}$
Glucaric acid	38.4	26.8	12.2
Gluconic acid	30.4	44.5	17.8
Formic acid	13.9	15.2	54.2
Oxalic acid	traces	traces	traces
Tartaric acid	traces	traces	traces
Glycolic acid	traces	traces	traces

Although a good selectivity to glucaric acid is achieved at the lower potentials, 0.84 and 1.11 V_{RHE} , the catalyst activity is too low (i.e. limited current density of 0.1 mA cm⁻²) to achieve acceptable conversions (6.4% obtained at 0.84 V_{RHE} and 7.5% at 1.11 V_{RHE}). From the Cyclic Voltammetry study it was concluded that copper, at these potentials, corresponding to peak B and C in Figure 3.2(a), oxidizes the C1 aldehyde group, which is confirmed by the results of the electrolysis. Moreover, the percentage of glucaric acid suggests that, at these potentials, also the C6 hydroxymethyl group is able to complete its oxidation to carboxyl, which was not easily deducible from the CV. Finally, our hypothesis (based on CV combined with a literature study) that cuprite species, formed at 1.80 V_{RHE} , are responsible for the cleavage of the C-C bonds and thus the formation of mainly formic acid is confirmed by the obtained high selectivity (> 50%) to this product at this potential. For gold and platinum a constant decrease of current density was observed during the electrolysis process, which was ascribed to active surface poisoning during the oxidation process. To avoid this poisoning, the electrolysis experiments were carried out using an optimized program of potential which included three potential plateaus, in order to maintain the electrode activity at a sufficient level [88, 159]. The oxidation plateau over 30 s was followed by a reactivation procedure consisting of two short potential pulses (1 s): one at 2.40 V_{RHE} , that allowed to reactivate the electrode by clearing out the poisoning species, and the second at 0 V_{RHE} that served to reduce the metal surface and allowed the adsorption of the organic molecule. These steps were repeated at the length of the experiments until 65 h passed. The electrolysis experiments of D-glucose on platinum were carried out at two oxidation potentials: 0.70 and 1.10 V_{RHE} . The selectivity of the products in the liquid phase after 65 h of reaction at 5°C are given in table 3.3. The products whose concentration is below 100 ppm are indicated as “traces”.

Table 3.3. Chromatographic analyses of the solutions of D-glucose after 65 h electrolysis on Pt at 0.70 V_{RHE} (Potential program 1) and 1.10 V_{RHE} (Potential program 2) at 5°C.

Product	Selectivity (%)	
	Potential program 1 ^[a]	Potential program 2 ^[b]
Glucaric acid	12.6	6.3
Gluconic acid	68.0	78.4
Formic acid	12.0	7.8
Oxalic acid	traces	traces
Tartaric acid	traces	traces
Glycolic acid	traces	traces

[a] Potential program 1: 0.70 V_{RHE} for 30 s, 2.40 V_{RHE} for 1 s, 0 V_{RHE} for 1 s. Initial conditions: 0.04 M D-glucose in 0.1 M NaOH.

[b] Potential program 2: 1.10 V_{RHE} for 30 s, 2.40 V_{RHE} for 1 s, 0 V_{RHE} for 1 s. Initial conditions: 0.04 M D-glucose in 0.1 M NaOH.

For both oxidation potentials, gluconic acid is the main product of the electrochemical reaction as expected based on previous literature. Nevertheless, at the end of the electrolysis at 0.70 V_{RHE} , a higher amount of glucaric acid and a lower amount of gluconic acid were detected, while the total amount of lower molar mass products remained the same. This confirms the results obtained from the cyclic voltammetry study: at this potential, corresponding to peak B in the voltammogram of platinum electrode (Figure 3.5(b)), both oxidations, of the aldehyde and of the hydroxymethyl groups, are promoted so that the intermediate product, d-gluconic acid, is able to further convert into the corresponding aldaric acid more effectively than at higher overpotentials (1.10 V_{RHE} , peak C). The electrolysis of D-glucose on gold were carried out at two oxidation potentials: 0.55 and 1.34 V_{RHE} . The selectivity % of the products in the liquid phase after 65 h of reaction at 5 °C is given in Table 3.4. The products whose concentration is below 100 ppm are indicated as “traces”.

Table 3.4 Chromatographic analyses of the solutions of D-glucose after 65 h electrolysis on Au at 0.55 V_{RHE} (potential program 3) and 1.34 V_{RHE} (potential program 4) at 5°C.

Product	Selectivity (%)	
	Potential program 3 ^[a]	Potential program 4 ^[b]
Glucaric acid	traces	13.5
Gluconic acid	86.6	65.8
Formic acid	6.0	8.8
Oxalic acid	traces	traces
Tartaric acid	traces	traces
Glycolic acid	traces	traces

[a] Potential program 3: 0.55 V_{RHE} for 30 s, 2.40 V_{RHE} for 1 s, 0 V_{RHE} for 1 s. Initial conditions: 0.04 M D-glucose in 0.1 M NaOH.

[b] Potential program 4: 1.34 V_{RHE} for 30 s, 2.40 V_{RHE} for 1 s, 0 V_{RHE} for 1 s. Initial conditions: 0.04 M D-glucose in 0.1 M NaOH

At lower oxidation potential, 0.55 V_{RHE} , glucose converts exclusively to gluconic acid, while at higher potential, 1.34 V_{RHE} , part of the glucose further converts into glucaric acid through oxidation of both, the aldehyde and the hydroxymethyl group. Again, the results of the electrolysis confirm our hypothesis based on the cyclic voltammogram of gold that can therefore oxidize C1 at lower overpotentials, and C1 and C6 at higher overpotentials. As expected, for both oxidation potentials, gluconic acid is the main product of the electrochemical reaction. The electrolysis of D-glucose on Pt and Au over 65 h at 5°C was selective towards D-gluconic acid. The further oxidation of the latter to D-glucaric acid in these conditions was promoted at lower potentials on Pt (0.70 V_{RHE}) and at higher potentials on Au (1.34 V_{RHE}) and, in both cases, was accompanied by the formation of lower molar mass carboxylic acids (mainly formic acid). We suspect that the formation of products in which the molecular structure of d-glucose is disrupted (tartaric, glycolic, formic and oxalic acids), in all the experiments, might also occur due to the formation of small quantities of d-fructose in the reaction system. Indeed, despite minimalizing the chemical side-reactions by optimizing the reaction conditions, 10 to 15% of the total glucose is still isomerized to d-fructose at 5°, which is a reversible process. For this reason, we reported only the products of the electrochemical reaction. A participation of the ketose in the electrochemical reaction, could, indeed, have an impact on the product distribution. Our results demonstrate that the sole electrochemical reaction, performed in a simple H-cell on bare (unmodified) metal electrodes, i.e. platinum and gold, effectively yields gluconic and glucaric acid (more than 80% of the glucose reacted is converted to gluconic and glucaric acid) and that the selectivity towards one product or the other can be controlled by adjusting the electrochemical parameters.

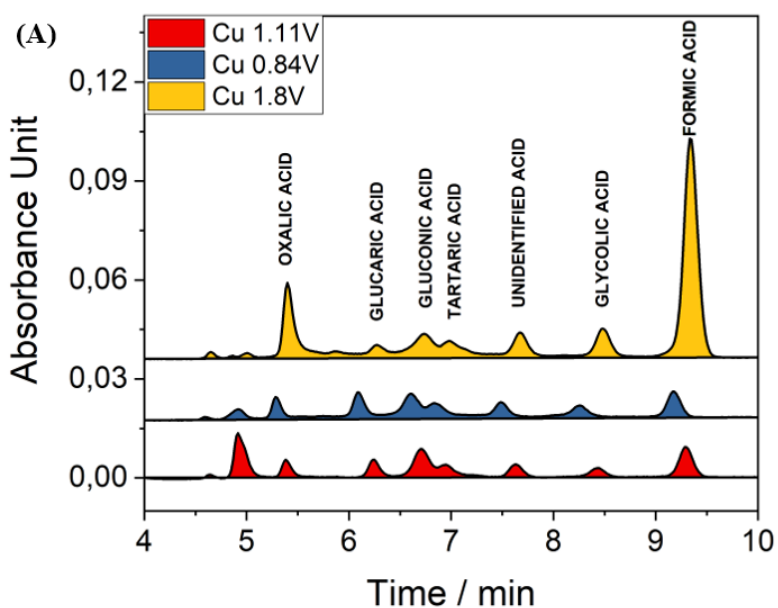
3.4 Conclusions

The results of the cyclic voltammetry study performed in the three solutions containing 0.04 M of gluconic acid, glucuronic acid and glucaric acid in 0.1 M aqueous NaOH are confirmed by the electrolysis: the selectivity of the electrooxidation of D-glucose on copper, platinum and gold is potential-dependent. The potential-reactivity relationship of the functional group is verified for the three catalysts examined in this work. Gold is the catalyst with the highest activity and selectivity to gluconic and glucaric acid. In fact, for this electrode, at low potential, i.e. 0.55 V_{RHE} , a current density of $\sim 2 \text{ mA cm}^{-2}$ is observed in the CV of glucose, and D-gluconic acid is the main product of long term electrolysis (with a selectivity of 86.6 % at 5 °C after 65 h). At higher potentials, i.e. 1.34 V_{RHE} , a current density of $\sim 4 \text{ mA cm}^{-2}$ is observed in the CV of glucose and D-gluconic acid is still the main product but a selectivity of 13.5% of D-glucaric acid shows that the produced gluconic acid undergoes further oxidation. An important impact of the applied potential was also found for the oxidation on platinum. As for gold, the main oxidation product is the intermediate d-gluconic acid, but, in this case, it is at lower potentials, i.e. 0.70 V_{RHE} that it further oxidizes to D-glucaric acid (with a 12.6% of selectivity after 65 h). Copper is the least active catalyst of the ones examined in this work: even though the selectivity to d-glucaric acid is quite high at low potentials (38.4% at 0.84 V_{RHE} and 26.8% at 1.11 V_{RHE}), its activity (current density) is too low and the formation of C-C cleavage products too high. At the highest potential, i. e. 1.80 V_{RHE} , the current density is high but here formic acid becomes the main oxidation product and the selectivity to d-gluconic acid and d-glucaric acid is very low. In conclusion, in this work we developed a method that allows a controlled, selective, oxidation of a highly functionalized compound as D-

glucose, into two value-added products, D-gluconic acid and D-glucaric acid, in batch, using bare metals as heterogeneous catalysts and without making use of any mediator/oxidizing agent/co-oxidant. The relationship between oxidation potential and reactivity of the functional groups demonstrated in this work, together with the findings on the role of the chemical side-reactions competing with the electrochemical process, open the doors to further developments, which are the subject of the next chapters: 1) the optimization of the operating conditions to maximize the selectivity to D-glucaric acid (chapter 4); 2) the up-scaling of the process through catalyst and reactor design (chapter 5).

3.5 Supporting information

HPLC graphs of the solutions of D-glucose after 65h electrolysis on copper, platinum and gold at each oxidation potentials examined in our study.



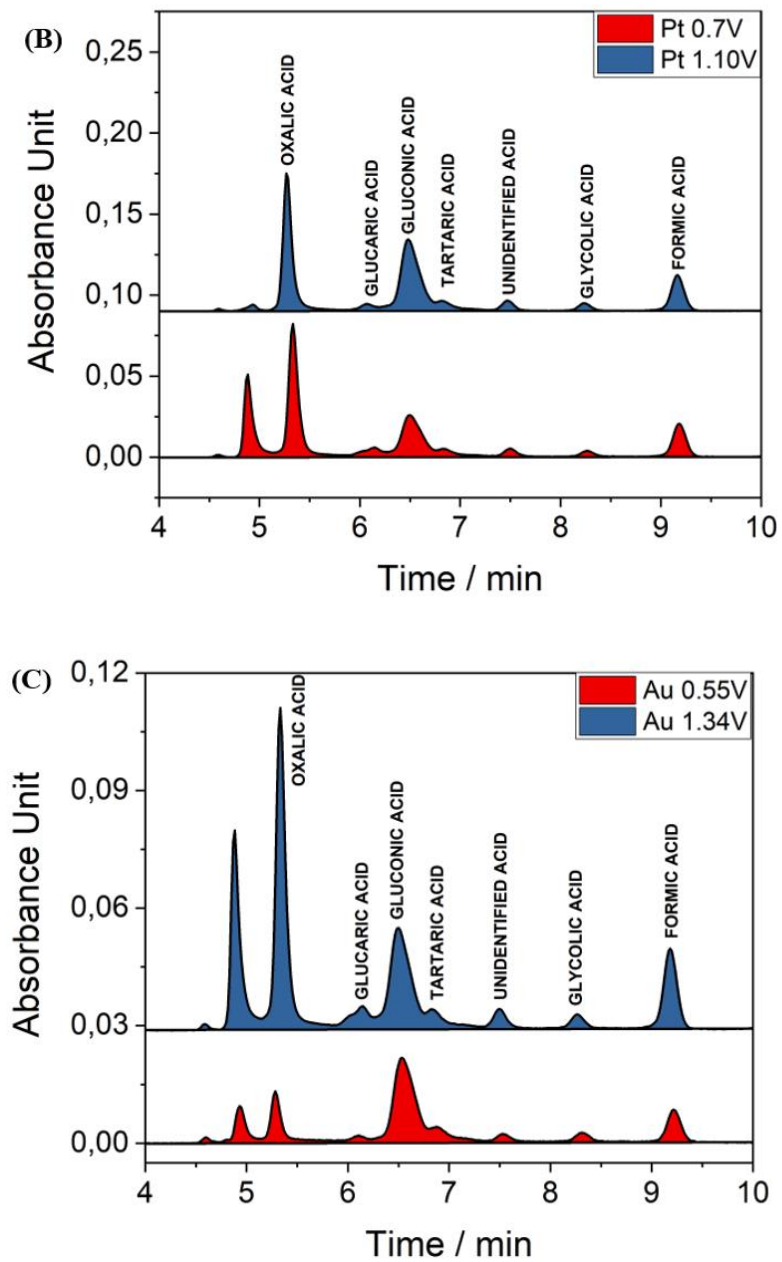


Figure 3.7. HPLC graphs of the reaction solutions after 65h electrolysis on (A) copper, (B) platinum and (C) gold.

Chapter 4

Two-steps synthesis of D-glucaric acid via D-gluconic acid on gold electrode: influence of operational parameters

This chapter has been published as a research paper: [G. Moggia](#), J. Schalck, N. Daems, T. Breugelmans “Two-steps synthesis of D-glucaric acid via D-gluconic acid by electrocatalytic oxidation of D-glucose on gold electrode: Influence of operational parameters”, *Electrochimica Acta*, vol. 374 (2021) special issue: “Electrochemistry towards Excellence (ISE 2020)”, article number: 137852.

4.1 Introduction

It is well known that gold is the most efficient electrocatalyst for glucose oxidation because of its high activity and stability in alkaline media [78]. In the previous chapter, we showed the correlation between oxidation potential and reactivity of the functional groups of the glucose molecule and highlight its role in the determination of the selectivity to gluconic and glucaric acid [168]. It is found that, in all cases, the predominant product is gluconic acid, which could indicate that the formation of glucaric acid is the rate-determining step [86, 88, 158, 159, 169–172]. However, it was also found that, while at low oxidation potential ($\sim 0.6 V_{\text{RHE}}$) the formation of D-gluconic acid is predominant through the oxidation of the aldehyde group on C1, at higher potential ($\sim 1.3 V_{\text{RHE}}$) the oxidation of the hydroxymethyl group on C6, allows the further oxidation to D-glucaric acid [168]. Based on these results, Au appears to be able to oxidize glucose to glucaric acid in two consecutive oxidation steps, each characterized by an oxidation potential: the first step allowing the oxidation of D-glucose to the intermediate D-gluconic acid and the second step completing the oxidation to D-glucaric acid.

Besides the type of metal, the reaction conditions also play an important role in determining the efficiency of this process. In fact, it has been pointed out recently that the kinetics of glucose oxidation are strongly affected by the experimental conditions such as temperature, pH and glucose concentration [173, 174]. First of all, because glucose is consumed by two chemical reactions in alkaline media: i.e. the isomerization of D-glucose into D-fructose and its subsequent thermal oxidative degradation [152], whose kinetics are controlled by thermodynamic parameters and, for which, bases are common homogeneous catalysts [152]. Secondly, the presence of these chemical side-reactions, competing with the electrochemical one, has a dramatic impact on the selectivity of the process. Therefore, in this chapter, we systematically investigate the influence of different operational parameters, i.e., pH, initial substrate concentration, applied potential, reaction temperature and time, on both oxidation steps, to gain a better understanding of the reaction mechanism. Once the optimal operational parameters are selected, the two steps are carried out in cascade, to prove the ability of gold to oxidize glucose to gluconic acid and promote its further oxidation to glucaric acid. A final parameter, often overlooked, is the stability of the catalyst, which needs to be high in order for the catalyst to be effective. This parameter is investigated here by measuring the quantity of Au leaching in the reaction solution and following the eventual loss of electrocatalytic activity during the long-term electrolysis.

4.2 Experimental

4.2.1 Chemicals and reagents

The supporting electrolytes were prepared with ultrapure water (Synergy UV system), sodium carbonate (Sigma-Aldrich, 98%) and sodium hydroxide (Sigma-Aldrich, 98%). Anhydrous D-glucose was purchased from VWR (99.5%), D-gluconic acid potassium salt (98%) and D-saccharic acid potassium salt (98%) from Sigma Aldrich and D-gluconic acid sodium salt (99%) from Acros Organics. All chemicals were used without further modifications.

4.2.2 Electrochemical setup

Electrolysis measurements were conducted in an in-house designed and developed two-compartment thermostated batch cell with a volume of 50 mL at the cathode side and 3.5 mL at

the anode, separated by a Nafion 117 cation-exchange membrane (Fig. 4.1). A cation-exchange membrane was used to allow only protons to move between compartments. Unless otherwise stated, the temperature was set at 20°C.

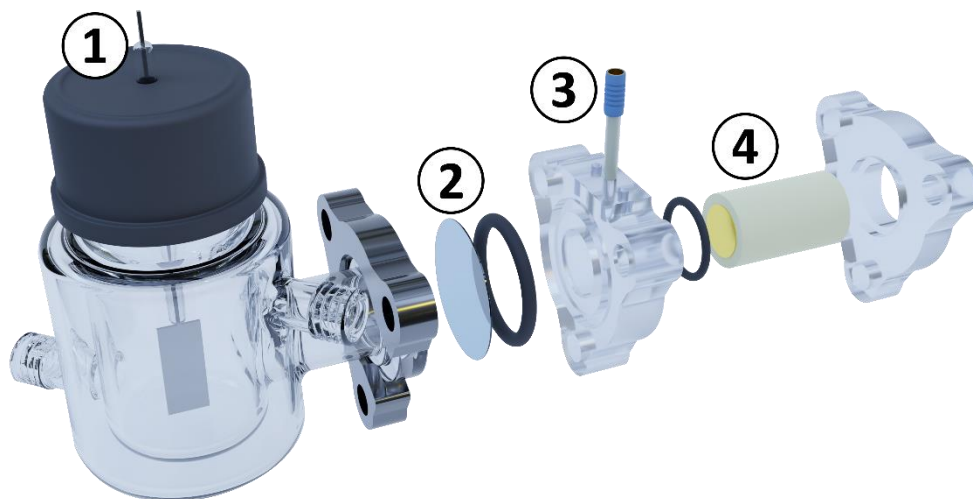


Figure 4.1. Electrochemical set-up designed for the long-term electrolysis: (1) Pt counter electrode (CE), in the cathodic compartment; (2) Nafion membrane; (3) reference electrode (RE) and (4) working electrode (WE), both in the anodic compartment.

A silver-silver chloride electrode (Ag/AgCl) and a platinum plate were used as reference and counter electrode, respectively. A gold (0.08 cm²) RDE purchased from AISI 304, Goodfellow was used as working electrode. The electrochemical instrumentation consisted of a Bio-Logic VSP-300 Potentiostat. All the electrode activities reported are represented with current densities (measured at the beginning of every electrolysis), utilizing the geometric area as active area and with respect to the reversible hydrogen electrode (RHE). The tested potential vs. Ag/AgCl was converted into potential vs. RHE using the Nernst equation (Eq. 14):

$$E_{RHE} = E_{Ag/AgCl} + \ln(10) \cdot \frac{RT}{F} \cdot pH + 0.197 \quad [14]$$

With R being the universal gas constant (8.314472 J K⁻¹ mol⁻¹), F the Faraday constant (96485.332 C mol⁻¹) and T the temperature.

Before every electrochemical measurement, the working electrode surface was carefully polished with aluminum (Φ 1 μm) slurry on a polishing cloth and then sonicated in MilliQ water for 5 min. Finally, the electrode was dried with high purity N₂ (99.999%).

4.2.3 Reaction procedure

The long-term experiments (24 h) were carried out using a technique of potential-programmed electrolysis first developed by the authors Belgsir *et al.* and intended to keep the activity of the Au electrode high for long periods, by avoiding the blockage of the active sites by poisoning species [86]. The optimized potential program included three potential plateaus, in order to ensure an optimal electrocatalytic activity throughout the course of the experiment [88, 159, 168]. The oxidation plateau (30 s) was followed by a reactivation procedure consisting of two short potential pulses (1 s): one at 2.40 V_{RHE}, that allowed to reactivate the electrode by clearing out the poisoning

species, and the second at 0 V_{RHE} that served to reduce the metal surface and allowed the adsorption of the organic molecule (Fig. 4.2). These steps were repeated over the whole course of the experiments. A CV was performed before each electrolysis to select the exact potential corresponding to the oxidation peak. The identification of reaction products was carried out by gas chromatography coupled with mass spectrometry (GC-MS) using an RXI-1ms (Restek) capillary (30 m, 0.32 mm i.d. and 0.25 μm film thickness). The electrolytic solutions were treated before analysis according to the following procedure: (1) the water was removed by lyophilization to leave dry samples of electrolyzed material. (2) This material was then trimethylsilylated using Supelco HMDS+TMCS+pyridine, 3:1:9 (Sylon HTP) Kit, as described in [165]. (3) The resulting materials were then analyzed by GC-MS. Authentic samples of the expected reaction products were also trimethylsilylated and their chromatographic data were used for the product identification. Moreover, to have an additional confirmation of the formation of gluconic and glucaric acid, we performed liquid chromatography mass spectrometry (LC-MS) analysis using an Acquity Arc UHPLC (Waters) fitted with a KC811 Ion-exclusion column (Shodex) and coupled to a QDa single quad mass spectrometer (Waters). Detailed procedure and results of this analysis are reported in the SI (Fig. 4.9 and 4.10), from which it can be concluded that gluconic and glucaric acid are indeed produced.

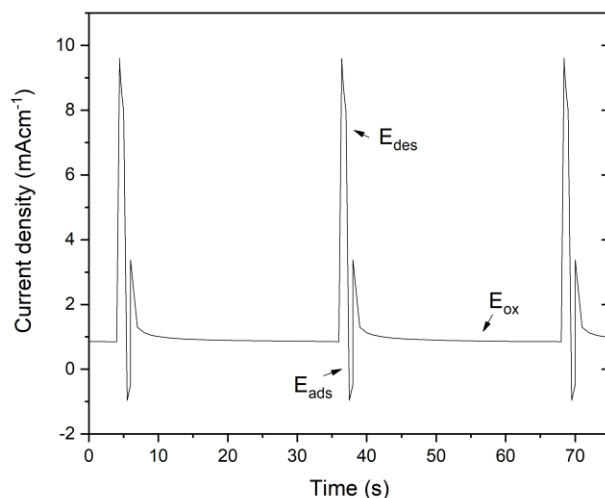


Figure 4.2. The optimized potential program used for the long-term electrolysis (adapted from [86]).

The quantification of the reaction products was performed by HPLC (Alliance 2695, Waters, USA) fitted with a Waters IC-Pak Ion Exclusion column (IC-Pak, Waters, USA) and equipped with a UV detector set at $\lambda=210$ nm and a refractive index (RI) detector. A solution with 0.1% v/v perchloric acid was used as the mobile phase at 1 mL min⁻¹ flow rate. The instrument was calibrated with high purity standards purchased from Sigma Aldrich prior to product analysis. Authentic samples of D-glucose and of the expected reaction products were analyzed and their chromatographic data were used for the identification of the products present after reaction. The aqueous solutions of HPLC references were prepared from standard products >99% pure for gluconic, glucaric, glycolic, tartaric, formic and oxalic acids. The conversion (X_G), productivity (P_i) and selectivity (S_i) were calculated using the following equations (Eqs. 15-17):

$$X_G(\%) = \frac{n_{reagent\ initial} - n_{reagent\ final}}{n_{reagent\ initial}} \cdot 100 \quad [15]$$

$$P_i(\%) = \frac{n_{product\ i}}{S_{catalyst} \cdot t_{electrolysis}} \cdot 100 \quad [16]$$

$$S_i(\%) = \frac{n_{product\ i}}{n_{reagent\ consumed}} \cdot \frac{\mu}{\vartheta} \cdot 100 \quad [17]$$

Where $S_{catalyst}$ and $t_{electrolysis}$ are, respectively, the geometrical area of the catalyst (in cm^2) and the electrolysis time (in h). The symbols μ and δ in Eq. 4 represent the stoichiometric coefficients of the reaction. All the measurements were performed three times and the errors measured on the values of conversion, selectivity and productivity were, in all cases, lower than 3%. The analysis of the gas phase was performed by Gas Chromatography (GC): no gaseous product was formed during the electrolysis. The pH was measured at the end of each electrolysis to check its possible development: in all experiments, no evident pH change was detected.

4.2.4 Catalyst stability

For the study of the catalyst stability, two deactivation parameters were analyzed in this work: dissolution and loss in current response. To determine the quantity of catalyst leaching, samples of the reaction solution, taken after prolonged electrolysis time (24h) were analyzed using an Agilent 7500 series inductively coupled plasma mass spectrometry (ICP-MS). The samples were diluted to a 1:20 ratio in a 2% HCl matrix and a calibration curve was fitted from 1 to 1000 ppb to determine the sample Au contents. Standards for gold were purchased from Alfa Aesar. In addition, the current density was monitored during the course of all the chronoamperometry experiments to detect any signs of activity loss. The results of cyclic voltammetry performed in a fresh solution before and after the prolonged electrolysis were compared to detect possible losses in catalyst activity.

4.3 Results and discussion

The anodic reactions taking place at the Au working electrode, leading to the formation of D-gluconic acid (first reaction) and D-glucaric acid (second reaction) are illustrated in Fig. 4.3 and reported in Eq. 18-19 in SI. In the cathodic compartment, at the Pt counter electrode, the hydrogen evolution reaction (HER) takes place (Eq. 20 in SI) [175].

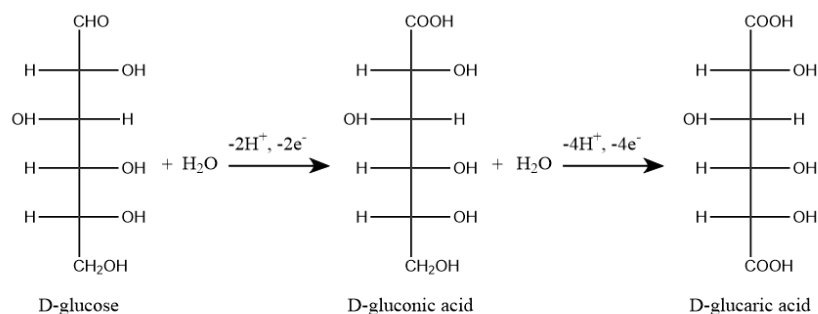


Figure 4.3. The oxidation of D-glucose to D-gluconic acid in two-steps (for simplicity D-glucose is represented in the open-chain form).

In the following paragraphs, we analyze single-variably the influence of pH, substrate concentration, applied potential, temperature and reaction time on the selectivity to D-gluconic acid (first process) and to D-glucaric acid (second process) by measuring the products of long-term electrolysis. To do so, long-term electrolysis measurements were carried out under different operating conditions (i.e., pH, substrate concentration, cell voltage, temperature and reaction time) in the 3.5 mL anodic compartment.

4.3.1 The oxidation of glucose to gluconic acid: impact of the operational parameters

pH

The D-glucose oxidation was studied under alkaline conditions, in a pH range between 11 and 13. In fact, it is well established that alkaline conditions are required for glucose electrooxidation since, at high pH, D-glucose is transformed into β -D-glucopyranose, its most active anomeric form [88, 159]. For this reason, only alkaline pH conditions were considered in this work. However, strong bases (like alkali bases, such as NaOH) also initiate glucose isomerization (production of D-fructose) and oxidative degradation reactions (production of low molar mass carboxylic acids i.e. formic and oxalic acid), which would result in a reduced glucose availability for the electrochemical oxidation [152]. For this reason, a weaker base, Na_2CO_3 , was also used in the pH range between 11 and 12 and the results were compared with those obtained at higher pH using NaOH as electrolyte.

The influence of the pH (11-13) on the 2-electron oxidation of glucose is represented in Fig. 4.4 (selectivity) and Table 4.1 (conversion and productivity). The results confirm our initial idea that the pH has a strong impact on the products' distribution: electrochemical product (gluconic acid) vs. chemical degradation products (fructose and small molar mass carboxylic acids). When a strong alkaline solution (high pH) is used as electrolyte, the selectivity to gluconic acid remains below 50%, while the selectivity to fructose goes up to 50% (Fig. 4.4). On the contrary, when a less strong base as Na_2CO_3 is used as electrolyte (lower pH), D-gluconic acid becomes the main product, reaching a selectivity up to 90% for pH 11.3 (Fig. 4.4). At the lowest concentration of Na_2CO_3 (0.01 M, pH 11.0), glucose conversion is very low due to both the poor conductivity of the solution and the small amount of glucose that is converted into active β -D-glucopyranose at this "low" pH (Table 4.1). Increasing the concentration of the base, Na_2CO_3 , from 0.01 M (pH

11.0) to 0.1 M (pH 11.3), results in a higher amount of D-glucose that is converted into D-gluconic acid, as evidenced by the increase of glucose conversion and gluconic acid productivity (Table 4.1). However, a further increase to 1.0 M Na_2CO_3 (pH 11.4) causes a decrease of the selectivity to D-gluconic acid until a value of 53.6%, indicating that isomerization and degradation reactions are taking over due to the high concentration of the base, which is a catalyst for these reactions. Furthermore, it is interesting to note that, while initially D-glucose conversion and D-gluconic acid productivity increase with the concentration of Na_2CO_3 (from, respectively, 5.7% and 1.1 $\text{mmol cm}^{-2} \text{h}^{-1}$ at 0.01 M, to 23.3% and 4.7 $\text{mmol cm}^{-2} \text{h}^{-1}$ at 0.1 M), for concentrations >0.5 M, both parameters drop to lower values (Table 1). The same trend is followed by the current density (Fig. 4.11 in SI). One possible explanation is that higher concentrations of electrolyte (Na_2CO_3 or NaOH) provide more reacting hydroxyl (OH^-) species, which are essential for glucose oxidation [89, 99, 173, 176, 177], thus enhancing the reaction kinetic. But, as pointed out by the authors Holade *et al.*, a too high concentration of electrolyte might decrease the number of active sites available for glucose adsorption, thus diminishing the cell performance [173]. This behavior of the current density with the electrolyte concentration (pH) had also been observed by the authors Tung *et al.* who attributed it to the passivation of the electrode by gold oxides [178]. From this analysis, we could conclude that, for this reaction step, Na_2CO_3 in concentrations of ca. 0.1 M, corresponding to a pH of ca 11.3, yields the highest selectivity and productivity (Table 4.1). All further experiments starting from glucose have been, therefore, conducted using 0.1 M Na_2CO_3 as electrolyte.

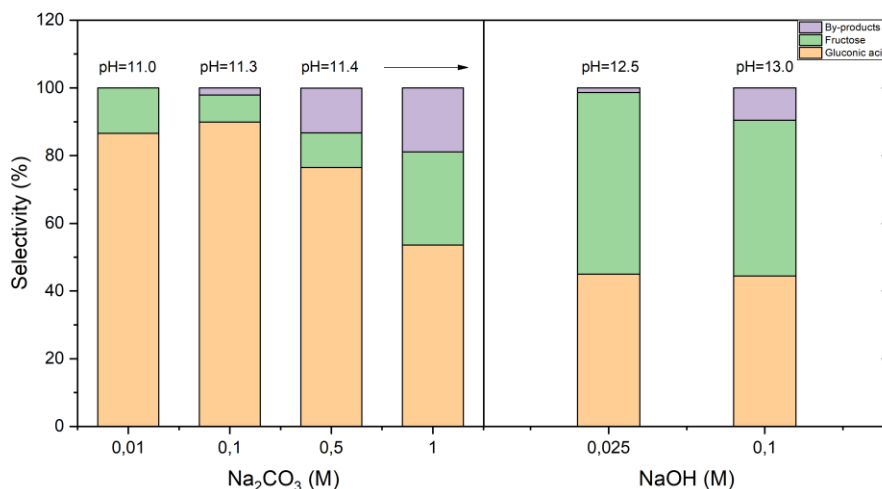


Figure 4.4. Influence of the pH on the selectivity to D-gluconic acid (orange), D-fructose (green) and by-products (violet) for the oxidation of 0.04 M D-glucose on Au at 20°C after 24 h using the optimized potential program as described in 4.2.3.

Table 4.1. Summary of the results obtained in the glucose electrooxidation to gluconic acid in function of the pH.

Operating conditions					Catalytic results		
t ^a (h)	C _G ^b (M)	C _E ^c (M)	pH	T ^d (°C)	X _G ^e (%)	S _{GO} ^f (%)	P _{GO} ^g (mmol cm ⁻² h ⁻¹)
24	0.04	Na₂CO₃ 0.01	11.0	20	5.7	86.6	1.1
24	0.04	Na₂CO₃ 0.1	11.3	20	23.3	90.8	4.7
24	0.04	Na₂CO₃ 0.5	11.4	20	22.0	76.5	3.6
24	0.04	Na₂CO₃ 1.0	11.4	20	17.2	53.6	1.9
24	0.04	NaOH 0.025	12.5	20	16.7	45.0	1.6
24	0.04	NaOH 0.1	13.0	20	45.6	44.4	4.5

^a Reaction time, h; ^b Substrate (glucose) initial concentration, M; ^c Electrolyte concentration, M; ^d Reaction temperature, °C; ^e Glucose conversion, %; ^f Selectivity to gluconic acid, %; ^g Productivity of gluconic acid, mmol cm⁻² h⁻¹.

D-glucose initial concentration

The initial D-glucose concentration was varied in the range 0.01-0.16 M. Fig. 4.5 shows the current density response to the variation of glucose concentration from 0.01 M to 0.16 M as derived from the peak potentials in the respective CV curves. The electrocatalytic activity values strongly increased with the initial D-glucose concentration up to 0.1 M, where the further increments get smaller and smaller, until a plateau is reached for concentrations >0.1 M (Fig. 4.5). The initial activity enhancement can simply be attributed to the presence of an increased reactant availability at the active surface and thus a decrease in the mass transfer limitations [178]. After the maximum performance is reached, further increase of the reactant concentration becomes ineffective. This saturation effect has been previously observed by the authors Kokoh *et al.* who studied the influence of the concentration of glucose (from 1 mM to 50 mM) on the reaction mechanism and kinetic on a pure gold anode by cyclic voltammetry [88]. Indeed, they found that, at low initial concentration of glucose, the reaction had order 1, while, at higher concentration, a saturation mechanism takes place, dropping the order to 0 [88]. There are simply not enough Au sites available to accommodate the growing number of glucose molecules, explaining this stagnation. The results of 24 h electrolysis experiments at various D-glucose initial concentrations are shown in Fig. 4.6 (selectivity) and Table 4.2 (conversion and productivity). It is observed that, at low initial concentration of glucose (0.01 M), the productivity of the electrochemical product, D-gluconic acid, is low due to the mass transfer limitation (Table 4.2) and so is its selectivity. Due to the presence, in this system, of homogeneous side-reactions that compete with the electrochemical (heterogeneous) process, when increasing the initial concentration of glucose, a greater amount of reactant reaches the electrode surface, thus increasing the selectivity towards gluconic acid (Fig. 4.6). Nevertheless, as for the current density, after a maximum value of 92.0% is reached at 0.07 M initial D-glucose, a decrease in cell performance is observed for concentrations >0.1 M, until a selectivity as low as 60.7% is obtained at 0.16 M (Fig. 4.6). At the same time, glucose conversion and gluconic acid productivity also decrease, while the amount of fructose formed keeps increasing with the available amount of glucose in the solution (Table 4.2). Three possible explanations have been given for this behavior: 1) at high concentration of glucose, the coverage rate of the electrode surface is so high that the catalyst surface rapidly becomes saturated.

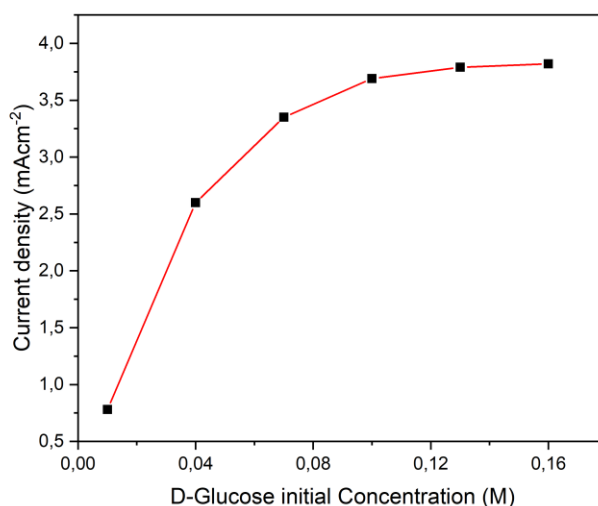


Figure 4.5. Current density response to the variation of initial glucose concentration derived from the respective cyclic voltammogram at 10 mVs^{-1} (Na_2CO_3 0.1 M).

Under these conditions, the hydroxyl species cannot adsorb on the active sites, which diminishes the kinetics of the electrochemical reaction [173]; 2) the second explanation is based on the fact that an increase of glucose concentration increases the viscosity of the solution, which hinders the mass transfer towards the Au active sites, required for the heterogeneous, electrochemical reaction. It must be pointed out that a decrease in cell performance at high concentrations has been observed for a wide range of systems of other organic molecules even when a flow cell is used [179–182]. Glucose, in particular, has a rather low diffusivity ($D=6.9 \times 10^{-10} \text{ m}^2 \text{ s}^{-1}$) compared to other, smaller, organic molecules like, for example, formic acid, which has a diffusion coefficient of ca $14.7 \times 10^{-10} \text{ m}^2 \text{ s}^{-1}$ [183–185]. So, especially in batch, it becomes clear why the system is subjected to such mass transfer limitations; 3) the third, and last, explanation is based on the fact that more fructose is also formed at higher glucose concentrations, which may occupy the Au active sites as such impeding adsorption of glucose [164].

From this section we could conclude that the initial glucose concentration is best taken in between 0.04-0.1 M, as this yields the best performance in terms of selectivity (>90%) and productivity (> $4.7 \text{ mmol cm}^{-2} \text{ h}^{-1}$) (Table 4.2). For this reason, we chose an initial concentration of glucose of 0.04 M for all remaining experiments.

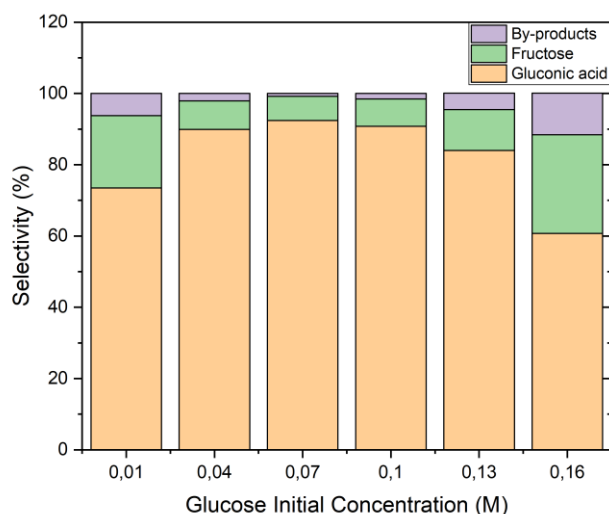


Figure 4.6. Selectivity to D-gluconic acid (orange), D-fructose (green) and by-products (violet) in dependence of initial amount of glucose. Reaction conditions: 0.1 M Na₂CO₃, 20°C, pH 11.3, 24h, using the optimized potential program as described in 4.2.3.

Table 4.2. Summary of the results obtained in the glucose electrooxidation to gluconic acid in function of the initial concentration of glucose.

Operating conditions					Catalytic results		
t ^a (h)	C _G ^b (M)	C _E ^c (M)	pH	T ^d (°C)	X _G ^e (%)	S _{GO} ^f (%)	P _{GO} ^g (mmol cm ⁻² h ⁻¹)
24	0.01	Na ₂ CO ₃ 0.1	11.3	20	43.3	73.5	1.8
24	0.04	Na ₂ CO ₃ 0.1	11.3	20	23.3	90.8	4.7
24	0.07	Na ₂ CO ₃ 0.1	11.3	20	17.6	92.0	6.2
24	0.1	Na ₂ CO ₃ 0.1	11.3	20	15.5	90.8	7.6
24	0.13	Na ₂ CO ₃ 0.1	11.3	20	10.8	84.0	6.4
24	0.16	Na ₂ CO ₃ 0.1	11.3	20	4.7	60.7	2.4

^a Reaction time, h. ^b Substrate (glucose) initial concentration, M. ^c Electrolyte concentration, M. ^d Reaction temperature, °C. ^e Glucose conversion, %. ^f Selectivity to gluconic acid, %. ^g Productivity of gluconic acid, mmol cm⁻² h⁻¹.

Reaction temperature

The influence of the reaction temperature on D-glucose oxidation to D-gluconic acid was studied in the range 5-50°C. Based on the electrocatalytic activity values derived from the voltammograms recorded at different temperatures, an Arrhenius plot was established for T>20°C (Fig. 4.12 in SI). The apparent activation energy was calculated to be 19.1 kJ mol⁻¹ (using Eq. 21 in SI), confirming that the electrochemical process is dominated by the diffusion of the reactants and/or products, with a substantial contribution from adsorption [173, 186, 187].

The obtained values of selectivity are shown in Fig. 4.7, while the values of conversion and productivity are given in Table 4.3. As expected, the selectivity to D-gluconic acid decreases with the reaction temperature, with the maximum of 97.6% reached at 5°C. In fact, higher temperatures promote the isomerization to fructose and the oxidative degradation reactions leading to low molar mass carboxylic acids (glycolic, oxalic, formic and tartaric acid), thus decreasing the selectivity to the electrochemical process. Moreover, while below 40°C the selectivity decreases only slightly with the temperature, remaining over 80%, at 50°C, in agreement with literature, the solution degrades rapidly assuming a yellowish color [164, 188] and the selectivity to gluconic acid drops to a value of ca 60% (Fig. 4.7).

As for conversion, productivity (Table 4.3) and current density (results not shown) we observe slightly higher values at 5 and 10 °C compared to those at 20°C, and then again, an increase for $T > 20$ °C, due to the increased reaction kinetics. A maximum conversion of 48.5% is reached at 50°C, with as unfortunate downside that gluconic acid selectivity and productivity drop dramatically due to the above-mentioned rapid degradation of the solution. In fact, it seems that, from a certain point, by increasing the temperature, the rate of conversion of glucose into fructose increases so rapidly that it overtakes the electrochemical reaction (Table 4.3). This fluctuating behavior of the current density had been already observed in a previous study by the authors Yei *et al.*, who interpreted it assuming an inhibiting effect on the electrocatalytic activity caused by the formation of fructose, that starts being pronounced above 20 °C [164]. They concluded that the real reactivity of glucose can only be observed at low temperatures (below 10 °C), where the rate of isomerization to fructose is negligible [164]. Then, above 20°C, the temperature raise affects the kinetics of the electrocatalytic reaction more strongly, resulting in an activity enhancement (Fig. 4.12 in SI) and increase of the conversion rate (Table 4.3). Our results seem to confirm these assumptions: at 5 °C, glucose conversion is 25 % but fructose has not formed, so the selectivity to gluconic acid is maximum (97.6 %). Instead, at 20 °C, despite the quantity of glucose converted is similar (23.3%), a greater amount of it is transformed to fructose which inhibits the productivity of gluconic acid (Table 4.3). Then, above 20 °C, both conversion and productivity increase again because of the improved reaction kinetics.

From this analysis, we concluded that, if the aim is to obtain the maximum selectivity, the best temperature to work at is 5 °C, but to have the highest conversion rate and the highest productivity of gluconic acid, albeit losing a bit of selectivity, then 40 °C is the optimum. For our next experiments, we decided to work at ambient temperature, 20 °C.

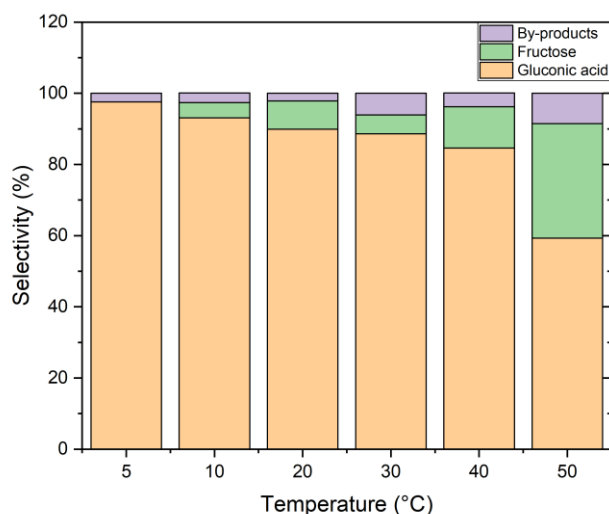


Figure 4.7. Dependence of the selectivity to D-gluconic acid (orange), D-fructose (green) and by-products (violet) with the reaction temperature for the oxidation of 0.04 M D-glucose in 0.1 M Na_2CO_3 for 24 h using the optimized potential program as described in 4.2.3.

Table 4.3. Summary of the results obtained in the glucose electrooxidation to gluconic acid in function of the reaction temperature.

Operating conditions					Catalytic results		
t^a (h)	C_G^b (M)	C_E^c (M)	pH	T^d (°C)	X_G^e (%)	S_{GO}^f (%)	P_{GO}^g (mmol $\text{cm}^{-2} \text{h}^{-1}$)
24	0.04	Na_2CO_3 0.1	11.3	5	25.0	97.6	5.4
24	0.04	Na_2CO_3 0.1	11.3	10	27.0	93.1	5.3
24	0.04	Na_2CO_3 0.1	11.3	20	23.3	90.8	4.7
24	0.04	Na_2CO_3 0.1	11.3	30	34.5	88.6	6.5
24	0.04	Na_2CO_3 0.1	11.3	40	41.9	84.6	7.6
24	0.04	Na_2CO_3 0.1	11.3	50	48.5	59.3	6.1

^a Reaction time, h. ^b Substrate (glucose) initial concentration, M. ^c Electrolyte concentration, M. ^d Reaction temperature, °C. ^e Glucose conversion, %. ^f Selectivity to gluconic acid, %. ^g Productivity of gluconic acid, $\text{mmol cm}^{-2} \text{h}^{-1}$.

Oxidation potential and reaction time

Next, the analysis of the impact of the applied potential on the selectivity of the reaction was conducted using the optimized potential program as described in 4.2.3. The results (shown in Table 4.8. in the SI) highlight that, whatever potential is chosen, as long as it stays within the oxidation peak, the selectivity remains about the same. It was thus concluded that this parameter does not have a significant impact on the outcome of the first reaction step.

Finally, the impact of the reaction time was investigated and, for this, the Au catalyst was tested for prolonged reaction times using the optimized potential program as described in 4.2.3) to evaluate the evolution of the products over time and to assess the deactivation behavior. Conversion and selectivity to gluconic acid as a function of time are shown in Fig. 4.8 in while the

productivity values are reported in Table 4.4. The maximum selectivity to gluconic acid (ca. 98%) was obtained for low reaction times (6 h). After 12 h, the selectivity decreases to ca. 90%, where it remains constant for the remainder of the electrolysis experiment. The cause for this higher selectivity at short reaction times could either be attributed to the fact that fructose and by-products are not formed yet at this point due to the slower kinetics of the catalytic reactions or simply because their presence cannot be detected by the analytical instrumentation as these compounds have a higher detection limit (~10 ppm).

Glucose conversion increases continuously with time (Fig. 4.8), although, a slight reduction of the conversion rate discovered after 24 h of electrolysis was attributed to the limited mass transfer in the batch cell due to the reduced concentration of glucose in the solution at this point. A logarithmic fit was calculated for the values of glucose conversion and the resulting curve is shown in Fig. 4.8. In an optimal process, the electrolysis should be stopped after 18-24 h because, in this range, a good value of conversion is reached (~20 %) and the conversion rate is still high.

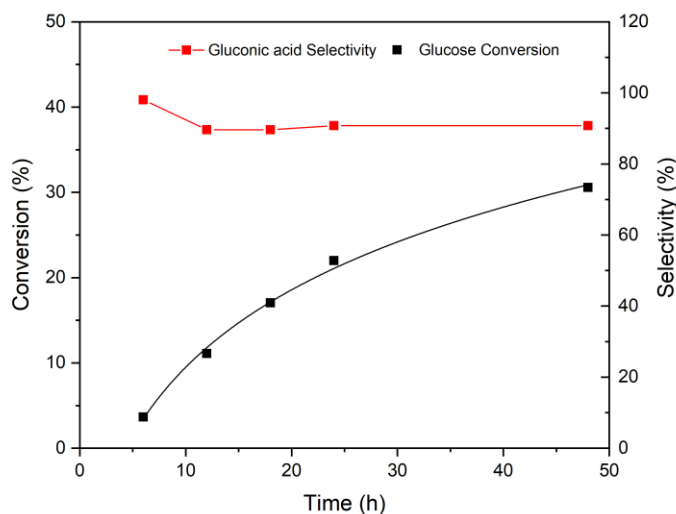


Figure 4.8. Variation with the reaction time of glucose conversion (black line) and gluconic acid selectivity (red line).

The LC-MS Chromatogram of the product solution of 24 h electrolysis of a starting solution 0.04 M D-glucose in 0.1 M Na_2CO_3 at 20 °C is reported in Fig. 4.13 of the SI showing the formation of gluconic acid and no trace of glucaric acid, proving that gluconic acid is the product of the electrolysis of glucose. The HPLC spectrum with all the products resulting from the electrolysis of glucose at 0.6 V_{RHE} is reported in Fig. 4.14(a) in the SI.

Table 4.4. Summary of the results obtained in the glucose electrooxidation to gluconic acid in function of the reaction time.

Operating conditions					Catalytic results		
t^a (h)	C_G^b (M)	C_E^c (M)	pH	T^d (°C)	X_G^e (%)	S_{GO}^f (%)	P_{GO}^g (mmol cm⁻² h⁻¹)
6	0.04	Na ₂ CO ₃ 0.1	11.3	20	3.6	98.1	0.8
12	0.04	Na ₂ CO ₃ 0.1	11.3	20	11.1	89.6	2.1
18	0.04	Na ₂ CO ₃ 0.1	11.3	20	17.0	89.6	3.1
24	0.04	Na ₂ CO ₃ 0.1	11.3	20	23.3	90.8	4.7
48	0.04	Na ₂ CO ₃ 0.1	11.3	20	30.6	90.0	6.1

^a Reaction time, h. ^b Substrate (glucose) initial concentration, M. ^c Electrolyte concentration, M. ^d Reaction temperature, °C. ^e Glucose conversion, %. ^f Selectivity to gluconic acid, %. ^g Productivity of gluconic acid, mmol cm⁻² h⁻¹.

4.3.2 The oxidation of gluconic acid to glucaric acid: impact of the operational parameters

As done for the first oxidation step, we also investigated the impact of the operational parameters (pH, gluconic acid initial concentration, reaction temperature and time) on the performance of the second oxidation reaction (results shown in Table 4.5). In this case, contrary to the oxidation of glucose, gluconic acid is stable in alkaline solution, so, it does not undergo degradation.

Table 4.5. Summary of the results obtained in the gluconic acid electrooxidation to glucaric acid, at 1.3 V_{RHE}, in function of pH, gluconic acid initial concentration, reaction temperature and time.

Operating conditions					Catalytic results		
t^a (h)	C_{GO}^b (M)	C_E^c (M)	pH	T^d (°C)	X_{GO}^e (%)	S_{GA}^f (%)	P_{GA}^g (mmol cm⁻² h⁻¹)
24	0.04	Na ₂ CO ₃ 0.1	11.5	20	2.6	66.3	0.4
24	0.04	NaOH 0.025	12.5	20	4.1	72.3	0.6
24	0.04	NaOH 0.1	13.0	20	7.4	60.4	0.9
24	0.04	NaOH 0.8	13.5	20	15.6	60.6	1.9
24	0.01	NaOH 0.025	12.5	20	21.0	75.2	0.8
24	0.07	NaOH 0.025	12.5	20	1.9	72.3	0.5
24	0.04	NaOH 0.025	12.5	10	4.5	76.1	0.7
24	0.04	NaOH 0.025	12.5	40	6.4	72.7	0.9
6	0.04	NaOH 0.025	12.5	20	0.8	64.1	0.1
18	0.04	NaOH 0.025	12.5	20	3.0	73.0	0.4

^a Reaction time, h. ^b Substrate (gluconic acid) initial concentration, M. ^c Electrolyte concentration, M. ^d Reaction temperature, °C. ^e Gluconic acid conversion, %. ^f Selectivity to glucaric acid, %. ^g Productivity of glucaric acid, mmol cm⁻² h⁻¹.

It was found that none of the operational parameters examined had an appreciable impact on the selectivity of this process. The only observable trend is an increase of gluconic acid conversion with the pH and with the reaction temperature (Table 4.5). It is possible that, as for the oxidation of glucose to gluconic acid, the presence of more reacting hydroxyl (OH^-) species and higher temperatures enhance the reaction kinetics, thus increasing the conversion rate. However, while, on one hand, pH, substrate initial concentration, reaction temperature and time had no substantial effect (Table 4.5), the applied potential seems to play an important role in the determination of the products' distribution, and thus on the selectivity (Table 4.6). In fact, the selectivity to glucaric acid varies from a minimum of 64.9% obtained at 1.4 V_{RHE} , to a maximum of 89.5% reached at 1.1 V_{RHE} . It has been reported in literature that, depending on the applied potential, three species of Au are involved in the oxidation of glucose in alkaline media [89, 99, 173, 176, 177]: Au metal, around 0.6 V_{RHE} (peak 1 in Fig. 4.15(a) in SI), which, in our work, is responsible for the oxidation of glucose to gluconic acid; $\text{Au}(\text{OH})_x$, around 1.1 V_{RHE} (left shoulder of peak 2 in Fig. 4.15(a) and (b) in SI); and AuO_x , around 1.3 V_{RHE} (peak 2 in Fig. 4.15(a) and (b) in SI). The authors Holade *et al.* performed chronoamperometry experiments coupled with FTIR spectroscopy and chromatographic analysis of the products to monitor glucose electrooxidation reaction at various electrode potentials, from 0.2 to 1.4 V_{RHE} [173]. Surprisingly, although the CA results changed from one potential to another, they did not report any appreciable difference in the distribution of the products [173]. In our case, for the oxidation of gluconic acid, the applied potential for the electrolysis does have an impact on the products' distribution. We believe that this variation is ascribed to distinct reaction mechanisms taking place at the different Au oxide species. Similarly, also Belgsir *et al.* reported a variation of the product distribution (selectivity) with the potential at which the glucose oxidation reaction was conducted (0.5, 0.6, and 0.9 V_{RHE}) for a system consisting of Au modified with Pb adatoms [86].

Table 4.6. Summary of the results obtained in the gluconic acid electrooxidation to glucaric acid in function of the applied potential.

Operating conditions						Catalytic results		
t^a (h)	C_{GO}^b (M)	C_E^c (M)	pH	T^d (°C)	E^e (V_{RHE})	X_{GO}^f (%)	S_{GA}^g (%)	P_{GA}^h ($\text{mmol cm}^{-2} \text{h}^{-1}$)
24	0.04	NaOH 0.025	12.5	20	1.0	3.2	84.6	0.6
24	0.04	NaOH 0.025	12.5	20	1.1	4.6	89.5	0.8
24	0.04	NaOH 0.025	12.5	20	1.2	4.9	82.0	0.8
24	0.04	NaOH 0.025	12.5	20	1.3	4.1	72.3	0.6
24	0.04	NaOH 0.025	12.5	20	1.4	3.2	64.9	0.4

^a Reaction time, h. ^b Substrate (gluconic acid) initial concentration, M. ^c Electrolyte concentration, M. ^d Reaction temperature, °C. ^e Oxidation potential, V_{RHE} . ^f Gluconic acid conversion, %. ^g Selectivity to glucaric acid, %. ^h Productivity of glucaric acid, $\text{mmol cm}^{-2} \text{h}^{-1}$.

However, as it is evidenced by the very low values of conversion obtained in all experiments, independent on the reaction conditions/time (Table 4.6), for this reaction step there was a limit on the maximum achievable concentration of glucaric acid, which was rather low (~ 1.2 mM). In addition to this, we noticed that the current density decreased drastically already in the first hours of electrolysis (Fig. 4.16 in SI), where the reaction, in fact, stopped, which explains also the very

low productivity values. This behavior indicates a deactivation process, involving the Au catalyst, which will be further discussed in paragraph 4.3.4, “Catalyst stability”.

The LC-MS Chromatogram of a sample of the starting solution of 0.04 M gluconic acid in 0.025 M NaOH and of the solution resulting from 24 h electrolysis at 20°C are reported in Fig. 4.17 and 4.18 in the SI. While Glucaric acid is not detected in the starting solution, it is present in the solution resulting from the electrolysis, proving that it is product of the electrolysis of gluconic acid. The HPLC spectrum with all the products resulting from the electrolysis of gluconic acid at 1.1 V_{RHE} is reported in Fig. 4.14(b) in the SI.

4.3.3 The two steps in cascade

Despite the limit in the achievable concentration of glucaric acid due to the deactivation phenomena, we did attempt the two electrolysis steps in cascade as proof of concept. A set of optimal operating parameters was selected to first convert D-glucose to D-gluconic acid at 0.6 V_{RHE} , the potential corresponding to this oxidation step, and then to convert the latter to glucaric acid, at 1.1 V_{RHE} . A concentration of 0.1 M Na_2CO_3 (corresponding to pH 11.3) was chosen for the electrolyte because it gave the best selectivity to gluconic acid (Table 4.1). The quantity of glucose converted to gluconic acid in the first step had to be high enough to guarantee a sufficient concentration of gluconic acid in solution to initiate the second oxidation step and to allow accurate detection of the final products by the analytical device. For this reason, the first electrolysis step was conducted at 40°C for 48h, starting from a solution of 0.1 M glucose (all values corresponding to the maximum productivity, see Table 4.2-4.3-4.4). Therefore, after 48h, the second electrolysis was immediately started by switching the oxidation potential from 0.6 V_{RHE} (used for the first step) to 1.1 V_{RHE} , which was kept for an additional 18 h of electrolysis, without modification of any of the other reaction parameters. In fact, after 18 h the catalyst was completely deactivated, as the current density dropped to zero, so the electrolysis was stopped.

The results, reported in Table 4.7, show that only 2.4% of the gluconic acid formed in the first reaction step is converted to glucaric acid in the second oxidation step, with a selectivity of 89.0%.

Table 4.7. Summary of the results of the cascade process.

Oxidation step		Catalytic results				
Nr	X_G^a (%)	S_{GO}^b (%)	X_{GO}^c (%)	S_{GA}^d (%)	P_{GO}^e (mmol $cm^{-2} h^{-1}$)	P_{GA}^f (mmol $cm^{-2} h^{-1}$)
1	17.5	83.9	-	-	3.8	-
2	25.0	87.4	2.4*	89.0*	4.1	0.2

^a Glucose conversion, %. ^b Selectivity to gluconic acid, %. ^c Gluconic acid conversion, %. ^d Selectivity to glucaric acid, %. ^e Productivity of gluconic acid, mmol $cm^{-2} h^{-1}$. ^f Productivity of glucaric acid, mmol $cm^{-2} h^{-1}$. *These results refer to the sole oxidation of gluconic acid.

In fact, while the first oxidation proceeds rather effectively, with 17.5% of the initial glucose converted mainly to gluconic acid (83.9% of selectivity), the second reaction step is characterized by a very limited productivity (only 0.2 mmol $cm^{-2} h^{-1}$), which is justified considering that the reaction actually starts slowing down already after a few hours of electrolysis due to deactivation of the catalyst.

It is important to point out that, during the second oxidation step, at the constant potential of 1.1 V_{RHE} , gluconic acid is still produced by the much easier oxidation of the aldehyde group on C1. In fact, as we showed in our previous work, at this potential, gold is able to oxidize both the aldehyde group on C1 and the hydroxymethyl group on C6 [168]. The final conversion of glucose, obtained with the two electrolysis in cascade, is 25%, with a total selectivity to gluconic acid of 87.4%, which remains, for the major part, unreacted.

In the next paragraph we investigate the catalyst stability and try to address the cause of the rapid deactivation of the catalyst during the second oxidation step.

4.3.4 Catalyst stability

The stability of the Au catalyst was studied in two ways: firstly, by comparing the activity of the electrocatalyst before and after electrolysis, secondly by measuring the dissolution of the active phase in the reaction solution after long electrolysis times. The comparison of the CVs of Au in a fresh solution of 0.04 M glucose and 0.1 M Na_2CO_3 recorded before and after 48h electrolysis at 0.6 V_{RHE} (Fig. 4.15(a) in SI), evidences no loss of electrocatalytic activity during the oxidation of glucose to gluconic acid, mainly thanks to the use of the potential-program that assures the cleaning of the electrode surface after each electrolysis sequence (see “Experimental” section). On the other hand, the CVs of Au in a fresh solution of 0.04 M gluconic acid and 0.025 M NaOH recorded before and after 18h electrolysis at 1.1 V_{RHE} (Fig. 4.15(b) in SI) appear different, with a larger left shoulder and a surprisingly higher current density in the CV of the recovered catalyst (which was thoroughly rinsed with MilliQ water before the CV). This might be explained assuming that, after one cycle of electrolysis, a greater amount of hydroxyl (OH^-) species adsorbed onto the catalyst’s surface to form active $\text{Au}(\text{OH})_x$ species, thus increasing its activity.

Next, in order to exclude possible losses of gold active phase due to dissolution, the reaction solution was analyzed after electrolysis with ICP-MS to determine the quantity of metal leaching. The results, shown in Table 4.9 in the SI, indicate no significant loss of metal during both oxidations, confirming the inherent stability of the catalyst itself.

A recent review article from the authors Iglesias *et al.*, reports that, due to the blockage of the catalyst active sites by strongly adsorbed glucaric acid, the oxidation of gluconic acid requires more drastic conditions than that of glucose [57]. The results to which they refer are those from the authors Lee *et al.*, who estimated the free energy of adsorption of various compounds on a Pt catalyst in the aerobic oxidation of glucose to glucaric acid, in order to rationalize an observed difference in reactivity of the aldehyde group of glucose and of the $-\text{CH}_2\text{OH}$ of gluconic acid [72]. They found out that the $\text{C}=\text{O}$ group interacts more strongly with the catalyst compared to the alcoholic group thus, while glucose and gluconic acid adsorb with similar strengths, glucaric acid adsorbs more strongly [72]. As a consequence, glucaric acid may block the active sites and slow down the reaction [72]. Moreover, they also ascribe the lower oxidation rate of gluconic acid, compared to that of glucose, to the slow kinetics of the dehydrogenation of $-\text{CH}_2\text{OH}$ as compared to $-\text{CHO}$, which is an important step for activating the molecule and is unnecessary in the oxidation of glucose to gluconic acid [72]. In light of their results, we suspected that the same phenomena as observed for Pt are also at play here for Au and were responsible for the deactivation encountered during our experiments. To verify this hypothesis, we conducted some additional tests.

First, a sample of water, brought in contact with the catalyst right after the electrolysis, was analyzed with HPLC to evaluate the presence of glucaric acid coming off the catalyst. Glucaric acid was found in the sample at concentrations comparable to those measured in the bulk after the electrolysis, thus providing a first proof for our hypothesis. Secondly, an electrolysis experiment was performed starting from a solution of gluconic acid containing already a small amount of glucaric acid, to see if the presence of glucaric acid at the beginning of the electrolysis inhibited the reaction already from the start of the experiment. Indeed, we observed that in the cyclic voltammetry study (Fig. 4.19 in SI) in presence of glucaric acid, the current density corresponding to the oxidation peak is much lower than in its absence, meaning that the glucaric acid introduced in the solution may adsorb onto the catalyst surface, thereby deactivating it. The subsequent electrolysis showed a very low starting current (as compared to that in the glucaric acid free solution) which further decreased during the experiment. The products analysis confirmed our conclusion: at the end of the electrolysis, we measured a lower concentration of glucaric acid compared to that introduced at the start, thus indicating that part of it may have remained on the Au surface, as such deactivating it. This further confirmed our original hypothesis that glucaric acid acts as an inhibitor through fouling of the Au surface.

In case of physical adsorption, an easy solution would be working in a flow configuration, as this might shift the equilibrium towards desorption as a consequence of the constant product removal and/or enhanced mass transport (away from the surface). To verify if an increased mass transfer could facilitate the glucaric acid desorption, we conducted an electrolysis (24h, 20°C, starting solution: 0.04 M gluconic acid in 0.025 M NaOH) with a rotating disk electrode. The results showed, again, the occurrence of Au deactivation as similar glucaric acid productivity and concentration were achieved.

So, in conclusion, the deactivation of the catalyst during the oxidation of gluconic acid to glucaric acid may be ascribed to fouling by glucaric acid, which once formed, remains on the catalyst surface, blocking it.

This work was intended to gain an understanding on the electrooxidation of glucose to glucaric acid on gold using a 2-steps process, thus, the use of a simple Au flat electrode in a batch reactor was suitable for such small-scale application. Although, to increase the productivity and assess the performance of this catalytic technology, we intend to 1) synthesize an Au-based catalyst characterized by higher electrocatalytic activity and stability and 2) scale the process to an industrial-like level by applying flow conditions. To improve the catalyst's activity and stability, we will modify the catalyst's morphology, increasing its electroactive surface area, and composition, to prevent occurrence of deactivation processes.

One method to avoid deactivation could be to alloy gold with a second metal. For example, Rafaideen *et al.* demonstrated that alloyed PdAu bimetallic nanocatalysts own a much higher stability and selectivity compared to the corresponding monometallic systems proposed in literature under similar experimental conditions [189]. Another way, often reported in literature, to minimize deactivation and improve the selectivity is adding a promoter to the catalytic system, such as Bi or Pb [86, 190–195]. This should thus be investigated further under the ideal conditions found in this work to further advance the field of glucose to glucaric acid oxidation.

4.4 Conclusions

In conclusion, we reported a novel, two-steps oxidation of D-glucose to D-glucaric acid using a bare Au electrode in a batch cell. The impact of the operating parameters has been investigated for both oxidation steps to understand the reaction mechanisms and identify the conditions that maximize the selectivity. In the glucose electrooxidation to gluconic acid, pH, glucose initial concentration, reaction temperature and time had a major impact on selectivity and conversion. A maximum 97.6% selectivity at pH 11.3, 0.04 M initial glucose and 5°C was achieved, which, to the best of our knowledge, is the highest value ever obtained in literature for the electrochemical process. Higher temperatures increase the conversion rate but cause also the rapid degradation of glucose due to the increased kinetics of the chemical side-reactions (48.5% conversion is achieved at 50°C after 24h but the selectivity drops to 59.3%). Similarly, by increasing the pH, glucose conversion also increases (up to 45.6% at pH 13.0), but the selectivity to gluconic acid drops to 44.4% due to an excessive adsorption of the hydroxyl ions (OH^-) onto the Au surface which decreases the number of active sites available for glucose, thus diminishing the cell performance. The electrolysis of more concentrated solutions of glucose resulted in a lower selectivity to gluconic acid because of the rapid saturation of the catalyst surface and increased viscosity of the solution, which hinders the mass transfer towards the Au active sites, thus limiting the (heterogeneous) electrochemical reaction. Finally, it was found that, while the selectivity remains constant even for prolonged reaction time (up to 48 h), glucose conversion continuously increases, with a slight reduction of the conversion rate due to mass transfer limitations. As for the oxidation of gluconic acid to glucaric acid, a variation of the products' distribution was observed when changing the potential at which the gluconic acid oxidation reaction was conducted. A maximum selectivity of 89.5%, one of the highest reported in literature, was obtained at 1.1 V_{RHE} , where $\text{Au}(\text{OH})_x$ is the main species of gold involved in the catalytic process. In this case, no chemical side-reaction competed with the electrochemical process, because gluconic acid is stable in alkaline media. Therefore, none of the operational parameters examined (pH, gluconic acid initial concentration, reaction temperature and time) had a significant impact on the products' distribution. Nevertheless, higher pH and temperature slightly affected the reaction kinetics, thus increasing the conversion rate. In all cases, a very limited concentration of glucaric acid was obtained due to an early deactivation of the Au electrode, which may be ascribed to fouling by glucaric acid itself. Importantly, no Au leaching was detected during both oxidation reactions and the catalyst itself remained active after long electrolysis time (after rinsing product off). In the next chapter, we focus on improving the catalyst morphology aiming at higher EASA compared to that of the bulk electrode.

4.5 Supporting information

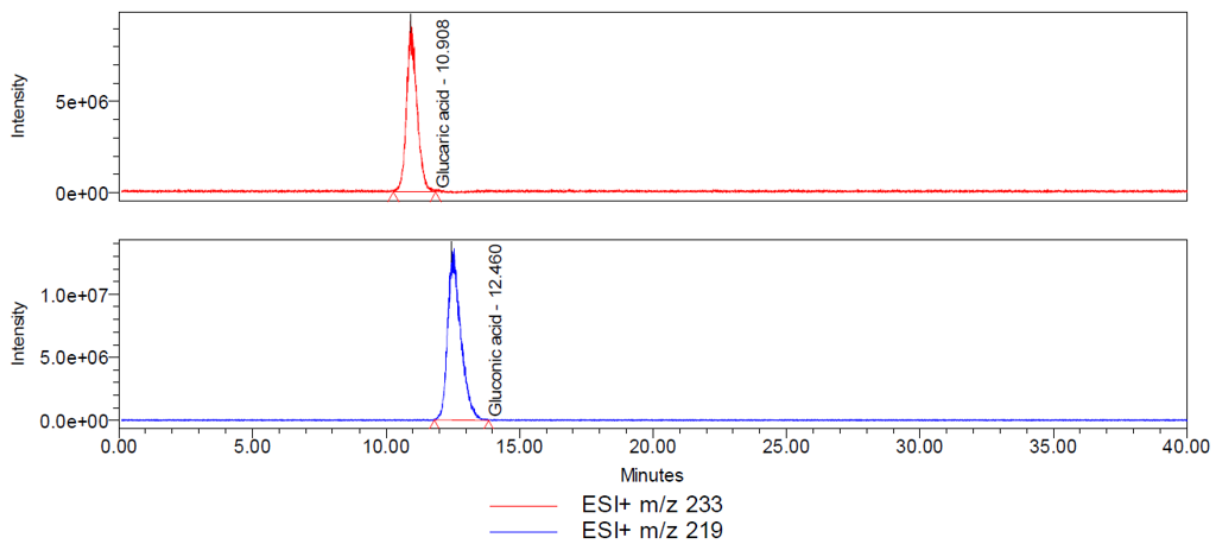
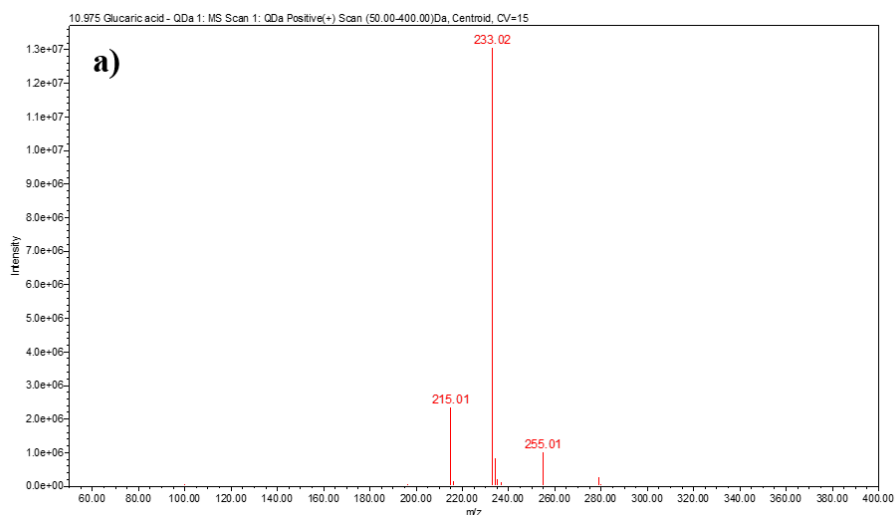


Figure 4.9. Chromatogram of a high purity standard mixture of glucaric and gluconic acid. Glucaric acid is observed at 10.9 min in the mass chromatogram taken at m/z 233. Gluconic acid is observed at 12.5 min in the mass chromatogram taken at m/z 219.

The liquid chromatography mass spectrometry (LC-MS) analysis was conducted using an Acquity Arc UHPLC (Waters) fitted with a KC811 Ion-exclusion column (Shodex) and coupled to a QDa single quad mass spectrometer (Waters). A solution of 10mM formic acid in water was used as the mobile phase. In a high purity standard mixture of glucaric and gluconic acid, both compounds were observed as the $M+Na$ ion at resp. m/z 233 and m/z 219 (Fig. 1 and 2). In addition, the mass spectrum of glucaric acid showed the formation of $M+Na-H_2O$ and $M-H+CH_3COOH$ (Fig. 2(a)), which are all expected to be present. Since the sensitivity was best for $M+Na$ m/z , the mass chromatograms for subsequent samples were extracted at these masses. Samples were diluted 100 times in LC-MS grade water before measurements.



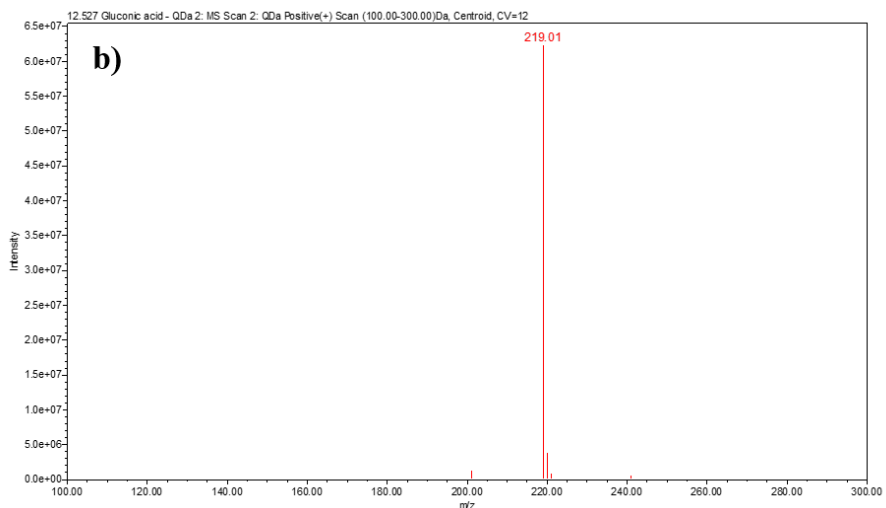
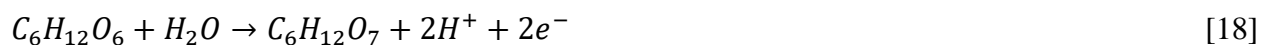


Figure 4.10. Mass spectra of a) the glucaric acid peak, appearing at 10.9 min retention time, and b) the gluconic acid peak, at 12.5 min. retention time, obtained from authentic samples of high purity standards. In the mass spectrum of glucaric acid, the M+Na ion is observed at m/z 233, as well as the M+Na-H₂O ion (m/z 215) and the M-H+CH₃COOH ion (m/z 255). In the mass spectrum of gluconic acid, only the M+Na ion is observed at m/z 219

Anodic and cathodic reactions involved in the glucose electrooxidation process.

At the anode, the oxidation reactions take place at the Au working electrode:



The H⁺ ions generated by the oxidation reactions at the anode, can diffuse through the cation-exchange membrane to the cathodic compartment where the Hydrogen evolution reaction (HER) takes place at the Pt counter electrode:



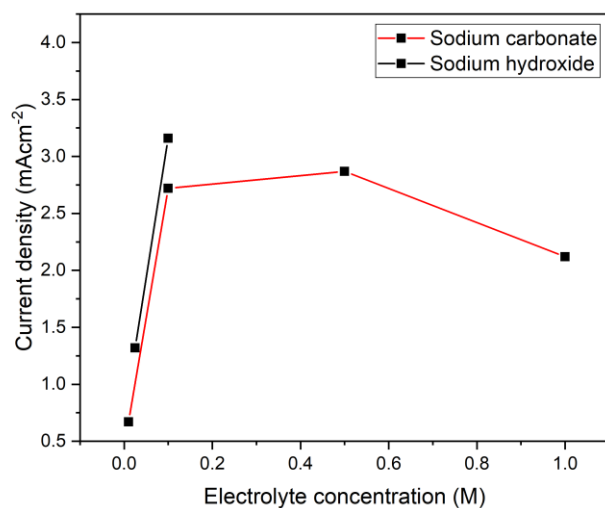


Figure 4.11. Current density response to the variation of the electrolyte concentration, so of the pH, derived from the respective cyclic voltammograms recorded at 10 mVs^{-1} , 20°C , in a solution with 0.04 M of glucose. The red line represents the values of current density obtained with Na_2CO_3 as electrolyte while the black line is that obtained with NaOH .

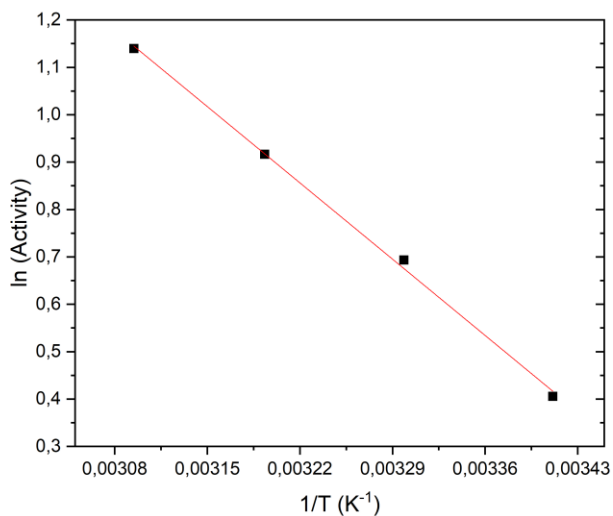


Figure 4.12. Arrhenius plot derived from the cyclic voltammograms of Au in a solution $0.1 \text{ M Na}_2\text{CO}_3$ and 0.04 M glucose, recorded at 10 mVs^{-1} at various temperatures (in the range $20\text{-}50^\circ\text{C}$).

Equation to calculate the apparent activation energy [186]:

$$E_a = R \left(\frac{d(\ln j)}{d(1/T)} \right) \quad [21]$$

Where j is the current density, R the ideal gas constant and T the temperature.

Table 4.8. Summary of the results obtained in the glucose electrooxidation to gluconic acid in function of the applied potential. The table shows that the variation of the potential applied for the electrolysis, within the oxidation peak, has no appreciable impact on glucose conversion nor on D-gluconic acid selectivity and productivity.

Operating conditions						Catalytic results		
t^a (h)	C_G^b (M)	C_E^c (M)	pH	T^d (°C)	E^e (V_{RHE})	X_G^f (%)	S_{GO}^g (%)	P_{GO}^h ($\text{mmol cm}^{-2} \text{h}^{-1}$)
24	0.04	Na_2CO_3 0.1	11.3	20	0.5	3.6	6.0	83.7
24	0.04	Na_2CO_3 0.1	11.3	20	0.6	11.1	5.7	86.6
24	0.04	Na_2CO_3 0.1	11.3	20	0.8	30.6	6.1	84.9

^a Reaction time, h. ^b Substrate (glucose) initial concentration, M. ^c Electrolyte concentration, M. ^d Reaction temperature, °C. ^e Oxidation potential, V_{RHE} . ^f Glucose conversion, %. ^g Selectivity to gluconic acid, %. ^h Productivity of gluconic acid, $\text{mmol cm}^{-2} \text{h}^{-1}$.

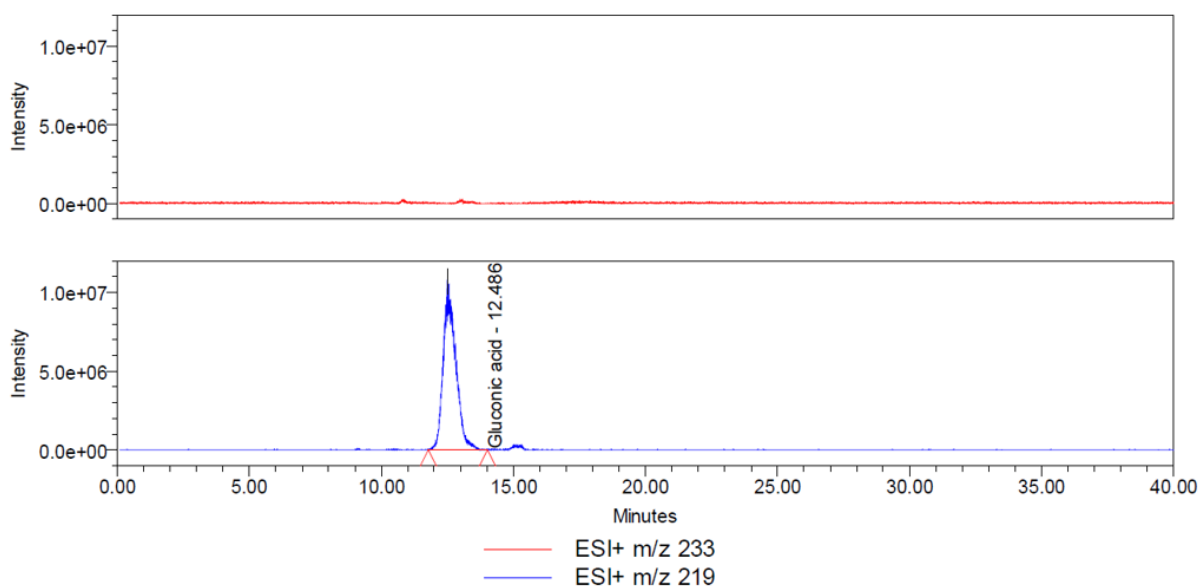


Figure 4.13. Chromatogram of the product of 24 h electrolysis of a starting solution 0.04 M D-glucose in 0.1 M Na_2CO_3 at 20 °C. No trace of glucaric acid is observed in the mass chromatogram taken at m/z 233, while, in the mass chromatogram of m/z 219, the product peak at 12.5 min retention time coincides with that found for gluconic acid (Fig. 4.9 (blue trace)), proving that gluconic acid is the product of the electrolysis of glucose.

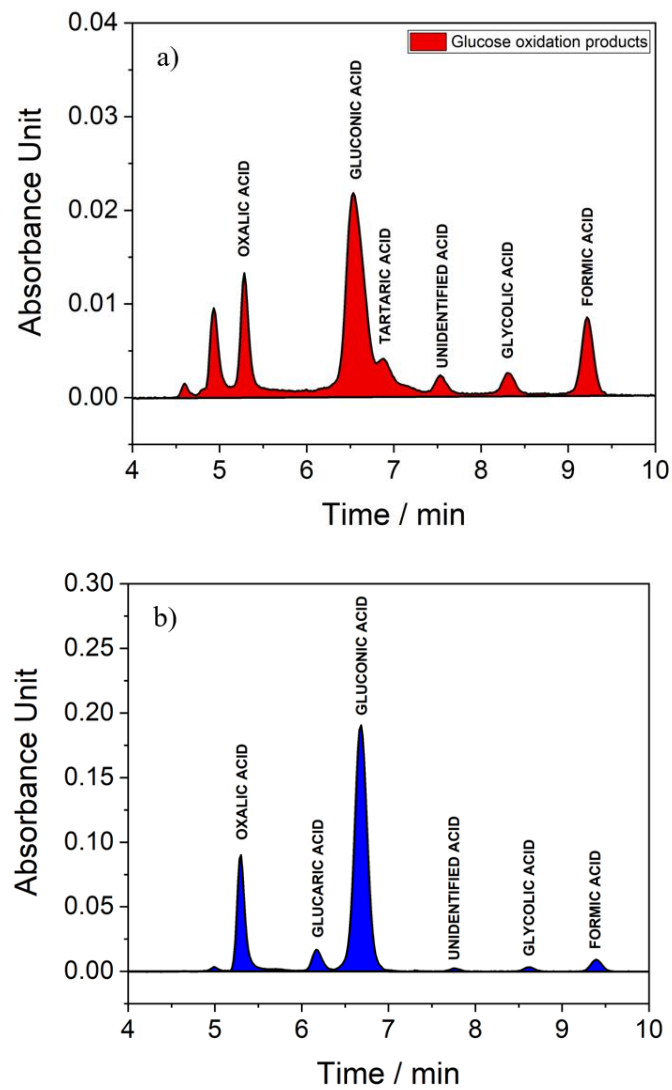


Figure 4.14. HPLC spectrum of the products resulting from the electrolysis of glucose (a) and of gluconic acid (b), respectively at 0.6 and 1.1 V_{RHE} .

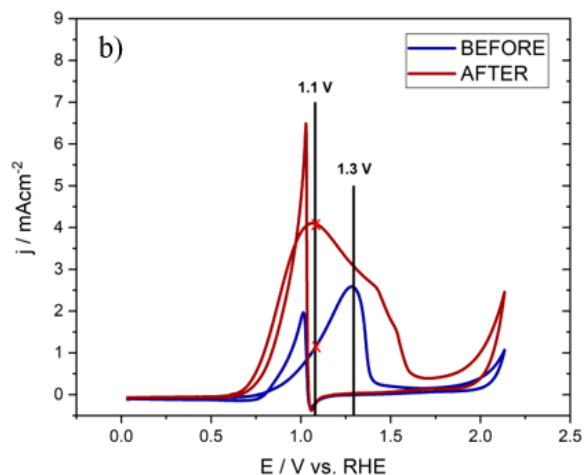
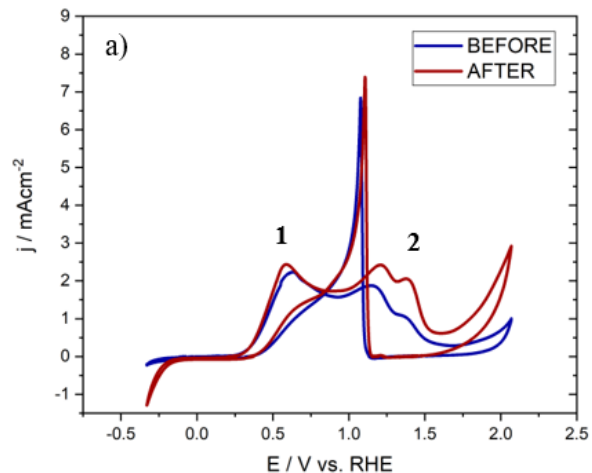


Figure 4.15. Cyclic voltammograms (II cycles) of Au electrode in a fresh solution of a) 0.1 M Na_2CO_3 and 0.04 M glucose and b) 0.025 M NaOH and 0.04 M gluconic acid recorded at 20 mV s^{-1} and 20°C , before (blue line) and after (red line) electrolysis at a) $0.6 \text{ V}_{\text{RHE}}$ (for 48h) and b) $1.1 \text{ V}_{\text{RHE}}$ (for 18h). Prior use, the recovered electrodes were thoroughly rinsed with MilliQ water

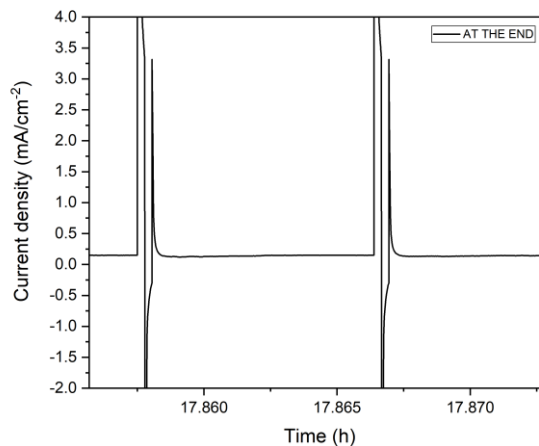
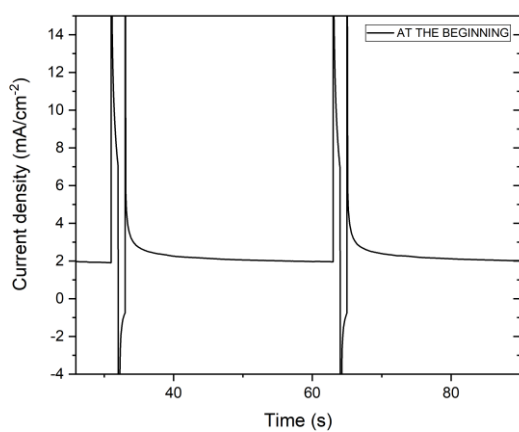


Figure 4.16. Comparison of Chronoamperometry data before (left) and after (right) 18h electrolysis at the potential of 1.1 V_{RHE}, corresponding to the second oxidation step. The graphs highlight the important loss of current density registered during this oxidation step. The current density decreases constantly from the initial value of ~2.0 mA cm⁻² until a practically null value, at the end of the electrolysis.

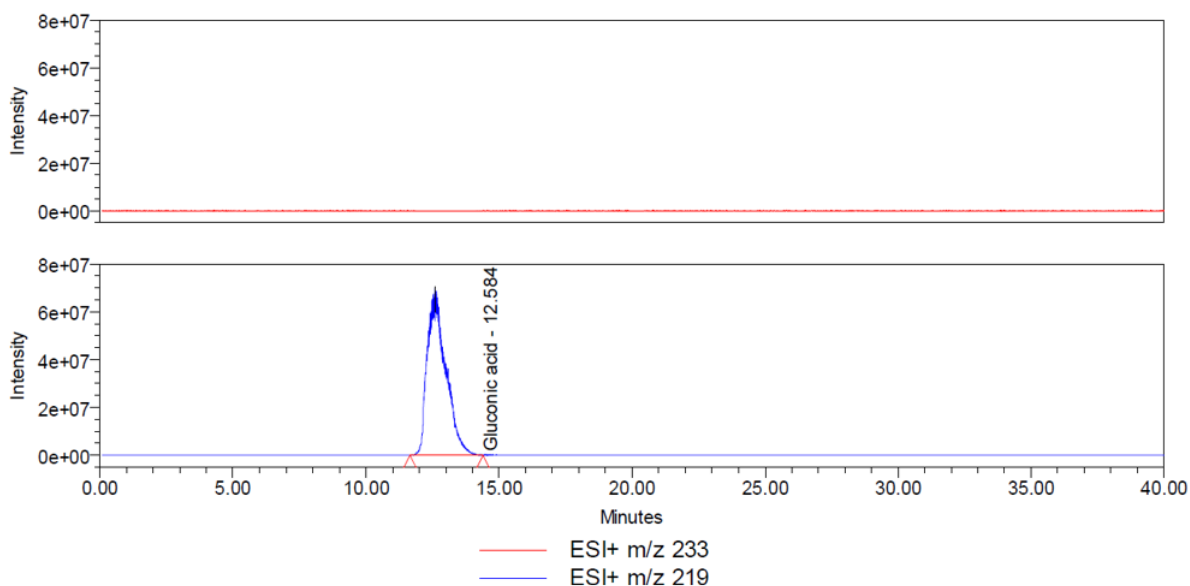


Figure 4.17. Chromatogram of a sample of the starting solution of 0.04 M gluconic acid in 0.025 M NaOH. In the mass chromatogram of m/z 233 (red trace) no product peak is observed, which indicates absence of glucaric acid. Gluconic acid is observed at 12.5 min in the mass chromatogram taken at m/z 219.

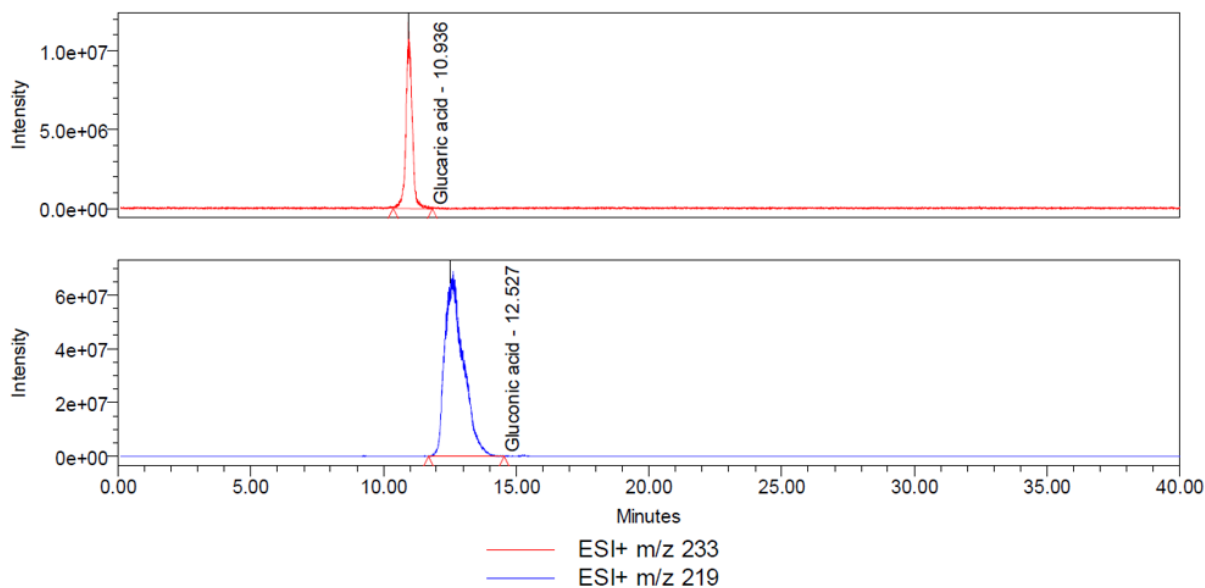


Figure 4.18. Chromatogram of the sample of 24 h electrolysis of a solution 0.04 M gluconic acid in 0.025 M NaOH at 20 °C. Glucaric acid, not detected in the starting solution, is present here at 10.9 min in the mass chromatogram taken at m/z 233, proving that it is product of the electrolysis of gluconic acid. Gluconic acid unreacted is observed at 12.5 min in the mass chromatogram taken at m/z 219.

Table 4.9. The table shows the amount of Au dissolved in the reaction solution (in ppm) before (Initial concentration) and after (Final concentration) each electrolysis. In both cases, the Au leaching is irrelevant.

	Initial concentration [ppm]	Final concentration [ppm]
1 st Oxidation step	0.0	0.0
Cascade process	0.0	0.619

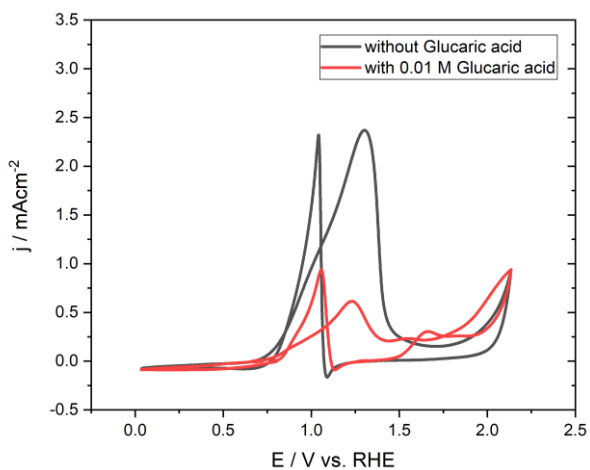


Figure 4.19. Cyclic voltammograms (V cycles) of Au electrode in 0.04 M gluconic acid and 0.025 M NaOH recorded at 20 mV s^{-1} and $20 \text{ }^\circ\text{C}$, without (grey line) and with (red line) 0.01 M glucaric acid. The graph shows that, in the presence of glucaric acid, the current density corresponding to the oxidation peak drops as a consequence of the passivation of the Au surface.

Chapter 5

Synthesis, Characterization of a Highly Electroactive Composite based on Au Nanoparticles Supported on Nanoporous Activated Carbon for Electrocatalysis

This chapter has been published as a research paper: [G. Moggia](#), S. Hoekx, N. Daems, S. Bals, T. Breugelmans, "Synthesis and characterization of a Highly Electroactive Composite based on Au Nanoparticles Supported on Nanoporous Activated Carbon for Electrocatalysis", *ChemElectroChem*, vol. 10 (2023) issue 21.

5.1 Introduction

Electrode materials can consist of: bulk metals, nanoparticles or bimetallic nanoparticles. Thus far, we have been studying systems in which the catalyst material consisted of a bulk electrode, which is implicitly characterized by very limited catalytic activity, in terms of current density, and so only able to generate low conversion and productivity [168, 196]. To improve their electrocatalytic activity while keeping limited usage of the expensive active phase, metal catalysts can be made of nanoparticles and thin films deposited over various, high surface area, supports [100, 178, 197–205]. The basic principle is that the increased catalyst surface-to-volume ratio allows to achieve higher activity with lower total metal loadings. Moreover, altering the properties of an electrocatalyst, as the morphology or the EASA, can result in enhanced mass transport and charge transfer, or stronger or weaker adsorption of the reagents and/or better desorption of the products, which could potentially address deactivation issues [206]. In fact, as evidenced by several studies, the impact of the mass transfer can be significant on certain electrocatalytic processes as it controls the diffusion of the reactants from the bulk to the surface of the catalyst and of the products from the surface to the bulk [79, 207–211]. For all these reasons, in this chapter we develop a very simple chemical method to synthesize a Au-based catalyst with very high electroactive surface area and, at the same time, low Au loading. The catalyst proposed consists of Au nanoparticles deposited over a porous carbon matrix, activated carbon, with a very high specific surface. After describing the synthesis method, the AuNP/C composite is physically characterized and its electrocatalytic activity determined by calculation of the EASA. Finally, the as-developed system is tested for gluconic acid electrooxidation in batch and flow-reactors, to also see the impact of the flow conditions on the electroactivity of the AuNP/C catalyst towards this reaction

5.2 Experimental

5.2.1 Chemicals and reagents

The synthesis bath was prepared using tetrachloroauric acid trihydrate (Sigma-Aldrich, 99%), ultrapure water (Synergy UV system), sodium hydroxide (Sigma-Aldrich, 98%), Polyvinylpyrrolidone (PVP40) (Sigma Aldrich), activated carbon Norit® SX1G (Total surface area, BET, 1000 m² g⁻¹, Nederland BV [212]), used as received, and sodium borohydride (Sigma Aldrich, 98%). The ink was prepared using 2-propanol (ChemLab, >99%) as solvent and Sustanion® (suspension of 5 wt% in lower aliphatic alcohols and water), purchased from Sigma Aldrich, as solvent. The supporting electrolytes were prepared with ultrapure water (Synergy UV system), sodium carbonate (Sigma-Aldrich, 98%) and sodium hydroxide (Sigma-Aldrich, 98%). Anhydrous D-glucose was purchased from VWR (99.5%), D-gluconic acid potassium salt (98%) and D-saccharic acid potassium salt (98%) from Sigma Aldrich and D-gluconic acid sodium salt (99%) from Acros Organics. All chemicals were used without further modifications.

5.2.2 Preparation of AuNPs supported on activated carbon

The catalyst was prepared using a modification of the wet impregnation method developed by Hermans et al. [213–215]: 30 mg HAuCl₄·3H₂O was dissolved in 150 mL MilliQ water under stirring at 600 rpm and ambient temperature (solution 1). The pH of the solution was adjusted to the target value (9–11) by adding an appropriate amount of a 1 M NaOH solution.

Polyvinylpyrrolidone (PVP) was added from a 2% wt solution in order to obtain a concentration of $64 \mu\text{g mL}^{-1}$ in the final solution. PVP was used as stabilizing agent/capping agent as it can bind onto the particle surfaces and protect them from aggregation [216], which, based on the findings from a previous study of our group, decreases the electrochemical charge transfer resistance and increases the electrochemically active surface area of the catalyst [217]. Then, 150 mL of a solution obtained dissolving 135 mg of activated carbon (Norit) in MillQ water (pH corrected with 1 M NaOH to target: 9 to 11) was added to solution 1. The resulting solution (solution 2) was left under stirring for 24 h. Following, a 0.1 M NaBH_4 solution was added dropwise to solution 2 such that the concentration of NaBH_4 in the final solution matched the one of Au. NaBH_4 was used as the reducing agent and to remove the strongly adsorbed PVP, thus avoiding treatment at high temperature (PVP decomposition temperature is between 200 and 350 °C) that can cause particle agglomeration and shape change [218]. The solution was left under stirring (600 rpm) for 2 h (immobilization time). After this time, the slurry was filtered and washed with water six times to remove all the Cl^- . To verify that all the Cl^- had been removed, AgNO_3 was added to the filtrate to check for the absence of precipitate. The catalyst was then dried in an oven at 70 °C for 5 h and calcined at 200 °C for 3 h. The whole synthesis process has been conducted under Argon to avoid alteration of the pH due to the presence of CO_2 .



Figure 5.1. Schematic representation of the synthesis of AuNPs/C catalyst by impregnation.

5.2.3 Physical characterization of the Au/AC catalyst

The AuNP/C catalyst was investigated using a set of physicochemical characterization techniques. Standards for all metallic species analyzed were purchased from VWR (Belgium). The Au weight percentage in the catalyst powders was analyzed by Thermo-gravimetric analysis (TGA), using a Q500 thermogravimetric analyzer (TA Instruments) and inductively coupled plasma mass spectrometry (ICP-MS), using an Agilent 7500 series spectrometer. For the TGA analysis, the temperature of the furnace was ramped from 40°C to 600°C-800°C at 5°C/min. Platinum pans were used in all measurements. The Au wt.% was calculated from the residue at 600°C, which was found to be metallic Au by XRD analysis. To measure the Au content in the catalyst by ICP-MS analysis, 10 mg sample was dissolved in 500 μL of aqua regia and destructed at 70 °C overnight. The samples were diluted to a 1:100 ratio and a calibration curve was fitted from 100 to 10 000 ppb. However, with this method the Au content (%wt.) measured was only 0.3%, too low compared to the theoretical one, given by the difference between the quantity of Au added during the synthesis and that left in the filtrate solution, and also compared to Au content

measured by TGA. Matching results were only obtained when the samples of Au/C powder were ashed prior to the ICP-MS analysis, thus eliminating the carbon matrix and leaving the sole metal. The procedure used was the following: first, porcelain crucibles were pre-heated for 1h in a muffle furnace at 700°C. Crucibles were weighed after cooling; second, 50-100 mg of sample was placed in the crucible, weighed and placed in the muffle furnace for 4h at 700°C; third, after cooling, the crucible was weighed and the ash content was calculated. Ash was transferred to a falcon tube and digested in 1mL of aqua regia overnight. Finally, the samples were diluted to perform the ICP-MS measurement. In order to characterize the crystalline structure of the catalysts, X-Ray diffraction (XRD) was employed. X-ray diffraction experiments were performed on a Huber X-ray diffractometer equipped with a G670 Guinier camera (Huber GmbH&Co, Germany) using the Cu K α 1 radiation ($\lambda=1.5405981\text{\AA}$).

Scanning Electron Microscopy and Energy-dispersive X-Ray Spectroscopy (SEM-EDX) were used in order to assess the morphology and distribution of the metal nanoparticles over the carbon support. The microscope used was a Quanta 250 FEI operated at an acceleration voltage of 5kV and equipped with a Super-X EDX detector to study the morphology of the obtained catalysts and verify the atomic distribution.

For more detailed characterization and to determine the 3D structure of the supported Au nanoparticles, HAADF-STEM electron tomography experiments were performed on a Thermo Fischer Tecnai Osiris microscope operated at 200 kV. Tilt series for the materials were acquired using incremental fast tomography between -75° and 75° with a 2° tilt increment and a frame time of 6 s [219]. The projection images were acquired with a 50 pA beam current and image resolution of 1024×1024 pixels. The series were aligned using cross-correlation and the reconstructions were completed using the Expectation Maximization (EM) algorithm in the ASTRA Toolbox [220]. To determine the composition of the materials, EDX maps were obtained using the Super-X detector on the Tecnai Osiris microscope. The maps were acquired for 8 minutes at a 50 pA beam current.

Nitrogen (N₂) physisorption was performed at 77 K with a Quantachrome Quadrasorb SI (Quantachrome Instruments, Boynton Beach, FL, USA) automated surface area & pore size analyzer. Prior to the measurements, all samples were degassed for 16 h at 200 °C. The specific surface area was calculated using the Brunauer-Emmet-Teller (BET) equation.

5.2.4 Electrochemical setups

A thermostated three-electrode glass cell was used for the EASA experiments and for the cyclic voltammetry study to screen the electro-reactivity of the catalyst in gluconic acid and blank solution. A silver-silver chloride electrode (Ag/AgCl) and a platinum wire were used as reference and counter electrodes, respectively. The working electrode used for the cyclic voltammetry experiments consisted of a glassy carbon RDE (Goodfellow) with an active diameter of 8 mm which was covered with 14 μL of catalyst ink deposited by drop-casting until a loading of ca 50 μg (0.099 mg cm^{-2}). Before the catalyst deposition, the surface of the glassy carbon electrode was carefully polished with aluminum (Φ 1, 0.3 and 0.05 μm) slurry on a polishing cloth and then sonicated in MilliQ water for 5 min. The electrochemical instrumentation consisted of a Bio-Logic VSP-300 Potentiostat. All the electrode activities are represented as current densities, utilizing the EASA as active area and with respect to the reversible hydrogen electrode (V_{RHE}). The cyclic voltammetry studies were conducted between 0 and 2.5 V_{RHE} at 50 mV s^{-1} at ambient temperature

from solutions containing 0.1 M aqueous NaOH while stirring at 700 rpm. All the voltammograms shown correspond to the cycle once a stable state is reached. An initial solution containing 0.05 M of gluconic acid in 0.1 M NaOH (pH 13) was used for the electrolysis. A CV was performed before the electrolysis to select the exact potential corresponding to the oxidation peak. The continuous flow experiments were executed in an adapted micro flow cell (ElectroCell, Denmark), allowing to operate in a three-electrode mode (Fig. 5.2).

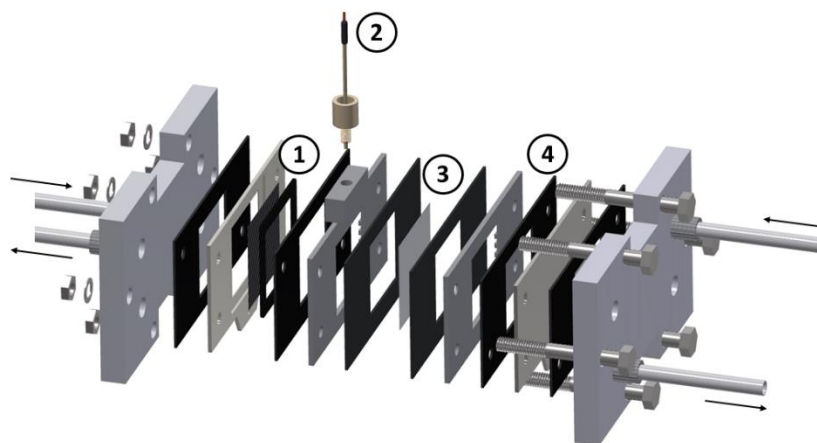


Figure 5.2. Scheme of the reactor setup used for the continuous flow experiments: (1) anodic compartment containing the working electrode (WE); (2) reference electrode (RE); (3) Nafion membrane and (4) SS counter electrode (CE), in the cathodic compartment.

A detailed description can be found in a previous work [221]. A 10.2 cm² electrode (Titanium fiber felt, Fuel Cell Store) was used as anode. The catalyst ink was prepared dispersing the catalyst powder in a solution of 2-propanol and 20wt% Sustanion, so that the ratio Sustanion/catalyst was 1/7. The ink, consisting of catalyst, Sustanion suspension and isopropanol was sprayed onto its microporous layer, until a total loading of 2.45 mg cm⁻² was reached. The ink was ultra-sonicated for 25 min prior to airbrushing. The anodic potential was controlled versus a leak-free Ag/AgCl reference anode (Innovative Instruments, Inc.) with a multichannel Autolab potentiostat M204 equipped with a 10 A booster. The catholyte and anolyte used were both 0.1 M aqueous NaOH. In both, the flow rate was kept at 20 mL min⁻¹ with a multichannel peristaltic pump. A Nafion® 117 cation exchange membrane separated the two compartments. The system was operated in recirculation mode as shown in Figure 2 and the electrolyte volumes were 250 mL for both anolyte and catholyte. The reactor was operated in a vertical position with the electrolyte being fed from the bottom of the reactor and leaving on the top, at room temperature and atmospheric pressure. The products were analyzed by HPLC (Alliance 2695, Waters, USA) combined with an ionexclusion column (Shodex KC-811). A photodiode array (PDA) detector set to 210 nm was used to detect organic acids while a refractive index (RI) detector thermostated at 30°C was used to detect glucose. A perchloric acid solution (0.1 %) was used as the eluant for the HPLC analysis. Prior to analysis, 1 mL samples were acidified with 200 µL perchloric acid 6 M solution, sonicated and finally filtered.

All the electrode activities reported are represented with current densities (measured at the beginning of every electrolysis), utilizing the EASA as active area and with respect to the reversible hydrogen electrode (RHE). The tested potential vs. Ag/AgCl was converted into potential vs. RHE using the Nernst equation (Eq. 22):

$$E_{RHE} = E_{Ag/AgCl} + \ln(10) \cdot \frac{RT}{F} \cdot pH + 0.197 \quad [22]$$

With R being the universal gas constant (8.314472 J K⁻¹ mol⁻¹), F the Faraday constant (96485.332 C mol⁻¹) and T the temperature. All current densities are calculated with respect to the geometrical area.

5.2.5 Electroactive surface area measurement

The electroactive surface area (EASA) of the synthesized catalyst was calculated using the capacitance, measured as the slope of the plot of the current vs. the scan rate (selected scan rates: 20, 40, 60, 80 and 100 mV s⁻¹) at 0.71 V_{RHE} in the electrolyte solution (0.1 M NaOH) (Fig. 5.12). To obtain the EASA, this value (i.e. 0.0131 F or 13100 μF) was divided by the value of capacitance of EDL for bulk gold found in literature [222], 14.25 μF cm⁻². The specific EASA, 282.4 m² g⁻¹, was obtained by dividing the EASA, 919.3 cm², by the quantity of gold in the catalyst, 0.0003255 g.

5.3 Results and discussion

The AuNP catalysts were prepared on Norit activated carbon by a controlled adsorption method in which the interactions between the Au precursor and the carbonaceous support in aqueous solution were optimized by controlling the pH of the impregnating solutions. In fact, the surface of the activated carbons presents different types of functional groups containing heteroatoms (O, N, and S) [223], in varying amounts, which can be divided into acidic, neutral, and basic functions. This influences their surface characteristics and adsorption behavior. In particular, the carbon surface can be either positively or negatively charged in aqueous solution, below or above a characteristic pH value, called the point of zero charge (PZC), which is equal to 9.0 for Norit carbon [224, 225]. At the pH corresponding to the PZC, the net overall surface charge would be zero; at pH > PZC, the negatively charged carbon surface attracts cations from solutions, while at pH < PZC, it attracts anions. Therefore, it is important to know at which pH the interactions between the metallic precursor and the carbonaceous support are maximized. For this reason, the synthesis of the Au/C catalyst was conducted at 4 different pH's, in the range 8-11.5, in order to identify at which pH the maximum adsorption occurs. Fig. 5.13 shows the thermogravimetric plots for 4 samples of catalysts obtained, respectively, from the synthesis conducted at pH 8.5, 9.5, 10.5 and 11.5. All the samples show a small mass loss (ca 5% wt.) from room temperature to around 100 °C due to the evaporation of adsorbed water. Another slight weight loss (ca 5% wt.) is encountered between 300 and 350 °C, which could be related to the decomposition of the residual polyvinylpyrrolidone (PVP) used as surfactant during the synthesis. The major mass loss (ca 75% wt.) between 400 and 800 °C is attributed to the loss of the carbon support (Norit). The residual values shown in Fig. 5.13 (b) represent the total amount of metallic composite in the

catalyst samples. The Au loading was calculated by subtracting the residual mass of a blank Norit carbon sample (i.e., non-carbon contaminations, ca. 5.4%) from the total residual amount of metallic composite in the catalyst samples (Fig. 5.13 (b)). In order to identify which species of gold was generated during the TG analysis, a sample of residual composite was analyzed by XRD, which revealed it was metallic gold. The resulting gold loading (Au% wt) was then plotted versus the pH in order to identify the pH at which the maximum adsorption occurs (Fig. 5.3). To double-check the residual mass trends, the amount of non-adsorbed metal in solution – after filtration – was also determined by ICP-MS. As shown in Fig. 5.3, the maximum adsorption of Au (9.3%) on the activated carbon occurs at a pH of 9.5, which is just above 9.0 (the PZC of Norit). The explanation for this is that, at a pH between 9 and 10, the carbon surface holds negative charges which attract the Au³⁺ cations from solution: the interaction between the Au precursor and the carbon support leads to the high loading. On the other hand, at pH > 10, the carbon surface is also negatively charged but the metal precursor, is less available due to its preferential complexation with OH⁻ at these conditions, leading to a weaker metallic precursor-carbon surface interaction and a lower loading. At pH < 9 the carbon surface is positively charged, so it attracts anions rather than cations from the solution, meaning that the interaction will be weak and the resulting loading low. For this reason, the optimal pH of 9.5, which resulted in the highest metal loading, was used to synthesize the AuNP/C catalyst used in the rest of this study. A similar behavior was observed by the authors Hermans et al. in the preparation of Au-Pd/C catalysts for glyoxal and glucose chemical oxidation [213–215].

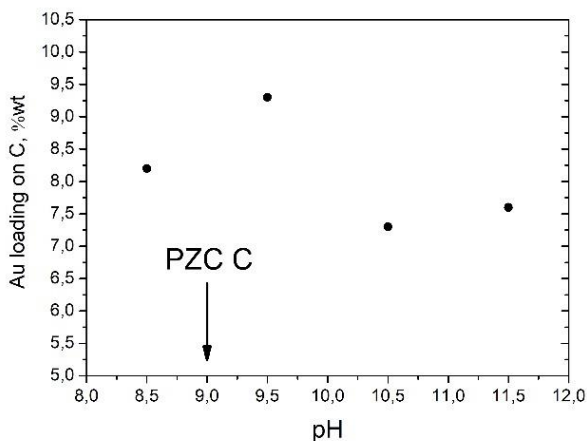


Figure 5.3. Au loading (%wt) on activated carbon, C, plotted versus the pH used for the synthesis. The point of zero charge for Norit® SX1G is ca 9.0 [225].

5.3.1 Physical characterization of the catalyst

Samples of Au/C were characterized by XRD and SEM coupled with EDX. The crystallinity of synthesized AuNPs was investigated by an X-ray diffraction (XRD) technique, and corresponding XRD patterns were shown in Fig. 5.4. Gold nanocrystals exhibited four distinct peaks at $2\theta = 38.2^\circ$, 44.4° , 64.6° and 74.6° in the diffraction pattern, corresponding to (1 1 1), (2 0 0), (2 2 0) and (3 1 1) Bragg's reflection of face-centred-cubic (fcc) lattice (JCPDS no. 04-0784) [226]. The intense diffraction peak at 38.1° indicates that the preferred growth orientation of zero-valent gold was fixed in (111) direction [227]. This XRD pattern is typical of pure Au nanoparticles [226, 227].

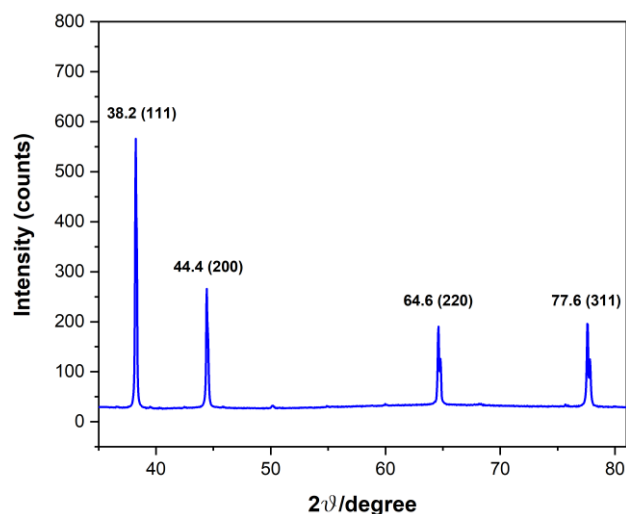
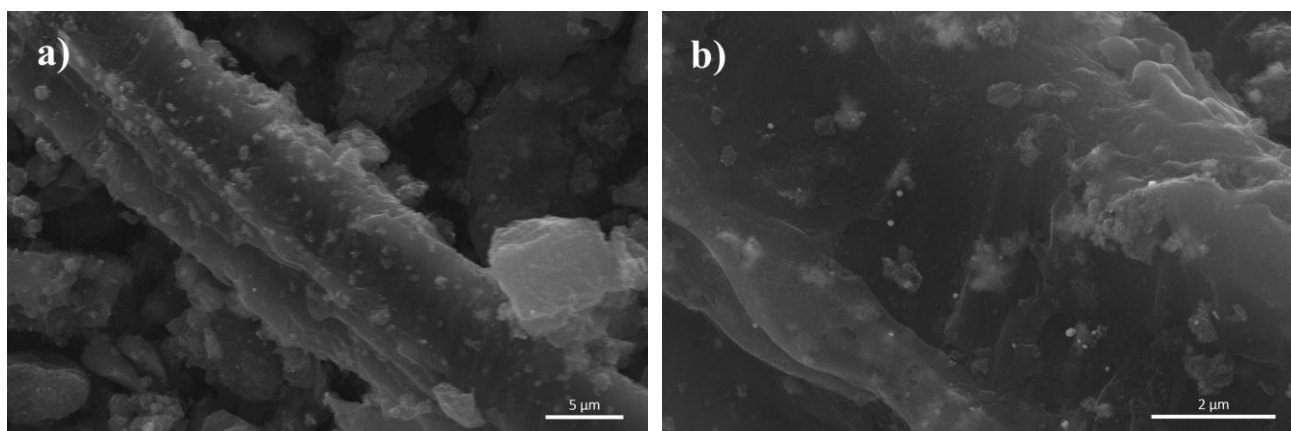


Figure 5.4. XRD pattern of the Au nanoparticles grown on activated carbon at optimized pH (9.5). The crystalline nanoparticles are represented by four peaks corresponding to standard Bragg reflections (111), (200), (220), and (311) of face centers cubic lattice. The intense peak at 38.2 represents preferential growth in the (111) direction.

The AuNP/C samples were further characterized by SEM and EDX. Fig. 5.5 (a) and (b) show the surface of the carbon after the deposition of the Au nanoparticles at pH 9.5. The coverage of the support appears uniform, with nanoparticles in the range <100 nm. Some aggregates were also spotted (not shown). Fig. 5.5 (c) shows the energy dispersive X-ray (EDX) spectra of the synthesized AuNP/C composite, confirming that the Au nanoparticles are supported on the carbon matrix. The peaks of O and Cl elements are residues from the synthesis and/or functional groups of the carbon support.



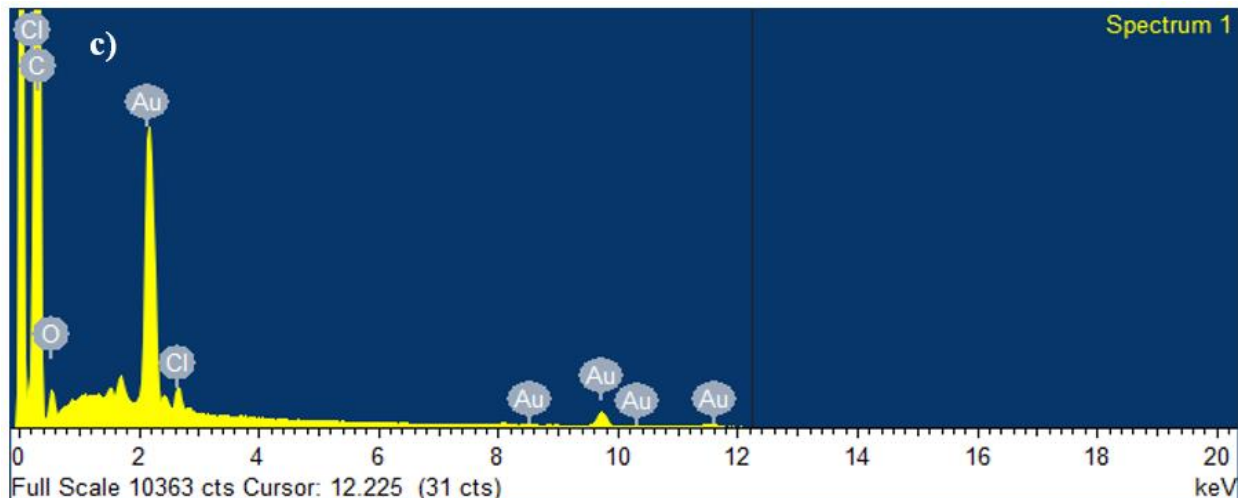


Figure 5.5. SEM images, (a) and (b), and EDX spectra (c) of the Au nanoparticles deposited on carbon synthesized at the optimized pH of 9.5 (9.3% loading).

More detailed information about the size and distribution of the Au nanoparticles across the support was obtained by HAADF-STEM characterization. Figure 5.6 (a) shows a HAADF-STEM image of the Au nanoparticles deposited onto the activated carbon. This investigation confirms that the Au nanoparticles are reasonably homogeneously distributed across the activated carbon (as was already suggested by SEM analysis). The particle size distribution was determined and is shown in Figure 5.6 (b). This shows that the mean particle size is 6.9 nm with a standard deviation of 2.8 nm. Figure 5.6 (a) shows that the Au nanoparticles are well spread out across the entire support. Some sporadic larger nanoparticles in the range of 50-100 nm can also be observed (see Fig. 5.14 for their particle size distribution).

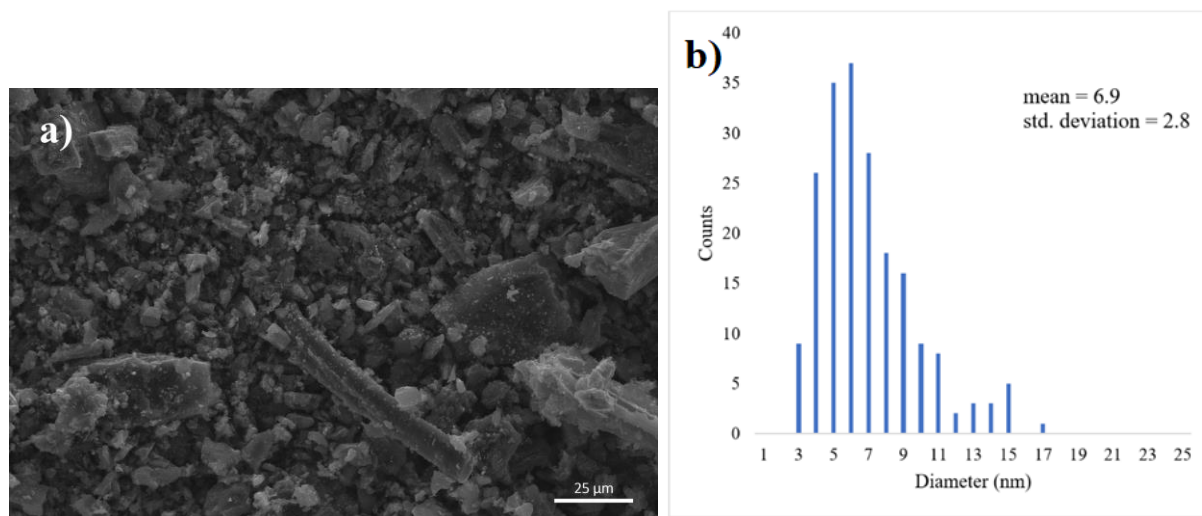


Figure 5.6. (a) HAADF-STEM image of the 9.3 wt % Au nanoparticles on activated carbon and (b) a histogram showing the particle size distribution of the nanoparticles for this sample.

Electron tomography was utilized for complete 3D characterization. This involves the acquisition of images at various projection angles allowing for visualization of the materials in 3D and therefore the determination of whether or not the Au nanoparticles are situated inside of the activated carbon, as was hypothesized, or are simply deposited onto the surface. Figure 5.7 shows

an ortho-slice taken from the 3D reconstruction in the xz direction, approximately halfway through the volume of the AuNP/C. This ortho-slice shows the presence of Au NPs (in the middle of the activated carbon). Therefore, it can be concluded that the particles are situated inside of the pores of the carbon support. This was further confirmed by comparing the total surface area of the bare Norit SX1G support (i.e., 1000 m² g⁻¹ according to the product data sheet) with that of AuNP@Norit, which showed a significant decrease to 517 m² g⁻¹. This is a further indication that the Au NPs are present in the pores and blocking them (*vide infra*).

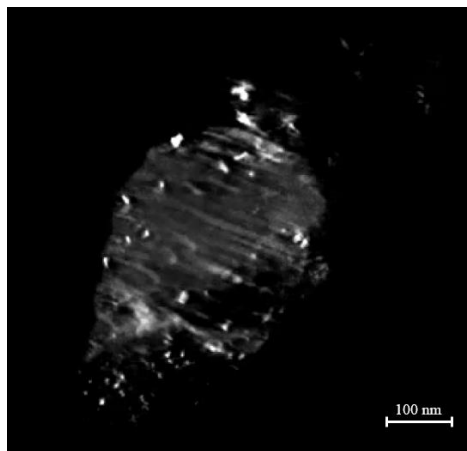


Figure 5.7. Ortho-slice in the xz direction approximately halfway through the volume of of Au/C sample at pH 9.5 (9.3% loading).

Energy-dispersive X-ray spectroscopy (EDX) maps were acquired from various areas of the sample to determine the composition, and confirm that there are Au NPs deposited on carbon. Figure 5.8 shows a HAADF-STEM image and the respective elemental maps for Au and C, obtained on a representative area of the sample. The results clearly indicate the presence of Au nanoparticles, homogeneously spread across the carbon matrix, with a low degree of agglomeration. The presence of Cu in the spectrum is due to the Cu grid and holder used for these measurements.

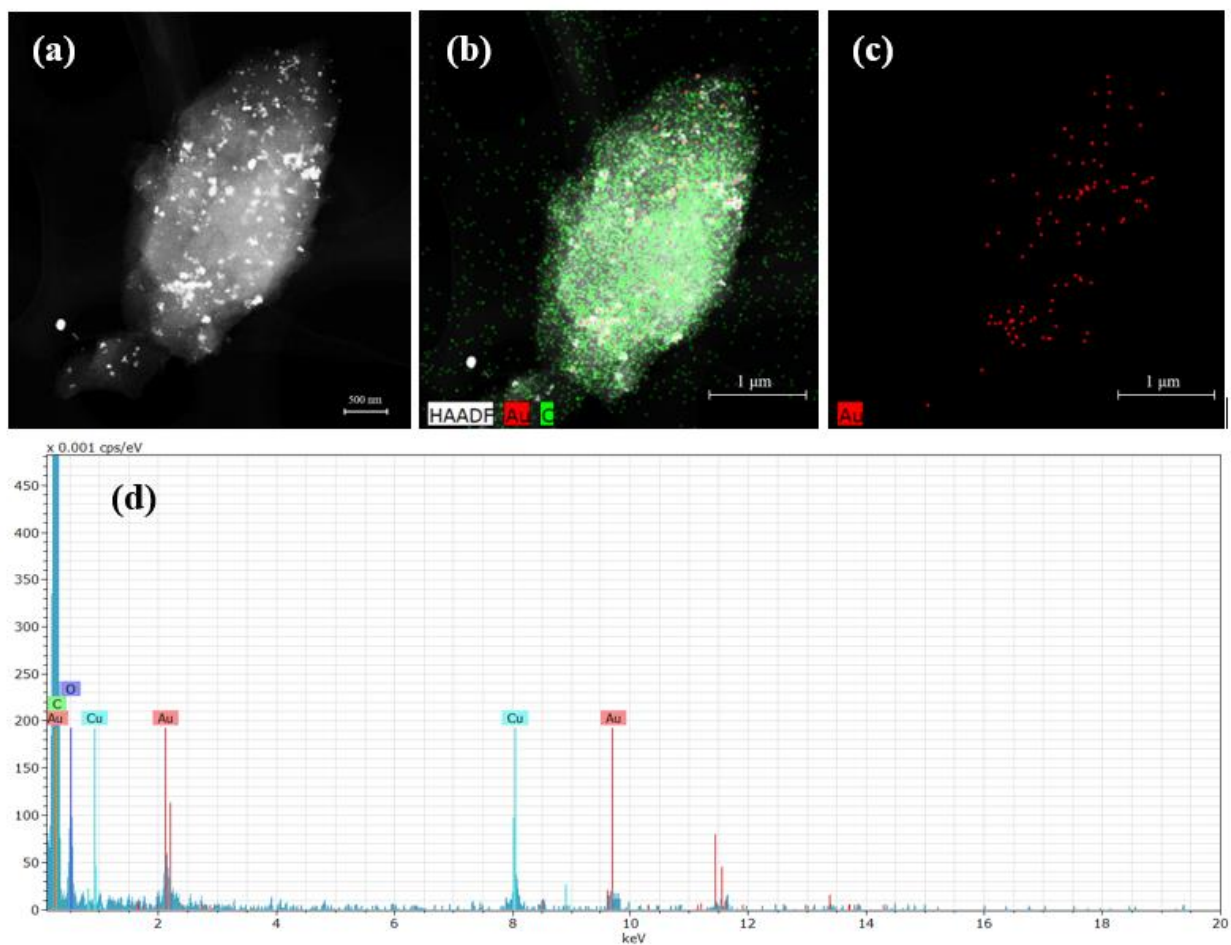


Figure 5.8. (a) HAADF-STEM image, (b, c) the respective EDX elemental distributions and (d) an EDX spectrum showing which elements are present for the Au/C composite with 9.3% Au-loading. For the EDX maps, Au is marked in red and C in green.

5.3.2 Catalytic activity testing

The very high specific EASA which was found for the AuNP/C catalyst, $282.4 \text{ m}^2/\text{g}_{\text{Au}}$, is mainly ascribed, in addition to the Au loading, to the Au nanoparticles size and homogeneous spread onto the activated carbon support, which has a particularly high specific surface area, most of which is concentrated inside its pores (ca 99.8%). A high EASA, typically boosts electrons transfer and mass transport of reactants and intermediates, leading to enhanced electrocatalytic activity [206]. To understand the electrocatalytic activity of the as-synthesized AuNP/C@GC catalyst towards gluconic acid oxidation, a cyclic voltammogram was recorded at ambient temperature, with a stirring velocity of 700 rpm, in 0.1 M NaOH (pH 13) with increasing amount of gluconic acid (Fig. 5.9).

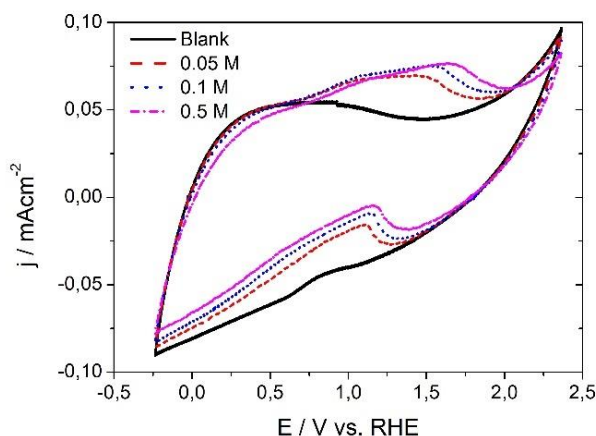


Figure 5.9. Voltammograms of AuNP/C@GC electrode in 0.1 M NaOH recorded at 50 mVs^{-1} , at $20 \text{ }^\circ\text{C}$ and stirring the solution at 700 rpm, with increasing amount of gluconic acid (from 0 to 0.5 M).

As expected, no oxidation peaks are observed in the cyclic voltammogram in the blank solution while, when gluconic acid is added, a small oxidation peak characterized by a left shoulder appears between 1 and 2 V_{RHE} , which was found, in our previous study, to be specific for the oxidation of the hydroxymethyl group on C6 in the gluconic acid molecule on gold [168]. Thus, the increase of current density with the concentration of gluconic acid in solution indicates reaction of the substrate with the gold active sites in this potential range. However, the current density reaches a maximum of only ca 0.08 mA cm^{-2} . Considering the high value of EASA of this catalyst (39.5 cm^2), we expected to observe a much higher electrocatalytic activity, and thus current density, at this potentials. Indeed, previously, we measured a similar current density, in the range of 0.22 mA cm^{-2} (in respect to the EASA), using a bare gold flat electrode with an EASA of only 0.702 cm^2 [168, 196]. Unfortunately, a 10^2 increase in EASA did not result in an increase in activity. To understand if a deactivation process was responsible for the limited reactivity of the catalyst, we recalculated the EASA of the catalyst after cycling it in a gluconic acid solution. The measurement of the EASA was repeated on the catalyst after cyclic voltammetry in 0.05 M gluconic acid and 0.1 M NaOH, and the result remained unchanged, proving that the catalyst does not get deactivated during the cycling. In addition, particle size upon electrochemical cycling also does not alter (Fig. 5.15 in SI), which leaves two possible explanations for the low electrocatalytic activity that is detected. 1. Based on the 3D reconstruction (*vide supra*) it is possible that the substrate, gluconic acid (molecule size $\sim 1 \text{ nm}$ [228, 229]), cannot easily access the majority of the electroactive surface area of the catalyst, located inside the micropores ($< 2 \text{ nm}$) of the activated carbon [230, 231]. In such case, the EASA available for the reaction would be only a small fraction of the total calculated EASA, which means it becomes close to that of the flat electrode. 2. Another hypothesis is that the stabilising agent, PVP, was not removed completely during catalyst preparation, or that, at the chosen conditions (i.e., concentration of NaBH_4 , immobilisation time), it reabsorbed on the AuNPs [218]. The presence of PVP on the AuNPs can block the access of reactant molecules to the surface atoms, thereby lowering activity of the NPs [216].

As a proof of concept, we performed the reaction in a flow reactor configuration where mass transfer limitations are excluded. For the continuous flow experiments, we used the reactor setup described in the Experimental section with the synthesized AuNP/C dispersed over a Ti felt as

catalyst, with a total EASA of 919.3 cm². In first instance, cyclic voltammetry experiments were performed at increasing concentrations of gluconic acid. Fig. 5.10 presents the current density vs. concentration of gluconic acid obtained at a fixed potential of 1.7 V_{RHE}, corresponding to the oxidation peak, at a flow rate of 20 mL min⁻¹ and a scan rate of 20 mV s⁻¹, utilizing a 0.1 M NaOH solution. For comparison, we report the results obtained for the AuNP/C@Ti system, consisting of the synthesized AuNP/C catalyst dispersed over a Ti felt, as well as the Ti felt alone, to confirm it does not contribute to the reaction.

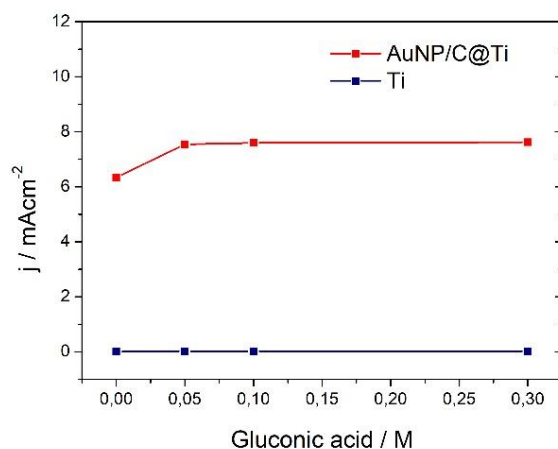


Figure 5.10. Plot current density vs. gluconic acid concentration obtained extracting the current density values at fixed potential of 1.7 V_{RHE} (corresponding to the oxidation peak) from the cyclic voltammetry study of AuNP/C@Ti (red line) and Ti felt alone (blue line) at 20 mVs⁻¹, 20 °C and 20 mLmin⁻¹, from a starting solution 0.1 M NaOH.

The data show clearly that, upon addition of gluconic acid, the current density has only a slight increase, of ca 1 mA cm⁻², and that it does not increase further when the concentration of gluconic acid in solution is raised. This confirms the results obtained in the batch cell, where only a small part of gluconic acid is able to react with the gold as saturation is quickly achieved here (no further increase in current density after adding only small amounts of gluconic acid). Despite the contribution of the higher convection given by the continuous flow, the mass transfer inside the pores of the carbon matrix remains hindered, as such limiting the reaction. Control experiments were also conducted at higher flow rates (> 20 mL min⁻¹), but no difference was observed. Given the very small difference in current density between the blank solution and the solutions containing gluconic acid, we can again assume that this is due to the limited availability of the active sites for reaction. Long-term electrolysis experiments were conducted applying a constant current density, and the product solutions were analyzed by HPLC. The results of chronopotentiometry experiments conducted at 10, 20 and 30 mA cm⁻², in a solution of 0.05 M gluconic acid and 0.1 M NaOH are shown in Fig. 5.11.

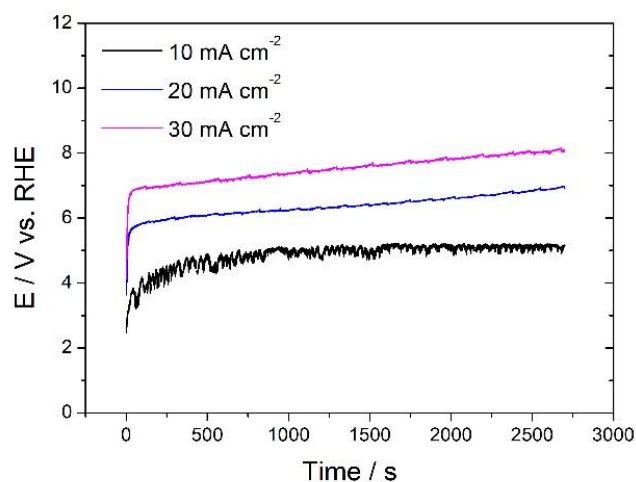


Figure 5.11. Results of chronopotentiometry experiments conducted at constant current densities of 10, 20 and 30 mAcm⁻² in the flow cell, in a solution 0.05 M gluconic acid and 0.1 M NaOH. At these currents, the O₂ evolution reaction takes place, as evidenced by the high potentials (y-axis) and the increasing O₂ bubbles formation with the current density at the anode.

The chronopotentiometry experiments confirm that when applying such high current density, the only reaction that occurs at the surface of the AuNP/AC@Ti electrode is the O₂ evolution reaction, which, in fact, takes place at these high potentials, and which was also evidenced by the heavy formation of bubbles at the anode, confirmed to be O₂ by gas chromatography (GC) measurements. Chromatographic analysis of the liquid product stream revealed what we expected: no glucaric acid or relevant amount of oxidation products is detected (Fig. 5.16 in SI).

In conclusion, in this work, we used an efficient synthesis method to produce an Au-based catalyst with very high EASA at low metal loading. The main advantages of this synthesis are its simplicity and an optimal Au utilization (up to 93%), with only 7% being lost during the different synthesis steps. This result was achieved by maximizing the interaction between the metallic precursor, the Au cations, and the carbonaceous support, activated carbon (Norit), during the immobilization step, by fine-tuning the pH of the synthesis broth. At pH 9.5 the maximum amount of gold was deposited on the Norit, resulting in a final loading of 9.3 wt%. Physical characterization revealed the successful deposition of very small nanoparticles, of average size between 5 and 20 nm, and their homogeneous distribution inside the pores of the AC. The specific EASA of the catalyst was found to be as high as 282.43 m² g_{Au}⁻¹, which is higher than typical values found in literature [197, 205, 232]. The as-synthesized catalytic system was tested for the electrooxidation of gluconic acid in alkaline media in an attempt to boost the productivity of glucaric acid exploiting its very high EASA. However, cyclic voltammetry experiments conducted both, in batch and in continuous flow reactor configurations, revealed a very limited reactivity towards gluconic acid oxidation, evidenced by the low current density registered at the gluconic acid oxidation peak, while, on the other hand, O₂ evolution reaction seemed to proceed favourably, as evidenced by the formation of O₂ bubbles, which increased with applied increasing current density. The low current density detected in presence of gluconic acid could be explained assuming that the gold active sites are not completely accessible to the reactant molecules. We have 2 hypothesis which could explain this behaviour. Our first hypothesis is that the reagent, gluconic acid, cannot easily diffuse inside

the catalyst pores because of its spacial hinderance: gluconic acid, like glucose, is a rather bulky molecule with a relatively low diffusivity compared to other, smaller, organic molecules [184]. This spatial hindrance may have prevented gluconic acid to penetrate inside the pores of the catalyst, leaving, as only accessible active sites the Au nanoparticles situated outside the pores of the carbon matrix. In fact, most of the EASA of the synthesized catalyst is located inside the pores of the carbon matrix (as evidenced by TEM tomography), as the area inside the pores can go up to 99.8% of the total available surface of the carbon support. This would result in an accessible EASA of only 0.2% of the total, corresponding to ca 0.079 cm² for the catalytic system used in the batch cell and 1.838 cm² for the one used in the flow cell, which are close to the value found for the flat Au electrode (0.702 cm²) and would thus explain the low performance. One way to prove this hypothesis would be to perform Fourier-transform infrared spectroscopy (FTIR) and verify whether gluconic acid is present on the gold active sites located inside the pores of the carbon support. In a recent work, Oña et al. have highlighted that carbon supports with relatively large pores (mesopores) are ideal candidates as catalytic supports for the conversion of high molecular weight compounds such as sugars [233]. In this case, one solution to overcome the low reactivity towards gluconic acid electrooxidation could be to deposit the Au NPs over a meso/macro-porous activated carbon instead of the microporous one used in this study, compromising on the specific surface area.

Our second hypothesis concerns the possible presence of residual PVP capping agent on the AuNPs, which may block the access of reactant molecules to the surface atoms, thus lowering the activity of the nanoparticles [216]. On the one hand, it is possible that the treatment with NaBH₄ (paragraph 5.2.2) removed only part of the PVP used during the synthesis, leaving another part still adsorbed on the AuNPs. On the other hand, it may be that, during the immobilisation time, the PVP re-adsorbed on the gold surface. In fact, it has been demonstrated that the effective and complete desorption of organothiols such as PVP from the surface of AuNPs, when treated with NaBH₄, strongly depends on the concentration of NaBH₄ and on the incubation time [218]. The authors Ansar et al. observed that: a) the rate of organothiols desorption increases with increasing NaBH₄ concentration (i.e., the higher the concentration of NaBH₄, the lower the time needed for complete desorption); b) the desorbed organothiols can be completely re-adsorbed onto the AuNPs upon prolonged sample incubation [218]. One way to verify this hypothesis could be to perform Raman or FTIR measurements to verify whether PVP is still present on the catalyst surface upon treatment with NaBH₄. In such case, further optimisation of the catalyst preparation procedure would be needed to identify the right concentration of NaBH₄ and incubation time to ensure complete removal of PVP.

5.4 Conclusions

The one-pot synthesis of a gold catalyst made of gold nanoparticles deposited onto the surface of activated carbon was achieved by a wet impregnation method at an optimal pH of the bath of 9.5, critical in determining the gold-carbon interaction, with a resulting loading of 9.3% and an Au utilization as high as 93%. The catalyst was characterized by SEM-EDX and HAADF-STEM electron tomography, showing a very uniform coverage of the carbon matrix with the Au nanoparticles, whose size ranged between 5 and 20 nm. The catalytic system was tested for the electrooxidation of gluconic acid in alkaline media in an attempt to boost the productivity of glucaric acid by exploiting the high specific EASA, which was calculated to be 282.43 m² g_{Au}⁻¹, which is 10² times higher than that found for the Au bulk electrode used for our previous studies.

A low catalytic activity towards gluconic acid electrooxidation was found, which may be ascribed to the inaccessibility of the gold active sites by the reactant molecules due to 1. a difficult diffusion of the reagent inside the catalyst nanopores caused by spacial hinderance, or 2. the presence of residual PVP strongly adsorbed on the AuNPs which blocks the access of reactant molecules to the surface atoms. Further research is still needed to address this limited catalytic activity: i.e., employing meso/macro-porous activated carbon supports instead of the microporous ones; or optimising the catalyst preparation procedure ensuring the complete removal of PVP.

We believe that the as-developed AuNP/C catalytic system may be a good fit for a wide range of applications in addition to sugars electrooxidation, for example, in reactions involving small molecules (i.e. gasses as O_2), which makes it an interesting potential candidate for reactions involving molecules with high diffusivity as CO_2 , CH_4 , N_2 . In particular, it could be a very good fit for application in the nitrogen reduction reaction (NRR), where gold is known to achieve the highest selectivity [234, 235].

5.5 Supporting information

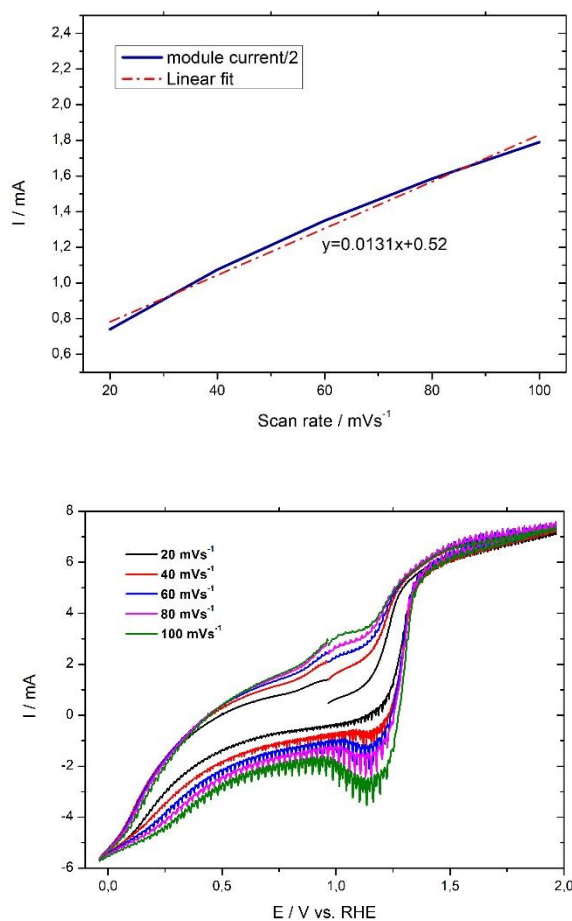


Figure 5.12. Plot of the module of the current vs. the scan rate at the potential of $0.71 V_{RHE}$ for the AuNP/C@Ti system in the electrolyte solution ($0.1 M NaOH$). The original data are reported in the plot of current vs. potential at different scan rates ($20, 40, 60, 80$ and $100 mVs^{-1}$) (bottom).

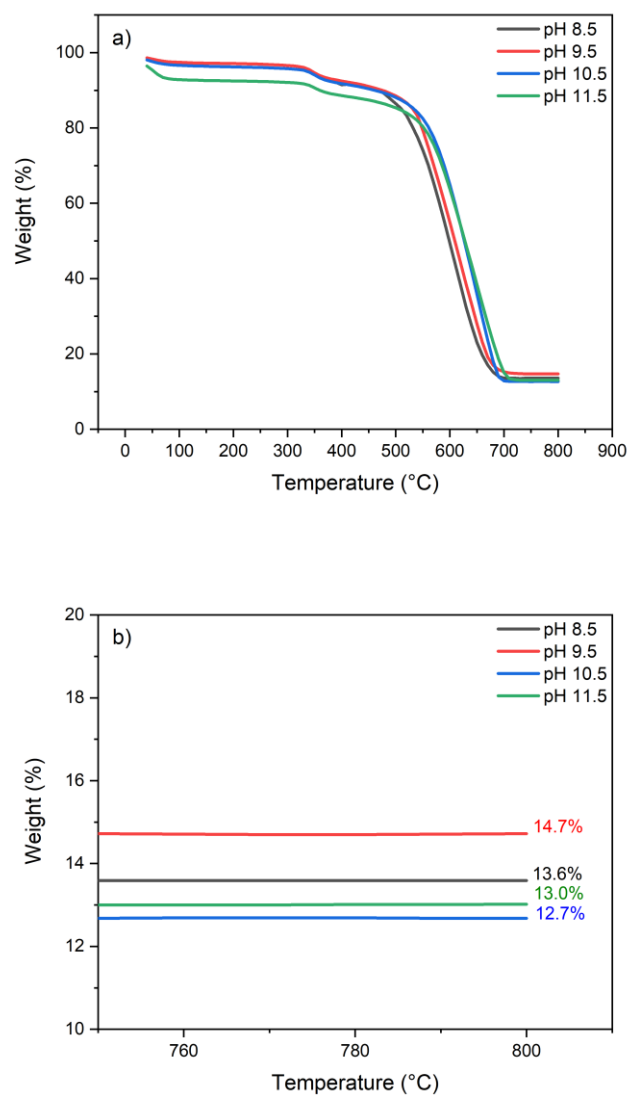


Figure 5.13. Thermogravimetric plots for 4 samples of catalysts obtained, respectively, from the synthesis conducted at pH 8.5, 9.5, 10.5 and 11.5.

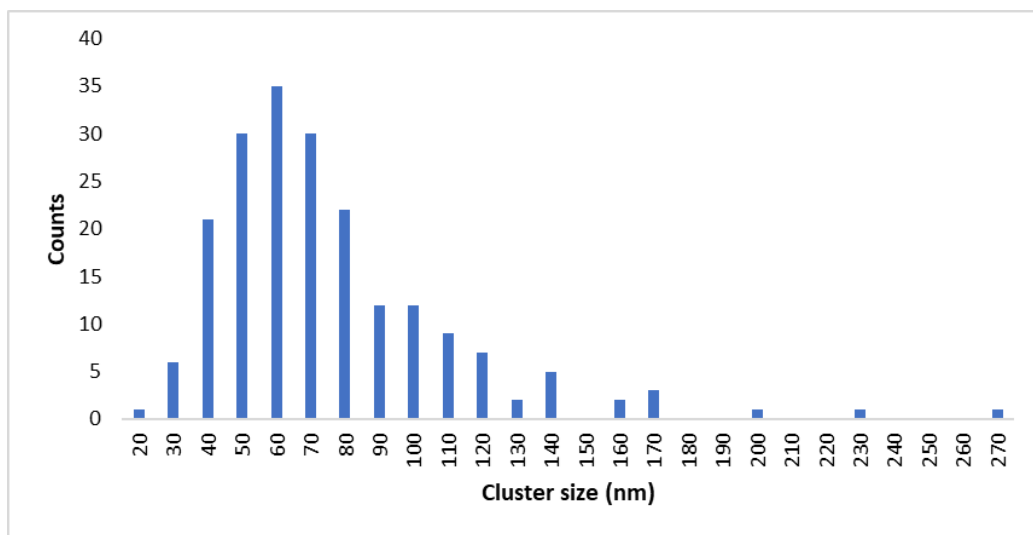


Figure 5.14. Particle size distribution (PSD) of the sporadic larger nanoparticles in the range of 50-100 nm (mean size 75 nm) obtained utilizing the TEM images.

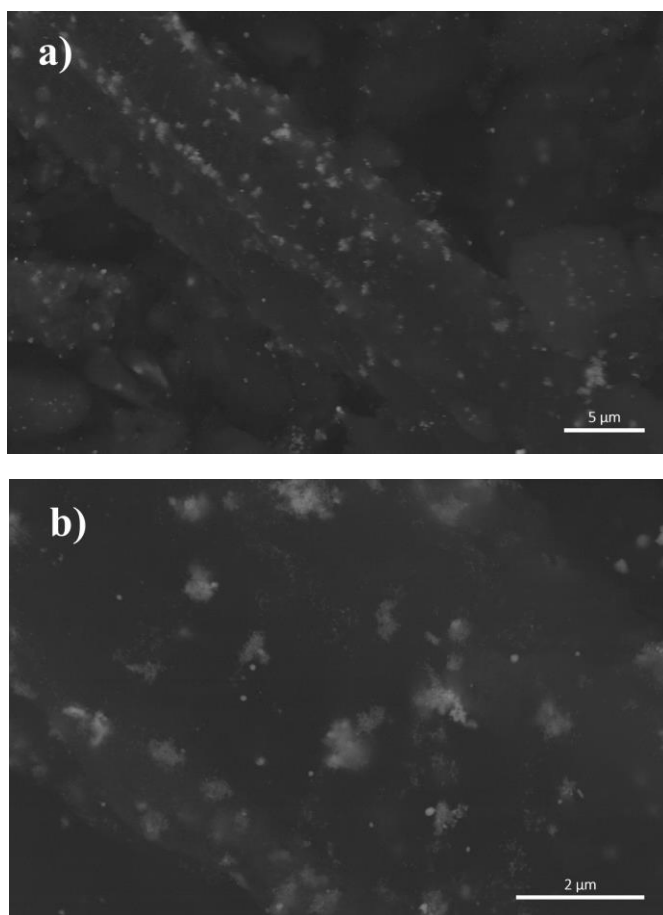


Figure 5.15. SEM pictures of the AuNP/C@GC system after 10 cycles in 0.1 M NaOH and 0.5 M gluconic acid recorded at 50 mV s^{-1} and $20 \text{ }^\circ\text{C}$ while stirring the solution at 700 rpm.

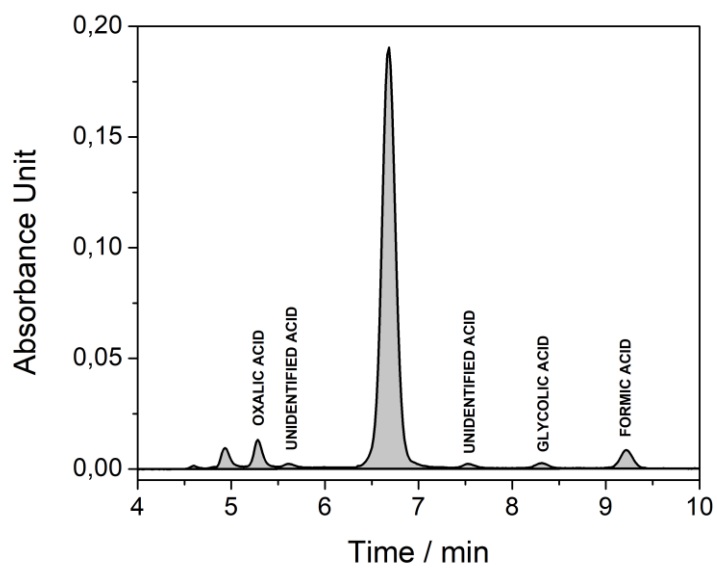


Figure 5.16. HPLC graphs of the reaction solutions after 1h electrolysis in the flow reactor.

Chapter 6

Conclusions and future perspectives

6.1 Conclusion

Carboxylic and di-carboxylic acids derived from the oxidation of glucose are considered one of the most important classes of chemicals that can be derived from biomass. Amongst these, gluconic and glucaric acid, are used as raw materials for the production of a variety of commodity products (including detergents, coatings/paints, cancer prevention therapies, etc.). The electrochemical oxidation of glucose is an environmentally friendly, viable alternative to the traditional chemical routes as it obeys to all the principles of Green Chemistry. However, the successful implementation of such process passes through some fundamental steps: 1) selection of the electrocatalyst, 2) optimization of the reaction conditions, and 3) up-scaling. The ultimate goal of this doctoral dissertation was to develop an electrocatalytic process for the selective oxidation of glucose to gluconic and glucaric acid. The work was divided into 4 experimental chapters, where the results of each chapter represent the starting point for the next. Chapters 2 and 3 comprised an investigation of various electrocatalysts for glucose oxidation; chapter 4 was dedicated to the study of the impact of the reaction parameters and; finally, in chapter 5, a facile synthesis method was developed for the production of a catalytic system with a high EASA.

6.1.1 Electrocatalysts for glucose oxidation to gluconic and glucaric acid

In the first part of the experimental work, Chapter 2 and 3, we investigated the activity of various catalysts towards glucose electrooxidation, with particular focus on their selectivity towards the products of interest: gluconic and glucaric acid. As shown in the literature study, Chapter 1, heterogeneous electrocatalysis is preferred over the homogeneous alternative as it brings the advantage of an easy separation and recovery of the catalyst after reaction. Amongst various heterogeneous catalysts with electro-reactivity for glucose oxidation, MnO_2 was the first one to be employed successfully for a selective production of gluconic and glucaric acid. For this reason, our research started with the investigation of the electrocatalytic activity of MnO_2 -based catalysts towards glucose oxidation, understanding the underlying mechanism and its potential application for the production of glucaric acid. To this end, nanostructured MnO_2 porous films were deposited over various supports using anodic and cathodic deposition as well as through a chemical impregnation method. Electrochemical evaluation revealed that, at equal loading, the catalyst with the smallest porosity (45 nm average pore size) also resulted in the highest electrocatalytic activity in presence of glucose ($\sim 10.5 \text{ mA cm}^{-2}$), suggesting a possible correlation between these two parameters. Unfortunately, none of the produced MnO_2 electrocatalysts yielded the desired products in significant quantities, which is why we did not pursue this material any further and shifted towards noble metals, given their promising performance in the glucose oxidation reaction. As a first step, in Chapter 3, we studied the reactivity of three noble metals, copper, platinum and gold, as they all had shown electrocatalytic activity in presence of glucose, using rotating disk electrodes. One important first observation here was that, in alkaline conditions, D-glucose is consumed by two chemical reactions: one is the isomerization of D-glucose into D-fructose, which is a reversible process, the other is its thermal, base-catalyzed, oxidative degradation to various low molar-mass carboxylic acids (i.e., formic, oxalic, tartaric, glycolic acid), which is irreversible and undesired. In order to maximally impede these side-reactions and promote the electrochemical reaction, it was found that lowering the temperature is beneficial, with an optimal performance occurring at a temperature of 5°C . Apart from the importance of the reaction conditions (i.e., alkaline pH and low temperature), the most interesting finding of this work was the strong

relationship between potential and reactivity of the functional groups in the glucose molecule. For all the three noble metals examined, distinct oxidation potentials were found, which preferably promote the oxidation of either the aldehyde or the hydroxymethyl terminal groups, without breaking the 6-carbons backbone. In the case of copper, however, the highest potential did lead to C-C cleavage and formation of lower molar mass carboxylic acids. Gold was found to be the catalyst with the highest activity and selectivity to gluconic and glucaric acid, owing to two distinct oxidation peaks for glucose, one at low potential, 0.55 V_{RHE}, which promoted the oxidation of the aldehyde group and formation of gluconic acid (86.6 % selectivity at 5 °C and 65 h), the other at higher potential, 1.34 V_{RHE}, which promoted the oxidation of the hydroxymethyl group and further conversion to glucaric acid (13.5 % selectivity to glucaric acid and 65.8 % to gluconic acid at 5 °C and 65 h reaction time). These first positive results achieved with gold, which showed, not only electrocatalytic activity towards glucose oxidation, but also high selectivity towards gluconic and glucaric acid, motivated us to continue the investigations focusing on this catalyst with the intent to optimize selectivity and productivity of glucaric acid.

6.1.2 Investigation of the influence of the reaction parameters

To understand the reaction mechanism and identify the conditions that maximize the selectivity, in Chapter 4 we investigated the influence of and optimized different operational parameters, i.e., pH, initial substrate concentration, applied potential, reaction temperature and reaction time, for the two reaction steps, the oxidation of glucose to gluconic acid and for the further oxidation of gluconic acid to glucaric acid. For the first oxidation to gluconic acid, we achieved maximum selectivity at moderately high pH, low temperature and low initial concentration of glucose (i.e., pH 11.3, 5 °C and 0.04 M initial glucose). Higher temperatures increased the conversion rate but went at the cost of the rapid degradation of glucose due to the increased kinetics of the chemical side-reactions. Similarly, increasing the pH also increased glucose conversion, but at the expense of a decreased selectivity to gluconic acid due to an excessive adsorption of hydroxyl ions (OH⁻) onto the Au surface, as such decreasing the number of active sites available for glucose oxidation. The electrolysis of more concentrated solutions of glucose resulted in a lower selectivity to gluconic acid because of the rapid saturation of the catalyst surface and increased viscosity of the solution, which hindered the mass transfer towards the Au active sites, thus limiting the (heterogeneous) electrochemical reaction. Finally, it was found that the selectivity of this reaction remains constant for very long reaction times, and glucose conversion continuously increases, but the conversion rate decreases due to mass transfer limitations. As for the electrooxidation of gluconic acid to glucaric acid, a very high selectivity was achieved in the potential range examined, where Au(OH)_x was found to be the main species of gold involved in the catalytic process. Since gluconic acid is stable in alkaline media (no side-reactions), pH, gluconic acid initial concentration, reaction temperature and time did not have a significant impact on the selectivity. However, even at optimized conditions, only limited concentrations of glucaric acid were obtained during the electrolysis. This may have been caused by an early deactivation of the flat Au electrode, due to fouling by glucaric acid. The good selectivity obtained, 97.6% for the first reaction step (at 5 °C, with 25 % glucose converted) and 89.5 % for the second reaction step (at 1.1 V_{RHE}, with 4.6 % gluconic acid converted), motivated us to try and address the deactivation issue which limited the conversion of gluconic acid to glucaric acid.

6.1.3 Synthesis of gold nanoparticles

In the final chapter, we synthesized a gold-based catalyst suitable for larger scale applications characterized by high electroactive surface area, $282.4 \text{ m}^2 \text{ g}_{\text{Au}}^{-1}$, relatively low metal loading, 9.3 %, and high specific surface, $517 \text{ m}^2 \text{ g}^{-1}$. To this purpose, we developed a synthesis approach to deposit gold nanoparticles onto an activated carbon support. Activated carbon was used as catalytic support because of its high porosity, which contributed to further increase the surface-to-volume ratio of the catalyst, and because of its positive interaction with the gold precursor, which allowed the deposition of gold nanoparticles during the synthesis. For its preparation, we developed a very simple impregnation method which allowed the synthesis of a catalyst with a very high electroactive surface area and, at the same time, low loading of precious gold. A critical parameter in this synthesis was found to be the pH of the synthesis bath. Indeed, between 8.5 and 11.5, an optimal pH was found at 9.5, where gold-carbon interaction was optimal and a maximum Au loading could be obtained. The physical characterization of the catalyst revealed uniform coverage of the carbon matrix with very small gold nanoparticles, distributed in a narrow size range (i.e., 5-20 nm). Utilizing TEM, it was observed that Au was mainly present inside the pores of the carbon support, where most of the surface area is located. The EASA was calculated to be 10^2 times higher than that of the Au bulk electrode used for our previous studies, which was extremely promising for our application. However, our experiments conducted both, in batch and in continuous flow reactor configurations, revealed a very limited activity towards gluconic acid oxidation, with a maximum current density of, respectively, 0.08 and 7.5 mA cm^{-2} , at $1.7 V_{\text{RHE}}$. Such low catalytic activity towards gluconic acid electrooxidation was ascribed to the inaccessibility of the gold active sites by the reactant molecules. We gave 2 possible explanations for this behaviour: 1. a difficult diffusion of the reagent inside the catalyst nanopores caused by its spacial hinderance, or 2. the presence of residual PVP strongly adsorbed on the AuNPs blocking the access of reactant molecules to the surface atoms. The occurrence of oxygen evolution reaction on this catalyst, even at moderate voltages, suggests its potential use for applications involving small gas molecules as O_2 , CO_2 , CH_4 and N_2 .

6.2 Future perspectives

While this thesis has demonstrated the potential application of noble metals, such as gold, in the electrocatalytic oxidation of glucose to gluconic and of gluconic acid to glucaric acid, many opportunities for extending the scope of this doctoral dissertation are possible. The final paragraphs are dedicated to improvements, perspectives and suggestions for future research.

6.2.1 Mesoporous carbon supports and gold direct deposition

In chapter 5, to improve the electrocatalytic activity of the catalyst and overcome the early deactivation possibly caused by fouling by glucaric acid, we chose a catalyst design consisting of gold nanoparticles embedded in a microporous, activated carbon matrix. However, it was found that such catalyst configuration yielded a very limited reactivity towards gluconic acid oxidation. One possible explanation for this behaviour was given assuming that the gold active sites are not completely accessible to the reactant molecules because gluconic acid cannot easily diffuse inside the catalyst pores because of its spacial hinderance. In fact, gluconic acid, like glucose, is a rather bulky molecule with a relatively low diffusivity compared to other, smaller, organic molecules. One way to address this could be the use of meso/macro-porous carbon supports as, compared to the microporous ones, they are characterized by larger pores (for reference: average pore diameters

> 50 nm for macroporous materials, between 2 and 50 nm for mesoporous materials, and <2 nm for microporous materials). Electrocatalysts obtained by direct deposition of gold over a support characterized by large porosity, i.e., felts, nets, foams, etc., could be a possible alternative solution as high surface area catalyst for glucose/gluconic acid electrooxidation. Also in this case, to optimize the specific surface of the catalyst and minimize the loading, the active phase can consist of nanoparticles rather than thin films. One important factor to take into account when designing catalysts based on precious metals, is the maximization of the utilization of the active phase by the synthesis method. In fact, as noble metals are extremely expensive and rare, it is very important to develop synthesis techniques which result in little to no losses of active phase during the different steps. In our design, by utilizing activated carbon as support for the gold nanoparticles, we guaranteed an efficient metal utilization (~93%) by leveraging the favorable gold-carbon interaction, while also ensuring stability of the gold nanoparticles which did not aggregate during cycling. The direct deposition of gold on the final support, being it chemical or electrochemical, may be more challenging and would require a more in-depth investigation.

6.2.2 Bi-metallic catalysts and promoters

In chapters 3 and 4, we investigated the mechanism of the electrocatalytic oxidation of glucose on noble metals, particularly on gold, and identified 2 distinct electrocatalytic steps: the first being the transformation of glucose to gluconic acid and the second, the conversion of gluconic acid to glucaric acid. While the first reaction is fully unraveled, the mechanism of the transformation of gluconic acid to glucaric acid is not yet fully clear and requires further investigation. We have seen that, despite the high selectivity, very limited concentrations of glucaric acid were obtained during the electrolysis of gluconic acid due to an early deactivation of the gold electrode most probably caused by fouling by the product itself. One way to overcome the deactivation of the catalyst could be by altering its morphology and composition. To this purpose, one option is to alloy gold with a second metal. Indeed, bimetallic nanocatalysts have shown a much higher stability and higher selectivity compared to the corresponding monometallic systems. Some examples of alloys of gold with another metal which have been found to exhibit enhanced electrocatalytic activity towards glucose oxidation are: Pd-Au, Au-Pt, Au-Bi and Au-Ag. Another way, often reported in literature, to minimize deactivation and improve selectivity, is adding a promoter to the system. There are many cases in literature where dissolved Bi and Pb adatoms (the promoters) are used during the oxidation of sugars to boost the activity and selectivity of the precious metal catalyst (i.e., Pt, Pd or Au). Both these approaches should be investigated further under the ideal conditions found in this work to further advance the field of glucose to glucaric acid oxidation.

6.2.3 Optimization of the AuNP@AC catalyst and application for NRR

In Chapter 5, we developed a chemical method that allowed to fabricate an efficient gold-based catalyst with a high EASA and, at the same time, low metal loading, while utilizing almost the totality of gold invested in the synthesis procedure. Experiments conducted in both, batch and continuous flow reactor configurations, revealed a very limited reactivity towards gluconic acid oxidation. One possible explanation given for this behaviour concerned the presence of residual PVP capping agent on the AuNPs, which blocked the access of reactant molecules to the surface atoms, thus lowering the activity of the nanoparticles. Indeed, the effective removal of PVP from the surface of AuNPs using NaBH₄ is strongly dependent on the concentration of NaBH₄ and on the incubation time. Further research should focus on optimizing these synthesis parameters to ensure

complete removal of PVP. Raman or FTIR techniques should be used to detect the quantity of PVP on the AuNPs surface.

During the electrochemical activity testing, we observed that oxygen evolution reaction, for which gold is a well-established catalyst, proceeded favourably on the AuNPs/C catalyst, even at moderate potentials. We have not investigated further the use of the as-developed catalyst for application to ORR as it was out of the scope for this thesis. However, these observation may suggest a good fit for reactions involving small molecules with high diffusivity such as O₂, CO₂, CH₄ or N₂. Amongst these, one particularly interesting application would be the nitrogen reduction reaction (NRR), for which, gold is in fact the most selective single material. As the NRR is one of the subjects investigated in our group, we will utilize the as-synthesized catalyst for this reaction to contribute to the development of a more sustainable and environmentally friendly route for the production of ammonia. On the other hand, for the upscaling of glucose electrooxidation process, and, potentially, for application in other oxidation processes involving sugars and sugar derivatives (i.e. fructose, xylose, lactose, levulose, glycerol, xylitol, etc.), it could be interesting to investigate catalytic systems in which gold is directly deposited onto high surface area supports with large porosity, like felts, nets or foams.

List of Figures

Figure 1.1. Electricity as the main source of energy for all our applications in society [6, 7].....	2
Figure 1.2. Schematic representation of a circular economy [8].	3
Figure 1.3. Types of Biomass (adapted from [6])	5
Figure 1.4. Chemical structure depiction of D-glucaric acid, the D-enantiomer of glucaric acid (adapted from [25]).....	6
Figure 1.5. Derivatives of Glucaric acid (adapted from [26]).....	7
Figure 1.6. Scheme of the variety of applications of glucaric acid in different sectors (adapted from [18]).	7
Figure 1.7. Nitric acid oxidation of D-glucose (1) to D-glucaric acid (2) isolated as monopotassium D-glucarate (3) (adapted from [52]).....	8
Figure 1.8. Redox system for TEMPO-like nitroxide mediated oxidations [62].	9
Figure 1.9. Proposed genealogy of the degradation products observed in the nitroxide-mediated oxidation of D-glucose to D-glucaric acid [61].	10
Figure 1.10. TEMPO-mediated electro-oxidation of D-glucose (1) to D-glucaric acid (2) and the tricarboxylic acid (3) (adapted from [78]).	13
Figure 2.1. Schematic diagram to correlate deposition parameters change with manganese oxide morphology, anodically deposited on Au-coated glass (adapted from [84])	21
Figure 2.2. Cyclic voltammetric study of Pt in 0.01M MnSO ₄ and 0.5M Na ₂ SO ₄ solution recorded at a scan rate of 5 mV s ⁻¹	22
Figure 2.3. Cyclic voltammetric study of GC in 0.01 M MnSO ₄ and 0.5 M Na ₂ SO ₄ solution recorded at a scan rate of 5 mV s ⁻¹	23
Figure 2.4. SEM images, (a) and (b), and c) EDX spectra of the MnO ₂ inter-connected nanosheet layer deposited over the Pt electrode by anodic deposition at 1.91 V _{RHE} for 20 min at 50 mV s ⁻¹ from a 0.01M Mn ²⁺ in 0.5M Na ₂ SO ₄ solution.	24
Figure 2.5. SEM images, (a) and (b), and c) EDX spectra of the multi-scale micro/nano porous MnO ₂ film fabricated by cathodic deposition using hydrogen bubbling as dynamic template over the Pt RDE. .	26
Figure 2.6. SEM image, left, and EDX spectra, right, of the nano porous MnO ₂ film fabricated by sol-gel chemical deposition over a Ti rod electrode.	27
Figure 2.7. a) Cyclic voltammetric study of MnO ₂ @Pt in blank solution, 0.5 M Na ₂ SO ₄ , (blue line) and with increasing concentration of glucose (lines green, 0.04 M, and red, 0.4 M) recorded at 100 mV s ⁻¹ ; b) cyclic voltammetry study of Pt in blank solution, 0.5 M Na ₂ SO ₄ , (grey line) and in a solution 0.4 M glucose (light blue line).	28
Figure 2.8. Cyclic voltammetric study in a solution 0.5M Na ₂ SO ₄ and 0.4 M glucose of MnO ₂ @ Pt obtained by anodic deposition (red line) and with cathodic deposition (green line), and MnO ₂ @ Ti obtained by chemical deposition (blue line), recorded at 100 mV s ⁻¹	29
Figure 2.9. The two anomeric forms of D-glucopyranose: the difference between the two anomers lies on the position of the OH functional group on the anomeric carbon C1, axial in the α form and equatorial in the β form (adapted from [143]).	30
Figure 2.10. a) and b) show the SEM images of the MnO ₂ @Au electrode obtained by anodic deposition at a constant potential of 1.91 V _{RHE} , for 20 min at 50 mV s ⁻¹ from a 0.01M Mn ²⁺ in 0.5M Na ₂ SO ₄ solution.	32
Figure 2.11. a) and b) show the SEM images of the MnO ₂ @GC electrode obtained by anodic deposition at a constant potential of 1.91 V _{RHE} , for 20 min at 50 mV s ⁻¹ from a 0.01M Mn ²⁺ in 0.5M Na ₂ SO ₄ solution.	32

Figure 2.12. a) and b) show the SEM images of the MnO ₂ @SS electrode obtained by cathodic deposition: 10 min at -0.7 V _{RHE} and 10 mV s ⁻¹ in 0.1M MnCl ₂ and 0.1M NaCl (hydrogen bubbling, step 1); 10 cycles between 0.6 and 1.6 V _{RHE} in a solution: 0.1M Na ₂ SO ₄ (electrooxidation, step 2).....	33
Figure 2.13. Chromatogram (a) and corresponding PDA spectrum (b) of gluconic (black line is a) and blue line in b)) and glucaric acid (red line).	33
Figure 2.14. Chromatogram of the resulting solution of 18 h electrolysis of 0.4 M Glucose in 0.5M Na ₂ SO ₄ at neutral pH on anodically deposited MnO ₂ @Pt at 20 °C and oxidation potential 1.61 V _{RHE} (black line) and 1.80 V _{RHE} (red line). All peaks visible in the chromatogram are smaller than the injection peak (at around 4.6 min), thus neglectable. None of them corresponds to gluconic (retention time 5.156 min) or glucaric acid (retention time 5.663).	34
Figure 2.15. a) Chromatograms of the resulting solutions of the electrolysis of 0.4 M Glucose in 0.5M Na ₂ SO ₄ at neutral pH on anodically deposited MnO ₂ @Pt at 20 °C and oxidation potential 2.0 V _{RHE} . a) is the chromatogram of the products after 1 h electrolysis (red line) compared with the chromatogram of the reaction solution before electrolysis (black line), obtained using an injection volume of 100 μL, in an attempt to better identify the products' peaks; b) is the chromatogram of the product solution at increasing electrolysis times, from 0 to 5 h, obtained using an injection volume of 10 μL. All peaks visible in the chromatograms are smaller than the injection peak (4.6 min). None of them corresponds to gluconic (retention time 5.156 min) or glucaric acid (retention time 5.663).	34
Figure 2.16. Chromatogram of the resulting solution of 65 h electrolysis of 0.4 M Glucose in 0.1M NaOH at pH 13 on anodically deposited MnO ₂ @Pt at 5 °C and oxidation potential 2.0 V _{RHE} (blue line), compared to that of the starting solution (black line). One peak in the chromatogram is considered relevant as higher than the injection peak: the peak at ca. 5.8 min retention time, which corresponds to gluconic acid, as confirmed by overlapping the chromatogram with that of pure gluconic acid (light blue line). The other, smaller peaks remained unidentified but are sufficiently small to be neglectable.	35
Figure 3.1. Electrochemical set-up designed for the long-term electrolysis: (1) Pt counter electrode (CE), in the cathodic compartment; (2) Nafion membrane; (3) reference electrode (RE) and (4) working electrode (WE), both in the anodic compartment.	39
Figure 3.2. Voltammograms of a) copper, b) platinum and c) gold electrodes in alkaline medium (0.1 M NaOH) recorded at 10 mVs ⁻¹ , at 20 °C without (dashed lines) and with (solid lines) 0.04 M D-glucose. .	41
Figure 3.3. Structural formulas of D-glucose and its three derivatives.....	43
Figure 3.4. Voltammograms of copper electrode in 0.04 M a) glucose, b) glucuronic acid, c) gluconic acid and d) glucaric acid (solid lines) in alkaline medium (0.1 M NaOH) recorded at 10 mVs ⁻¹ , at 20°C, compared with the blank solution (dashed lines).	44
Figure 3.5. Voltammograms of platinum electrode in 0.04 M a) glucose, b) glucuronic acid, c) gluconic acid and d) glucaric acid (solid lines) in alkaline medium (0.1 M NaOH) recorded at 10 mVs ⁻¹ , at 20°C, compared with the blank solution (dashed lines).	45
Figure 3.6. Voltammograms of gold electrode in 0.04 M a) glucose, b) glucuronic acid, c) gluconic acid and d) glucaric acid (solid lines) in alkaline medium (0.1 M NaOH) recorded at 10 mVs ⁻¹ , at 20°C, compared with the blank solution (dashed lines).	46
Figure 3.7. HPLC graphs of the reaction solutions after 65h electrolysis on (A) copper, (B) platinum and (C) gold.	52
Figure 4.1. Electrochemical set-up designed for the long-term electrolysis: (1) Pt counter electrode (CE), in the cathodic compartment; (2) Nafion membrane; (3) reference electrode (RE) and (4) working electrode (WE), both in the anodic compartment.	55
Figure 4.2. The optimized potential program used for the long-term electrolysis (adapted from [144])...	56

Figure 4.3. The oxidation of D-glucose to D-glucaric acid in two-steps (for simplicity D-glucose is represented in the open-chain form).	58
Figure 4.4. Influence of pH on the selectivity to D-gluconic acid (orange), D-fructose (green) and by-products (violet) for the oxidation of 0.04 M D-glucose on Au at 20°C after 24 h.	59
Figure 4.5. Current density response to the variation of initial glucose concentration derived from the respective cyclic voltammogram at 10 mVs ⁻¹ (Na ₂ CO ₃ 0.1 M).	61
Figure 4.6. Selectivity to D-gluconic acid (orange), D-fructose (green) and by-products (violet) in dependence of initial amount of glucose. Reaction conditions: 0.1 M Na ₂ CO ₃ , 20°C, pH 11.3, 24h.	62
Figure 4.7. Dependence of the selectivity to D-gluconic acid (orange), D-fructose (green) and by-products (violet) with the reaction temperature for the oxidation of 0.04 M D-glucose in 0.1 M Na ₂ CO ₃ for 24 h.	64
Figure 4.8. Variation with the reaction time of glucose conversion (black line) and gluconic acid selectivity (red line).	65
Figure 4.9. Chromatogram of a high purity standard mixture of glucaric and gluconic acid. Glucaric acid is observed at 10.9 min in the mass chromatogram taken at m/z 233. Gluconic acid is observed at 12.5 min in the mass chromatogram taken at m/z 219.	72
Figure 4.10. Mass spectra of a) the glucaric acid peak, appearing at 10.9 min retention time, and b) the gluconic acid peak, at 12.5 min. retention time, obtained from authentic samples of high purity standards. In the mass spectrum of glucaric acid, the M+Na ion is observed at m/z 233, as well as the M+Na-H ₂ O ion (m/z 215) and the M-H+CH ₃ COOH ion (m/z 255). In the mass spectrum of gluconic acid, only the M+Na ion is observed at m/z 219.	73
Figure 4.11. Current density response to the variation of the electrolyte concentration, so of the pH, derived from the respective cyclic voltammograms recorded at 10 mVs ⁻¹ , 20°C, in a solution with 0.04 M of glucose. The red line represents the values of current density obtained with Na ₂ CO ₃ as electrolyte while the black line is that obtained with NaOH.	74
Figure 4.12. Arrhenius plot derived from the cyclic voltammograms of Au in a solution 0.1 M Na ₂ CO ₃ and 0.04 M glucose, recorded at 10 mVs ⁻¹ at various temperatures (in the range 20-50 °C).	74
Figure 4.13. Chromatogram of the product of 24 h electrolysis of a starting solution 0.04 M D-glucose in 0.1 M Na ₂ CO ₃ at 20 °C. No trace of glucaric acid is observed in the mass chromatogram taken at m/z 233, while, in the mass chromatogram of m/z 219, the product peak at 12.5 min retention time coincides with that found for gluconic acid (Fig. 4.9 (blue trace)), proving that gluconic acid is the product of the electrolysis of glucose.	75
Figure 4.14. HPLC spectrum of the products resulting from the electrolysis of glucose (a) and of gluconic acid (b), respectively at 0.6 and 1.1 V _{RHE}	76
Figure 4.15. Cyclic voltammograms (II cycles) of Au electrode in a fresh solution of a) 0.1 M Na ₂ CO ₃ and 0.04 M glucose and b) 0.025 M NaOH and 0.04 M gluconic acid recorded at 20 mV s ⁻¹ and 20°C, before (blue line) and after (red line) electrolysis at a) 0.6 V _{RHE} (for 48h) and b) 1.1 V _{RHE} (for 18h). Prior use, the recovered electrodes were thoroughly rinsed with MilliQ water.	77
Figure 4.16. Comparison of Chronoamperometry data before (left) and after (right) 18h electrolysis at the potential of 1.1 V _{RHE} , corresponding to the second oxidation step. The graphs highlight the important loss of current density registered during this oxidation step. The current density decreases constantly from the initial value of ~2.0 mA cm ⁻² until a practically null value, at the end of the electrolysis.	78
Figure 4.17. Chromatogram of a sample of the starting solution of 0.04 M gluconic acid in 0.025 M NaOH. In the mass chromatogram of m/z 233 (red trace) no product peak is observed, which indicates absence of glucaric acid. Gluconic acid is observed at 12.5 min in the mass chromatogram taken at m/z 219.	78

Figure 4.18. Chromatogram of the sample of 24 h electrolysis of a solution 0.04 M gluconic acid in 0.025 M NaOH at 20 °C. Glucaric acid, not detected in the starting solution, is present here at 10.9 min in the mass chromatogram taken at m/z 233, proving that it is product of the electrolysis of gluconic acid. Gluconic acid unreacted is observed at 12.5 min in the mass chromatogram taken at m/z 219.	78
Figure 4.19. Cyclic voltammograms (V cycles) of Au electrode in 0.04 M gluconic acid and 0.025 M NaOH recorded at 20 mV s ⁻¹ and 20 °C, without (grey line line) and with (red line) 0.01 M glucaric acid. The graph shows that, in the presence of glucaric acid, the current density corresponding to the oxidation peak drops as a consequence of the passivation of the Au surface.	79
Figure 5.1. Schematic representation of the synthesis of AuNPs/C catalyst by impregnation.	83
Figure 5.2. Scheme of the reactor setup used for the continuous flow experiments: (1) SS counter electrode (CE), in the cathodic compartment; (2) reference electrode (RE); (3) Nafion membrane and (4) anodic compartment containing the working electrode (WE).	85
Figure 5.3. Au loading (% wt) on activated carbon, C, plotted versus the pH used for the synthesis. The point of zero charge for Norit® SX1G is ca 9.0 [211].....	87
Figure 5.4. XRD pattern of the Au nanoparticles grown on activated carbon at optimized pH (9.5). The crystalline nanoparticles are represented by four peaks corresponding to standard Bragg reflections (111), (200), (220), and (311) of face centers cubic lattice. The intense peak at 38.1 represents preferential growth in the (111) direction.	88
Figure 5.5. SEM images, (a) and (b), and c) EDX spectra of the Au nanoparticles deposited on carbon synthesized at the optimized pH of 9.5 (9.3% loading).	89
Figure 5.6. (a) HAADF-STEM image of the 9.3 wt %. Au nanoparticles on activated carbon and (b) a histogram showing the particle size distribution of the nanoparticles for this sample.	89
Figure 5.7. Ortho-slice in the xz direction approximately halfway through the volume of of Au/C sample at pH 9.5 (9.3% loading).....	90
Figure 5.8. (a) HAADF-STEM image, (b, c) the respective EDX elemental distributions and (d) an EDX spectrum showing which elements are present for the Au/C composite with 9.3% Au-loading. For the EDX maps, Au is marked in red and C in green.	91
Figure 5.9. Voltammograms of AuNP/C@GC electrode in 0.1 M NaOH recorded at 50 mVs ⁻¹ , at 20 °C and stirring the solution at 700 rpm, with increasing amount of gluconic acid (from 0 to 0.5 M).	92
Figure 5.10. Plot current density vs. gluconic acid concentration obtained extracting the current density values at fixed potential of 1.7 V _{RHE} (corresponding to the oxidation peak) from the cyclic voltammetry study of AuNP/C@Ti (red line) and Ti felt alone (blue line) at 20 mVs ⁻¹ , 20 °C and 20 mLmin ⁻¹ , from a starting solution 0.1 M NaOH.....	93
Figure 5.11. Results of chronopotentiometry experiments conducted at constant current densities of 10, 20 and 30 mAcm ⁻² in the flow cell, in a solution 0.05 M gluconic acid and 0.1 M NaOH. At these currents, the O ₂ evolution reaction takes place, as evidenced by the high potentials (y-axis) and the increasing O ₂ bubbles formation with the current density at the anode.	94
Figure 5.12. Plot of the module of the current vs. the scan rate at the potential of 0.71 VRHE for the AuNP/C@Ti system in the electrolyte solution (0.1 M NaOH). The original data are reported in the plot of current vs. potential at different scan rates (20, 40, 60, 80 and 100 mVs ⁻¹) (bottom)	96
Figure 5.13. Thermogravimetric plots for 4 samples of catalysts obtained, respectively, from the synthesis conducted at pH 8.5, 9.5, 10.5 and 11.5.....	97
Figure 5.14. Particle size distribution (PSD) of the sporadic larger nanoparticles in the range of 50-100 nm (mean size 75 nm) obtained utilizing the TEM images..	98
Figure 5.15. SEM pictures of the AuNP/C@GC system after 10 cycles in 0.1 M NaOH and 0.5 M gluconic acid recorded at 50 mV s ⁻¹ and 20 °C while stirring the solution at 700 rpm	99

Figure 5.16. HPLC graphs of the reaction solutions after 1h electrolysis in the flow reactor. 99

List of Tables

Table 1.1. Summary of the most relevant electrocatalytic systems investigated so far for glucaric acid production and resulting performance, reported as selectivity or yield (%).	14
Table 3.1. Chromatographic analyses of the solutions of D-glucose after 65 h of reaction in absence of the catalyst at 5 and 20°C.....	47
Table 3.2. Chromatographic analyses of the solutions of D-glucose after 65 h electrolysis on Cu at 0.84 V_{RHE} , 1.11 V_{RHE} and 1.80 V_{RHE} at 5°C.....	48
Table 3.3. Chromatographic analyses of the solutions of D-glucose after 65 h electrolysis on Pt at 0.70 V_{RHE} (Potential program 1) and 1.10 V_{RHE} (Potential program 2) at 5°C.	49
Table 3.4 Chromatographic analyses of the solutions of D-glucose after 65 h electrolysis on Au at 0.55 V_{RHE} (potential program 3) and 1.34 V_{RHE} (potential program 4) at 5°C.....	49
Table 4.1. Summary of the results obtained in the glucose electrooxidation to gluconic acid in function of the pH.....	60
Table 4.2. Summary of the results obtained in the glucose electrooxidation to gluconic acid in function of the initial concentration of glucose.	62
Table 4.3 Summary of the results obtained in the glucose electrooxidation to gluconic acid in function of the reaction temperature.....	64
Table 4.4. Summary of the results obtained in the glucose electrooxidation to gluconic acid in function of the reaction time.....	66
Table 4.5 Summary of the results obtained in the gluconic acid electrooxidation to glucaric acid, at 1.3 V_{RHE} , in function of pH, gluconic acid initial concentration, reaction temperature and time.	66
Table 4.6. Summary of the results obtained in the gluconic acid electrooxidation to glucaric acid in function of the applied potential.	67
Table 4.7. Summary of the results of the cascade process.	68
Table 4.8. Summary of the results obtained in the glucose electrooxidation to gluconic acid in function of the applied potential. The table shows that the variation of the potential applied for the electrolysis, within the oxidation peak, has no appreciable impact on glucose conversion nor on D-gluconic acid selectivity and productivity.	75
Table 4.9. The table shows the amount of Au dissolved in the reaction solution (in ppm) before (Initial concentration) and after (Final concentration) each electrolysis. In both cases, the Au leaching is irrelevant.	79

Bibliography

- [1] Commission, E. Environmental challenges
https://ec.europa.eu/clima/policies/adaptation/how/challenges_en.
- [2] Commission, E. Climate Strategies & Targets.
- [3] An official website of the European Union. A European Green Deal Striving to be the first climate-neutral continent https://ec.europa.eu/info/strategy/priorities-2019-2024/european-green-deal_en (accessed Feb 20, 2022).
- [4] An official website of the European Union. Delivering the European Green Deal https://ec.europa.eu/info/strategy/priorities-2019-2024/european-green-deal/delivering-european-green-deal_en (accessed Feb 20, 2022).
- [5] Wei, M.; McMillan, C. A.; de la Rue du Can, S. Electrification of Industry: Potential, Challenges and Outlook. *Curr Sustain. Renew. Energy Rep*, 2019, 6, 140–148.
<https://doi.org/https://doi.org/10.1007/s40518-019-00136-1>.
- [6] Independent Statistics & Analysis, U. S. E. I. A. Biomass explained
<https://www.eia.gov/energyexplained/biomass/> (accessed Feb 20, 2022).
- [7] Appunn, K. Sector Coupling - Shaping an Integrated Renewable Energy System. *Journalism for the Energy Transition*. April 2018.
- [8] Banks, M. Consumers in the circular economy - EU Political Report
<https://www.eupoliticalreport.eu/consumers-in-the-circular-economy/> (accessed Feb 26, 2022).
- [9] Vasquez-medrano, R.; Ibanez, J. G.; Fitch, A.; Frontana-uribe, B. A. Encyclopedia of Applied Electrochemistry. *Encycl. Appl. Electrochem.*, 2014, No. January. <https://doi.org/10.1007/978-1-4419-6996-5>.
- [10] Paul T, Anastas; John, C. W. *Green Chemistry : Theory and Practice*; Oxford, Ed.; New York : Oxford University Press, 1998.
- [11] EPA United States Environmental Protection Agency, A. official website of the U. S. government. Basics of Green Chemistry <https://www.epa.gov/greenchemistry/basics-green-chemistry#definition> (accessed Feb 20, 2022).
- [12] Matthews, M. A. Green Electrochemistry. Examples and Challenges. *Pure Appl. Chem.*, 2001, 73 (8), 1305–1308. <https://doi.org/10.1351/pac200173081305>.
- [13] Steckhan, E.; Arns, T.; Heineman, W. R.; Hilt, G.; Hoormann, D.; Jörissen, J.; Kröner, L.; Lewall, B.; Pütter, H. Environmental Protection and Economization of Resources by Electroorganic and Electroenzymatic Syntheses. *Chemosphere*, 2001, 43 (1), 63–73. [https://doi.org/10.1016/S0045-6535\(00\)00325-8](https://doi.org/10.1016/S0045-6535(00)00325-8).
- [14] Krishnan, Rajeshwar, Jorge, G. I. *Environmental Electrochemistry: Fundamentals and Applications in Pollution Abatement*; Elsevier, Ed.; 1997.
- [15] Genders, J. D.; Pletcher, D. Electrosynthesis – ; A Tool for the Pharmaceutical Industry Today? *Chem. Ind.*, No. 682–686.
- [16] Albert, M. *Introduction to Green Chemistry (2nd Edition)*; CRC Press, 2010.
<https://doi.org/https://doi.org/10.1201/9781439882115>.

- [17] Commission, E. Horizon 2020 -Section Bioeconomy <https://ec.europa.eu/programmes/horizon2020/en/h2020-section/bioeconomy> (accessed Oct 30, 2019).
- [18] Saeed, K.; Pricel, P.; Lopez-Sanchez, J. A. Catalytic Routes towards Bio-Renewable Glucaric Acid. *Chim. Oggi/Chemistry Today*, 2017, 35 (5), 7–11.
- [19] Bioproduct Basics <https://www.energy.gov/eere/bioenergy/bioproduct-basics#:~:text=In addition to electricity and,plastics%2C chemicals%2C and fertilizers.> (accessed Feb 20, 2022).
- [20] Wikipedia. Biorefinery <https://en.wikipedia.org/wiki/Biorefinery> (accessed Feb 20, 2022).
- [21] Huber, G. W.; Chheda, J. N.; Barrett, C. J.; Dumesic, J. A. Chemistry: Production of Liquid Alkanes by Aqueous-Phase Processing of Biomass-Derived Carbohydrates. *Science (80-.)*, 2005, 308 (5727), 1446–1450. <https://doi.org/10.1126/science.1111166>.
- [22] Lichtenthaler, F. W. Carbohydrates as Organic Raw Materials. In *Ullmann's Encyclopedia of Industrial Chemistry*; 2010. https://doi.org/10.1002/14356007.n05_n07.
- [23] Jinliang, S.; Honglei, F.; Jun, M.; Buxing, H. Conversion of Glucose and Cellulose into Value-Added Products in Water and Ionic Liquids. *Green Chem.*, 2013, No. 10. <https://doi.org/DOI> <https://doi.org/10.1039/C3GC41141A>.
- [24] (HMDB), T. H. M. D. Glucaric acid <https://hmdb.ca/metabolites/HMDB0000663>.
- [25] European Bioinformatic Institute (EBI), C. E. of B. I. (ChEBI). D-glucaric acid <https://www.ebi.ac.uk/chebi/searchId.do?chebiId=CHEBI:16002>.
- [26] Werpy, T.; Petersen, G.; Aden, A.; Bozell, J.; Holladay, J.; White, J.; Manheim, A.; Eliot, D.; Lasure, L.; S., J. Top Value Added Chemicals from Biomass, Volume 1 - Results of Screening for Potential Candidates From Sugars and Synthesis Gas. *Off. Sci. Tech. Inf.*, 2004, 69. <https://doi.org/10.2172/15008859>.
- [27] Research, G. view. *Glucaric Acid Market Size, Share, Global Industry Trends Report*; 2017.
- [28] Besemer, A. C.; van Bekkum, H. Calcium Sequestering Agents Based on Carbohydrates. In *Carbohydrates as Organic Raw Materials III*; 2007. <https://doi.org/10.1002/9783527614899.ch15>.
- [29] Mehtiö, T.; Toivari, M.; Wiebe, M. G.; Harlin, A.; Penttilä, M.; Koivula, A. Production and Applications of Carbohydrate-Derived Sugar Acids as Generic Biobased Chemicals. *Critical Reviews in Biotechnology*. 2016. <https://doi.org/10.3109/07388551.2015.1060189>.
- [30] Gallagher, J. J.; Hillmyer, M. A.; Reineke, T. M. Degradable Thermosets from Sugar-Derived Dilactones. *Macromolecules*, 2014. <https://doi.org/10.1021/ma401904x>.
- [31] Kiely, D. E.; Chen, L.; Lin, T. H. Hydroxylated Nylons Based on Unprotected Esterified D-Glucaric Acid by Simple Condensation Reactions. *J. Am. Chem. Soc.*, 1994. <https://doi.org/10.1021/ja00081a018>.
- [32] Wu, Y.; Enomoto-Rogers, Y.; Masaki, H.; Iwata, T. Synthesis of Crystalline and Amphiphilic Polymers from D-Glucaric Acid. *ACS Sustain. Chem. Eng.*, 2016. <https://doi.org/10.1021/acssuschemeng.6b00530>.
- [33] Walaszek, Z.; Szemraj, J.; Hanausek, M.; Adams, A. K.; Sherman, U. D-Glucaric Acid Content of Various Fruits and Vegetables and Cholesterol-Lowering Effects of Dietary D-Glucarate in the Rat. *Nutr. Res.*, 1996. [https://doi.org/10.1016/0271-5317\(96\)00045-0](https://doi.org/10.1016/0271-5317(96)00045-0).

- [34] Zóltaszek, R.; Hanausek, M.; Walaszek, Z.; Kiliańska, Z. M. The Biological Role of D-Glucaric Acid and Its Derivatives: Potential Use in Medicine. *Postepy Hig. Med. Dosw.*, 2008.
- [35] Walaszek, Z. Potential Use of D-Glucaric Acid Derivatives in Cancer Prevention. *Cancer Letters*. 1990. [https://doi.org/10.1016/0304-3835\(90\)90083-A](https://doi.org/10.1016/0304-3835(90)90083-A).
- [36] Lampe, J. W.; Li, S. S.; Potter, J. D.; King, I. B. Serum β -Glucuronidase Activity Is Inversely Associated with Plant-Food Intakes in Humans. *J. Nutr.*, 2002. <https://doi.org/10.1093/jn/132.6.1341>.
- [37] Donald E. Kiely, Kirk R. Hash, Kylie Kramer-Presta, T. N. S. Hydroxycarboxylic Acids and Salts. US20120305832A1, 2012.
- [38] Korzh, E. N.; Sukhotin, A. M.; Borshchevskii, A. M. Corrosion of Steel in Calcium Chloride Solutions. *Prot. Met.*, 1982.
- [39] Sukhotin, A. M.; Borshchevskii, A. M.; Korzh, E. N.; Perel'Shtein, I. I.; Aref'Eva, L. N.; Kurslyaikin, G. A.; Perushin, E. B. Inhibition of Steel in Calcium Chloride Solutions. *Prot. Met.*, 1982.
- [40] Mehlretter, C. L.; Rist, C. E. Sugar Oxidation, Saccharic and Oxalic Acids by the Nitric Acid Oxidation of Dextrose. *J. Agric. Food Chem.*, 1953. <https://doi.org/10.1021/jf60012a005>.
- [41] Kohler, J. Detergent Phosphates: An EU Policy Assessment. *J. Bus. Chem.*, 2006.
- [42] Godfrey, P. J. The Eutrophication of Cayuga Lake: A Historical Analysis of the Phytoplankton's Response to Phosphate Detergents. *Freshw. Biol.*, 1982. <https://doi.org/10.1111/j.1365-2427.1982.tb00610.x>.
- [43] Mitchell, D. Eutrophication of Lake Water Microcosms: Phosphate versus Nonphosphate Detergents. *Science (80-.)*, 1971. <https://doi.org/10.1126/science.174.4011.827>.
- [44] Litke, D. W. *Review of Phosphorus Control Measures in the United States and Their Effects on Water Quality*; 1999.
- [45] Tyler N. Smith, Donald E. Kiely, K. K.-P. Corrosion Inhibiting Composition. US20120119152A1, 2012.
- [46] Mehlretter, C. L.; Alexander, B. H.; Rist, C. E. Sequestration by Sugar Acids. *Ind. Eng. Chem.*, 1953. <https://doi.org/10.1021/ie50528a060>.
- [47] Abbadi, A.; Gotlieb, K. F.; Meiberg, J. B. M.; Peters, J. A.; van Bekkum, H. New Ca-Sequestering Materials. *Green Chem.*, 1999. <https://doi.org/10.1039/a905197j>.
- [48] Van De Vyver, S.; Román-Leshkov, Y. Emerging Catalytic Processes for the Production of Adipic Acid. *Catal. Sci. Technol.*, 2013. <https://doi.org/10.1039/c3cy20728e>.
- [49] Shi, H.; Zhang, L.; Wu, Y.; Yu, R.; Peng, Y.; Wang, Y.; Li, T.; Yang, W. Production of Adipic Acid Derivatives from D-Glucaric Acid by Hydrodeoxygenation Mediated with Hydroiodic Acid. *Catal. Letters*, 2020. <https://doi.org/10.1007/s10562-020-03312-x>.
- [50] Skoog, E.; Shin, J. H.; Saez-Jimenez, V.; Mapelli, V.; Olsson, L. Biobased Adipic Acid – The Challenge of Developing the Production Host. *Biotechnology Advances*. 2018. <https://doi.org/10.1016/j.biotechadv.2018.10.012>.
- [51] Sohst, O.; Tollens, B. Über Krystallisirte Zuckersäure (Zuckerlactonsäure). *Justus Liebigs Ann. Chem.*, 1888. <https://doi.org/10.1002/jlac.18882450102>.

- [52] Smith, T. N.; Hash, K.; Davey, C. L.; Mills, H.; Williams, H.; Kiely, D. E. Modifications in the Nitric Acid Oxidation of D-Glucose. *Carbohydr. Res.*, 2012. <https://doi.org/10.1016/j.carres.2011.12.024>.
- [53] L Mehlretter, C. Process of Making D-Saccharic Acid. US2436659A, 1948.
- [54] Mustakas, G. C.; Slotter, R. L.; Zipf, R. L. Pilot Plant Potassium Acid Saccharate by Nitric Acid Oxidation of Dextrose. *Ind. Eng. Chem.*, 1954. <https://doi.org/10.1021/ie50531a019>.
- [55] Kiely, D. E.; Hash, K. R. S. Method of Oxidation Using Nitric Acid. US7692041B2, 2010.
- [56] Renewables, R. Rivertop Renewables and DTI Announce Commercial Production of Glucaric Acid <https://www.globenewswire.com/news-release/2015/10/06/1005693/0/en/Rivertop-Renewables-and-DTI-Announce-Commercial-Production-of-Glucaric-Acid.html> (accessed Sep 7, 2020).
- [57] Iglesias, J.; Martínez-Salazar, I.; Maireles-Torres, P.; Martín Alonso, D.; Mariscal, R.; López Granados, M. Advances in Catalytic Routes for the Production of Carboxylic Acids from Biomass: A Step Forward for Sustainable Polymers. *Chem. Soc. Rev.*, 2020. <https://doi.org/10.1039/d0cs00177e>.
- [58] Lee, D.; Taylor, M. S. Catalyst-Controlled Regioselective Reactions of Carbohydrate Derivatives. *Synthesis (Germany)*. 2012. <https://doi.org/10.1055/s-0032-1317483>.
- [59] Thaburet, J. F.; Merbouh, N.; Ibert, M.; Marsais, F.; Queguiner, G. TEMPO-Mediated Oxidation of Maltodextrins and D-Glucose: Effect of PH on the Selectivity and Sequestering Ability of the Resulting Polycarboxylates. *Carbohydr. Res.*, 2001. [https://doi.org/10.1016/S0008-6215\(00\)00263-9](https://doi.org/10.1016/S0008-6215(00)00263-9).
- [60] Weik, S.; Nicholson, G.; Jung, G.; Rademann, J. Oxoammonium Resins as Metal-Free, Highly Reactive, Versatile Polymeric Oxidation Reagents. *Angew. Chemie - Int. Ed.*, 2001. [https://doi.org/10.1002/1521-3773\(20010417\)40:8<1436::AID-ANIE1436>3.0.CO;2-X](https://doi.org/10.1002/1521-3773(20010417)40:8<1436::AID-ANIE1436>3.0.CO;2-X).
- [61] Ibert, M.; Marsais, F.; Merbouh, N.; Brückner, C. Determination of the Side-Products Formed during the Nitroxide-Mediated Bleach Oxidation of Glucose to Glucaric Acid. *Carbohydr. Res.*, 2002. [https://doi.org/10.1016/S0008-6215\(02\)00072-1](https://doi.org/10.1016/S0008-6215(02)00072-1).
- [62] Merbouh, N.; Francois Thaburet, J.; Ibert, M.; Marsais, F.; Bobbitt, J. M. Facile Nitroxide-Mediated Oxidations of D-Glucose to D-Glucaric Acid. *Carbohydr. Res.*, 2001. [https://doi.org/10.1016/S0008-6215\(01\)00231-2](https://doi.org/10.1016/S0008-6215(01)00231-2).
- [63] Schmeisser, M. Chlorine, Bromine, Iodine. In *Handbook of Preparative Inorganic Chemistry*; 1963. <https://doi.org/10.1016/b978-0-12-395590-6.50013-2>.
- [64] Merbouh, N.; Bobbitt, J. M.; Brückner, C. 4-AcNH-Tempo-Catalyzed Oxidation of Aldoses to Aldaric Acids Using Chlorine or Bromine as Terminal Oxidants. *J. Carbohydr. Chem.*, 2002. <https://doi.org/10.1081/CAR-120003738>.
- [65] Alexander, B. H.; Mehlretter, C. L. Process for the Preparation of D-Glucosaccharic Acid. US2472168A, 1949.
- [66] Acres, J. K. G.; Budd, E. R. A. Catalytic Oxidation of Glucose. US3607922A, 1971.
- [67] Boussie, T. R.; Dias, E. L.; Zachary, M. F.; Murphy, V. J.; Shoemaker, J.; Archer, R.; Jiang, H. Production of Adipic Acid and Derivatives from Carbohydrate-Containing Materials. US20100317823A1, 2010.

- [68] Murphy, V. J.; Shoemaker, J.; Zhu, G.; Archer, R.; Salem, G. F.; Dias, E. L. Oxidation Catalysts. US20110306790A1, 2011.
- [69] Dimitratos, N.; Lopez-Sanchez, J. A.; Hutchings, G. J. Green Catalysis with Alternative Feedstocks. *Top. Catal.*, 2009. <https://doi.org/10.1007/s11244-008-9162-4>.
- [70] Besson, M.; Gallezot, P.; Pinel, C. Conversion of Biomass into Chemicals over Metal Catalysts. *Chemical Reviews*. 2014. <https://doi.org/10.1021/cr4002269>.
- [71] Dimitratos, N.; Lopez-Sanchez, J. A.; Hutchings, G. J. Selective Liquid Phase Oxidation with Supported Metal Nanoparticles. *Chemical Science*. 2012. <https://doi.org/10.1039/c1sc00524c>.
- [72] Lee, J.; Saha, B.; Vlachos, D. G. Pt Catalysts for Efficient Aerobic Oxidation of Glucose to Glucaric Acid in Water. *Green Chem.*, 2016. <https://doi.org/10.1039/c6gc00460a>.
- [73] Jin, X.; Zhao, M.; Vora, M.; Shen, J.; Zeng, C.; Yan, W.; Thapa, P. S.; Subramaniam, B.; Chaudhari, R. V. Synergistic Effects of Bimetallic PtPd/TiO₂ Nanocatalysts in Oxidation of Glucose to Glucaric Acid: Structure Dependent Activity and Selectivity. *Ind. Eng. Chem. Res.*, 2016. <https://doi.org/10.1021/acs.iecr.5b04841>.
- [74] Jin, X.; Zhao, M.; Shen, J.; Yan, W.; He, L.; Thapa, P. S.; Ren, S.; Subramaniam, B.; Chaudhari, R. V. Exceptional Performance of Bimetallic Pt₁/Cu₃/TiO₂ Nanocatalysts for Oxidation of Gluconic Acid and Glucose with O₂ to Glucaric Acid. *J. Catal.*, 2015. <https://doi.org/10.1016/j.jcat.2015.05.018>.
- [75] Török, B. Chapter 2.2 - Sustainable Synthesis. In *Green Chemistry: An inclusive approach*; 2018; pp 49–89. <https://doi.org/https://doi.org/10.1016/B978-0-12-809270-5.00003-0>.
- [76] Ibert, M.; Fuertès, P.; Merbouh, N.; Fiol-Petit, C.; Feasson, C.; Marsais, F. Improved Preparative Electrochemical Oxidation of D-Glucose to d-Glucaric Acid. *Electrochim. Acta*, 2010. <https://doi.org/10.1016/j.electacta.2009.11.041>.
- [77] Ibert, M.; Fuerts, P.; Merbouh, N.; Feasson, C.; Marsais, F. Evidence of Benzilic Rearrangement during the Electrochemical Oxidation of D-Glucose to D-Glucaric Acid. *Carbohydr. Res.*, 2011. <https://doi.org/10.1016/j.carres.2010.12.017>.
- [78] Vedovato, V.; Vanbroekhoven, K.; Pant, D.; Helsen, J. *Electrosynthesis of Biobased Chemicals Using Carbohydrates as a Feedstock*; 2020. <https://doi.org/10.3390/molecules25163712>.
- [79] Bin, D.; Wang, H.; Li, J.; Wang, H.; Yin, Z.; Kang, J.; He, B.; Li, Z. Controllable Oxidation of Glucose to Gluconic Acid and Glucaric Acid Using an Electrocatalytic Reactor. *Electrochim. Acta*, 2014. <https://doi.org/10.1016/j.electacta.2014.02.128>.
- [80] Zhao, L.; Kuang, X.; Sun, X.; Zhang, Y.; Wei, Q. Synchronously Achieving Highly Efficient Hydrogen Evolution and High-Yield Synthesis of Glucaric Acid by MOF Nanorod Arrays. *J. Electrochem. Soc.*, 2019. <https://doi.org/10.1149/2.0831912jes>.
- [81] Liu, W.; Xu, Z.; Zhao, D.; Pan, X.; Li, H.; Hu, X.; Fan, Z.; Wang, W.; Zhao, G.; Jin, S.; et al. Efficient Electrochemical Production of Glucaric Acid and H₂ via Glucose Electrolysis. *Nat. Commun.*, No. 2020, 1–11. <https://doi.org/10.1038/s41467-019-14157-3>.
- [82] Lv, H.; Sun, L.; Chen, X.; Xu, D.; Liu, B. One-Step Fabrication of Trimetallic Core-Shell Au@PdAuCu Mesoporous Nanospheres for Ethanol Electrooxidation. *Green Chem.*, 2019, 21 (8), 2043–2051. <https://doi.org/10.1039/c9gc00263d>.
- [83] Solmi, S.; Morreale, C.; Ospitali, F.; Agnoli, S.; Cavani, F. Oxidation of D-Glucose to Glucaric

- Acid Using Au/C Catalysts. *ChemCatChem*, 2017. <https://doi.org/10.1002/cctc.201700089>.
- [84] Ragauskas, A. J.; Williams, C. K.; Davison, B. H.; Britovsek, G.; Cairney, J.; Eckert, C. A.; Frederick, W. J.; Hallett, J. P.; Leak, D. J.; Liotta, C. L.; et al. The Path Forward for Biofuels and Biomaterials. *Science*. 2006. <https://doi.org/10.1126/science.1114736>.
- [85] Aury, S.; Rubini, P.; Gérardin, C.; Selve, C. Amphiphilic Amide Derivatives of D-Glucaric Acid. Synthesis and Complexing Properties toward Lanthanide(III) Ions. *European J. Org. Chem.*, 2004. <https://doi.org/10.1002/ejoc.200300749>.
- [86] Belgsir, E. M.; Bouhier, E.; Essis Yei, H.; Kokoh, K. B.; Beden, B.; Huser, H.; Leger, J. M.; Lamy, C. Electrosynthesis in Aqueous Medium: A Kinetic Study of the Electrocatalytic Oxidation of Oxygenated Organic Molecules. *Electrochim. Acta*, 1991. [https://doi.org/10.1016/0013-4686\(91\)85103-E](https://doi.org/10.1016/0013-4686(91)85103-E).
- [87] Beden, B.; Largeaud, F.; Kokoh, K. B.; Lamy, C. Fourier Transform Infrared Reflectance Spectroscopic Investigation of the Electrocatalytic Oxidation of D-Glucose: Identification of Reactive Intermediates and Reaction Products. *Electrochim. Acta*, 1996. [https://doi.org/10.1016/0013-4686\(95\)00359-2](https://doi.org/10.1016/0013-4686(95)00359-2).
- [88] Kokoh, K. B.; Léger, J. M.; Beden, B.; Huser, H.; Lamy, C. "On Line" Chromatographic Analysis of the Products Resulting from the Electrocatalytic Oxidation of d-Glucose on Pure and Adatoms Modified Pt and Au Electrodes-Part II. Alkaline Medium. *Electrochim. Acta*, 1992. [https://doi.org/10.1016/0013-4686\(92\)87102-6](https://doi.org/10.1016/0013-4686(92)87102-6).
- [89] Pasta, M.; Ruffo, R.; Falletta, E.; Mari, C. M.; Della Pina, C. Alkaline Glucose Oxidation on Nanostructured Gold Electrodes. *Gold Bull.*, 2010. <https://doi.org/10.1007/bf03214967>.
- [90] Pasta, M.; La Mantia, F.; Cui, Y. Mechanism of Glucose Electrochemical Oxidation on Gold Surface. *Electrochim. Acta*, 2010. <https://doi.org/10.1016/j.electacta.2010.04.069>.
- [91] Di, F.; Matematiche, S.; Naturali, F. E.; Inorganica, C.; Analitica, M.; Malatesta, L.; Pasta, D. M. Tesi Di Dottorato Di Ricerca. 2010.
- [92] Li, J.; Li, J.; Wang, H.; Cheng, B.; He, B.; Yan, F.; Yang, Y.; Guo, W.; Ngo, H. H. Electrocatalytic Oxidation of N-Propanol to Produce Propionic Acid Using an Electrocatalytic Membrane Reactor. *Chem. Commun.*, 2013, 49 (40), 4501–4503. <https://doi.org/10.1039/C3CC41181H>.
- [93] Das, D.; Sen, P. K.; Das, K. Electrodeposited MnO₂ as Electrocatalyst for Carbohydrate Oxidation. *J. Appl. Electrochem.*, 2006, 36 (6), 685–690. <https://doi.org/10.1007/s10800-006-9126-y>.
- [94] Das, D.; Sen, P. K.; Das, K. Mechanism of Potentiostatic Deposition of MnO₂ and Electrochemical Characteristics of the Deposit in Relation to Carbohydrate Oxidation. *Electrochim. Acta*, 2008, 54 (2), 289–295. <https://doi.org/10.1016/j.electacta.2008.07.082>.
- [95] Das, D.; Ganguly, S.; Sen, P. K.; Das, K. Spectral and Electrochemical Behavior of Manganese Dioxide Nanodispersions Prepared in Reverse Micelle. 2008, 622, 59–63. <https://doi.org/10.1016/j.jelechem.2008.05.001>.
- [96] Das, D.; Sen, P. K.; Das, K. Carbohydrate Electro-Oxidation on Chemically Prepared MnO₂. *J. Electroanal. Chem.*, 2007, 611 (1–2), 19–25. <https://doi.org/10.1016/j.jelechem.2007.07.024>.
- [97] Babakhani, B.; Ivey, D. G. Effect of Electrodeposition Conditions on the Electrochemical Capacitive Behavior of Synthesized Manganese Oxide Electrodes. *J. Power Sources*, 2011, 196

- (24), 10762–10774. <https://doi.org/10.1016/j.jpowsour.2011.08.102>.
- [98] Marioli, J. M.; Kuwana, T. Electrochemical Characterization of Carbohydrate Oxidation at Copper Electrodes. *Electrochim. Acta*, 1992. [https://doi.org/10.1016/0013-4686\(92\)85055-P](https://doi.org/10.1016/0013-4686(92)85055-P).
- [99] Hebié, S.; Holade, Y.; Maximova, K.; Sentis, M.; Delaporte, P.; Kokoh, K. B.; Napporn, T. W.; Kabashin, A. V. Advanced Electrocatalysts on the Basis of Bare Au Nanomaterials for Biofuel Cell Applications. *ACS Catal.*, 2015. <https://doi.org/10.1021/acscatal.5b01478>.
- [100] Yan, L.; Brouzgou, A.; Meng, Y.; Xiao, M.; Tsiakaras, P.; Song, S. Efficient and Poison-Tolerant PdxAu/C Binary Electrocatalysts for Glucose Electrooxidation in Alkaline Medium. *Appl. Catal. B Environ.*, 2014, 150–151, 268–274. <https://doi.org/10.1016/j.apcatb.2013.12.026>.
- [101] Nikolaeva, N. N.; Khazova, O. A.; Vasil'ev, Y. B. Effect of Electrode Nature on the Electrooxidation of Glucose. *Elektrokhimiya*, 1982.
- [102] Brouzgou, A.; Tsiakaras, P. Electrocatalysts for Glucose Electrooxidation Reaction: A Review. *Top. Catal.*, 2015. <https://doi.org/10.1007/s11244-015-0499-1>.
- [103] Wei, W.; Cui, X.; Mao, X.; Chen, W.; Ivey, D. G. Morphology Evolution in Anodically Electrodeposited Manganese Oxide Nanostructures for Electrochemical Supercapacitor Applications - Effect of Supersaturation Ratio. *Electrochim. Acta*, 2011, 56 (3), 1619–1628. <https://doi.org/10.1016/j.electacta.2010.10.044>.
- [104] Nguyen, T.; Boudard, M.; Carmezim, M. J.; Montemor, M. F. Hydrogen Bubbling-Induced Micro/Nano Porous MnO₂ Films Prepared by Electrodeposition for Pseudocapacitor Electrodes. *Electrochim. Acta*, 2016, 202, 166–174. <https://doi.org/10.1016/j.electacta.2016.03.204>.
- [105] Wang, H.; Wang, H.; Li, J.; Bin, D.; Yin, Z.; Kang, J.; He, B. An Electrocatalytic Reactor for the High Selectivity Production of Sodium 2,2,3,3-Tetrafluoropropionate from 2,2,3,3-Tetrafluoro-1-Propanol. *Electrochim. Acta*, 2014, 123, 33–41. <https://doi.org/10.1016/j.electacta.2014.01.016>.
- [106] Liu, R.; Lee, S. B. MnO₂/Poly(3,4-Ethylenedioxythiophene) Coaxial Nanowires by One-Step Coelectrodeposition for Electrochemical Energy Storage. *J. Am. Chem. Soc.*, 2008, 130 (10), 2942–2943. <https://doi.org/https://doi.org/10.1021/ja7112382>.
- [107] Wu, M. S.; Ou, Y. H.; Lin, Y. P. Electrodeposition of Iron Oxide Nanorods on Carbon Nanofiber Scaffolds as an Anode Material for Lithium-Ion Batteries. *Electrochim. Acta*, 2010, 55 (9), 3240–3244. <https://doi.org/10.1016/j.electacta.2009.12.100>.
- [108] Xiao, R.; Cho, S. II; Liu, R.; Lee, S. B. Controlled Electrochemical Synthesis of Conductive Polymer Nanotube Structures. *J. Am. Chem. Soc.*, 2007, 129 (14), 4483–4489. <https://doi.org/https://doi.org/10.1021/ja068924v>.
- [109] Zheng, H.; Tang, F.; Lim, M.; Mukherji, A.; Yan, X.; Wang, L.; (Max) Lu, G. Q. Multilayered Films of Cobalt Oxyhydroxide Nanowires/Manganese Oxide Nanosheets for Electrochemical Capacitor. *J. Power Sources*, 2010, 195 (2), 680–683. <https://doi.org/10.1016/j.jpowsour.2009.08.002>.
- [110] Sinha, A. K.; Pradhan, M.; Pal, T. Supporting Information Morphological Evolution of 2D MnO₂ Nanosheets and Their Shape Transformation to 1D Ultra Long MnO₂ Nanowires for Robust Catalytic Activity. 2013.
- [111] Zhang, W.; Yang, Z.; Wang, X.; Zhang, Y.; Wen, X.; Yang, S. Large-Scale Synthesis of β -MnO₂ Nanorods and Their Rapid and Efficient Catalytic Oxidation of Methylene Blue Dye. *Catal. Commun.*, 2006, 7 (6), 408–412. <https://doi.org/10.1016/j.catcom.2005.12.008>.

- [112] Zhang, Y.; Yang, Y.; Zhang, Y.; Zhang, T.; Ye, M. Heterogeneous Oxidation of Naproxen in the Presence of α -MnO₂ Nanostructures with Different Morphologies. *Appl. Catal. B Environ.*, 2012, *127*, 182–189. <https://doi.org/10.1016/j.apcatb.2012.08.014>.
- [113] Shi, F.; Wang, F.; Dai, H.; Dai, J.; Deng, J.; Liu, Y.; Bai, G.; Ji, K.; Au, C. T. Rod-, Flower-, and Dumbbell-like MnO₂: Highly Active Catalysts for the Combustion of Toluene. *Appl. Catal. A Gen.*, 2012, *433–434*, 206–213. <https://doi.org/10.1016/j.apcata.2012.05.016>.
- [114] Lu, S.; Li, K.; Huang, F.; Chen, C.; Sun, B. Efficient MnO_x-Co₃O₄-CeO₂ Catalysts for Formaldehyde Elimination. *Appl. Surf. Sci.*, 2017, *400*, 277–282. <https://doi.org/10.1016/j.apsusc.2016.12.207>.
- [115] Zhu, L.; Wang, J.; Rong, S.; Wang, H.; Zhang, P. Cerium Modified Birnessite-Type MnO₂ for Gaseous Formaldehyde Oxidation at Low Temperature. *Appl. Catal. B Environ.*, 2017, *211*, 212–221. <https://doi.org/10.1016/j.apcatb.2017.04.025>.
- [116] Elamin, K.; Sjöström, J.; Jansson, H.; Swenson, J. Calorimetric and Relaxation Properties of Xylitol-Water Mixtures. *J. Chem. Phys.*, 2012, *136* (10), 1–8. <https://doi.org/10.1063/1.3692609>.
- [117] Nakayama, M.; Kanaya, T.; Inoue, R. Anodic Deposition of Layered Manganese Oxide into a Colloidal Crystal Template for Electrochemical Supercapacitor. *Electrochem. commun.*, 2007, *9* (5), 1154–1158. <https://doi.org/10.1016/j.elecom.2007.01.021>.
- [118] Chun, S. E.; Pyun, S. I.; Lee, G. J. A Study on Mechanism of Charging/Discharging at Amorphous Manganese Oxide Electrode in 0.1 M Na₂SO₄ Solution. *Electrochim. Acta*, 2006, *51* (28), 6479–6486. <https://doi.org/10.1016/j.electacta.2006.04.034>.
- [119] Toupin, M.; Brousse, T.; Bélanger, D. Charge Storage Mechanism of MnO₂ Electrode Used in Aqueous Electrochemical Capacitor. *Chem. Mater.*, 2004, *16* (16), 3184–3190. <https://doi.org/https://doi.org/10.1021/cm049649j>.
- [120] Hu, C.-C.; Wang, C.-C. Nanostructures and Capacitive Characteristics of Hydrous Manganese Oxide Prepared by Electrochemical Deposition. *J. Electrochem. Soc.*, 2003, *150* (8), A1079. <https://doi.org/10.1149/1.1587725>.
- [121] Wu, M. S.; Chiang, P. C. J. Electrochemically Deposited Nanowires of Manganese Oxide as an Anode Material for Lithium-Ion Batteries. *Electrochem. commun.*, 2006, *8* (3), 383–388. <https://doi.org/10.1016/j.elecom.2005.12.014>.
- [122] Wang, X.; Li, Y. Synthesis and Formation Mechanism of Manganese Dioxide Nanowires/Nanorods. *Chem. A Eur. J.*, 2002, No. 9, 300–306. <https://doi.org/https://doi.org/10.1002/chem.200390024>.
- [123] Nelson, P. A.; Elliott, J. M.; Attard, G. S.; Owen, J. R. Mesoporous Nickel/Nickel Oxide Nanoarchitected Electrode. *Chem. Mater.*, 2002, *14* (2), 524–529. <https://doi.org/https://doi.org/10.1021/cm011021a>.
- [124] Zhou, W. J.; Zhao, D. D.; Xu, M. W.; Xu, C. L.; Li, H. L. Effects of the Electrodeposition Potential and Temperature on the Electrochemical Capacitance Behavior of Ordered Mesoporous Cobalt Hydroxide Films. *Electrochim. Acta*, 2008, *53* (24), 7210–7219. <https://doi.org/10.1016/j.electacta.2008.05.007>.
- [125] Babakhani, B.; Ivey, D. G. Anodic Deposition of Manganese Oxide Electrodes with Rod-like Structures for Application as Electrochemical Capacitors. *J. Power Sources*, 2009, *195* (7), 2110–2117. <https://doi.org/10.1016/j.jpowsour.2009.10.045>.

- [126] Xia, H.; Feng, J.; Wang, H.; Lai, M. O.; Lu, L. MnO₂ Nanotube and Nanowire Arrays by Electrochemical Deposition for Supercapacitors. *J. Power Sources*, 2010, *195* (13), 4410–4413. <https://doi.org/10.1016/j.jpowsour.2010.01.075>.
- [127] Wei, W.; Cui, X.; Chen, W.; Ivey, D. G. Improved Electrochemical Impedance Response Induced by Morphological and Structural Evolution in Nanocrystalline MnO₂ Electrodes. *Electrochim. Acta*, 2009, *54* (8), 2271–2275. <https://doi.org/10.1016/j.electacta.2008.10.031>.
- [128] Wei, W.; Cui, X.; Chen, W.; Ivey, D. G. Electrochemical Cyclability Mechanism for MnO₂ Electrodes Utilized as Electrochemical Supercapacitors. *J. Power Sources*, 2009, *186* (2), 543–550. <https://doi.org/10.1016/j.jpowsour.2008.10.058>.
- [129] Babakhani, B.; Ivey, D. G. Improved Capacitive Behavior of Electrochemically Synthesized Mn Oxide/PEDOT Electrodes Utilized as Electrochemical Capacitors. *Electrochim. Acta*, 2010, *55* (12), 4014–4024. <https://doi.org/10.1016/j.electacta.2010.02.030>.
- [130] Pilla, A. S.; Duarte, M. M. E.; Mayer, C. E. Manganese Dioxide Electrodeposition in Sulphate Electrolytes: The Influence of Ferrous Ions. *J. Electroanal. Chem.*, 2004, *569* (1), 7–14. <https://doi.org/10.1016/j.jelechem.2004.01.032>.
- [131] Kao, W. H.; Weibel, V. J. Electrochemical Oxidation of Manganese(II) at a Platinum Electrode. *J. Appl. Electrochem.*, 1992, No. 22, 21–27. <https://doi.org/https://doi.org/10.1007/BF01093007>.
- [132] Nijjer, S.; Thonstad, J.; Haarberg, G. M. Oxidation of Manganese(II) and Reduction of Manganese Dioxide in Sulphuric Acid. *Electrochim. Acta*, 2000, *46* (2–3), 395–399. [https://doi.org/10.1016/S0013-4686\(00\)00597-1](https://doi.org/10.1016/S0013-4686(00)00597-1).
- [133] Carmezim, T. M. S. M. J. Electrodeposition and Characterization of Nickel – Copper Metallic Foams for Application as Electrodes for Supercapacitors. 2013. <https://doi.org/10.1007/s10800-013-0646-y>.
- [134] Wang, G.; Zhang, L.; Zhang, J. A Review of Electrode Materials for Electrochemical Supercapacitors. *Chem. Soc. Rev.*, 2012, *41* (2), 797–828. <https://doi.org/10.1039/c1cs15060j>.
- [135] Bryce C, T.; Stephen A, S.; Luther, E. P. Nanoporous Metal Foams. *Angew. Chemie - Int. Ed.*, 2010, *49* (27), 4544–4565. <https://doi.org/10.1002/anie.200902994>.
- [136] Ghaemi, M.; Khosravi-Fard, L.; Neshati, J. Improved Performance of Rechargeable Alkaline Batteries via Surfactant-Mediated Electrosynthesis of MnO₂. *J. Power Sources*, 2005, *141* (2), 340–350. <https://doi.org/10.1016/j.jpowsour.2004.10.004>.
- [137] Davies, G. Some Aspects of the Chemistry of Manganese(III) in Aqueous Solution. *Coord. Chem. Rev.*, 1969, *4* (2), 199–224. [https://doi.org/10.1016/S0010-8545\(00\)80086-7](https://doi.org/10.1016/S0010-8545(00)80086-7).
- [138] Kozlov, Y. N.; Zharmukhamedov, S. K.; Tikhonov, K. G.; Dasgupta, J.; Kazakova, A. A.; Dismukes, G. C.; Klimov, V. V. Oxidation Potentials and Electron Donation to Photosystem II of Manganese Complexes Containing Bicarbonate and Carboxylate Ligands. *Phys. Chem. Chem. Phys.*, 2004, *6*, 4905–4911. <https://doi.org/DOI> <https://doi.org/10.1039/B406569G>.
- [139] Paul, R. L.; Cartwright, A. The Mechanism of the Deposition of Manganese Dioxide. Part II. Electrode Impedance Studies. *J. Electroanal. Chem.*, 1986, *201* (1), 113–122. [https://doi.org/10.1016/0022-0728\(86\)90091-4](https://doi.org/10.1016/0022-0728(86)90091-4).
- [140] Wen-zhi, L.; You-qin, L.; Guang-qi, H. Preparation of Manganese Dioxide Modified Glassy Carbon Electrode By a Novel Film Plating/Cyclic Voltammetry Method for H₂O₂ Detection. *J. Chil. Chem. Soc.*, 2009, *54* (4), 2–7. <https://doi.org/10.4067/s0717-97072009000400009>.

- [141] Chrmmrque, I. D. G. Oxidation du MnSO₄ en dioxyde de manganese dans H₂SO₃ 30%, 1990, 35 (1).
- [142] Manivel, A.; Ilayaraja, N.; Velayutham, D.; Noel, M. Medium Effects on the Electro-Deposition of MnO₂ on Glassy Carbon Electrode A Comparative Study in Alkane , Perfluoro Alkane Carboxylic Acids and Methanesulphonic Acid. 2007, 52, 7841–7848. <https://doi.org/10.1016/j.electacta.2007.06.008>.
- [143] Bai, Y.; Du, Y.; Xu, J.; Chen, H. Choline Biosensors Based on a Bi-Electrocatalytic Property of MnO₂ Nanoparticles Modified Electrodes to H₂O₂. 2007, 9, 2611–2616. <https://doi.org/10.1016/j.elecom.2007.08.013>.
- [144] Plowman, B. J.; Jones, L. A.; Bhargava, S. K. Building With Bubbles: The Formation of High Surface Area Honeycomb-like Films via Hydrogen Bubble Templated Electrodeposition. *Chem. Commun.*, 2015, No. 21. <https://doi.org/10.1039/C4CC06638C>.
- [145] Shin, B. H.; Dong, J.; Liu, M. Nanoporous Structures Prepared by an Electrochemical Deposition Process **. 2003, 2 (19), 1610–1614. <https://doi.org/10.1002/adma.200305160>.
- [146] Duay, J.; Sherrill, S. A.; Gui, Z.; Gillette, E.; Lee, S. B. Self-Limiting Electrodeposition of Hierarchical MnO₂ Nanofibril / Nanowires : Synthesis Mechanism and Supercapacitor Properties. 1–6.
- [147] Mette, K.; Bergmann, A.; Tessonier, J. P.; Hävecker, M.; Yao, L.; Ressler, T.; Schlögl, R.; Strasser, P.; Behrens, M. Nanostructured Manganese Oxide Supported on Carbon Nanotubes for Electrocatalytic Water Splitting. *ChemCatChem*, 2012, 4 (6), 851–862. <https://doi.org/10.1002/cctc.201100434>.
- [148] Das, D.; Rani, Æ. P. Oxidation of Some Aliphatic Polyols on Anodically Deposited MnO₂. 2008, 743–749. <https://doi.org/10.1007/s10800-008-9503-9>.
- [149] Rajakylä, E. Separation and Determination of Some Organic Acids and Their Sodium Salts by High-Performance Liquid Chromatography. *J. Chromatogr. A*, 1981, 218, 695–701. [https://doi.org/https://doi.org/10.1016/S0021-9673\(00\)82095-6](https://doi.org/https://doi.org/10.1016/S0021-9673(00)82095-6).
- [150] Buch, M. L.; Montgomery, R.; Porter, W. L. Identification of Sulphonamides on Paper Chromatograms. *Anal. Chem.*, 1952, 24 (3), 489–491. <https://doi.org/https://doi.org/10.1021/ac60063a014>.
- [151] French, D. *Advances in Clinical Mass Spectrometry*, 1st ed.; Elsevier Inc., 2017; Vol. 79. <https://doi.org/10.1016/bs.acc.2016.09.003>.
- [152] Marianou, A. A.; Michailof, C. M.; Pineda, A.; Iliopoulou, E. F.; Triantafyllidis, K. S.; Lappas, A. A. Glucose to Fructose Isomerization in Aqueous Media over Homogeneous and Heterogeneous Catalysts. *ChemCatChem*, 2016. <https://doi.org/10.1002/cctc.201501203>.
- [153] Hong, C. H.; Kim, S. H.; Kim, Y. G.; Shin, N. R. Method for Producing Glucaric Acid. US9227904B1, 2016.
- [154] Brown, J. M.; Manley-Harris, M.; Field, R. J.; Kiely, D. E. An NMR Study of the Equilibration of d -Glucaric Acid with Lactone Forms in Aqueous Acid Solutions . *J. Carbohydr. Chem.*, 2007. <https://doi.org/10.1080/07328300701787172>.
- [155] Gehret, T. C.; Frobese, A. S.; Zerbe, J. S.; Chenault, H. K. Convenient Large-Scale Synthesis of D-Glucaro-1,4:6,3-Dilactone. *J. Org. Chem.*, 2009. <https://doi.org/10.1021/jo9015985>.

- [156] Besson, M.; Gallezot, P. Selective Oxidation of Alcohols and Aldehydes on Metal Catalysts. *Catal. Today*, 2000. [https://doi.org/10.1016/S0920-5861\(99\)00315-6](https://doi.org/10.1016/S0920-5861(99)00315-6).
- [157] Largeaud, F.; Kokoh, K. B.; Beden, B.; Lamy, C. On the Electrochemical Reactivity of Anomers: Electrocatalytic Oxidation of α - and β -d-Glucose on Platinum Electrodes in Acid and Basic Media. *J. Electroanal. Chem.*, 1995. [https://doi.org/10.1016/0022-0728\(95\)04139-8](https://doi.org/10.1016/0022-0728(95)04139-8).
- [158] Kokoh, K. B.; Parpot, P.; Belgsir, E. M.; Léger, J. M.; Beden, B.; Lamy, C. Selective Oxidation of D-Gluconic Acid on Platinum and Lead Adatoms Modified Platinum Electrodes in Alkaline Medium. *Electrochim. Acta*, 1993. [https://doi.org/10.1016/0013-4686\(93\)80070-G](https://doi.org/10.1016/0013-4686(93)80070-G).
- [159] Kokoh, K. B.; Léger, J. M.; Beden, B.; Lamy, C. "On Line" Chromatographic Analysis of the Products Resulting from the Electrocatalytic Oxidation of d-Glucose on Pt, Au and Adatoms Modified Pt Electrodes-Part I. Acid and Neutral Media. *Electrochim. Acta*, 1992. [https://doi.org/10.1016/0013-4686\(92\)87004-J](https://doi.org/10.1016/0013-4686(92)87004-J).
- [160] Kabbabi, A.; Faure, R.; Durand, R.; Beden, B.; Hahn, F.; Leger, J. M.; Lamy, C. In Situ FTIRS Study of the Electrocatalytic Oxidation of Carbon Monoxide and Methanol at Platinum-Ruthenium Bulk Alloy Electrodes. *J. Electroanal. Chem.*, 1998. [https://doi.org/10.1016/S0022-0728\(97\)00558-5](https://doi.org/10.1016/S0022-0728(97)00558-5).
- [161] Nikolaeva, N. N.; Khazova, O. A.; Vasil'ev, Y. B. Main Characteristics of Glucose Electrooxidation on a Gold Anode. *Elektrokhimiya*, 1983.
- [162] Vassilyev, Y. B.; Khazova, O. A.; Nikolaeva, N. N. Kinetics and Mechanism of Glucose Electrooxidation on Different Electrode-Catalysts. Part I. Adsorption and Oxidation on Platinum. *J. Electroanal. Chem.*, 1985. [https://doi.org/10.1016/0022-0728\(85\)85084-1](https://doi.org/10.1016/0022-0728(85)85084-1).
- [163] Yei, L. H. E.; Beden, B.; Lamy, C. Electrocatalytic Oxidation of Glucose at Platinum in Alkaline Medium: On the Role of Temperature. *J. Electroanal. Chem.*, 1988. [https://doi.org/10.1016/0022-0728\(88\)80171-2](https://doi.org/10.1016/0022-0728(88)80171-2).
- [164] Yei, L. H. E.; Beden, B.; Lamy, C. Electrocatalytic Oxidation of Glucose At Platinum in Alkaline Medium: On the Role of Temperature. 1988, *246*, 349–362.
- [165] O'Laughlin, J. W. Handbook of Analytical Derivatization Reactions (Knapp, Daniel R.). *J. Chem. Educ.*, 1980. <https://doi.org/10.1021/ed057pa196.3>.
- [166] Kano, K.; Torimura, M.; Esaka, Y.; Goto, M.; Ueda, T. Electrocatalytic Oxidation of Carbohydrates at Copper(II) -Modified Electrodes and Its Application to Flow-through Detection. *J. Electroanal. Chem.*, 1994. [https://doi.org/10.1016/0022-0728\(93\)03252-K](https://doi.org/10.1016/0022-0728(93)03252-K).
- [167] Xiang, C. H.; Xie, Q. J.; Yao, S. Electrochemical Quartz Crystal Impedance Study of Glucose Oxidation on a Nickel Hydroxide Modified Au Electrode in Alkaline Solution. *Electroanalysis*, 2003. <https://doi.org/10.1002/elan.200390120>.
- [168] Moggia, G.; Kenis, T.; Daems, N.; Breugelmans, T. Electrochemical Oxidation of d -Glucose in Alkaline Medium : Impact of Oxidation Potential and Chemical Side Reactions on the Selectivity to d -Gluconic and d -Glucaric Acid. *ChemElectroChem*, 2019, 1–11. <https://doi.org/10.1002/celec.201901592>.
- [169] Rao, M. L. B.; Drake, R. F. Studies of Electrooxidation of Dextrose in Neutral Media. *J. Electrochem. Soc.*, 1969. <https://doi.org/10.1149/1.2411841>.
- [170] Skou, E. M.; Larsen, E.; Winsnes, R.; Pajunen, P.; Koskikallio, J.; Swahn, C.-G. The Inhibition of the Electrochemical Oxidation of Glucose at Platinum at PH = 7.4 by Chloride Ions. *Acta Chem.*

- Scand.*, 1973. <https://doi.org/10.3891/acta.chem.scand.27-2239>.
- [171] Ernst, S.; Hamann, C. H.; Heitbaum, J. Electrooxidation of Glucose in Phosphate Buffer Solutions: Kinetics and Reaction Mechanism. *Berichte der Bunsengesellschaft/Physical Chem. Chem. Phys.*, 1980. <https://doi.org/10.1002/bbpc.19800840111>.
- [172] Ernst, S.; Heitbaum, J.; Hamann, C. H. The Electrooxidation of Glucose in Phosphate Buffer Solutions. *J. Electroanal. Chem. Interfacial Electrochem.*, 1979. [https://doi.org/10.1016/s0022-0728\(79\)80159-x](https://doi.org/10.1016/s0022-0728(79)80159-x).
- [173] Holade, Y.; Servat, K.; Napporn, T. W.; Morais, C.; Berjeaud, J. M.; Kokoh, K. B. Highly Selective Oxidation of Carbohydrates in an Efficient Electrochemical Energy Converter: Cogenerating Organic Electrosynthesis. *ChemSusChem*, 2016. <https://doi.org/10.1002/cssc.201501593>.
- [174] Sanghez de Luna, G.; Tabanelli, T.; Velasco-Vélez, J. J.; Monti, E.; Ospitali, F.; Albonetti, S.; Cavani, F.; Fornasari, G.; Benito, P. Electrification of Glucose Valorization over NiO/Ni Foam. *Sustain. Energy Fuels*, 2023, 7 (18), 4474–4485. <https://doi.org/10.1039/d3se00847a>.
- [175] Lamy, C.; Coutanceau, C.; Baranton, S. Principle of Hydrogen Production by Electrocatalytic Oxidation of Organic Compounds in a Proton Exchange Membrane Electrolysis Cell. In *Production of Clean Hydrogen by Electrochemical Reforming of Oxygenated Organic Compounds*; 2020; pp 7–20. <https://doi.org/10.1016/B978-0-12-821500-5.00002-3>.
- [176] Hsiao, M. W.; Adzic, R. R.; Yeager, E. B. The Effects of Adsorbed Anions on the Oxidation of D-Glucose on Gold Single Crystal Electrodes. *Electrochim. Acta*, 1992. [https://doi.org/10.1016/0013-4686\(92\)85024-F](https://doi.org/10.1016/0013-4686(92)85024-F).
- [177] Hebié, S.; Cornu, L.; Napporn, T. W.; Rousseau, J.; Kokoh, B. K. Insight on the Surface Structure Effect of Free Gold Nanorods on Glucose Electrooxidation. *J. Phys. Chem. C*, 2013. <https://doi.org/10.1021/jp401009r>.
- [178] Tung, S. P.; Huang, T. K.; Lee, C. Y.; Chiu, H. T. Electrochemical Growth of Gold Nanostructures on Carbon Paper for Alkaline Direct Glucose Fuel Cell. *RSC Adv.*, 2012. <https://doi.org/10.1039/c1ra00611h>.
- [179] Corti, H. R.; Gonzalez, E. R. *Direct Alcohol Fuel Cells: Materials, Performance, Durability and Applications*; 2014. <https://doi.org/10.1007/978-94-007-7708-8>.
- [180] Ilie, A.; Simoes, M.; Baranton, S.; Coutanceau, C.; Martemianov, S. Influence of Operational Parameters and of Catalytic Materials on Electrical Performance of Direct Glycerol Solid Alkaline Membrane Fuel Cells. *J. Power Sources*, 2011. <https://doi.org/10.1016/j.jpowsour.2011.02.003>.
- [181] Arechederra, R. L.; Treu, B. L.; Minter, S. D. Development of Glycerol/O₂ Biofuel Cell. *J. Power Sources*, 2007. <https://doi.org/10.1016/j.jpowsour.2007.08.012>.
- [182] Rice, C.; Ha, S.; Masel, R. I.; Waszczuk, P.; Wieckowski, A.; Barnard, T. Direct Formic Acid Fuel Cells. *J. Power Sources*, 2002. [https://doi.org/10.1016/S0378-7753\(02\)00271-9](https://doi.org/10.1016/S0378-7753(02)00271-9).
- [183] Basu, D.; Basu, S. Synthesis, Characterization and Application of Platinum Based Bi-Metallic Catalysts for Direct Glucose Alkaline Fuel Cell. *Electrochim. Acta*, 2011. <https://doi.org/10.1016/j.electacta.2011.04.072>.
- [184] Basu, D.; Basu, S. A Study on Direct Glucose and Fructose Alkaline Fuel Cell. *Electrochim. Acta*, 2010. <https://doi.org/10.1016/j.electacta.2010.05.016>.

- [185] Gharagheizi, F. Determination of Diffusion Coefficient of Organic Compounds in Water Using a Simple Molecular-Based Method. *Ind. Eng. Chem. Res.*, 2012. <https://doi.org/10.1021/ie201944h>.
- [186] Brouzgou, A.; Yan, L. L.; Song, S. Q.; Tsiakaras, P. Glucose Electrooxidation over PdRh/C Electrocatalysts in Alkaline Medium. *Appl. Catal. B Environ.*, 2014, *147*, 481–489. <https://doi.org/10.1016/j.apcatb.2013.09.024>.
- [187] Wang, Y.; Nguyen, T. S.; Liu, X.; Wang, X. Novel Palladium-Lead (Pd-Pb/C) Bimetallic Catalysts for Electrooxidation of Ethanol in Alkaline Media. *J. Power Sources*, 2010. <https://doi.org/10.1016/j.jpowsour.2009.11.072>.
- [188] Mirescu, A.; Berndt, H.; Martin, A.; Prüße, U. Long-Term Stability of a 0.45% Au/TiO₂ Catalyst in the Selective Oxidation of Glucose at Optimised Reaction Conditions. *Appl. Catal. A Gen.*, 2007. <https://doi.org/10.1016/j.apcata.2006.10.016>.
- [189] Rafaideen, T.; Baranton, S.; Coutanceau, C. Highly Efficient and Selective Electrooxidation of Glucose and Xylose in Alkaline Medium at Carbon Supported Alloyed PdAu Nanocatalysts. *Appl. Catal. B Environ.*, 2019, *243* (August 2018), 641–656. <https://doi.org/10.1016/j.apcatb.2018.11.006>.
- [190] Wenkin, M.; Ruiz, P.; Delmon, B.; Devillers, M. The Role of Bismuth as Promoter in Pd-Bi Catalysts for the Selective Oxidation of Glucose to Gluconate. *J. Mol. Catal. A Chem.*, 2002. [https://doi.org/10.1016/S1381-1169\(01\)00421-6](https://doi.org/10.1016/S1381-1169(01)00421-6).
- [191] Wenkin, M.; Touillaux, R.; Ruiz, P.; Delmon, B.; Devillers, M. Influence of Metallic Precursors on the Properties of Carbon-Supported Bismuth-Promoted Palladium Catalysts for the Selective Oxidation of Glucose to Gluconic Acid. *Appl. Catal. A Gen.*, 1996. [https://doi.org/10.1016/S0926-860X\(96\)00231-1](https://doi.org/10.1016/S0926-860X(96)00231-1).
- [192] Karski, S.; Witońska, I. Bismuth as an Additive Modifying the Selectivity of Palladium Catalysts. *J. Mol. Catal. A Chem.*, 2003. [https://doi.org/10.1016/S1381-1169\(02\)00359-X](https://doi.org/10.1016/S1381-1169(02)00359-X).
- [193] Karski, S. Activity and Selectivity of Pd-Bi/SiO₂ Catalysts in the Light of Mutual Interaction between Pd and Bi. *J. Mol. Catal. A Chem.*, 2006. <https://doi.org/10.1016/j.molcata.2006.03.013>.
- [194] Besson, M.; Lahmer, F.; Gallezot, P.; Fuertes, Patrick; Fleche, G. Catalytic Oxidation of Glucose on Bismuth-Promoted Palladium Catalysts. *J. Catal.*, 1995. <https://doi.org/10.1006/jcat.1995.1065>.
- [195] Wenkin, M.; Renard, C.; Ruiz, P.; Delmon, B.; Devillers, M. Promoting Effects of Bismuth in Carbon-Supported Bimetallic Pd-Bi Catalysts for the Selective Oxidation of Glucose to Gluconic Acid. *Stud. Surf. Sci. Catal.*, 1997. [https://doi.org/10.1016/s0167-2991\(97\)81013-0](https://doi.org/10.1016/s0167-2991(97)81013-0).
- [196] Moggia, G.; Schalck, J.; Daems, N.; Breugelmans, T. Two - Steps Synthesis of D - Glucaric Acid via D - Gluconic Acid by Electrocatalytic Oxidation of D - Glucose on Gold Electrode : Influence of Operational Parameters . *Electrochim. Acta*, 2021, 137852. <https://doi.org/10.1016/j.electacta.2021.137852>.
- [197] Steven, J. T.; Golovko, V. B.; Johannessen, B.; Marshall, A. T. Electrochemical Stability of Carbon-Supported Gold Nanoparticles in Acidic Electrolyte during Cyclic Voltammetry. *Electrochim. Acta*, 2016, *187*, 593–604. <https://doi.org/10.1016/j.electacta.2015.11.096>.
- [198] Chu, T. F.; Rajendran, R.; Kuznetsova, I.; Wang, G. J. High-Power, Non-Enzymatic Glucose Biofuel Cell Based on a Nano/Micro Hybrid-Structured Au Anode. *J. Power Sources*, 2020. <https://doi.org/10.1016/j.jpowsour.2020.227844>.

- [199] Cui, H. F.; Ye, J. S.; Liu, X.; Zhang, W. De; Sheu, F. S. Pt-Pb Alloy Nanoparticle/Carbon Nanotube Nanocomposite: A Strong Electrocatalyst for Glucose Oxidation. *Nanotechnology*, 2006. <https://doi.org/10.1088/0957-4484/17/9/043>.
- [200] Aoun, S. Ben; Taniguchi, I. Effective Electrocatalytic Oxidation of Glucose at Platinum Nanoparticle-Based Carbon Electrodes. *Chem. Lett.*, 2008. <https://doi.org/10.1246/cl.2008.936>.
- [201] Basu, D.; Basu, S. Synthesis and Characterization of Pt-Au/C Catalyst for Glucose Electro-Oxidation for the Application in Direct Glucose Fuel Cell. *Int. J. Hydrogen Energy*, 2011. <https://doi.org/10.1016/j.ijhydene.2011.03.042>.
- [202] Choukroun, D.; Daems, N.; Kenis, T.; Van Everbroeck, T.; Hereijgers, J.; Altantzis, T.; Bals, S.; Cool, P.; Breugelmans, T. Bifunctional Nickel-Nitrogen-Doped-Carbon-Supported Copper Electrocatalyst for CO₂ Reduction. *J. Phys. Chem. C*, 2020. <https://doi.org/10.1021/acs.jpcc.9b08931>.
- [203] Ustarroz, J.; Geboes, B.; Vanrompay, H.; Sentosun, K.; Bals, S.; Breugelmans, T.; Hubin, A. Electrodeposition of Highly Porous Pt Nanoparticles Studied by Quantitative 3D Electron Tomography: Influence of Growth Mechanisms and Potential Cycling on the Active Surface Area. *ACS Appl. Mater. Interfaces*, 2017. <https://doi.org/10.1021/acsami.7b01619>.
- [204] Geboes, B.; Ustarroz, J.; Sentosun, K.; Vanrompay, H.; Hubin, A.; Bals, S.; Breugelmans, T. Electrochemical Behavior of Electrodeposited Nanoporous Pt Catalysts for the Oxygen Reduction Reaction. *ACS Catal.*, 2016. <https://doi.org/10.1021/acscatal.6b00668>.
- [205] Geboes, B.; Mintsouli, I.; Wouters, B.; Georgieva, J.; Kakaroglou, A.; Sotiropoulos, S.; Valova, E.; Armanyanov, S.; Hubin, A.; Breugelmans, T. Surface and Electrochemical Characterisation of a Pt-Cu/C Nano-Structured Electrocatalyst, Prepared by Galvanic Displacement. *Appl. Catal. B Environ.*, 2014. <https://doi.org/10.1016/j.apcatb.2013.12.020>.
- [206] Md Rahim, S. A. N.; Lee, C. S.; Abnisa, F.; Wan Daud, W. M. A.; Aroua, M. K.; Cognet, P.; Pérès, Y. Activated Carbon-Based Electrodes for Two-Steps Catalytic/ Electrocatalytic Reduction of Glycerol in Amberlyst-15 Mediator. *Chemosphere*, 2022, 295 (August 2021). <https://doi.org/10.1016/j.chemosphere.2022.133949>.
- [207] Duarte, M.; De Mot, B.; Hereijgers, J.; Breugelmans, T. Electrochemical Reduction of CO₂: Effect of Convective CO₂ Supply in Gas Diffusion Electrodes. *ChemElectroChem*, 2019, 6 (22), 5596–5602. <https://doi.org/10.1002/celec.201901454>.
- [208] Hern, S. Electrochemical CO₂ Conversion. 2021.
- [209] Lim, C. F. C.; Harrington, D. A.; Marshall, A. T. Effects of Mass Transfer on the Electrocatalytic CO₂ Reduction on Cu. *Electrochim. Acta*, 2017, 238, 56–63. <https://doi.org/10.1016/j.electacta.2017.04.017>.
- [210] Gojković, S. L. Mass Transfer Effect in Electrochemical Oxidation of Methanol at Platinum Electrocatalysts. *J. Electroanal. Chem.*, 2004, 573 (2), 271–276. <https://doi.org/10.1016/j.jelechem.2004.07.013>.
- [211] Dumitrescu, I.; Crooks, R. M. Effect of Mass Transfer on the Oxygen Reduction Reaction Catalyzed by Platinum Dendrimer Encapsulated Nanoparticles. *Proc. Natl. Acad. Sci. U. S. A.*, 2012, 109 (29), 11493–11497. <https://doi.org/10.1073/pnas.1201370109>.
- [212] Bv, N. N. Norit SX 1 G <http://www.norit.com/>.
- [213] Hermans, S.; Deffernez, A.; Devillers, M. Au-Pd/C Catalysts for Glyoxal and Glucose Selective

- Oxidations. *Appl. Catal. A Gen.*, 2011, 395 (1–2), 19–27.
<https://doi.org/10.1016/j.apcata.2011.01.019>.
- [214] Hermans, S.; Deffernez, A.; Devillers, M. Preparation of Au-Pd/C Catalysts by Adsorption of Metallic Species in Aqueous Phase for Selective Oxidation. *Catal. Today*, 2010, 157 (1–4), 77–82.
<https://doi.org/10.1016/j.cattod.2010.04.010>.
- [215] Deffernez, A.; Hermans, S.; Devillers, M. Pd/C Catalysts Prepared by Controlled Adsorption of Pd(II) Species on SX PLUS Carbon in the Aqueous Phase. *J. Phys. Chem. C*, 2007, 111 (26), 9448–9459. <https://doi.org/10.1021/jp070402u>.
- [216] Luo, M.; Hong, Y.; Yao, W.; Huang, C.; Xu, Q.; Wu, Q. Facile Removal of Polyvinylpyrrolidone (PVP) Adsorbates from Pt Alloy Nanoparticles. *J. Mater. Chem. A*, 2015, 3 (6), 2770–2775.
<https://doi.org/10.1039/c4ta05250a>.
- [217] Irtem, E.; Arenas Esteban, D.; Duarte, M.; Choukroun, D.; Lee, S.; Ibáñez, M.; Bals, S.; Breugelmanns, T. Ligand-Mode Directed Selectivity in Cu-Ag Core-Shell Based Gas Diffusion Electrodes for CO₂ Electroreduction. *ACS Catal.*, 2020, 10 (22), 13468–13478.
<https://doi.org/10.1021/acscatal.0c03210>.
- [218] Ansar, S. M.; Ameer, F. S.; Hu, W.; Zou, S.; Pittman, C. U.; Zhang, D. Removal of Molecular Adsorbates on Gold Nanoparticles Using Sodium Borohydride in Water. *Nano Lett.*, 2013, 13 (3), 1226–1229. <https://doi.org/10.1021/nl304703w>.
- [219] Albrecht, W.; Bals, S. Fast Electron Tomography for Nanomaterials. 2020.
<https://doi.org/10.1021/acs.jpcc.0c08939>.
- [220] Moon, T. K. The Expectation-Maximization Algorithm. *IEEE Signal Process. Mag.*, 1996, 13 (6), 47–60. <https://doi.org/doi:10.1109/79.543975>.
- [221] Duarte, M.; Hereijgers, J.; Daems, N.; Daele, S. Van; Breugelmanns, T. The Importance of Target Product Engineering for Long-Term Operation of CO₂ Zero-Gap Electrolysers.
- [222] Moulton, S. E.; Barisci, J. N.; Bath, A.; Stella, R.; Wallace, G. G. Studies of Double Layer Capacitance and Electron Transfer at a Gold Electrode Exposed to Protein Solutions. *Electrochim. Acta*, 2004. <https://doi.org/10.1016/j.electacta.2004.03.034>.
- [223] Auer, E.; Freund, A.; Pietsch, J.; Tacke, T. Carbons as Supports for Industrial Precious Metal Catalysts. *Appl. Catal. A Gen.*, 1998, 173 (2), 259–271. [https://doi.org/10.1016/S0926-860X\(98\)00184-7](https://doi.org/10.1016/S0926-860X(98)00184-7).
- [224] Hao, X.; Quach, L.; Korah, J.; Spieker, W. A.; Regalbutto, J. R. The Control of Platinum Impregnation by PZC Alteration of Oxides and Carbon. *J. Mol. Catal. A Chem.*, 2004, 219 (1), 97–107. <https://doi.org/10.1016/j.molcata.2004.04.026>.
- [225] Carrott, P. J. M.; Nabais, J. M. V.; Ribeiro Carrott, M. M. L.; Menéndez, J. A. Thermal Treatments of Activated Carbon Fibres Using a Microwave Furnace. *Microporous Mesoporous Mater.*, 2001, 47 (2–3), 243–252. [https://doi.org/10.1016/S1387-1811\(01\)00384-5](https://doi.org/10.1016/S1387-1811(01)00384-5).
- [226] Sneha, K.; Sathishkumar, M.; Kim, S.; Yun, Y. S. Counter Ions and Temperature Incorporated Tailoring of Biogenic Gold Nanoparticles. *Process Biochem.*, 2010.
<https://doi.org/10.1016/j.procbio.2010.05.019>.
- [227] Krishnamurthy, S.; Esterle, A.; Sharma, N. C.; Sahi, S. V. Yucca-Derived Synthesis of Gold Nanomaterial and Their Catalytic Potential. *Nanoscale Res. Lett.*, 2014.
<https://doi.org/10.1186/1556-276X-9-627>.

- [228] LaMorte, W. W. From Molecules to Man - A perspective on size https://sphweb.bumc.bu.edu/otlt/mph-modules/ph/ph709_basiccellbiology/ph709_basiccellbiology8.html#:~:text=A Perspective on Size,-An angstrom is&text=A glucose molecule is about 9 angstroms (accessed Dec 19, 2022).
- [229] How big are biochemical nuts and bolts? <http://book.bionumbers.org/how-big-are-biochemical-nuts-and-bolts/> (accessed Dec 19, 2022).
- [230] Ilomuanya, M.; Nashiru, B.; Ifudu, N.; Igwilo, C. Effect of Pore Size and Morphology of Activated Charcoal Prepared from Midribs of *Elaeis Guineensis* on Adsorption of Poisons Using Metronidazole and *Escherichia Coli* O157:H7 as a Case Study. *J. Microsc. Ultrastruct.*, 2017, 5 (1), 32. <https://doi.org/10.1016/j.jmau.2016.05.001>.
- [231] Annemieke, H. W. Modification and Application of Carbon Supported Noble Metal Catalysts, 2000.
- [232] Yang, L.; Zhang, Y.; Chu, M.; Deng, W.; Tan, Y.; Ma, M.; Su, X.; Xie, Q.; Yao, S. Facile Fabrication of Network Film Electrodes with Ultrathin Au Nanowires for Nonenzymatic Glucose Sensing and Glucose/O₂ Fuel Cell. *Biosens. Bioelectron.*, 2014, 52, 105–110. <https://doi.org/10.1016/j.bios.2013.08.038>.
- [233] Oña, J. P.; Latonen, R. M.; Kumar, N.; Peurla, M.; Angervo, I.; Grénman, H. Electrocatalytic Hydrogenation and Oxidation of Glucose and Xylose on Mesoporous Carbon-Supported Au Nanocatalysts. *Electrochim. Acta*, 2023, 437 (October 2022). <https://doi.org/10.1016/j.electacta.2022.141536>.
- [234] Guo, X.; Du, H.; Qu, F.; Li, J. Recent Progress in Electrocatalytic Nitrogen Reduction. *J. Mater. Chem. A*, 2019, 7, 3531–3543. <https://doi.org/https://doi.org/10.1039/C8TA11201K>.
- [235] Sahoo, S. K.; Heske, J.; Antonietti, M.; Qin, Q.; Oschatz, M.; Ku, T. D. Electrochemical N₂ Reduction to Ammonia Using Single Au/Fe Atoms Supported on Nitrogen-Doped Porous Carbon. 2020. <https://doi.org/10.1021/acsaem.0c01740>.